

An Isotopic and Geochemical study
of Kimberlites and
Associated Alkaline Rocks
from Namibia

ANDREW JOHN SPRIGGS

Submitted in accordance with the
requirements for the degree of
Doctor of Philosophy.

University of Leeds,
Department of Earth Sciences.
October 1988



ETHOS

Boston Spa, Wetherby
West Yorkshire, LS23 7BQ
www.bl.uk

**BEST COPY AVAILABLE
VARIABLE PRINT QUALITY**

ABSTRACT

The Gibeon kimberlite province of Namibia (70 ± 10 Ma) comprises 74 intrusions of group I calcite-monticellite-kimberlite occurring as dykes and pipes (hypabyssal and diatreme facies). The kimberlites display limited mineralogical variations, and consist of olivine \pm phlogopite macrocrysts set in a groundmass of ulvospinel, ilmenite, magnesiochromite, calcite and monticellite \pm phlogopite, perovskite, apatite and baddelyite. Late stage crystallisation produces an SiO_2 , CaO, CO_2 and trace element rich liquid which causes precipitation of Ba rich groundmass phlogopite previously unrecorded in kimberlite.

The majority of the kimberlites, which were collected from fresh borehole samples, show very little geochemical variation: the magma represents a primary liquid derived directly from a single asthenospheric source, with very little fractionation or wallrock contamination. The geochemical effects of fractionation, crustal contamination and alteration are examined and evaluated.

The asthenospheric source region of the kimberlites is geochemically and isotopically equivalent to that of the Bouvet OIB source. The Gibeon kimberlites are temporally and spatially coincident with the location of the Vema hotspot trace at 70Ma. The Gibeon province is located geographically within the Dupal anomaly, but the kimberlites have non-Dupal OIB type signatures, supporting the concept of a shallow origin for the Dupal anomaly.

One kimberlite pipe (33/K2) is enriched in Pb, Rb, Ba, K, Sr and P and has enriched isotopic characteristics, interpreted as the result of assimilation, during ascent, of older phlogopite-K-richterite-peridotite (PKP) type metasomatised lithosphere. Isotopically and geochemically, this kimberlite is intermediate between previously recorded group I and II kimberlites.

Garnet and pyroxene megacrysts (hosted by the kimberlites) have distinctly different Sr, Nd and Pb isotopic compositions to the kimberlite indicating their xenocrystal origins. Geochemical and isotopic variations in the megacrysts indicate their origin from an OIB-type, fractionating parental magma which was synchronously assimilating enriched lithosphere in an AFC process.

Hotspot traces extending from the Gibeon area to the present day Vema and Discovery seamounts are also coincident with non-kimberlite alkaline magmatism. These alkaline intrusions have geochemical and isotopic signatures equivalent to the kimberlites and Bouvet. It is concluded that a gradation exists between kimberlite and alkali basalt, with depth of melting being the dominant control affecting magma type.

ACKNOWLEDGEMENTS

In completing this work, I am indebted to a large number of people who helped me with instruction, advice, discussion and technical and logistical assistance.

Firstly and foremost, my thanks go to my superbly tolerant supervisors Peter Nixon and Gareth Davies who gave me a great deal of their time, and were ever willing to help.

Thanks also go to:

The De Beers Mining Corporation, for logistical support, drill samples and instruction in kimberlite petrology, and in particular to John Bristow, Libby Colgan, Roger Clement, Mike McGurl, Jock Robey, Mike Skinner and Farnas Viljoen, plus the many others whose hospitality I enjoyed in South Africa.

Hennie v.d. Westhuizen, Nigel Hoad, Roman Wessolinski and the staff at CDM for their hospitality and support in Namibia.

Marge Wilson, Craig Smith, Kirsten Fraser, Martin Menzies, Anton LeRoex, Emil Jagoutz, John Gurney, Roger Mitchell, Martin Dodson, for invaluable discussion, help and advice.

Rod Green, Phil and Angela Guise, Dave 'fumes' Rex and Bob Cliff for isotopic help and for withstanding combustion, demolition, dissolution, explosion and toxification during my exploits in the lab.

Alan Grey (XRF), Nick Walsh (ICP), Nick Rogers (INAA), Eric Condliffe (probe) and Dave Chaffey (computers) for their technical assistance and useful discussion.

Special mention in despatches for help with sample preparation go to Dennis Pickles (for expert assistance in mineral separation) and Tom Oddy (for light entertainment and stories of parachuting, and deeds of daring do!).

Thanks to Qua Sumus and the parachute club for their friendship and also to the inmates of cell 8.10a, for their incisive wit, hope you escape soon!

Lastly and especially, thanks to Jackie and my parents, for their love, encouragement and support throughout.

CONTENTS

Chapter 1 :	INTRODUCTION TO KIMBERLITE GEOLOGY	1
1.1	INTRODUCTION	1
1.2	REVIEW OF KIMBERLITE GEOLOGY	3
1.2.1	Occurrence and tectonics setting	3
1.2.2	Age of kimberlites	3
1.2.3	Intrusive style	5
1.2.4	Textural and mineralogical variations	7
1.2.5	Geochemistry	9
1.2.6	Radiogenic isotope studies	10
1.2.7	Experimental petrology	13
1.2.8	The Megacryst suite	14
1.2.8	Xenoliths	15
1.3	PROBLEMS IN KIMBERLITE GEOLOGY	15
1.4	AIMS OF THE PROJECT	16
Chapter 2 :	NAMIBIA	17
2.1	REGIONAL GEOLOGY	17
2.1.1	Crustal development	18
2.1.2	Proterozoic Orogenic Activity	19
2.1.3	Nama Sediments	22
2.1.4	Karoo Sediments	22
2.1.5	Karoo Volcanics	23
2.1.6	Alkali Complexes	26
2.1.7	Post Rifting	26
2.2	GEOPHYSICS	27
2.3	INTRODUCTION TO FIELD AREA	28
2.3.1	The Gibeon Kimberlite Province	30
2.3.2	The Zaris Cluster	32
2.3.3	The Tiras Cluster	33
2.3.4	Klinghardt Mountains	33
2.3.5	Carbonatites	35
2.3.6	Grunau Melilitites	35
2.3.7	Megacrysts	36
2.4	ROCK NUMBER SYSTEM	37
2.5	SAMPLE SELECTION	38
2.6	AGES OF INTRUSIONS	42
2.6.1	Previous Work	42
2.6.2	Radiometric Dating, This Work	44
2.6.3	Discussion of Results	45

Chapter 3 :	PETROGRAPHY, MINERALOGY AND GEOCHEMISTRY :	
	INTRAKIMBERLITE VARIATIONS	61
3.1	36/K35 BERSEBA RESERVE 2	61
3.1.1	Mineralogy	62
3.1.2	Geochemistry	76
3.2	36/K39 BERSEBA RESERVE 6	82
3.2.1	Mineralogy	83
3.2.2	Geochemistry	86
3.3	36/K53 RIETKUIL 7	87
3.3.1	Mineralogy	88
3.3.2	Geochemistry	94
3.4	33/K2 ANIS KUBUB	95
3.4.1	Mineralogy	96
3.4.2	Geochemistry	98
3.5	ALTERED SAMPLES	102
3.5.1	33/K4 Gibeon Reserve 4	102
3.5.2	33/K5 Zaris Sill	103
3.5.3	33/K12 Uitkoms 4	104
3.5.4	33/K13 Hatzium Dome	106
3.5.5	33/K14 Gibeon Reserve 3	107
3.5.6	36/K12 Hanaus 2	108
3.5.7	36/K16 Deutsche Erde 1	109
3.5.8	36/K43 Berseba Reserve 10	110
3.6	SUMMARY OF KIMBERLITE PETROLOGY	114
Chapter 4 :	INTERKIMBERLITE VARIATIONS: GEOCHEMISTRY	
	AND PETROGENESIS	117
4.1	FRACTIONATION	118
4.2	CRUSTAL CONTAMINATION	122
4.3	ALTERATION	125
4.4	COMMENT ON CLEMENT'S CONTAMINATION INDEX	138
4.5	CHEMICAL VARIATIONS IN THE KIMBERLITES	139
4.6	MANTLE SOURCE REGIONS	146
4.6.1	Location of OIB	147
4.6.2	Geochemical Characteristics of OIB	148
4.6.3	Comparison of kimberlites and OIB	153
4.7	THE TRACE ELEMENT COMPOSITION OF K2	162
4.8	COMPARISON WITH KIMBERLITE FROM OTHER AREAS	168
4.9	CONCLUSIONS	177

Chapter 5 :	THE KIMBERLITE-MEGACRYST RELATIONSHIP	179
5.1	INTRODUCTION	179
5.2	SAMPLES	182
5.3	ISOTOPE SYSTEMATICS	188
5.3.1	Pb Isotopes	188
5.3.2	Nd Isotopes	191
5.3.3	Sr Isotopes	197
5.4	DISCUSSION	198
5.5	CONCLUSIONS	201
Chapter 6 :	ASSOCIATED ALKALINE ROCKS	203
6.1	INTRODUCTION	203
6.2	GROSS BRUKKAROS AND THE BLUE HILLS	204
6.2.1	Location	204
6.2.2	Samples	205
6.2.3	Genesis of Monticellite Peridotite by partial melting of carbonated peridotite?	210
6.2.4	Derivation by kimberlite devolatilisation	226
6.3	THE SCHWARZEBERG NEPHELINITE	227
6.3.1	Mineralogy	228
6.3.2	Petrogenesis	229
6.3.3	Source regions	232
6.4	THE GRUNAU PROVINCE	234
6.5	CONCLUSIONS	235
Chapter 7 :	SYNTHESIS	237
7.1	MANTLE SOURCE REGIONS	237
7.2	MELTING	238
7.3	ASCENT	240
7.4	GROUP I - GROUP II	242
7.5	ASSOCIATED ROCKS	244
7.6	HOTSPOTS	245
7.7	MEGACRYSTS	247
REFERENCES		253

APPENDIX 1		271
A1.1	PREPARATION AND XRF ANALYSIS OF WHOLE ROCK	271
A1.1.1	Crushing	
A1.1.2	Preparation for XRF major element analysis	271
A1.1.3	Preparation for XRF trace element analysis	272
A1.1.4	Measurement of Loss-on-ignition	272
A1.1.5	XRF machine conditions	272
A1.2	ANALYSIS OF REE BY ICP SPECTROSCOPY	273
A1.3	ANALYSIS OF REE, Th, U, Ta, AND Hf BY INAA	274
A1.4	MINERAL ANALYSIS BY ELECTRON MICROPROBE	275
A1.5	Sr, Nd AND Pb ISOTOPE ANALYSIS	276
A1.5.1	Whole rock Sr and Nd chemistry	276
A1.5.2	Whole rock Pb chemistry	277
A1.5.3	Mass Spectrometry	278
A1.5.4	Standards	279
A1.5.5	Analytical blanks	280
A1.5.6	Data presentation	281
A1.6	COMPARISON OF ANALYTICAL TECHNIQUES	285
A1.7	ANALYSIS OF MINERAL SEPARATES	289
A1.7.1	Phlogopite separation	289
A1.7.2	Megacryst preparation	290
APPENDIX 2	MICROPROBE DATA	293

FIGURES

1.1	Distribution of crustal provinces and diamond bearing kimberlites.	4
1.2	Distribution and ages of group I and group II kimberlites.	5
1.3	Schematic diagram of a kimberlite pipe.	6
1.4	Textural classification of kimberlite.	8
1.5	Isotopic composition of kimberlites.	11
2.1	Map of Field Area.	18
2.2	Late Precambrian structural framework of Southern Africa and South America.	20
2.3	Volcanic provinces in Namibia.	29
2.4	The Gibeon kimberlite province.	31
2.5	The Luderitz area.	34
2.6	K39 Rb/Sr isochron plot.	47
2.7	K2 Rb/Sr isochron plot.	49
2.8	K43 Rb/Sr isochron plot.	52
2.9	K14 Rb/Sr isochron plot.	52
2.10	$^{39}\text{Ar}/^{40}\text{Ar}$ age plots for PK61 and PK62.	55
3.1	Forsterite composition of olivine phenocrysts and macrocrysts.	63
3.2	MgO v Cr_2O_3 for ilmenites from K35.	65
3.3	TiO_2 v $\text{FeO}/(\text{FeO}+\text{MgO})$ for groundmass spinels.	67
3.4	TiO_2 v $\text{Fe}^{3+}/\text{Fe}^{2+}$ for groundmass spinels.	68
3.5	BaO v K_2O for phlogopites.	70
3.6	BaO v TiO_2 for phlogopites.	72
3.7	Al/Si v Ba/K for groundmass phlogopites.	73
3.8	Transition element plot for K35.	78
3.9	REE plot for K35.	79
3.10	Trace element plot for K35.	81
3.11	Transition element plot for K39.	84
3.12	REE plot for K39.	84
3.13	Trace element plot for K39.	85
3.14	Spinel composition prism.	90
3.15	Transition element plot for K53.	92
3.16	REE plot for K53.	92
3.17	Trace element plot for K53.	93
3.18	Transition element plot for K2.	100
3.19	REE plot for K2.	100
3.20	Trace element plots for K2.	101
3.21	REE plot for altered kimberlites.	105
3.22	Trace element plots for altered kimberlites.	112
3.23	Transition element plots for altered kimberlite	113
4.1	Major elements v MgO for kimberlites.	120
4.2	Trace elements v MgO for kimberlites.	121
4.3	Comparison of crust and kimberlite compositions	124
4.4	Major elements v Nb for kimberlites.	129
4.5	Trace elements v Nb for kimberlites.	130

4.6	REE patterns for fresh and altered kimberlites.	132
4.7	REEs v Nb for fresh and altered kimberlites.	133
4.8	$^{87}\text{Sr}/^{86}\text{Sr}$ v Sr and $^{143}\text{Nd}/^{144}\text{Nd}$ v Nd.	135
4.9	$^{143}\text{Nd}/^{144}\text{Nd}$ variations and errors.	135
4.10	Trace element ratio variations in kimberlites.	140
4.11	Kimberlite normalised plot for K53.	141
4.12	Kimberlite normalised plot for K39.	143
4.13	Kimberlite normalised plot for K2.	145
4.14	Location of OIB in South Atlantic.	147
4.15	Trace element plots for South Atlantic OIB.	149
4.16	Trace element ratios of kimberlites and OIB.	150
4.17	Dupal anomaly map.	152
4.18	cNd v cSr for kimberlites and OIB.	158
4.19	Pb isotope diagram for kimberlites and OIB.	159
4.20	$^{87}\text{Sr}/^{86}\text{Sr}$ and $^{143}\text{Nd}/^{144}\text{Nd}$ v $^{206}\text{Pb}/^{204}\text{Pb}$.	160
4.21	Trace element plots showing enrichment in K2.	163
4.22	Kimberlite normalised plots showing possible sources for enrichment in K2.	165
4.23	Crichtonite mineral compositions.	167
4.24	K35-normalised plot for group IA kimberlites.	170
4.25	K35-normalised plot for group IB kimberlites.	171
4.26	K35-normalised plot for group II kimberlites.	174
4.27	Comparison of K35, K2, Finsch and Jwaneng.	175
5.1	Ca-Mg-Fe plot for megacrysts.	183
5.2	Pb isotopic composition of megacrysts.	189
5.3	Nd isotopic composition of megacrysts.	193
5.4	Nd isotopic growth curves for megacrysts.	194
5.5	cSr v cNd diagram for megacrysts and kimberlite	196
6.1	TiO_2 v $\text{FeO}/(\text{FeO}+\text{MgO})$ for groundmass spinels.	207
6.2	TiO_2 v $\text{Fe}^{3+}/\text{Fe}^{2+}$ for groundmass spinels.	208
6.3	Schematic diagram of the peridotite solidus and carbonate stability fields.	211
6.4	Chondrite normalised trace element plot for PK2	218
6.5	Kimberlite-K35 normalised plot for PK2.	219
6.6	cSr v cNd diagram for PK2, Schwarzeberg and the Gibeon kimberlites.	221
6.7	Pb isotope diagram for PK2, Schwarzeberg and the Gibeon kimberlites.	223
6.8	La/Nb v Ba/Nb for various magma types.	224
6.9	Major element plots for PK2.	226
6.10	Major element plots for PK2 and Schwarzeberg.	230
6.11	Chondrite normalised trace element plot comparing kimberlite, nephelinite and OIB.	233
7.1	Schematic diagram showing relationships between different magma types	249
7.2	Flow diagram showing possible events in megacryst formation	

PLATES

3.1	Photomicrograph of K35	62
3.2	Photomicrograph of K39	82
3.3	Photomicrograph of K53	88
3.4	Photomicrograph of K2	96
3.5	Photomicrograph of K4	103
3.6	Photomicrograph of K5	104
3.7	Photomicrograph of K12	106
3.8	Photomicrograph of K14	108
3.9	Photomicrograph of K12	109
3.10	Photomicrograph of K16	110
3.11	Photomicrograph of K43	111
6.1	Photomicrograph of PK2/A15	206
6.2	Photomicrograph of A20	209
6.3	Photomicrograph of Schwarzeberg nephelinite	228

TABLES

2.1	Sample summary	40
2.2	Previous work: age determinations.	43
2.3	This work : Age determinations.	45
2.4	K39 Rb/Sr data.	47
2.5	K2 Rb/Sr data.	49
2.6	K43 Rb/Sr data.	51
2.7	K14 Rb/Sr data.	53
2.8	$^{39}\text{Ar}/^{40}\text{Ar}$ data.	56
2.9	K/Ar data.	57
3.1	Wholerock kimberlite data.	79
4.1	Alteration state of altered kimberlites.	127
4.2	Sr and Nd isotopic composition of kimberlites.	136
4.3	Pb isotopic composition of kimberlites.	137
5.1	Megacryst sample list.	184
5.2	Composition of garnet megacrysts.	186
5.3	Composition of pyroxene megacrysts.	187
5.4	Pb isotope composition of pyroxene megacrysts.	191
5.5	Nd isotope composition of megacrysts.	195
5.6	Sr isotope composition of megacrysts.	198
6.1	melting parameters for PK2.	217
6.2	composition of associated alkaline rocks.	215
6.3	isotopic composition of associated rocks.	216

CHAPTER 1

1.1 INTRODUCTION

Kimberlite is a rare volatile-rich, potassic, ultrabasic igneous rock whose importance both economically and scientifically exceeds its abundance, being both the main source of natural diamond and, as xenoliths, of our only samples of the deep mantle. Through their chemistry kimberlites provide some insight into mantle processes, both chemical and dynamic, and, through studies of diamond inclusions and xenoliths, about the age and formation of the continental lithosphere.

This thesis presents a detailed geochemical study of kimberlite from the Gibeon province in Namibia. The province comprises some 74 occurrences which are related in time and space. The study aims to determine the petrogenesis of these kimberlites in particular, and then to consider wider aspects of kimberlite petrogenesis, including their mantle source regions, possible associations with 'hotspots' and the influence of the thickness, composition and temperature of the continental lithosphere on their evolution. The study also investigates the relationships between kimberlite and other similar alkalic volcanics. The origin of the enigmatic megacryst suite is considered in the light of Pb, Sr and Nd isotope evidence.

Recent commercial interests in kimberlite research have brought about great advances in the understanding of these rocks, but there is still disagreement on almost every aspect of kimberlite petrogenesis. Several major reviews document the periodic leaps in which the understanding and knowledge of kimberlite magmatism have accrued. Wagner (1914) summarised the discovery and development of

the diamond fields of South Africa and completed a major petrographic study, describing the occurrence and petrography of kimberlite and introducing a twofold division into basaltic and micaceous types.

Williams (1932) and Dawson (1980) updated and expanded on Wagner's lead, reiterating the two petrographic subdivisions and documenting a large variety of hypotheses concerning kimberlite magmatism. Mitchell (1986) provides by far the best review of kimberlite geology to date, clearly separating fact and hypothesis with chapters covering occurrence, structure, mineralogy, chemistry and petrogenesis of kimberlite. The sheer variety of current theories and lack of consensus in kimberlite geology is clearly shown by his inability to conclude with a general model compatible with all known data.

Some of the most important recent contributions have been made by the DeBeers research group and co-workers, providing an understanding of intrusive mechanisms, and a classification of different mineralogical types and textural facies of kimberlite. This work (eg Clement and Skinner 1979) dispelled the popular ideas of fluidised intrusion(eg Mikhayenko and Nenashev 1962, Dawson 1980) and provided a solid framework upon which geochemical studies (Smith et al. 85, Frazer et al. 1985) have been performed. The two petrographic subdivisions of kimberlite were defined on isotopic grounds by Smith (1983) as group I and group II kimberlites. Geochemical and isotope studies mark the latest moves forwards in the understanding of kimberlite petrogenesis, in seeking mantle source regions and in understanding enrichment processes.

1.2.1 Occurrence and tectonic setting.

Kimberlite was first discovered and described in South Africa and have since been found elsewhere in Africa and in Asia, Australia, North and South America. Always they are restricted to continental environments, and particularly to old cratonic areas with ages in excess of 1Ga. Kimberlites have not been found in young fold belts or oceanic environments

Southern Africa has probably the greatest concentration of kimberlite intrusions in the world, and has been the focus of the most detailed studies. It has long been realised that kimberlites bearing diamond have all been intruded through particularly old (>2.4 Ga) thick (>150km) central cratons such as the Kaapvaal craton in Southern Africa, and that in the younger surrounding 'mobile belts' the kimberlites are non-diamondiferous. The effect of the thickness age and composition of the craton on kimberlite geochemistry is still an open question and is a subject addressed in this work.

1.2.2 Age of kimberlites

Known ages of kimberlites in Africa range from the Proterozoic 1600Ma Kuruman occurrences (Bristow et al. 1986) in South Africa to the 70Ma Gibeon kimberlites (this work) in Namibia. A several hundred million year periodicity of kimberlite activity has been noted in Siberia (Vladimirov pers comm.) and also in South Africa. South Africa records periods of kimberlite intrusion at 1600Ma (Kuruman), 1200Ma (Premier), 500Ma (Zimbabwe) and the major period of activity from 240-70Ma. This latter period produced a large number of kimberlites in Southern Africa. Between 200 and 114Ma a 'line' of group II kimberlites was intruded from Dokolwayo (200Ma) in the

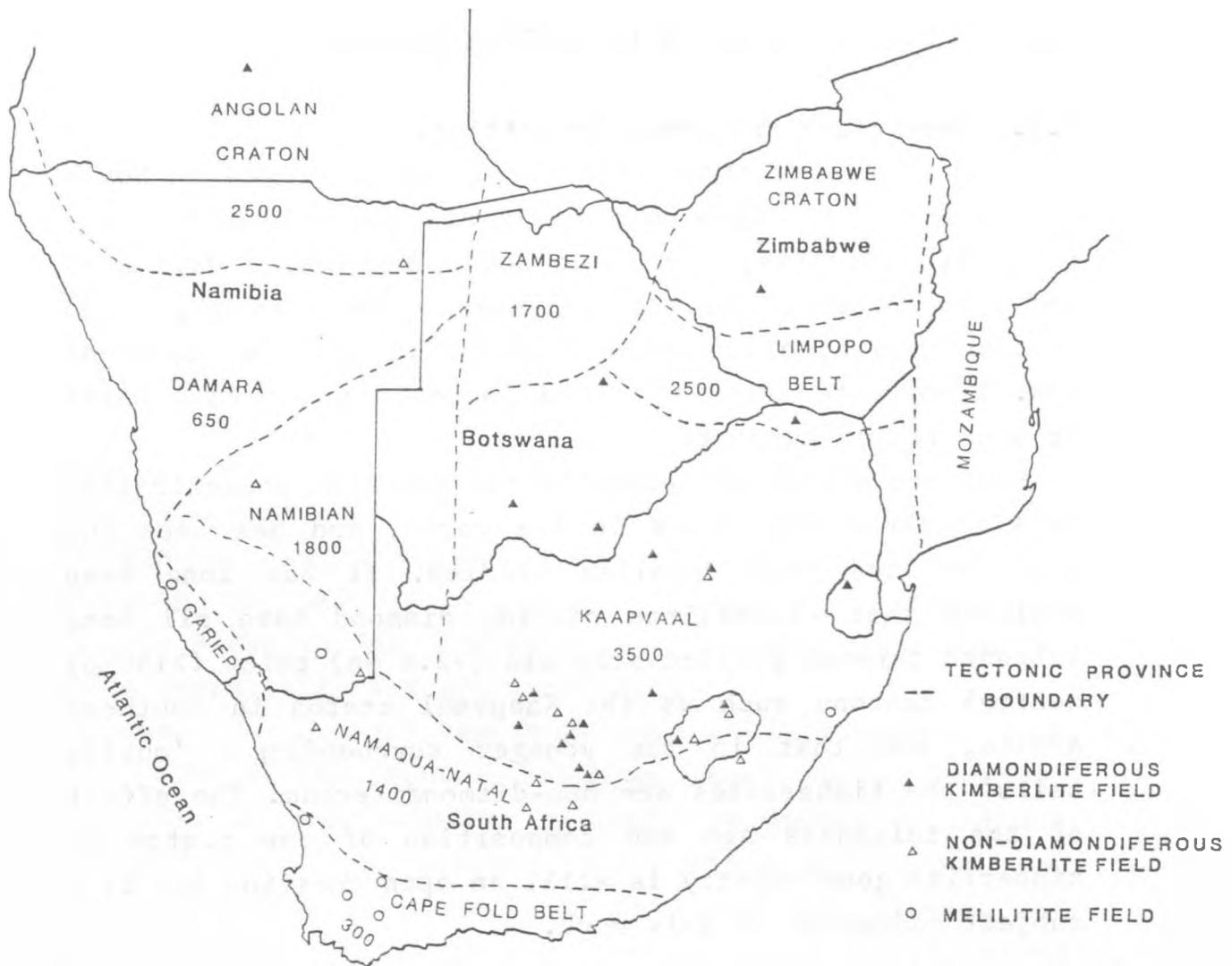


Fig 1.1: Map showing distribution of crustal province boundaries and the locations of diamondiferous kimberlite, after Tankard et al (1982) and Nixon (1987). Approximate ages of crustal provinces shown in Ma.

northeast to Eendekuil (114) in the southwest. From 114Ma to 70Ma a large number of group I kimberlites were intruded (including the Kimberley pipes at 90Ma) all over Southern Africa with no apparent chronological progression.

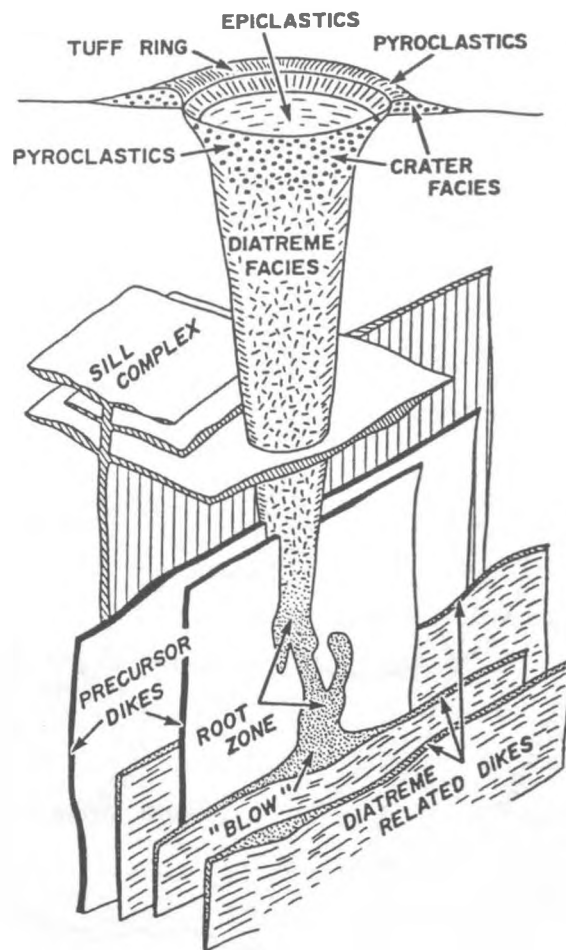


Fig 1.3: Schematic diagram of a kimberlite pipe showing sills, dykes, diatreme and crater. Not to scale. From Mitchell 1986.

trends. When the magma reaches the surface, devolatilization and explosive eruption occurs, followed by a slumping back of magma and fractured wallrock, forming the characteristic diatreme. The diatreme contains high percentages of crustal xenoliths together with

altered kimberlite magma, whereas dykes and sills may contain unaltered and uncontaminated magma.

In areas with a thick sedimentary cover, diatremes may be fully developed, whereas in areas of crystalline basement, kimberlites are usually restricted to dykes.

1.2.4 Textural and mineralogical variations

Clement and Skinner (1979) presented a textural-genetic classification together with a mineralogical classification (Skinner and Clement 1979) of kimberlite. Texturally the kimberlite pipe is divided into hypabyssal (dyke), diatreme and crater facies, with subdivisions based on the abundance of phenocrysts, xenocrysts and xenoliths. An understanding of the textural significance is crucial when selecting samples for geochemical analysis. It must be recognised that it is impossible to sample primary kimberlite magma, though restricting analysis to fresh hypabyssal material will yield the most meaningful data. Clement and Skinner's terminology is used throughout this work.

Skinner and Clement's (1979) mineralogical classification distinguishes kimberlite on the predominance of one or two of five major groundmass minerals: phlogopite, calcite, monticellite, serpentine or diopside. Olivine is ubiquitous, and though a necessary mineral to define kimberlite, is no aid to a subdividing classification. Other minerals present can include apatite, spinels, perovskite and ilmenite. Mitchell (1986) presents a comprehensive account of the range in mineralogy found in kimberlite.

Wagner (1914) recognised two petrographic types of kimberlite (basaltic and micaceous) which correlate to the group I and group II distinction now recognised by Smith (1983) on the basis of geochemical grounds. Skinner (1986) has summarised the petrographic differences. Group I

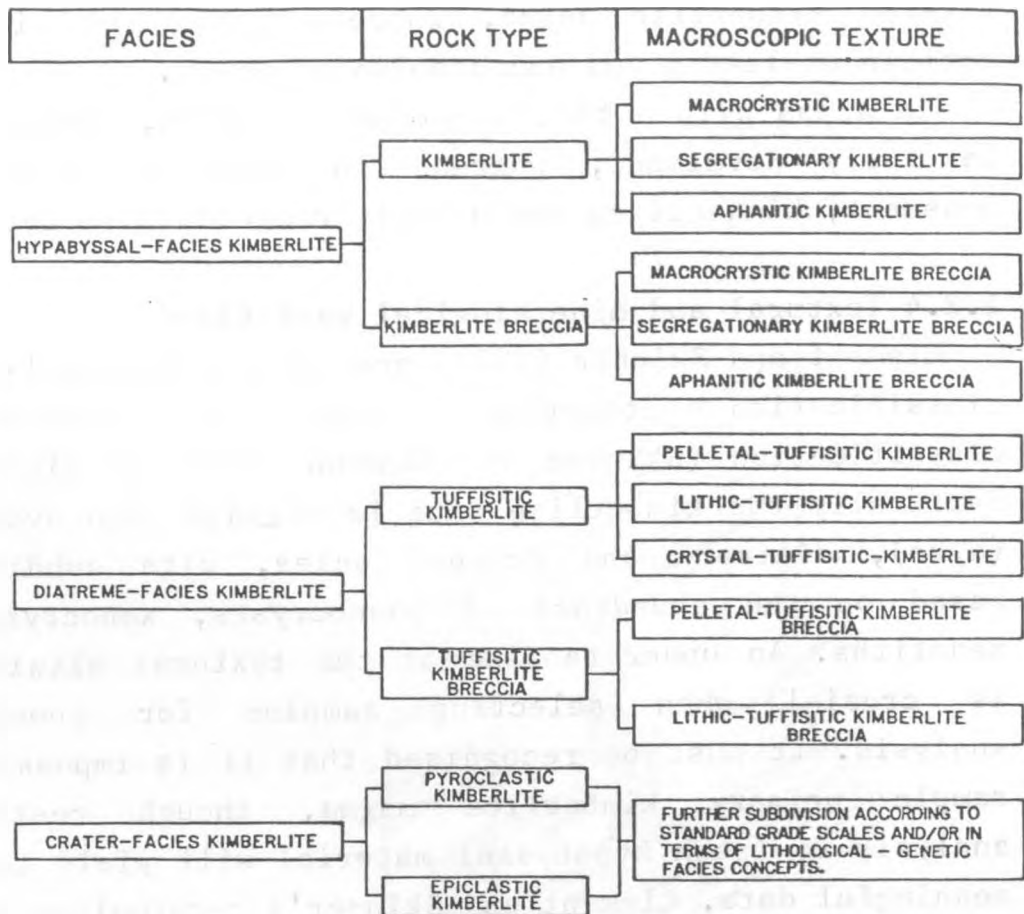


Fig 1.4: The textural classification of Clement and Skinner (1985).

kimberlites are dominated by olivine phenocrysts, whereas group II has olivine plus abundant phlogopite phenocrysts. Rutile inclusions are common in group I olivines, but are not found in group II. Group I kimberlites have abundant spinel or perovskite in the groundmass, whereas these are rare or absent in group II. Ilmenite may occur in group I but not group II kimberlites, and the reverse is true for diopside.

The lack of understanding of basic kimberlite petrology has resulted in misleading results from chemical studies. Fesq (1975) addressed the problem of crustal contamination and alteration due to weathering and showed the importance of careful sample selection. Clement (1982) introduced a contamination index (CI):

$$CI = \frac{(SiO_2 + Al_2O_3 + Na_2O)}{(MgO + 2K_2O)}$$

CI = 1 for non-contaminated rocks, and is greater than one when the kimberlite is contaminated by crust. This index can be used to identify crustal contamination by virtue of the high SiO₂ and Al₂O₃ usually found in crustal contaminants. A more elaborate filter based on trace element and isotope data is developed in this work.

1.2.5 Geochemistry

Severe problems impede the acquisition of meaningful geochemical data from kimberlites. Firstly there is the problem of alteration (weathering) and crustal contamination, which can be circumvented by careful sample selection. Secondly, the kimberlite magma includes mantle xenoliths and xenocrysts which cannot be separated from the sample, but do not however, always affect the trace element composition. Thirdly, there are few samples of glassy or aphyric parental kimberlite magma, so complex modelling as performed on basalts cannot be done.

Geochemical studies show that kimberlite is ultrabasic in nature, with MgO= 20-30%, SiO₂=25-35%, Al₂O₃=2-5%, FeO=2-10% and CaO=5-15%. The rock is highly alkaline with up to 1% Na₂O and 3.5% K₂O and has up to 10% volatiles (H₂O+CO₂). These compositions are highly variable as fractional crystallisation can greatly affect the magma

composition.

Kimberlites have particularly high concentrations of the incompatible trace elements Rb, Ba, K, U, Th, Sr, Nb, LREE etc, with abundances up to 1000 times chondritic values. The compatible trace elements, Sc, V, Cr, Co, Ni, Cu and Zn are also found in high concentrations relative to basalts.

The unusual combination of a very primitive ultrabasic magma with exceptionally high concentrations of incompatible trace elements must be explained in any petrogenetic theory and will be addressed in later chapters.

1.2.6 Radiogenic Isotope Studies

The use of radiogenic isotopes, coupled with trace element compositions has brought perhaps the greatest advances in the understanding of kimberlite petrogenesis in recent years. Smith (1983a,b), in an isotopic study of some 23 kimberlites from Southern Africa, showed that kimberlite can be divided into two distinct groups. Smith's group I and II kimberlites are roughly equivalent to Wagner and Dawson's basaltic and micaceous kimberlites. Smith et al. (1985) then showed that these two groups can be distinguished, though sometimes less clearly, on geochemical grounds. Because the two groups appeared to be quite distinct isotopically (see fig 1.5), with no intermediate members, it was deduced that the two groups had distinctly different sources. Smith concluded that group I kimberlites were derived from fertile asthenosphere, and group II kimberlites from trace element enriched subcontinental lithosphere. If this is correct, it implies fundamental differences in the processes involved in forming what are very similar rock types. However, a clear understanding of the petrogenesis of the two groups is still elusive.

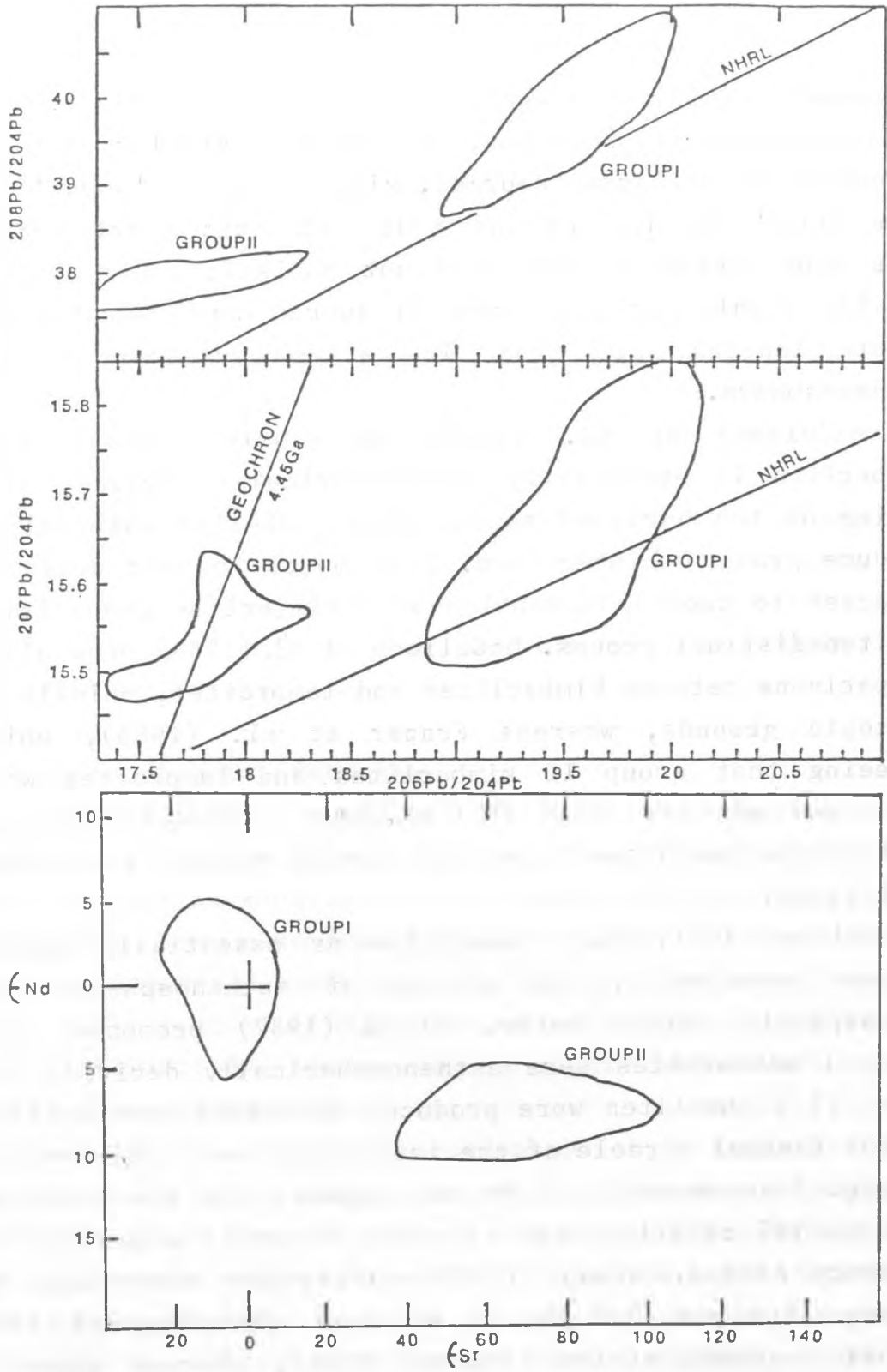


Fig 1.5: Sr, Nd and Pb isotope compositions of group I and group II kimberlites. After Smith 1983.

LeRoex (1987) suggests that both groups are asthenospherically derived, undergoing similar melting processes of different sources, similar to the 'Dupal' and 'non-Dupal' domains in the South Atlantic (Hart 1984). This explanation however does not satisfactorily explain how the highly enriched group II source could survive for great lengths of time in a convectively mixing asthenosphere.

McCulloch et al. (1983) conversely propose that kimberlite is essentially lithospherically derived, with mixing of the enriched source with MORB-like material to produce group I kimberlites. This model however would be expected to produce a continuum of kimberlite composition not two distinct groups. McCulloch et al (1983) drew close comparisons between kimberlites and lamproites, chiefly on isotopic grounds, whereas Frazer et al. (1985), while agreeing that group II kimberlites and lamproites were both derived from enriched lithosphere, showed important differences in the enrichment processes evident in the two rock types.

Nixon (1981) sees kimberlite as essentially hybrid magmas produced by the mixing of asthenospheric and lithospheric melts. Later, Nixon (1987) proposed that group I kimberlites were asthenospherically derived, and group II kimberlites were produced by lithosphere melting in the thermal aureole of the impinging group I kimberlite diapir. This appears not to be supported by the temporal and spatial relationships of group I and II magmatism in Southern Africa. Group II kimberlites are restricted to between 114 and 200 Ma in a rough chronological line across Southern Africa (Skinner 1986), whereas group I kimberlites are widespread in time and space.

Skinner (1986) suggested that both groups may be derived from the lithosphere by melting depleted or enriched domains. Thus the question of mantle source

regions has yet to be conclusively answered, and this work will address the problem.

It should be noted however, that as group II kimberlites have only (as yet) been described from South Africa, it may well be that they represent a special case, perhaps due to the elevated lithospheric temperatures evident at the time of their formation, which was contemporaneous with the Karoo volcanic episode and the breakup of Gondwana. Such possibilities are explored in chapter 7.

Richardson (1984) finally closed the debate on whether diamond is a xenocrystic or phenocrystic phase with his isotope work on silicate inclusions within diamonds, yielding ages up to 3.3 Ga compared to kimberlite intrusion ages of 90 Ma.

1.2.7 Experimental Petrology

Experimental work on the melting conditions of kimberlite has been relatively scarce because of the difficulties in running natural samples with volatiles and analysing the reaction products. There are, however, several important contributions from Olafsson and Eggler (1983), Brey et al (1983), Eggler and Wendlandt (1979) and Wyllie (1980,1987) which discuss conditions of melting in the kimberlite source.

In general there is consensus that kimberlite is generated by melting of a phlogopite-magnesite-garnet lherzolite in the range 35-50 kbar at 1000-1300°C. There are however, important differences in the proposed theories, partly derived from the uncertainty in determining dolomite and magnesite stability. This is important as the presence of these phases on the solidus buffers the amount of CO₂ present. CO₂ presence at melting appears to be critical in producing highly undersaturated (high Mg, low Si,Al,Ca) magmas by eutectic melting of a

carbonate-silicate system.

Experiments to determine the crystallisation conditions of kimberlite have also encountered difficulties because of the extremely complex phase relations, the problems of selecting a sample with a realistic parental magma composition and difficulties in analysing the experimental products. Kimberlite crystallisation is a non-equilibrium process with phlogopite olivine and spinel crystallising at early stages, and apatite, monticellite, calcite and serpentine crystallising in the groundmass

1.2.8 The Megacryst Suite

Megacrysts or 'discrete nodules' are large (>1cm) single crystals of olivine, diopside, orthopyroxene, garnet and ilmenite, which occur extensively in group I kimberlite (Nixon and Boyd 1973). Their origin is somewhat enigmatic. While it is clear that they represent the products of fractionation of magma at depths of 150-200 km over the temperature range of 1300-900°C, the nature of the parental magma is unknown.

Present debate centres on whether megacrysts are of phenocrystal origin, by crystallisation from a parental kimberlite magma, or of xenocrystal origin, merely incorporated into the kimberlite on eruption. Most studies has proved somewhat equivocal on this subject, as phase relations and distribution coefficients for the minerals involved are not well known for the pressures and temperatures in question.

Isotope systematics, however, are not affected by the high pressures and temperatures involved and hold out the best hope of resolving the problem. Few such studies have been undertaken because of the analytical problems involved, and those that have (eg Kramers 1981, Jones 1987), have not been decisive as detailed analysis of the megacrysts and host kimberlites have not been precise

enough.

Chapter 5 considers the problems involved in the megacryst question and uses Pb, Sr and Nd isotope data together with REE and trace element compositions to reach a more conclusive answer.

1.2.9 Xenoliths

Kimberlites are unique in the variety of mantle xenoliths they carry to the surface (Nixon 1987). Xenoliths provide us with direct samples of the deep mantle. Their study has revealed the ultrabasic and highly variable nature of the lithosphere and asthenosphere. Pressure and Temperature (P,T) studies (eg Boyd and Nixon 1975) have been used to construct geotherms and to constrain the depths of origin of kimberlite. The chemical compositions of mantle peridotites have been used to constrain the major element composition of possible source regions for mantle derived melts. Isotope studies (eg Hawkesworth et al 1984) have been used to decipher formation, depletion and enrichment events which have taken place in the lithosphere.

This work is not directly concerned with mantle xenoliths, but conclusions drawn from their study are invaluable in the understanding of kimberlite magmatism in particular and mantle evolution in general.

1.3 PROBLEMS IN KIMBERLITE GEOLOGY

Major questions still to be answered conclusively include:

- 1) Are kimberlites derived from the asthenosphere, lithosphere or both? Can we identify mantle source areas
- 2) Are group I and II kimberlites fundamentally different or are they end members of a continuum of processes? Do

group II kimberlites represent a special event in Southern Africa or are they the product of a more general process?

3) Can kimberlite and OIB type magmatism be related? What can kimberlites tell us about the Dupal anomaly?

4) Are kimberlite, melilitite and carbonatite related petrogenetically, forming under different P,T conditions from a similar source?

5) What effect does lithospheric age, thickness and history have on the chemical composition of kimberlite and melilitite?

6) Are megacrysts phenocrysts or xenocrysts?

1.4

AIMS OF THE PROJECT

This work aims to provide a detailed geochemical study of the Gibeon kimberlite province, and to answer a range of questions about kimberlite petrogenesis, as follows:

1) To geochemically define the Gibeon kimberlite province, in terms of characteristic chemistry both within and between separate intrusions, and to radiometrically date the kimberlites and to note geographic variations.

2) To compare the Gibeon kimberlites to other off-craton and on-craton (group Ia and Ib of Smith 1985) group I and II kimberlites, to note similarities and differences and to account for them.

3) To determine mantle source regions, in terms of asthenosphere/lithosphere and to compare them with the sources of other types of volcanism in the area (OIB, Karoo, melilitite).

4) To compare melting and fractionation between kimberlite and melilitite.

5) To examine the megacryst suite and determine any genetic links with kimberlite.

CHAPTER 2

INTRODUCTION TO NAMIBIA

2.1 REGIONAL GEOLOGY

Namibia's geology spans from the Early Proterozoic to the present, recording some long periods of stability, interspersed by major orogenic events. Though the rocks studied in this work represent events occurring in the last fraction of Namibia's history, it is useful to consider them in the context of the evolution of the subcontinent.

The geology of Southern Africa records periods of initial crustal formation (Archaean and Early Proterozoic), with successive orogenic additions building up to the supercontinent of Gondwana. After a long quiescent period, the Gondwanan supercontinent was broken apart amid the great volcanic episode of the Karoo. Africa remained as a stable continent into which the Jurassic and Cretaceous kimberlites were intruded.

Although kimberlites are derived from great depths in the mantle (>200km, Boyd and Nixon 1973, Boyd et al. 1985) their petrogenesis is significantly affected by the subcontinental lithosphere. The link between the Archaean Kaapvaal Craton and the presence of diamond has long been known (Kennedy 1966), suggesting that the evolution of the lithosphere may have some important consequences concerning the composition of the kimberlite that finally reaches the surface.

A detailed study of the evolution of Southern Africa is beyond the scope of this work, and the reader is referred to the comprehensive coverage presented by Tankard et al 1982.

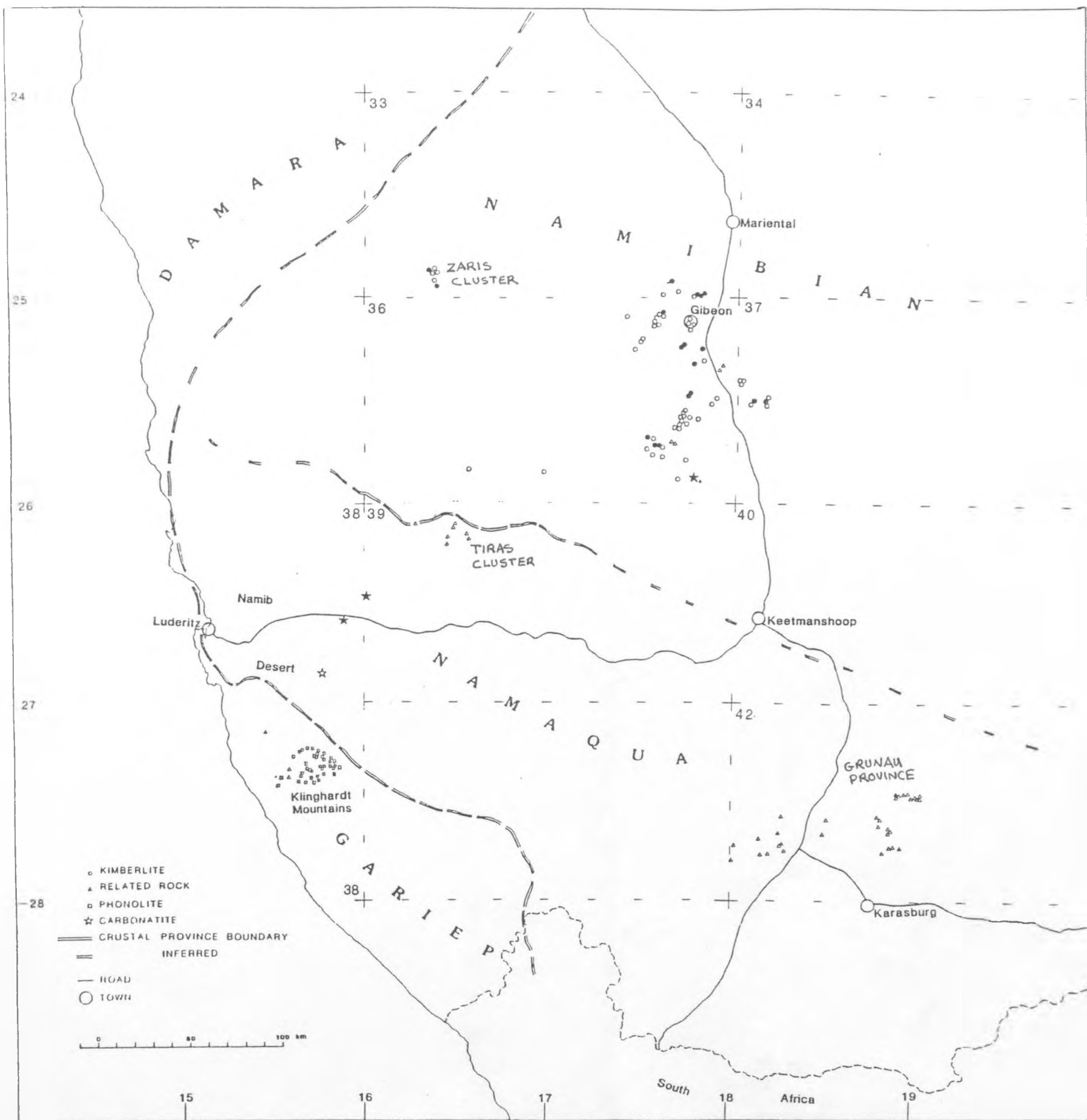
2.1.1 Crustal development

Namibia can be divided into several major tectonic units (fig 2.1). Each province was built through a number of crust forming events such that it is impossible to designate discrete ages on whole provinces.

In southern ^{Africa} the Archaean was a time of rapid crustal growth, relative to the Proterozoic, which was a time of crustal stabilization and sedimentation. This is a simplistic view as the Archaean-Proterozoic boundary is diachronous (1.7-3.0 Ga) if drawn at the time of cratonic stabilization. Tankard et al. (1982) take 2.5Ga as the Archaean-Proterozoic boundary.

The earliest known crust in southern Africa is the 3.55Ga Ancient Gneiss Complex on the eastern side of the Kaapvaal Province. The earliest evidence of cratonisation is the epicontinental Pongola Supergroup (3.0-2.8Ga). The Archaean crustal development saw the formation of the Kaapvaal, Limpopo and Zimbabwe provinces by 2.5 Ga. Crustal formation continued into the Early Proterozoic, with granite intrusions and regional metamorphism. The Early Proterozoic is characterised by large sedimentary sequences (eg the Witwatersrand Supergroup) which were deposited on the now stabilized cratons.

Figure 2.1. Map of Southern Namibia showing locations of kimberlites, associated alkaline rocks and crustal province boundaries. Filled symbols represent localities from which samples were analysed. Related rocks include nephelinite and melilitite



The Namibian Province, although unseen because of overlying sediments is a roughly triangular province bounded on the east by a north-south lineament defined on geophysical grounds, (Reeves 1976), to the southwest by a partially exposed boundary with the Namaqua province, and to the northwest by a well defined thrust zone in which the Damaran orogenic belt overthrusts the Namibian foreland. The Namibian province is believed to have been stable since at least 2.1 Ga (Tankard et al. 1982), forming a central continental block together with the Kaapvaal and Namaqua provinces which grew by orogenic additions at the margins. It is into the Namibian province that the kimberlites of this study were intruded.

Further crustal addition occurred between 1360 and 940 Ma as the Rehoboth Arc, a possible subduction-related magmatic belt of basic lavas and granitoid plutons, formed on the northern margin of the Namibian province. Further south the Sinclair group of volcanics added large lava piles between 1300 and 1000 Ma.

2.1.2 Proterozoic orogenic activity

After the long period of Early Proterozoic stability, the Mid Proterozoic was a time of major orogenic events. The Namaqua Natal mobile belt represents crust uplifted between 1.8 and 1.2 Ga (Tankard et al. 1982), stabilizing between 1.4 and 1.0 Ga (Hawkesworth et al. 1984).

In the late Proterozoic there were several major orogenic events caused by continental rifting and subsequent collision. Namibia was at the site of part of a triple junction which opened and subsequently closed between 1000 and 500 Ma respectively, forming the Damaran orogenic belt. Similar orogenies occurred in other parts

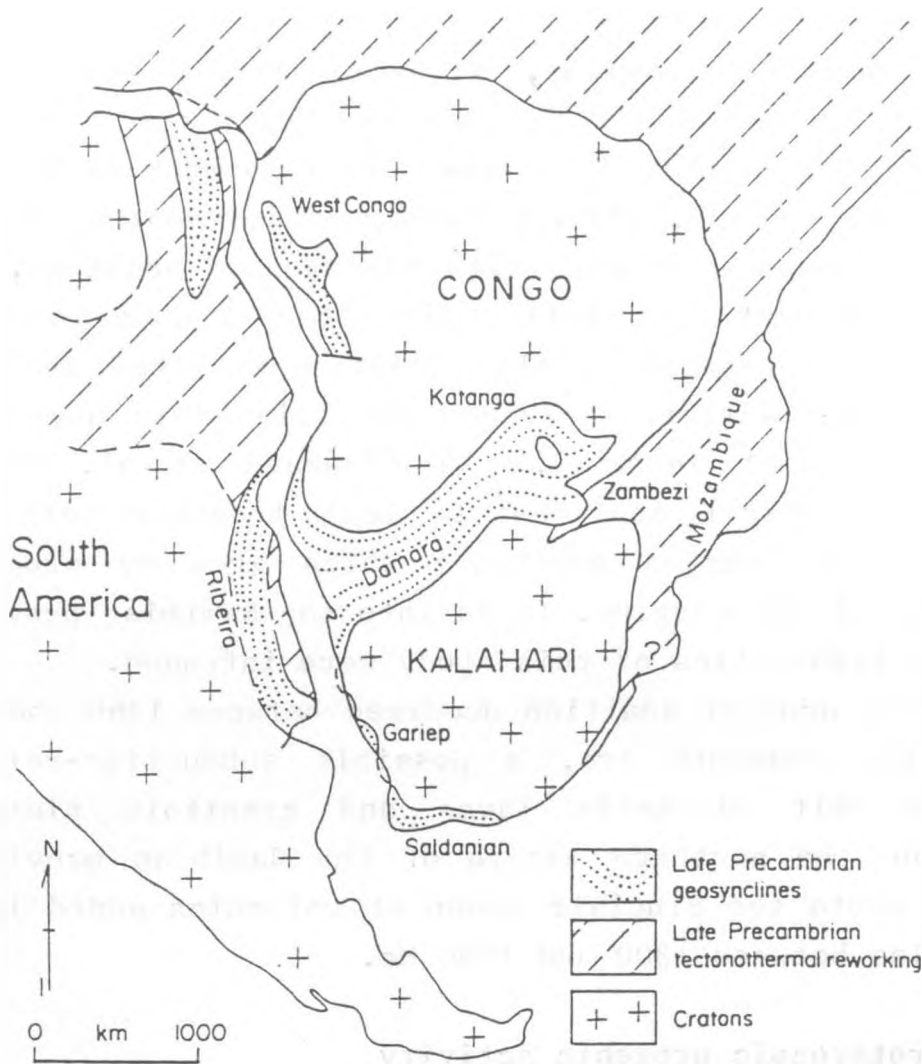


Figure 2.2. Late Precambrian structural framework of central and southern Africa and eastern South America, from Tankard et al. (1982)

of Africa, known widely as the 'Pan African' which was a major tectonothermal event affecting large parts of the continent.

Extension and rifting is first recorded (circa 1.0 Ga) by the accumulation of sediment in E-W trending grabens forming between the Namibian and Angolan provinces. Rifting then occurred along a N-S axis as 'South America'

broke free from Africa, forming a 'proto-Atlantic' ocean. Sediments and volcanoclastics filled the troughs being formed at 900 Ma ago. Full oceanic development occurred on the N-S trough, but the third (E-W) arm failed to develop fully into an oceanic basin. By 830 Ma, the oceanic basin to the west had developed and the continental margin was transgressed with widespread sedimentation.

The E-W (Damaran) zone of extension reverted to a compressional zone by 700 Ma, and limited crustal subduction occurred. The resultant orogenic belt (The Damara belt) formed between 700 and 500 Ma, producing an asymmetric orogenic belt as the southern (Kalahari, in fig 2.2) continent was partially subducted beneath the northern (Angolan) continent, producing large thrust zones.

Roughly synchronously (though precise ages are unknown) the oceanic basin to the west was closing, with deposition ceasing and orogeny beginning at around 550 Ma, producing the Gariep and Ribeira provinces, by subduction of the African plate beneath the South American. Strong easterly verging folds and thrusts developed in the Gariep province, while subduction related magmatism occurred in the Reibeira province of Brazil.

The Gondwana supercontinent was thus assembled. It is worth noting here that subduction has not occurred beneath the Namibian province since at least 1 Ga when the Rehoboth Arc magmatic event occurred.

2.1.3 Nama Sediments

The central area of Namibia (including that into which the Gibeon kimberlites are intruded) is covered with a thick sedimentary pile, collectively known as the Nama group which is a platform succession up to 2500m thick with a minimum age of 520 Ma. The lower Nama comprises a westward (seaward) thickening clastic and carbonate wedge, deposited unconformably over the Namibian province basement, in a shallow shelf to alluvial environment. Glaciogenic fluctuations of sea level and tectonic control of the Nama basin combined to control patterns of sedimentation. The upper Nama comprises alluvial, tidal flat and fan delta clastic sediments shed from the rising Damara mountain belt.

The Nama sediments have survived the Phanerozoic with almost no metamorphism or deformation, apart from small areas of thrusting around the basin edge, due to final stages of oceanic closure. The Gibeon kimberlites are intruded into almost flatlying sediments, dipping slightly eastwards. Nama xenoliths are common in the kimberlites. Limestone xenoliths are most common, but sandstone and shales are also found.

2.1.4 Karoo Sedimentation

As Gondwanaland drifted northwards during the Permo-Carboniferous, the climate changed from polar (as Africa was centred over the South Pole) to tropical. These changes were recorded in the thick pile of sediments deposited in the intracratonic basin in South Africa. The main depocentre was the Karoo trough in South Africa, with Namibia on the northern margin. In Namibia, the basal glaciogenic sediments of the Dwyka formation unconformably overlie the Nama group. The Gibeon kimberlite province extends into the western (basal) Karoo sediments, with

several intrusions emplaced into Dwyka tillite. Classic Kimberlite diatremes are best formed in sedimentary country rocks, whereas when the magma is emplaced into crystalline basement, the intrusions are usually dykes (DeBeers pers comm.).

2.1.5 Karoo volcanics

Karoo sedimentation was abruptly terminated in the Jurassic by the onset of the Karoo Volcanism, a vast outpouring of mainly basaltic lavas. These lavas were the first manifestations of the breakup of Gondwanaland (Eales 1984). A full account of Karoo volcanism is beyond the scope of this work, but the findings of the Karoo project (Erlank et al. 1984) are pertinent to any work dealing with magmatism in Southern Africa.

Erosional remnants of the Karoo lavas (covering 140 000 km²) are to be found scattered throughout Southern Africa, in Namibia, South Africa, Lesotho, Botswana, Zimbabwe, Zambia and Mozambique. The magmatic province also extends to South America in the Parana basin in Brazil (>1200 000 km²), and to Antarctica (>50 000 km²)(Eales et al 1984).

The lavas show evidence of igneous fractionation. Crustal contamination rarely greatly affects the composition of the lavas, though in some areas crustal anatexis has produced rhyolites and latites. Trace element compositions are variable both locally and between regions, due to variations in mantle source rocks (Erlank et al. 1984).

In Southern Africa, the Karoo basalts can be divided into three major types; Firstly a southern province of tholeiitic basalt which forms the bulk of the main phase of volcanism. This type is typified by the Lesotho formation, and can be found in Namibia near Mariental as the Kalkrand formation, (some 30km north of the Gibeon kimberlite

province) These basalts contain 6-8% MgO and 50-55% SiO₂ and appear to have evolved by the fractionation of olivine and pyroxene from a picritic parental magma (Cox 1983, Erlank et al. 1984) Fractionation has affected the abundances of compatible and incompatible trace elements, but it is clear that not all variations are a consequence of fractionation, leading Erlank et al (1984) to invoke variations in source regions. Crustal contamination is both localised and rare and plays little part in the petrogenesis of the basalts. Trace element abundances are elevated to greater concentrations than those found in MORB, and Nd and Sr isotope ratios are lower and higher respectively than those found in oceanic basalts. Elevated Rb/Sr and Nd/Sm ratios have produced the 'enriched' isotope characteristics over long periods of time (1-2 Ga).

The source region for these basalts is believed by Cox (1983) and Erlank et al (1984) to be MORB-like mantle enriched in K, Rb and Ba.

The second (northerly) province consists of more alkalic and generally evolved rocks of, for example, the Etendeka in Namibia, or the Nuanetsi in Zimbabwe. These lavas consist of basalts and dacites with markedly high and variable concentrations of the incompatible elements (K, Ti, P, Rb, Ba, Sr, Zr, Nb and LREE). The trace element variations cannot be modelled by fractionation or crustal contamination, and are due to variations in mantle source regions (Erlank et al 1984). The trace element enrichment is coupled with the high ⁸⁷Sr/⁸⁶Sr and low ¹⁴³Nd/¹⁴⁴Nd isotope ratios, indicative of long term mantle enrichment, which is of Proterozoic model age (1-2 Ga). This second province records greater enrichment than the main phase Lesotho type magmas.

In the Etendeka region, there are also some quartz latites which are the product of crustal anatexis. Similar

evolved rocks are found in Mozambique. It would appear that in the final stages of continental rifting, crustal thinning, uplift and magmatic intrusion occurs, which, supplies enough heat to melt the crust, whereas in central regions, anatexis is rare and localised (Erlank et al 1984, White and McKenzie 1988).

A third magma type is found in coastal Namibia as the Horingbaai dolerites. These dykes are of olivine normative MORB like basaltic composition, and are believed to represent the final stages of continental magmatism before the opening of the Atlantic Ocean.

The age relationships of the Karoo show that magmatism first started in the lower Jurassic, when the main phase of volcanism produced the widespread Lesotho magma type. There was then sporadic activity throughout the Jurassic, and finally a major pulse as the Etendeka was extruded in the lower Cretaceous. The MORB like dyke intrusions represented the end of the Karoo episode. The main phase of basaltic magmatism can be seen to predate rifting, whereas the Etendeka is roughly synchronous with the opening of the Atlantic.

White and MacKenzie 1988, using geophysical reasoning, proposed that continental flood basalts are derived from the melting of asthenosphere during continental rifting in the vicinity of a hotspot. They do not, however, offer an explanation of the 'continental' characteristics of their geochemistry.

The effects of the Karoo episode on the lithosphere are obviously an important part of its evolution. The effects of melting the lithosphere would be to deplete it in incompatible trace elements, and leave behind a refractory, trace element depleted lithosphere. Addition of asthenospherically derived melts could cause the opposite effect - metasomatising the lithosphere.

2.1.6 Alkali Complexes

There are several alkaline igneous complexes in coastal Africa (Luderitz, Damara, and Angola) and South America (Uruguay and Brazil) comprising multiple intrusions of silica saturated and undersaturated lavas. These complexes form along distinct lineaments (Marsh 1973), extending inland from the coast. These lineaments have been related by Marsh (1973) to transform faults and fracture zones in the Atlantic Ocean. The alkaline complex near Luderitz (Marsh 1975a,b,c) has been dated at 130Ma, coincident with the opening of the South Atlantic. The Angolan and Brazilian complexes are of similar ages, but are later reactivated at 51-83Ma. The transform faults and alkaline provinces are found to lie on small circles with the same poles of rotation as the Atlantic Ocean. The Luderitz complex lies on the same small circle as the Uruguay complex (120Ma). Thus Marsh concludes that these alkaline provinces are continental expressions of transform faults initiated during continental fragmentation. Reactivation of the Brazilian and Angolan complexes are associated with tensions caused during a shift in the pole of rotation of the Atlantic Ocean.

The alkaline complexes are not related to kimberlite or other 'hotspot' type magmatism.

2.1.7 Post Rifting

Subsequent to the formation of the Atlantic Ocean, Namibia has remained tectonically stable, as part of Southern Africa. Minor alkali volcanism occurred, of which the Gibeon kimberlites represent the majority. Minor sedimentation occurred in coastal areas and inland basins.

Very little published geophysical data is available from Namibia. However, heat flow and teleseismic data have been used to assess relative lithospheric thickness. Jones (1981,1987) using heat flow measurements from the Kaapvaal Craton and Namaqua belt found that (after compensating for heat production in the crust) there is a lower heat flow from the mantle, through the Kaapvaal craton, than through the Namaqua mobile belt to the west. Jones inferred that the lithospheric thickness of the Kaapvaal craton is greater than that of the surrounding mobile belts, a conclusion supported by geothermometry studies of kimberlite-borne mantle nodules by Boyd and Gurney (1986).

Combined gravity and teleseismic studies (Fairhead and Reeves 1977, and Fairhead pers comm.) also indicate that there is a decrease in lithospheric thickness away from the Kaapvaal craton, westwards across Namibia. Together, these studies show that the Gibeon kimberlites were intruded through thinner lithosphere than the 'on craton' kimberlites. Lithospheric thickness is widely believed (Nixon 1987 and refs therein) to be a controlling factor influencing the presence of diamond in on-craton kimberlites and their absence in off-craton kimberlites.

Southern Namibia comprises the central Nama plateau, bounded to the East by the Kalahari basin, and to the West by the Namib desert. The main subject of this study is the Gibeon kimberlite province, located between 25° and 26° S and $17^{\circ} 30'$ and $18^{\circ} 30'$ E, in an area some 100 by 80 km. This province is part of an arid upland plain, on the Nama Plateau. At about 100km to the NW and SW of the Gibeon province, are two smaller subclusters of kimberlites referred to here as the Zaris and Tiras clusters respectively. Some 30km north of the Gibeon kimberlite province the basaltic lavas of the Kalkrand formation outcrop (8000km^2) as the erosional remnant of the once more extensive Karoo.

To the southeast between $27^{\circ}30'$ and 28° S and 18° and 19° E, is the Grunau melilitite province, in a hilly area of granitic intrusions. These rocks are thought to be some 500Ma old (DeBeers pers comm.) and not related to the Gibeon kimberlites (see chapter 7).

In the Namib desert, 35km inland from the coast at $27^{\circ}10'S$, $15^{\circ}40'E$, outcrop a range of small hills, consisting of phonolite plugs and domes (Lock and Marsh (1981)).

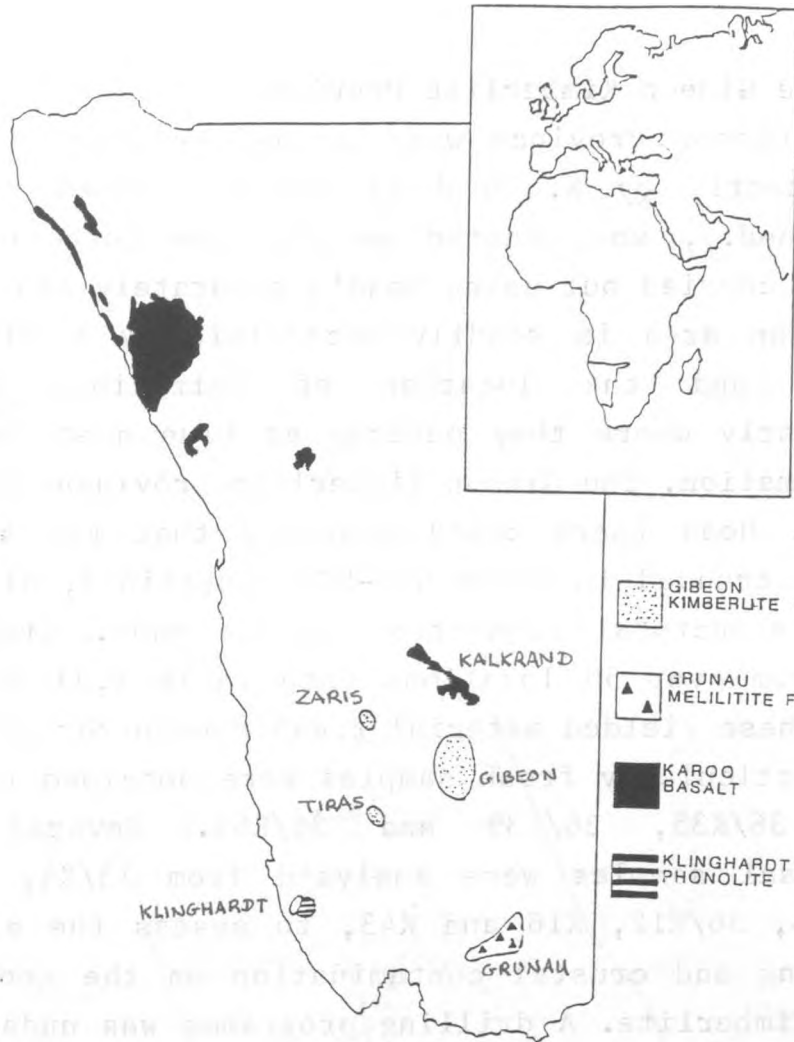


Figure 2.3. Volcanic Provinces in Namibia, showing extent of Etendeka basalts, and locations of kimberlites and associated rocks studied in this work.

Nearby, several pipes of kimberlite like rocks have been located (CDM pers comm.). These represent the most South-westerly occurrences of kimberlite related rocks.

On the broadest scale it can be seen that there is a general NE-SW lineament of kimberlites and related rocks.

2.3.1 The Gibeon Kimberlite Province

The Gibeon Province was mapped by Janse (1964) and more recently by N. Hoad of CDM Ltd (Hoad pers comm, unpublished.), who located several new intrusions. This work was carried out using Hoad's accurately plotted maps. The Gibeon area is readily accessible by 4 wheel drive vehicle, and the location of intrusions is easy, particularly where they outcrop as blue dust in the red Nama Formation. The Gibeon kimberlite province is shown in fig 2.4. Hoad (pers comm) observed that the kimberlite outcrops trended in vague NNE-SSW lineations, although no obvious structural connection can be made. Samples were taken from over 50 locations (see table 2.3) but only a few of these yielded material fresh enough for geochemical work. Particularly fresh samples were obtained from pipes 33/K2, 36/K35, 36/K39 and 36/K53. Several altered hyperbyssal samples were analysed from 33/K4, K5, K12, K13, K14, 36/K12, K16 and K43, to assess the effects of weathering and crustal contamination on the geochemistry of the kimberlite. A drilling programme was undertaken by C.D.M. ltd to provide core samples of the kimberlites. The drilling programme was biased towards the larger intrusions, which are often diatreme facies pipes, whereas the (hyperbyssal facies) dykes were less frequently drilled.

All kimberlite samples were taken from drillcore. A drilling programme was initiated for this project, and samples were obtained by the author from the recovered core which was stored by CDM Ltd. The drilling project was abandoned prematurely due to political/economic reasons in Namibia, hence many intrusions which were due to be sampled were not drilled.

GIBEON KIMBERLITE PROVINCE

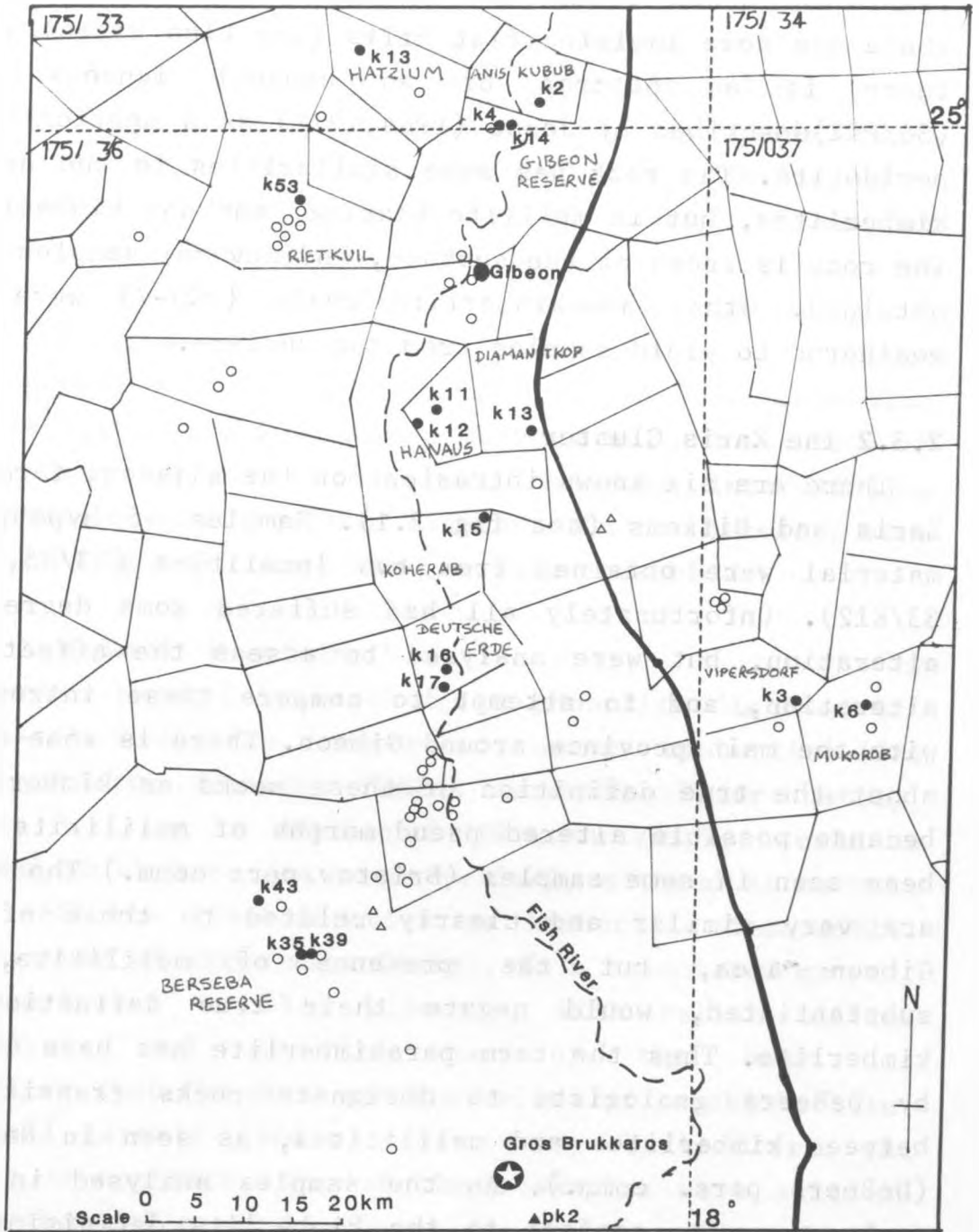


Figure 2.4. The Gibeon kimberlite province. Symbols as in Fig 2.1.

Within the Gibeon province, there are several intrusions which are not kimberlite. On the south-eastern flanks of Gross Brukkaros, an eroded volcanic complex, there are some lowlying flat hills (The Blue Hills) where there is an outcrop of an unusual igneous rock (36/PK2) described by Janse (1964,1971) as a monticellite-peridotite. The rock has some similarities to the nearby kimberlites, but is melilitite bearing, and not kimberlite. The rock is fresh at the surface, and several samples were obtained. Other non-kimberlite rocks (PK3-7) were too weathered to yield samples from the surface.

2.3.2 The Zaris Cluster

There are six known intrusions on the adjacent farms of Zaris and Uitkoms (see fig 2.1). Samples of hypabyssal material were obtained from two localities (33/K5, and 33/K12). Unfortunately all had suffered some degree of alteration, but were analysed to assess the affects of alteration, and to attempt to compare these intrusions with the main province around Gibeon. There is some doubt about the true definition of these rocks as kimberlites because possible altered pseudomorphs of melilitite have been seen in some samples (Bristow pers comm.) The rocks are very similar and clearly related to those of the Gibeon area, but the presence of melilitite, if substantiated, would negate their true definition as kimberlite. Thus the term parakimberlite has been coined by DeBeers geologists to designate rocks transitional between kimberlites and melilitites, as seen in Namibia (DeBeers pers. comm.). As the samples analysed in this work appear to conform to the kimberlite definition (of Clement and Skinner 1984) they are called kimberlites here.

2.3.3 The Tiras Cluster

The Tiras cluster (see fig 2.1) comprises some 11 intrusions on the farms Tiras, Excelsior, Mario, Numis, Barby, Conradie and Awas Sud. The cluster is more extensive in area than the Zaris cluster, and includes some rocks that are possibly parakimberlites (the chemistry of their indicator minerals is transitional between those of kimberlite and melilitite, McGurl pers comm.) Despite drilling to more than 100m, all samples obtained from this area were so pervasively altered as to make them totally unsuitable for geochemical analysis.

These rocks were considered important because 1) they could reveal the nature of the transition from kimberlite to melilitite, and 2) because they lie in the middle of the 'Gibeon-Luderitz lineament', intruded into Namaqua belt basement, not Namibian basement. It is therefore very disappointing that these samples were unusable.

2.3.4 Klinghardt Mountains

Located several km west of the phonolite field of the Klinghardt mountains, there are seven kimberlite-like pipes yielding diatreme facies material. Unfortunately, despite drilling to depths of 100m, no samples could be obtained which were not so pervasively altered as to make their definite identification as kimberlite impossible. The presence of large mica flakes, in a brecciated matrix, now decomposed to clay minerals, with relict olivine macrocrysts, and the pipe shape of the body was indicative that the rock was kimberlite or parakimberlite.

Small garnets and pyroxenes were obtained from the surface concentrate. None of these samples were suitable for geochemical analysis.

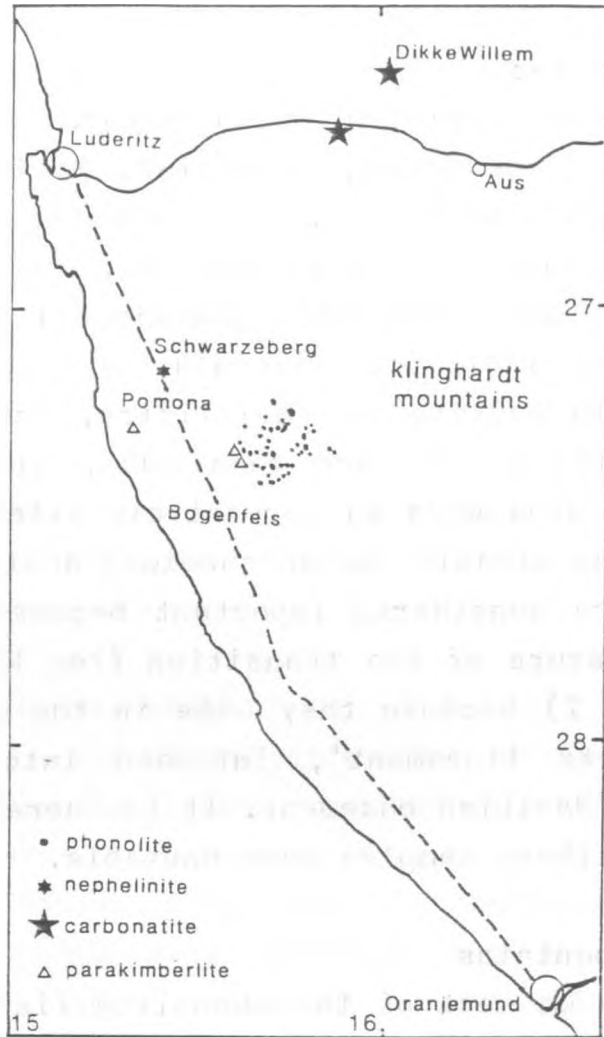


Figure 2.5. Map of the Luderitz area showing Schwarzeberg and Dikke Willem.

However, at Schwarzeberg ($27^{\circ}17'S$, $15^{\circ}25'E$), some 50km south of Kolmanskop, on the road from Luderitz to Oranjemund, there is a large nephelinite dyke, outcropping as a ridge 50m high, and several hundred metres long. Several very fresh samples were taken from this dyke. Other, smaller, nephelinite sills in the region were found but were also heavily weathered. Thus this dyke provided

the only fresh material from the southwest end of the 'Luderitz-Gibeon lineament' and there is no obvious relation between the kimberlites and the nephelinite.

2.3.5 Carbonatites

Several carbonatite samples were obtained from different localities:

1) Gross Brukkaros. (fig 2.4, Janse 1964, 1969) At the southern side of this large volcanic feature there are several small carbonatite plugs, with some small sills. The plugs were, in general, highly brecciated, but the sills provided relatively fresh carbonatite.

2) Dikke Willem. (fig 2.5, Wervoerd 1967) This large volcanic feature, 2km in diameter and several hundred metres high, consists entirely of carbonatite. Many different intrusions are evident, with a central core surrounded by an outer ring of breccia. Later dykes cross cut the intrusions. Igneous layering is evident in some parts, with magnetite/calcite bands. Several samples were taken from different parts of the intrusion.

3) Garub. A smaller carbonatite dome occurs to the south of Dikke Willem, a few hundred metres south of the Aus-Luderitz road, 12km west of the Garub railway stop. It, like Dikke Willem, has a central core, surrounded by a brecciated margin, with later cross-cutting dykes. Several samples were obtained.

2.3.6 Grunau Melilitites

The Grunau melilitite province (fig 2.1) covers an area of 120 x 50 km, and includes some 78 known occurrences, mostly dykes, of which 23 were sampled. These rocks were sampled to confirm the suspected 500Ma age of these rocks, to disassociate them from the Gibeon kimberlites, and also to compare their mantle sources with that of the later kimberlites. The melilitites commonly contained abundant

crustal xenoliths which are often streaked out and recrystallised. This evidence of crustal anatexis indicates that these magmas were intruded into the crust at higher temperatures than the kimberlites. Calcite alteration was usually pervasive. Some samples had large fresh micas, which were used for radiometric dating. Several samples were analysed, but as alteration was obvious, the analytical results are treated with caution.

2.3.7 Megacrysts

Megacryst samples were obtained from surface concentrations at most kimberlite localities, but only a few were large and fresh enough to yield material suitable for isotope analysis (see chapter 5). Other megacrysts analysed in this work were supplied by R. Mitchell and J. Gurney.

The DeBeers international system for numbering localities is used in this thesis. This system uniquely designates each recorded kimberlite/parakimberlite locality with a number for ease of reference. It was decided to use this system as it is becoming increasingly used by kimberlite geologists, and is very convenient to use. A typical number used would be as follows:

175/36/K39

175 represents Namibia, thus all samples used in this work start with 175. (the 175 is generally omitted for convenience in this thesis)

36 represents map sheet number 36 (of 42), see fig 2.1

K39 represents kimberlite intrusion number 39, as designated by DeBeers. (PK represents a parakimberlite).

These locality numbers were further suffixed by the author to aid sample numbering. Thus W represents a sample collected from the Windhoek core store, otherwise the sample was collected at the Kimberley core store. Final suffixes of M and X are used for analysed samples to record that the sample had minimal (M), or visible (X) crustal xenoliths.

This system has proved to be very convenient for data storage and referencing.

Careful sample selection is of the utmost importance when collecting kimberlite for geochemical analysis. The dual problems of crustal contamination (xenoliths) and secondary alteration (weathering) are particularly common in kimberlite. The vulnerability of kimberlite to alteration is so extreme that the only way to get fresh material is from underground mine workings, or from drill cores. The effects of alteration and contamination on whole rock geochemistry are discussed later (chapter 3), and by Smith (1983), Mitchell (1986), Clement (1982) and Fesq (1975). Good samples were selected by the use of several eliminating criteria:

1) Facies. The first criteria is that the sample is a hyperbyssal facies kimberlite. Diatreme facies materials must be discarded as they are not representative samples of kimberlite magma. An easy distinguishing criterion in the field is that the crustal xenoliths in hyperbyssal kimberlite have baked margins, whereas they do not in tuffisitic kimberlite breccia (TKB). There is also a fairly obvious brecciation in TKB, not evident in hyperbyssal kimberlite.

2) Freshness. The sample must look fresh in hand specimen, with glassy olivines and a dark matrix. Calcite veins, or a pale grey matrix, are obvious signs of alteration.

3) Xenoliths. Preferably there should be no xenoliths at all, but such samples are rare. Samples with >10% crustal or mantle xenoliths were rejected. It is shown in Chapter 3 and 4 that a small amount of crustal contamination has little effect on the trace element content of the rock. If present, xenocrysts cannot be

avoided. Garnet and pyroxene are easily recognised, but are not always abundant. Olivine xenocrysts are unavoidable. These xenocrysts have low abundances of trace elements, so tend to dilute trace element concentrations in the kimberlite sample.

4) If the rock passes these criteria, a thin section examination is necessary. Alteration can take several forms, replacing the kimberlite with calcite, chlorite, clay minerals, serpentine or silica. It is possible for kimberlite to be serpentinised by deuteric alteration on eruption, without affecting the bulk rock composition. Such rocks are suitable for analysis, and can be recognised by the texture of the serpentine and freshness of the groundmass, as in general it is only the olivines that suffer deuteric serpentinisation. Where secondary serpentinisation can be recognised overprinting the original rock texture the samples were rejected. Primary calcite forms blocky grains in the matrix, whereas secondary calcite is fine grained, forming in patches, overprinting the original texture, and often accompanied by veins. If secondary mineralisation is identified in thin section, the rock was considered unsuitable for geochemical analysis.

Table 2.1 : Sample Summary

locality	sample type	facies	preservation state	micas	geochemical analysis
33/K1	drill	TKB			
33/K2	drill	HYP	fresh	*	*
33/K4	drill	HYP	clay alt.		*
33/K5	surface	HYP	calcite alt.		*
33/K6	surface	TKB			
33/K7	surface	TKB			
33/K11	surface	TKB			
33/K12	drill	HYP	chlorite alt		*
33/K13	drill	HYP	calcite alt.		*
33/K14	drill	HYP	chlorite alt.	*	*
33/K15	drill	TKB			
36/K1	drill	TKB			
36/K2	surface	HYP	clay alt.		
36/K3	drill	HYP	serp. alt.		
36/K4	drill	SEG	chlorite alt		
36/K5	drill	TKB			
36/K6	drill	TKB			
36/K7	drill	SEG	calcite alt.		
36/K8	drill	TKB			
36/K9	drill	TKB			
36/K10	drill	TKB			
36/K11	surface	HYP	clay/calcite.		
36/K12	drill	HYP	clay/calcite		*
36/K16	drill	HYP	clay alt		*
36/K17	drill	TKB			
36/K18	drill	TKB			
36/K22	surface	HYP	calcite alt.		
36/K23	surface	HYP	calcite alt.		
36/K24	surface	HYP	calcite alt.		
36/K25	surface	HYP	calcite alt.		
36/K26	surface	HYP	calcite alt.		
36/K27	surface	HYP	calcite alt.		
36/K28	surface	HYP	calcite alt.		
36/K29	drill	TKB			
36/K30	surface	HYP	calcite alt.		
36/K33	drill	SEG	clay/calcite		
36/K34	drill	TKB			
36/K35	drill	HYP	fresh		*
36/K36	drill	TKB			

locality	sample type	facies	preservation state	mica	geochemical analysis
36/K38	drill	TKB			
36/K39	drill	HYP	fresh	*	*
36/K40	drill	TKB			
36/K41	drill	TKB			
36/K42	drill	TKB			
36/K43	drill	HYP	chlorite alt.	*	*
36/K47	surface	HYP	chlorite alt.		
36/K52	surface	HYP	chlorite alt.		
36/K53	drill	HYP	fresh		*
36/PK2	surface	HYP	fresh		*
36/PK7	surface	HYP	calcite alt.		
37/K1	drill	TKB			
37/K3	surface	TKB			
37/K5	drill	TKB			
37/K7	surface	HYP	calcite alt.		
37/K9	surface	HYP	calcite alt.		
38/PK1	drill	TKB			
42/PK3	surface	crater			
42/PK6	surface	crater			
42/PK13	surface	crater			
42/PK14	surface	HYP	clay alt.		
42/PK24	surface	HYP	calcite alt.		
42/PK25	surface	HYP	calcite alt.		
42/PK26	surface	HYP	calcite alt.		
42/PK28	surface	HYP	calcite alt.		
42/PK30	surface	HYP	calcite alt.		
42/PK32	surface	HYP	calcite alt.		
42/PK33	surface	HYP	calcite alt.		
42/PK34	surface	HYP	calcite alt.		
42/PK36	surface	HYP	calcite alt.		
42/PK48	surface	HYP	calcite alt.		*
42/PK55	surface	HYP	calcite alt.		*
42/PK56	surface	HYP	calcite alt.		
42/PK57	surface	HYP	calcite alt.		
42/PK61	surface	HYP	calcite alt.	*	
42/PK62	surface	HYP	calcite alt.	*	*
42/PK65	surface	HYP	calcite alt.		
42/PK66	surface	HYP	calcite alt.		
42/PK70	surface	HYP	calcite alt.		
42/PK72	surface	HYP	calcite alt.		

HYP=hypabyssal, TKB=tuffisitic kimberlite breccia, SEG=segregational, alt=alteration.

2.6.1 Previous work

Few Namibian kimberlites and parakimberlites have been dated, but previous attempts suggest ages of around 65Ma for the Gibeon kimberlites, and rather younger ages for the intrusions in the Klinghardt Mountains. Much older ages are suspected for the Grunau melilitite province (DeBeers pers. comm.).

Rb/Sr-mica dates were obtained using a technique developed by H. Allsopp, and described in appendix 1 and by Smith 1983, Smith et al 1985. The technique is based on the fact that kimberlites often have two or more generations of phlogopite, which, although in isotopic equilibrium at the time of kimberlite emplacement, have different Rb/Sr ratios, which lead, in time, to different $^{87}\text{Sr}/^{86}\text{Sr}$ ratios. The phlogopites are separated from the rock sample by crushing, and sieved to obtain different size fractions. The different size fractions represent different generations of phlogopite which can in practise (despite possible mixing) be treated as different minerals. Together with a whole rock sample, the phlogopite fractions are used to obtain an isochron. Good isochrons have been produced on rather poor samples affected by alteration or containing inclusions, but this is not always the case. This technique has been used successfully (Smith et al 1985, Bristow et al. 1986) to date several pipes, and is used in this work.

Table 2.2 : Previous work, age determinations (Ma)

Location	Age	method	worker
175/36/K16 Deutsche Erde	66.5+/-0.3	U/Pb zircon	Davis *
175/37/K5 Mukarob	61 +/-1	U/Pb zircon	Davis *
175/33/K5 Zaris	55 +/-5	Rb/Sr mica	Hunziker *
175/33/K6 Uitkomst	59 +/-4	Rb/Sr mica	Bristow *
Klinghardt Phonolite	37.5	K/Ar	Kroner 1973
Schwarzeberg nephelinite	35	K/Ar	Kroner 1973
Grunau melilitite, Garub	500	K/Ar	Kroner 1973
Gross Brukkaros Carb.	145 +/-5	K/Ar	D.C. Rex +

* = unpublished work, DeBeers internal report, pers. comm.
 + = unpublished work, P.H. Nixon pers comm.

The above two dates obtained by Bristow and Hunziker are in accordance with the regional geology (Janse 1964), but must not be taken as accurate age determinations (Bristow pers comm.) because:

- 1) The age is derived from a two point isochron.
- 2) The phlogopite fractions obtained were very poor (ie were altered around the edges and along lattice planes).
- 3) The lower end of the isochron could not be constrained accurately, as the whole-rock sample was affected by calcite alteration (see chapter 3). Instead, an estimate of the pre-alteration whole rock was made, based on typical group I kimberlites.
- 4) The isotope analyses were not of good precision.

The zircon technique has been used successfully (Davis 1976,1977,1978) to date zircons in kimberlites. However, there are problems with this method, which stem from the very low (<10ppm) U concentrations (and therefore low Pb concentrations) in kimberlitic zircons. Zircon is a very rare mineral in kimberlite, it is not, therefore easy to obtain large amounts of sample material. Because of small samples and low U concentrations, it is necessary to have very low analytical blanks, and very precise isotope analyses, especially for young zircons. $^{235}\text{U}/^{207}\text{Pb}$ ages are unreliable as a correction for any common ^{207}Pb in the sample (inclusions or cracks) must be made. This is less of a problem for $^{238}\text{U}/^{206}\text{Pb}$ ages as the ^{206}Pb correction is smaller, therefore ^{206}Pb ages have in general been regarded as more reliable, though Pb loss may affect the ages. Davis's Pb data is unavailable for comment, though his published data are generally regarded as accurate (Bristow et al 1986).

In the light of these problems it was decided that the Rb/Sr mica technique offered the best prospects of dating the kimberlites.

2.6.2 Radiometric dating, this work.

Where possible, attempts were made to date the kimberlites using the Rb/Sr mica technique. In some instances this was difficult as only one generation of rather poor quality mica was present. The relatively anhydrous parakimberlites and melilitites were dated by D.C. Rex using the standard K/Ar technique of Briden et al. (1979), and two samples with abundant micas were dated, again by D.C. Rex, using the $^{39}\text{Ar}/^{40}\text{Ar}$ step heating technique of Parsons et al. (1988).

Table 2.3 : Age determinations (Ma)

175/33/K2	Anis Kubub	75.9	+/- 1	Rb/Sr mica
175/33/K14	Gibeon Res. 3	73	+/- 8	Rb/Sr mica
175/36/K39	Berseba Res. 6	77.9	+/- 6.0	Rb/Sr mica
175/36/K43	Berseba Res. 10	72	+/- 4	Rb/Sr mica
175/36/PK2	Blue Hills	116	+/- 4	K/Ar
A44	Schwarzeberg	29	+/- 1	K/Ar
A45	Schwarzeberg	29	+/- 1	K/Ar
A73	Schwarzeberg	31	+/- 1	K/Ar
A74	Schwarzeberg	29	+/- 1	K/Ar
175/40/PK48		317	+/- 12	K/Ar *
175/40/PK55		392	+/- 12	K/Ar *
175/40/PK62		458	+/- 14	K/Ar *
175/40/PK61		524	+/- 0.8	$^{39}\text{Ar}/^{40}\text{Ar}$
175/40/PK62		514	+/- 0.8	$^{39}\text{Ar}/^{40}\text{Ar}$

* minimum age

2.6.3 Discussion of results

Rb/Sr mica technique.

Several practical difficulties arose which made it difficult to obtain radiometric dates from the Gibeon kimberlites:

1) Low abundance of phlogopite in the rock. The Gibeon kimberlites, in general, have rather low abundances of phlogopite. Only four kimberlites yielded enough fresh phlogopite from the available samples to obtain isotope analyses.

2) Poor quality of phlogopite. Most phlogopite grains separated were either altered around the rims, contained inclusions (titanomagnetite), or had calcite forming in

cracks. Leaching dissolves extraneous calcite, but altered grains do not yield good isochrons (Smith pers. comm.).

3) Only one generation of phlogopite. The technique depends upon the presence of several generations of phlogopite, to give a spread in Rb/Sr ratios. If there is only one generation (eg groundmass), only a two point isochron (whole-rock and phlogopite) can be obtained.

As a result of these problems, the analyses effectively gave two point isochrons, which do not yield precise ages. However, because of the consistency of the ages derived, a reasonable indication of the age of the Gibeon province can be inferred, although the data are not precise enough to reveal geochronological variations within the province.

Each case is considered separately:

36/K39 is a very fresh rock, with fairly sparse but large macrocrystal phlogopite. The grains are kinked, sometimes with altered rims, but are generally fresh. Phlogopite xenocrysts have been shown to equilibrate with kimberlite magma (Allsopp and Barrett 1975, Smith et al 1985). The groundmass contains rare fine grained, colourless phlogopite. Two phlogopite separates were obtained, coarse (+60 mesh) and fine (-60 mesh), which corresponded to the two generations of phlogopite. Four analyses of the whole-rock sample had similar $^{87}\text{Sr}/^{86}\text{Sr}$, but slightly different Rb/Sr. The two mica fractions had much greater Rb/Sr and $^{87}\text{Sr}/^{86}\text{Sr}$ ratios. The points are not colinear, with an M.S.W.D. of 7.5, so the regression line fitting of York (1969) was used to obtain an errorchron of $77.9 \pm 2.2\text{Ma}$, giving an age of $77.9 \pm 6.0\text{Ma}$.

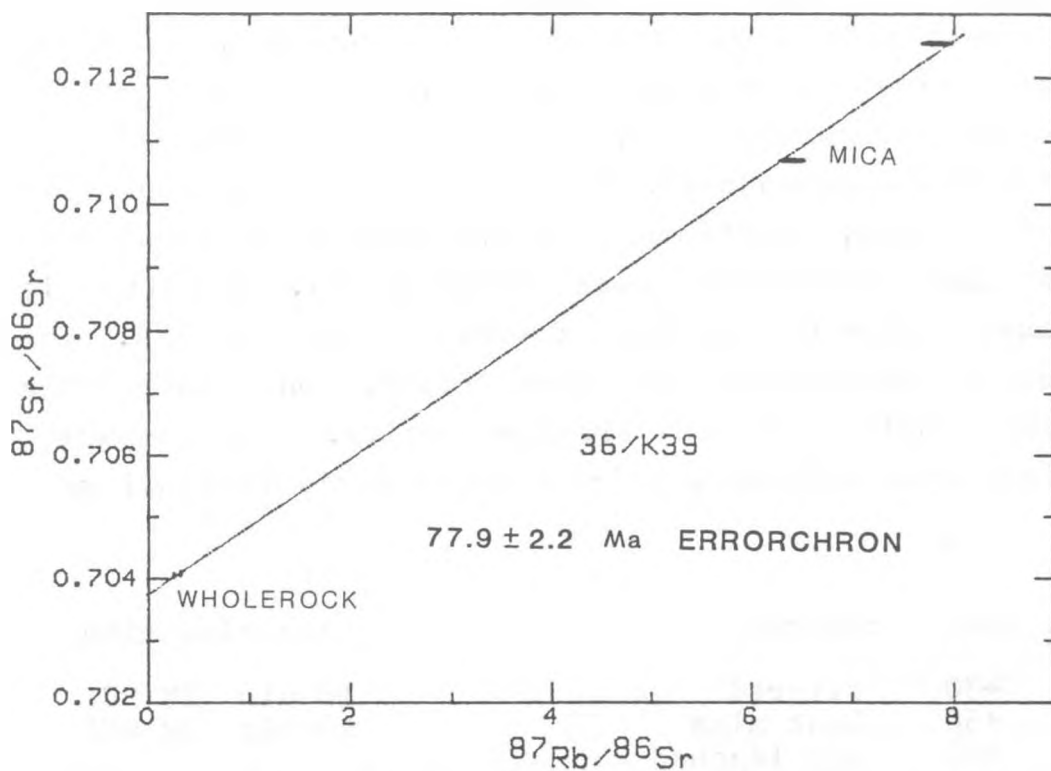


Figure 2.6. K39 Rb/Sr Wholerock-Mica Isochron plot.

Table 2.4 : 33/K39 Rb/Sr data

Sample	Rb	Sr	$^{87}\text{Rb}/^{86}\text{Sr}$	$^{87}\text{Sr}/^{86}\text{Sr}$
K39/W/M	27	1264	0.2568 +/-40	0.704048+/-10
K39/W/X	34	1400	0.2647 +/-40	0.703986+/-10
K39/1/M	61	1310	0.32468+/-48	0.704039+/-10
K39/1/X	65	1365	0.32751+/-48	0.704031+/-10
K39/c	376.3	163.6	6.40 +/-10	0.710634+/-10
K39/f	409.2	144.5	7.83 +/-12	0.712476+/-10

33/K2 contains two generations of phlogopite, an early coarser grained macrocrystal variety, and a finer grained colourless groundmass type, set in a fresh monticellite-calcite-spinel groundmass. The macrocrystal phlogopite is generally fresh, sometimes with overgrowths of groundmass composition phlogopite (see chapter 3). Calcite is sometimes evident invading cracks in the grains. The groundmass phlogopite is also fresh, but invariably contains inclusions of titanomagnetite. Six separate fractions were obtained, which were of variable quality:

sample	mesh	comment	leaching time	
1	+30	altered	10 min	2M HCl
2	+60	best mica	10 min	2M HCl
3	+60	not leached		
4	+60	magnetic inclusions	5 min	2M HCl
5	-60	magnetic inclusions	10 min	2M HCl
6	+60	altered	10 min	2M HCl

The coarsest fraction (1) consisted of macrocryst grains somewhat altered around the edges. Fraction 2 was exhaustively picked, and consisted of particularly fresh, clean macrocrystal phlogopite. Sample 3 was similar to 2, but not leached, to test the effect of the leaching technique. Samples 4 and 5 were groundmass phlogopite which contained abundant inclusions of ulvospinel. Fraction 6 was rather poor quality groundmass phlogopite with ulvospinel inclusions and calcite in cracks. The whole rock sample was very fresh.

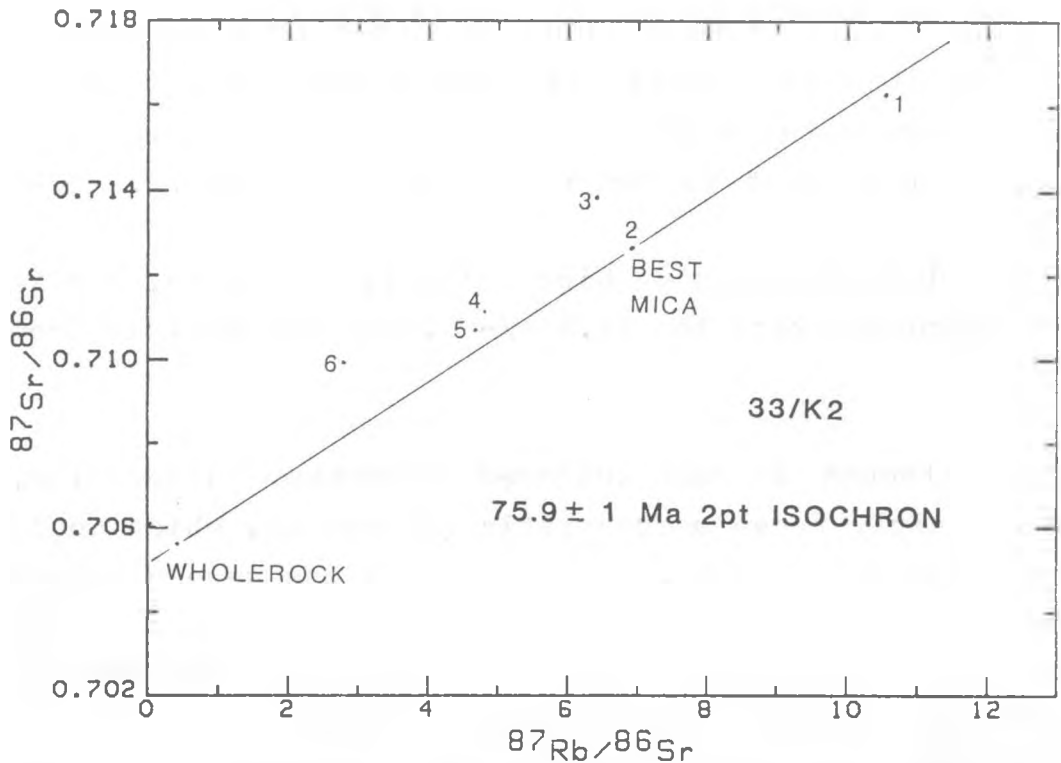


Figure 2.7. K2 Rb/Sr Wholerock-Mica isochron plot.

Table 2.5 : 33/K2 Rb/Sr data

Sample	Rb	Sr	$^{87}\text{Rb}/^{86}\text{Sr}$	$^{87}\text{Sr}/^{86}\text{Sr}$
K2/WR	137	1915	0.3924 +/-40	0.705585+/-10
1	375.9	97.47	10.59 +/-12	0.716145+/-160
2	210.0	84.56	6.891 +/-68	0.712595+/-16
3	334.0	143.9	6.452 +/-70	0.713751+/-50
4	226.7	132.6	4.807 +/-52	0.710954+/-62
5	124.6	74.47	4.708 +/-50	0.710583+/-66
6	42.27	44.61	2.752 +/-30	0.709420+/-52

The data obtained provided a spread of Rb/Sr and $^{87}\text{Sr}/^{86}\text{Sr}$. They did not however define an isochron (see fig 2.7). The whole rock sample and the best two mica separates (1 and 2) are almost colinear, but the poorer micas (3 to 6) all plot above this line. It is reasonable to discard these latter four points because they are derived from impure separates. The remaining three points define a crude errorchron of 73.7 +/- 24 Ma, with a M.S.W.D. of 10.8. When fraction 1 is discarded (because

the phlogopite was slightly altered) a two point isochron can be drawn between the fresh mica (2) and the whole rock. This two point isochron defines an age of 75.9 +/-1 Ma.

The age determination of pipe 33/K2 is imprecise, but it is in accordance with the 77.9 +/- 6.0 Ma age derived from 36/K39.

36/K43, although it has suffered groundmass alteration, contains fairly fresh macrocrystic phlogopite, which could be separated and cleaned. Two mica fractions were obtained which had very high Rb/Sr ratios, due to low Sr, which was reflected in the high $^{87}\text{Sr}/^{86}\text{Sr}$ ratios. The Rb and Sr compositions were considerably higher and lower respectively than micas from the other pipes. The reason for this is unknown, but presumably reflects heterogeneity in the source of the micas in the mantle.

A two point isochron using these data has a slope of 37 Ma. However, the two points are too close together to give a realistic age determination, and it would be better to constrain the lower end of the isochron using a whole rock sample.

The wholerock sample is not colinear with the phlogopites (see fig 2.8) but a best fit line between the whole rock and the micas has a slope of 68Ma.

Because the groundmass has been altered, it is known (chapter 4) that the $^{87}\text{Sr}/^{86}\text{Sr}$ ratio of the altered whole rock sample is higher than it would have been in the fresh rock. Therefore it would be appropriate to estimate the Rb/Sr and $^{87}\text{Sr}/^{86}\text{Sr}$ of the fresh rock by using data from the nearby pipe 36/K35, whose composition is typical of the Gibeon kimberlites (Chapter 4).

Table 2.6 : 36/K43 Rb/Sr data

Sample	Rb	Sr	$^{87}\text{Rb}/^{86}\text{Sr}$	$^{87}\text{Sr}/^{86}\text{Sr}$
K43 WR	97.0	496.3	0.7269+/-50	0.708686+/-10
K35 WR			0.3608	0.7038
K43 f	535.5	19.55	73.97 +/-50	0.781704+/-12
K43 c	552.6	17.39	85.79 +/-50	0.787873+/-18

The best fit line between the estimated whole rock data and the two mica samples has a slope of 72 Ma.

These data obviously do not provide an accurate age determination, but the age derived is similar to the ages derived above for other pipes, so some indication of age can be attained.

33/K14 has also suffered groundmass alteration, but contains fairly fresh macrocrystic phlogopite. No groundmass mica was obtained, but two size fractions of macrocrystic phlogopite were separated, which had similar $^{87}\text{Sr}/^{86}\text{Sr}$ ratios and Sr concentrations, but variable Rb/Sr. This variation could possibly be due to slightly excessive leaching, removing Rb from the mica, reducing the Rb/Sr in the fine fraction. Alternatively, the Rb/Sr difference could be inherent in the phlogopite grains.

The mica appeared fresh under the binocular microscope, and altered grains were removed by hand picking.

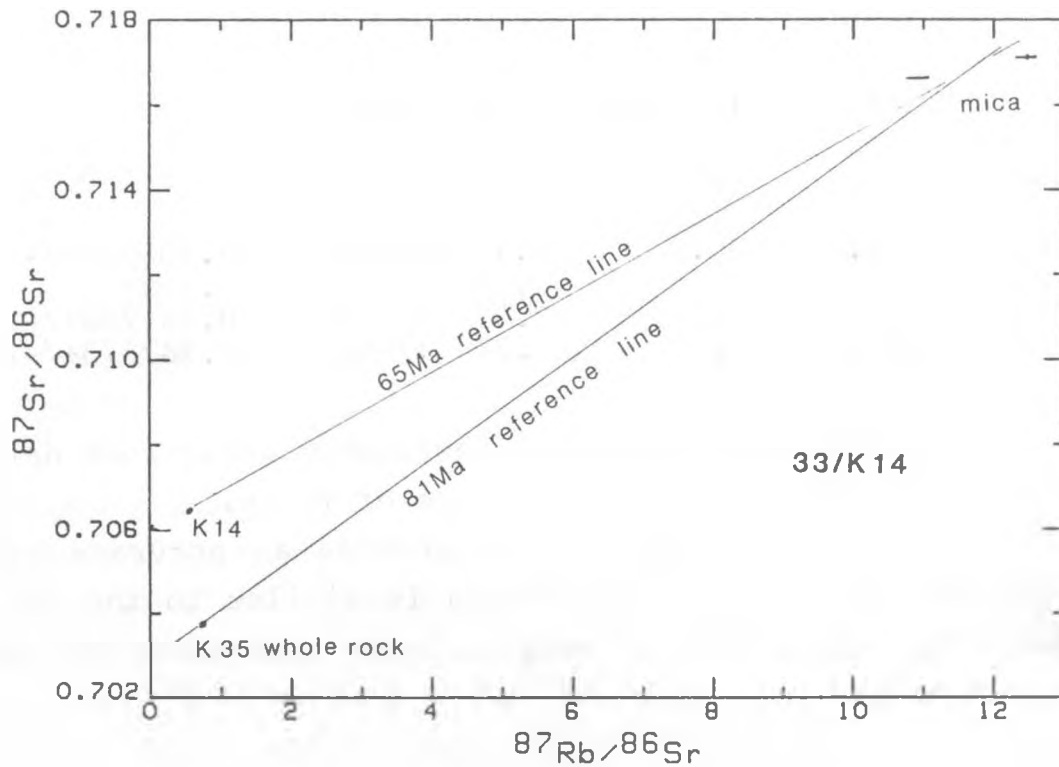


Figure 2.9 K14 Rb/Sr Wholerock-Mica isochron plot.

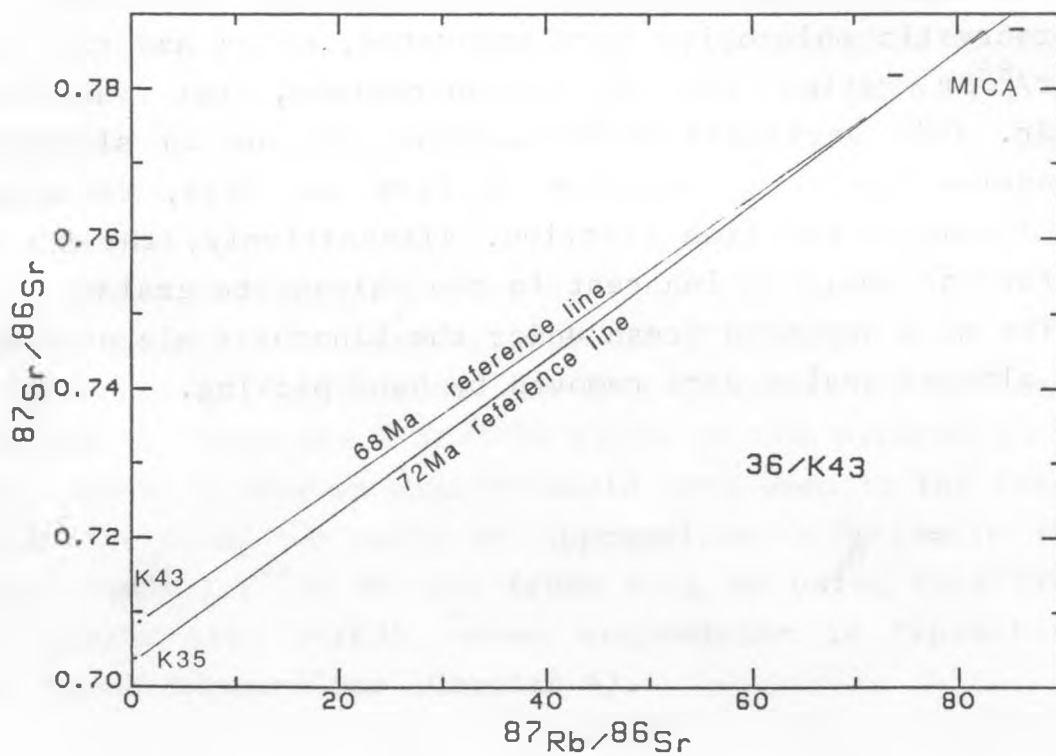


Figure 2.8 K43 Rb/Sr Wholerock-Mica isochron plot.

As with K43, the two mica separates are too similar to yield a two point isochron, and a whole rock sample must be sought to constrain the lower end of an isochron. The whole rock sample has suffered alteration, so again an estimate must be made for the pre-alteration composition of the rock. Using K35 again as a minimum estimate of the $^{87}\text{Sr}/^{86}\text{Sr}$ ratio, an 81Ma reference line can be drawn through the points. However, pipe K14 is very close to pipe 33/K2, which has variable and higher $^{87}\text{Sr}/^{86}\text{Sr}$, so the choice of K35 to represent the whole rock may be a poor approximation. Using the altered K14 whole rock sample, a 65 Ma reference line can be drawn through the data points.

Table 2.7 33/K14 Rb/Sr data

Sample	Rb	Sr	$^{87}\text{Rb}/^{86}\text{Sr}$	$^{87}\text{Sr}/^{86}\text{Sr}$
K14 WR	79.0	805.5	0.4641+/-70	0.706437+/-10
K35 WR			0.3608	0.7038
K14 f	382.8	96.9	10.84 +/-16	0.716486+/-10
K14 c	434.4	95.94	12.40 +/-18	0.716985+/-10

Thus in conclusion, it was not possible to accurately date K14, but it's age can be realistically constrained between 65 and 81 Ma, which is also in accordance with the ages derived above for the other pipes.

Conclusions

None of the four age determinations gave precise results, but they all gave similar dates, which is thought to be significant. The ages produced are in agreement with regional geological information (Janse 1964) and also consistent with the whole rock isotope systematics of the kimberlites (chapter 4). These results indicate an age of 70-80 Ma for the Gibeon kimberlites, whereas Davis' two Pb zircon dates indicate ages of 60-70 Ma. The data are too poor to show any chronological variations within the province. The age of the Gibeon kimberlite province can be confidently constrained as 70 ± 10 Ma and for the purpose of age correction of isotope ratios, 70 Ma is used in this work as the age of the province. The use of 60 or 80 Ma for age correction would have made no significant difference to the data or interpretation.

^{39}Ar - ^{40}Ar dates

The $^{39}\text{Ar}/^{40}\text{Ar}$ step heating method was used to date two samples, 42/PK61 and 42/PK62 (Uitkomst 4 and 5) which are two dykes outcropping on hillsides some 400m apart. They are both melilitites which have particularly large mica phenocrysts (2cm) which are exceptionally fresh, even though the groundmass has secondary alteration. The integrated ages calculated were:

PK61 524 Ma

PK62 514 Ma

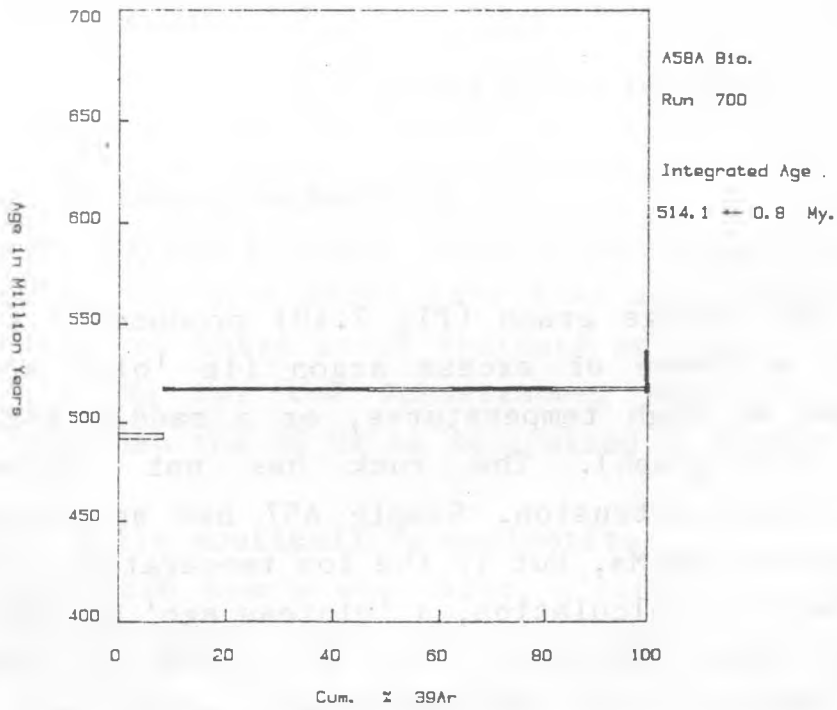
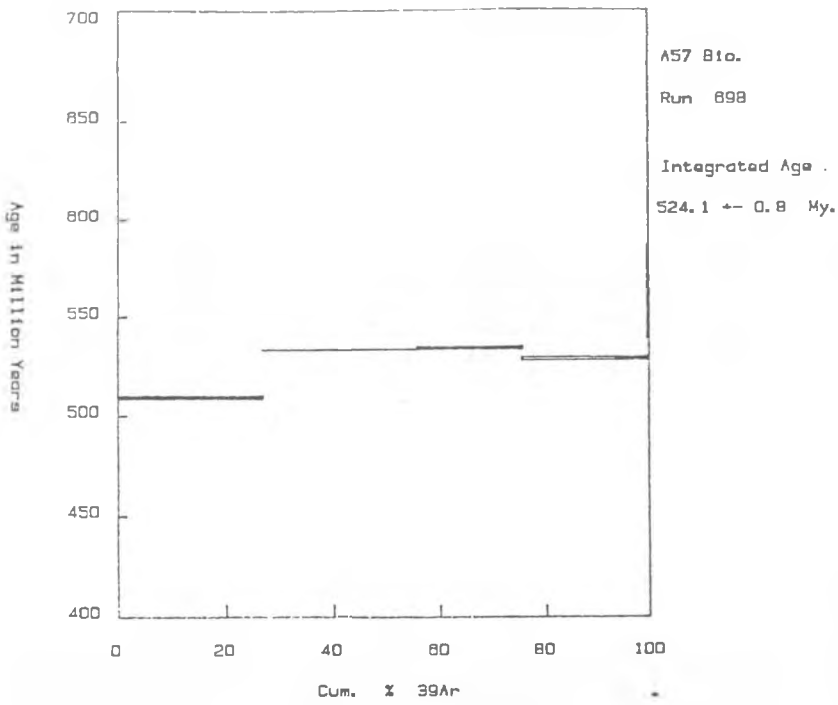


Figure 2.10. $^{39}\text{Ar}/^{40}\text{Ar}$ age plots for 42/PK61 (sample A57) and 42/PK62 (sample A58a).

Table 2.8: $^{39}\text{Ar}/^{40}\text{Ar}$ data

PK61

Temp	^{39}K (vol. $\times 10^{-9}$)	^{37}Ca ^{37}Ca (cc)	^{38}Cl ^{38}Cl (cc)	Ca/K	$^{40}\text{Ar}/^{39}\text{K}$	%Atm 40Ar	% ^{39}Ar	Age
830	100.208	10.401	0.898	0.2066	11.439	4.3	27.1	507.52 \pm 0.6
935	106.930	0.599	0.802	0.0112	12.069	0.8	28.9	531.71 \pm 0.54
1000	73.269	0.515	0.563	0.0140	12.075	1.1	19.8	531.94 \pm 0.55
1055	66.372	0.271	0.517	0.0081	11.946	1.2	17.9	527.00 \pm 0.56
1166	22.986	0.192	0.178	0.0166	11.941	1.0	6.2	526.82 \pm 0.74
1360	0.588	0.076	0.007	0.2587	12.824	4.6	0.2	560.31 \pm 23.1

integrated values $*^{40}/^{39}\text{K}=11.871$

Age 524.14 Ma. errors: analytical 0.82, J 9.13Ma.

PK62

Temp	^{39}K (vol. $\times 10^{-9}$)	^{37}Ca ^{37}Ca (cc)	^{38}Cl ^{38}Cl (cc)	Ca/K	$*^{40}/^{39}\text{K}$	%Atm 40Ar	% ^{39}Ar	Age
875	26.171	30.902	0.332	2.3498	10.976	12.9	8.3	492.53 \pm 1.17
940	121.081	0.914	0.936	0.0150	11.579	0.8	38.4	516.05 \pm 0.51
995	50.181	0.436	0.385	0.0173	11.583	0.9	15.9	516.23 \pm 0.67
1066	57.922	0.319	0.451	0.0110	11.561	0.8	18.4	515.37 \pm 0.56
1160	58.388	0.323	0.454	0.0110	11.589	0.4	18.5	516.44 \pm 0.48
1360	1.722	0.419	0.022	0.4848	11.778	1.1	0.5	523.75 \pm 10.2

integrated values $*^{40}/^{39}\text{K}=11.529$

Age 514.13 Ma. errors: analytical 0.79, J 8.98 Ma

The $^{39}\text{Ar}/^{40}\text{Ar}$ vs age graph (fig 2.10) produces a flat plot with no evidence of excess argon (ie 'old' argon being released at high temperatures, or a saddle shaped profile on the graph). The rock has not suffered metamorphism since intrusion. Sample A57 had an overall integrated age of 524 Ma, but if the low temperature argon is omitted from the calculation, a 'plateau age' of 530 Ma is obtained. Thus confidence can be placed in these results as reliable age determinations, which are in accordance with the 500Ma K-Ar age determined by Kroner (1973) on a similar nearby intrusion at Garub.

K-Ar dates

The K-Ar technique of Briden et al (1979) was used to date several volatile free rocks with little or no mica. Four samples of the Schwarzeberg nephelinite, one sample of the Blue Hills monticellite peridotite and three samples of melilitite from the Grunau area were analysed.

Table 2.9 : K/Ar data

sample	%K	vol ^{40}Ar rad cc STP/g	% ^{40}Ar rad	Age(Ma)
PK2 Blue Hills	1.75	81470	77.8	116+/-4
A44 Schwarzeberg	1.23	13800	40.6	29+/-1
A45 Schwarzeberg	1.21	13560	21.5	29+/-1
A73 Schwarzeberg	1.06	12800	65.9	31+/-1
A74 Schwarzeberg	1.31	14930	44.6	29+/-1
PK48	1.07	14392	87.3	317+/-12
PK55	1.11	18883	95.5	392+/-12
PK62	1.32	26787	84.4	458+/-14

1) Schwarzeberg nephelinite

Four extremely fresh samples were taken from different parts of the dyke which gave K/Ar ages within error. The coherence of these dates indicate an age determination of 30+/- 1 Ma for the Schwarzeberg nephelinite, slightly younger than the 35 Ma as determined by Kroner (1973).

2) Blue Hills monticellite peridotite

One fresh sample was dated, giving an age of 116 +/- 4 Ma, significantly older than the kimberlites. As a clue to the accuracy of this age determination, it is useful to consider the whole rock isotope systematics of this rock (see ch 6). The whole rock has a $^{87}\text{Sr}/^{86}\text{Sr}$ ratio of 0.7041 and a $^{143}\text{Nd}/^{144}\text{Nd}$ ratio of 0.51272 which are slightly

higher and lower respectively than those of the nearby kimberlites. These ratios are consistent with the rock being derived from the mantle relatively recently (ie <200 Ma). An age similar to or slightly older than the kimberlites is predicted if the rock is derived from a similar asthenospheric source.

Any alteration of the rock would tend to give an age younger than the emplacement age, so the age determined should be considered a minimum age. Regional geology (Janse 1964) supports the contention that PK2 is of broadly similar age to the kimberlites. PK2 outcrops on the Blue Hills ridge which appears to be younger than the carbonatite at Gross Brukkaros, which was dated by D.C. Rex at 145 +/-5 Ma.

Thus in conclusion, circumstantial evidence tentatively supports the 116 Ma age determined for this intrusion.

3)Grunau melilitites

Three melilitite samples were chosen (for K-Ar dating)because they had suffered less alteration than other samples collected, though they did have secondary calcite in the groundmass. The melilitites are all believed to be about 500Ma old (Skinner pers. comm.) and unrelated to the Gibeon kimberlite activity. Because of the alteration of these rocks it is expected that the resulting dates would be younger than the emplacement age, because of argon loss. The ages therefore can only be interpreted as minimum ages.

PK62 yields a 458 Ma age by K-Ar, but a 514 Ma age by $^{39}\text{Ar}/^{40}\text{Ar}$. Thus the discordant K-Ar age is interpreted as being a minimum age, affected by secondary alteration of the rock. PK48 and PK55 have suffered a greater degree of alteration than PK62, and their K-Ar ages are probably even more affected by alteration. The age variation is therefore interpreted as being due to variable degrees of

argon loss due to alteration.

The significant conclusion is that the rocks are much older than the Gibeon kimberlites and unrelated to them. Their ages are probably all around 520 Ma. The whole rock isotope systematics ($^{143}\text{Nd}/^{144}\text{Nd} = 0.5124$, much lower than the younger kimberlites, and consistent with the greater age).

CHAPTER 3

PETROGRAPHY, MINERALOGY AND GEOCHEMISTRY :

INTRAKIMBERLITE VARIATIONS

The petrography and mineralogy of the four fresh, and eight altered kimberlites are described in this chapter. The aim is to detail the internal geochemical and mineralogical variations within pipes. Whole rock geochemistry is introduced, but a full discussion of the interpretation of the geochemistry is deferred until chapter 4.

3.1 36/K35 BERSEBA RESERVE 2

Pipe K35 is one of a cluster of small pipes on the Berseba Reserve. Surface outcrop consists of blue/grey clay covering an oval area some 100x50m. Small garnet, ilmenite and dark green pyroxene megacrysts are scattered on the surface; no peridotite nodules were present. Any possible evidence of multiple intrusion has been obscured by surface weathering.

A borehole drilled into the pipe encountered fresh hypabyssal kimberlite at a depth of 50m, from which two samples were obtained. The rock is a hard dark kimberlite with rare (1%) crustal xenoliths, which have thin (1-2mm) reaction rims.

The rock is exceptionally fresh, the only alteration being slight serpentinization of the olivine macrocrysts by deuteric processes.

The low abundance of xenoliths coupled with the excellent preservation state, make this an ideal rock for geochemical analysis. Texturally, the rock is a

macrocrystic-hypabyssal kimberlite. Mineralogically it is a monticellite kimberlite and chemically it is a group I kimberlite.

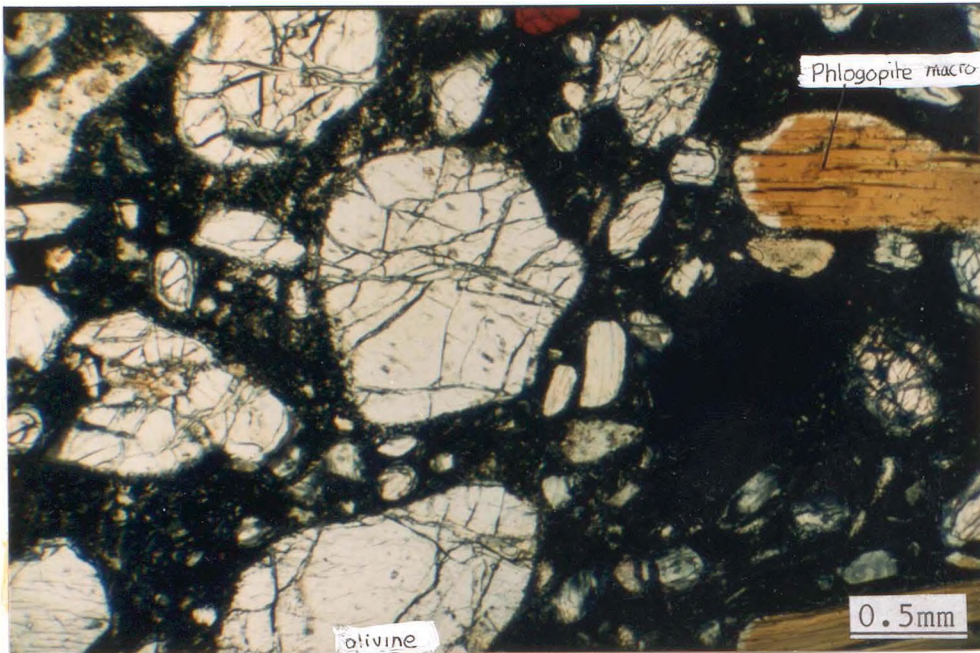


Plate 3.1: photomicrograph of K35, showing fresh olivine and phlogopite macrocrysts set in a dark spinel rich matrix

3.1.1 Mineralogy

The kimberlite consists of 40% olivine, comprising large anhedral fresh macrocrysts (up to 5mm) and small euhedral phenocrysts (<0.2mm) together with occasional large phlogopite macrocrysts, set in a fine grained matrix of chromite, ilmenite, phlogopite, magnesian-ulvospinel, perovskite, monticellite, apatite and primary calcite. Petrographic and chemical studies of these minerals show how the composition of the magma evolves from a 'basaltic' silicate melt to a carbonate rich fluid, precipitating a variety of minerals. Microprobe analyses of minerals are presented in appendix 2.

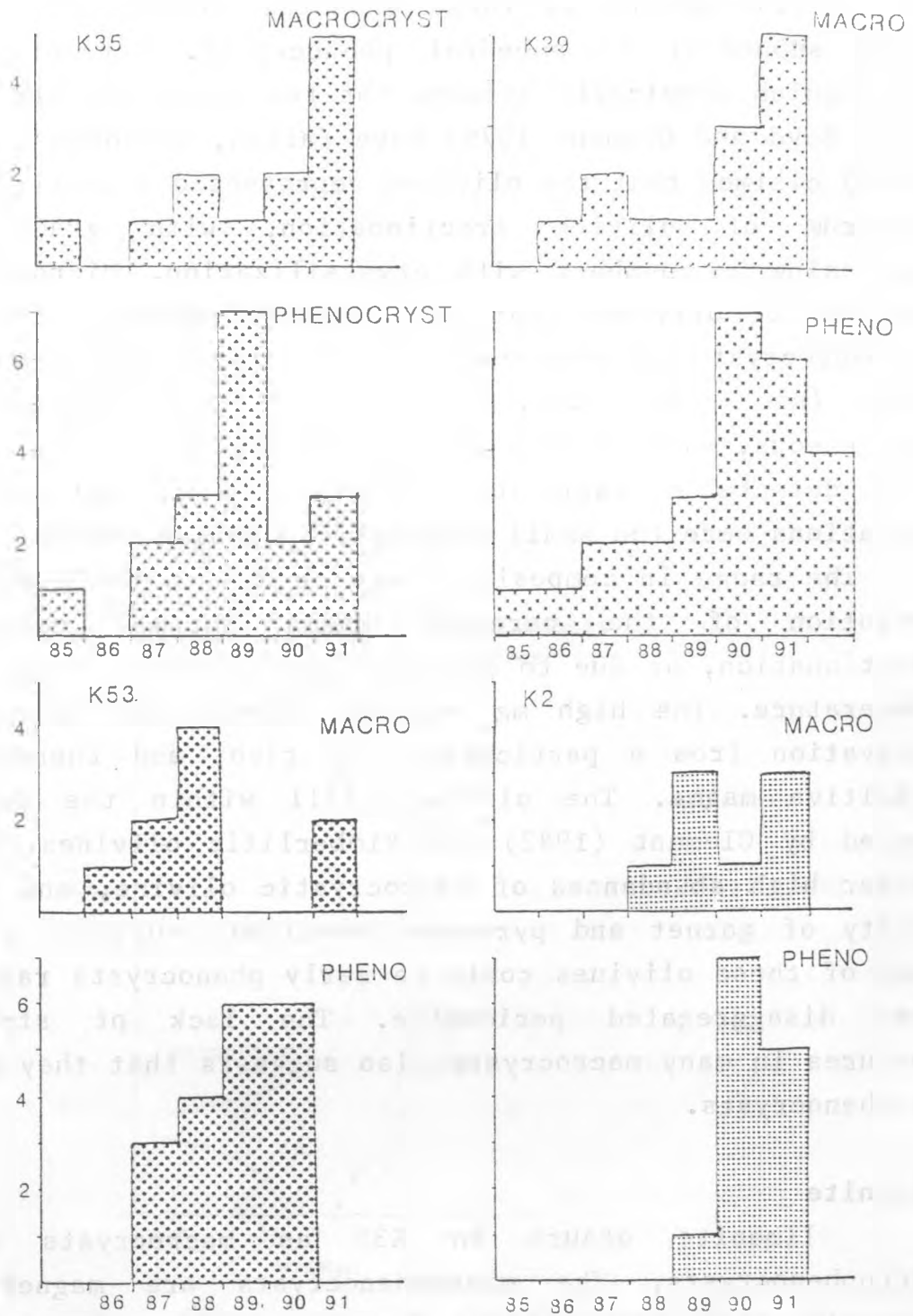


Figure 3.1. Forsterite compositions of olivine phenocrysts and macrocrysts from four fresh kimberlites

Olivine

Olivine occurs as large anhedral macrocrysts, and small subhedral to euhedral phenocrysts. Attempts to distinguish chemically between the two types (eg Clement 1982, Boyd and Clement 1979) have failed, although Moore (1986) claimed that the olivines represented a continuous spectrum of olivine fractionation, with gradually decreasing mg numbers with crystallization. Microprobe analyses of olivines from K35 reveal overlapping ranges in macrocryst and phenocryst compositions from Fo₈₆ to Fo₉₁ (see fig 3.1). Phenocrysts are relatively homogeneous, with little evidence of zoning. Macrocrysts have detectable variations within grains, but these variations were too small to establish zoning trends.

The range in composition may be due to the gradual evolution of the parental magma through crystal fractionation, or due to crystallization over a range in temperature. The high mg numbers (around 90) indicate derivation from a particularly Mg rich, and therefore primitive magma. The olivines fall within the range quoted by Clement (1982) for kimberlitic olivines. The rather high abundances of macrocrystic olivine, and the rarity of garnet and pyroxene xenocrysts suggests that many of these olivines could be early phenocrysts rather than disaggregated peridotite. The lack of strain features in many macrocrysts also suggests that they may be phenocrysts.

Ilmenite

Ilmenite occurs in K35 as macrocrysts and microphenocrysts. The microphenocrysts are magnesian ilmenite with compositions broadly similar to those determined by Shee (1984) and Apter et al. (1984) from Wesselton and Mayeng respectively (see fig 3.2 a,b). Wesselton is a large 'on craton' group I kimberlite with

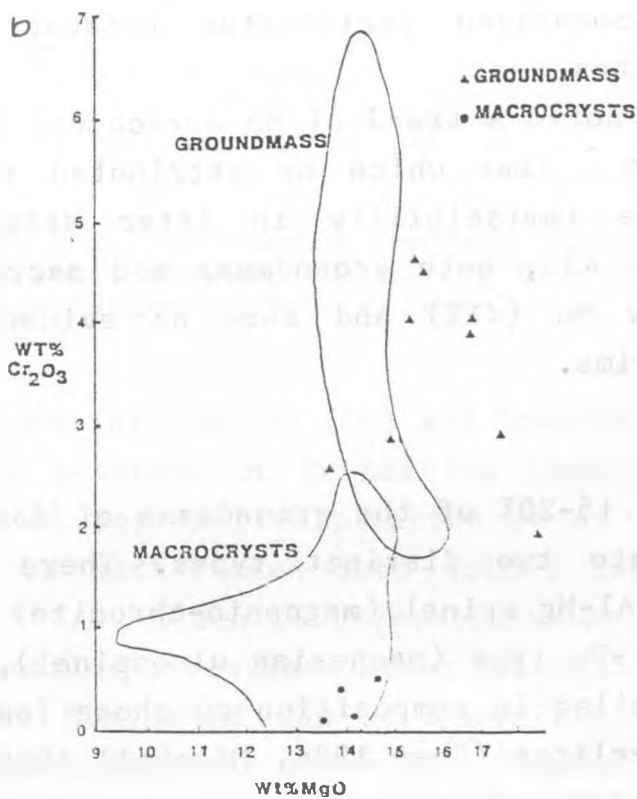
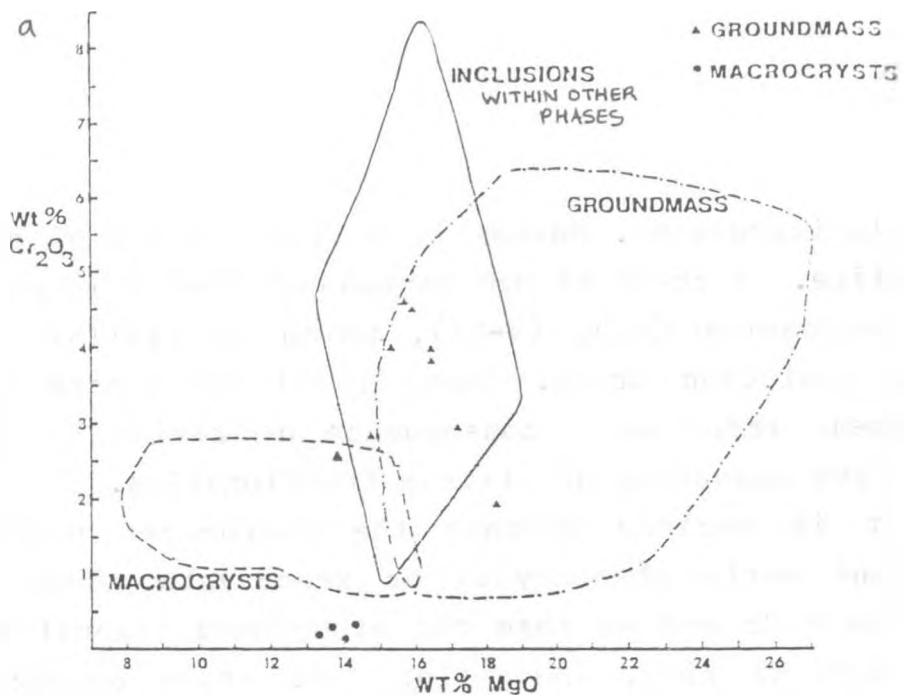


Figure 3.2. MgO v Cr₂O₃ in groundmass and macrocryst ilmenites from K35, compared with fields for ilmenite from (a) Wesselton (Shee 1984), and (b) The Mayeng Sills (Apter et al. 1984).

multiple intrusions. Mayeng is a sill complex of evolved kimberlite. A trend of MgO enrichment 15-19% is possible, with decreasing Cr₂O₃ (4-2%), which is similar to the Mayeng evolution trend. Shee (1984) interprets the Mg enrichment trend as a consequence of rising Mg in the melt after cessation of olivine fractionation.

It is unclear whether the macrocryst population represent early phenocrysts or xenocrysts. Macrocrysts have lower Cr and Mg than the groundmass ilmenites, and have high Mg rims, indicating late stage overgrowths. Thus the macrocrysts are not in equilibrium with the kimberlite magma which crystallised the groundmass. It is unlikely that the macrocrysts are derived from disaggregated metasomatised peridotites because these have Cr rich ilmenites.

Haggerty (1979) noted a trend of Mn enrichment in the groundmass ilmenite rims which he attributed to the onset of carbonate immiscibility in later stages of crystallisation. In K35, both groundmass and macrocryst ilmenites have low Mn (<1%) and show no evidence of enrichment in the rims.

Spinels

Spinels make up 15-20% of the groundmass of K35, and can be divided into two distinct types. There is a relatively rare Cr-Al-Mg spinel (magnesio-chromite) and a more abundant Mg-Ti-Fe type (magnesian ulvospinel). Both spinel types are similar in composition to those found in other group I kimberlites (Shee 1984, Mitchell 1986) and follow the magnesian ulvospinel - magnetite (MUM) magmatic trend described by Mitchell (1986). There is a compositional hiatus between the early forming Cr-spinels and the later magnesian ulvospinels, possibly due to the presence of a solvus in the spinel system, producing a

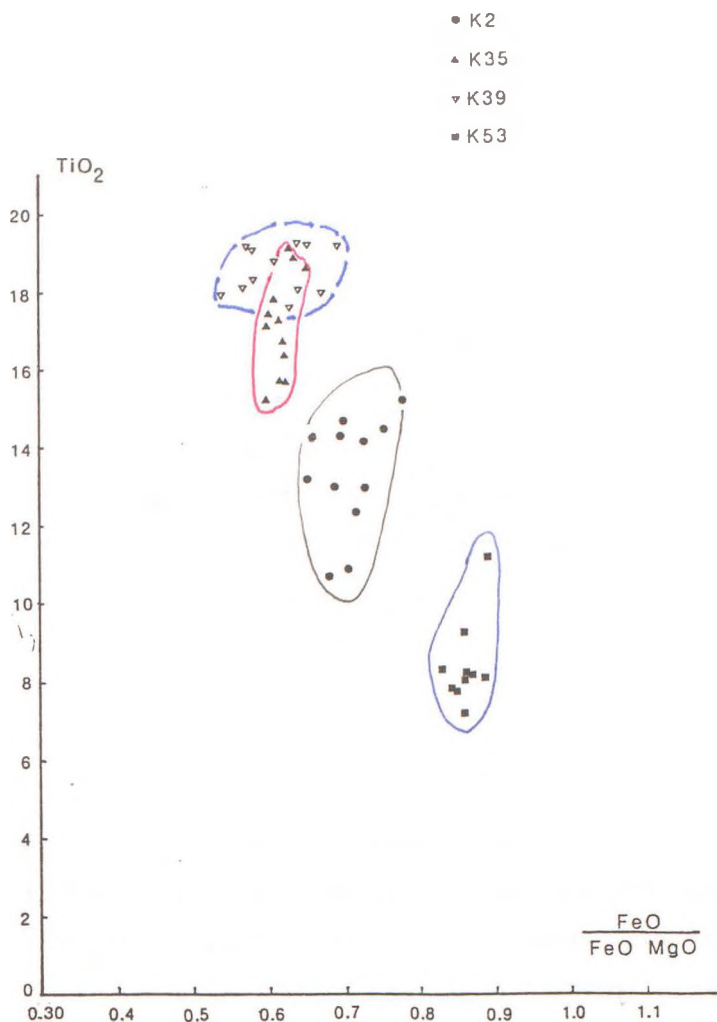


Figure 3.3. Groundmass spinel compositions of Gibeon kimberlites, showing increasing TiO_2 with limited (within pipe) variation in $\text{FeO}/(\text{FeO}+\text{MgO})$.

breakdown into normal (Cr) and inverse (Ti) spinels.

The presence of Cr bearing ilmenites indicates that Cr-spinel ceased precipitation at an early stage, as Cr would be partitioned into spinel rather than ilmenite (Shee 1984). Ilmenite crystallisation was then succeeded by magnesian ulvospinel, then perovskite.

The MUM trend can be seen (fig 3.3) to be one of increasing Ti at constant $\text{FeO}/(\text{FeO}+\text{MgO})$. As Ti increases, there is an increase in $\text{Fe}^{3+}/\text{Fe}^{2+}$ (fig 3.4) and total Fe. In some kimberlites (eg Green Mountain, Boctor and Meyer 1979) the spinels ^{may} evolve ^{further, and} sometimes pure magnetite is precipitated.

- K2
- ▲ K35
- ▼ K39
- K53

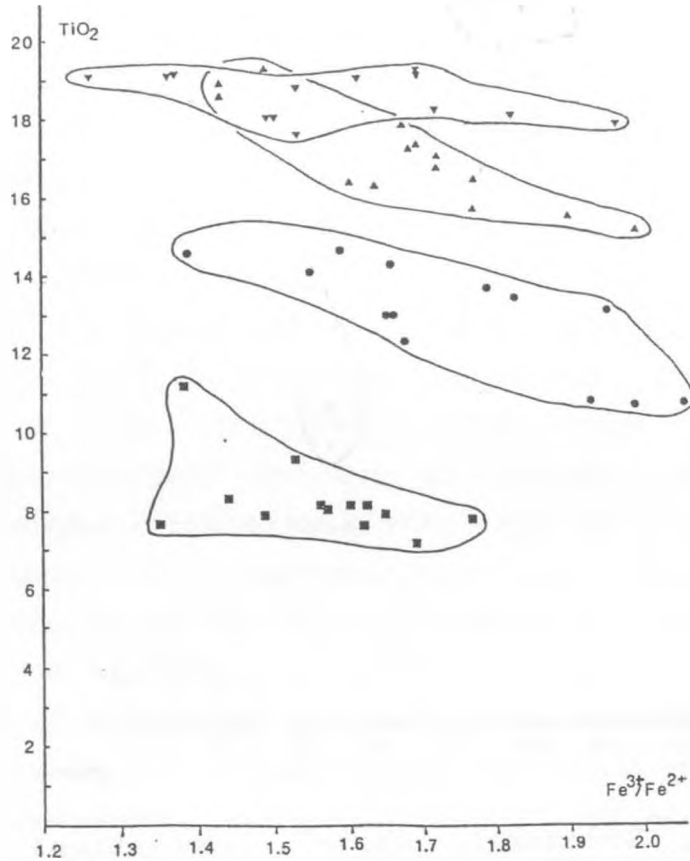


Figure 3.4. Groundmass spinel compositions of Gibeon kimberlites, showing increasing TiO₂ with decreasing Fe³⁺/Fe²⁺.

Perovskite

Perovskite occurs as a common phase in the groundmass as small subhedral grains and as overgrowth rims on spinels. Perovskite is a common phase in kimberlites (Mitchell 1986), though is much less abundant than spinel. Perovskite crystallises late in the groundmass, after spinel, but before monticellite, phlogopite and calcite. Occasionally it is found as inclusions within groundmass phlogopite. Perovskite compositions are relatively pure CaTiO₃ with little substitution, except for U, Nb and the REE, which are hosted by this phase.

Macrocryst Phlogopite

The macrocryst phlogopites are of a composition typically found in kimberlites (Smith et al.1978). They are typically 0.5 to 2mm, brown pleochroic grains, often kinked or deformed, with some chlorite or calcite replacement along cleavage planes, and rounded resorbed outlines. Some grains are rimmed with a phlogopite of groundmass composition, but otherwise their compositions tend to be homogeneous. Macrocrysts do not contain inclusions of groundmass spinel. These grains clearly preceeded groundmass crystallisation, and were separated from them by a hiatus in phlogopite crystallisation. It is not clear whether the macrocrysts represent early phenocrysts or xenocrysts. Their abundance in K35 suggests they are phenocrysts as other mantle xenocryst phases (apart from olivine) are relatively scarce. However, although macrocryst phlogopites are commonly found in the Gibeon kimberlites, their abundance varies from up to 3% in K2 to a complete absence in K53. The variations in macrocryst phlogopite abundance in kimberlites of similar geochemistry (table 3.1) and mineralogy lends support to the xenocryst theory. The deformation of the grains, their resorption and disequilibrium with the groundmass also favour their origins as xenocrysts.

The macrocryst phlogopites have compositions similar to those quoted by Smith et al (1978) and designated type I micas. These have relatively high TiO_2 (4-5%), and uniform K_2O contents at around 10.5%. BaO is less than 1% and Cr_2O_3 is relatively high (0.5-1.2%). Smith et al.(1978) were unable to define the origin of these micas, concluding that they could be phenocrysts from a precursor magma or xenocrysts from some mantle source.

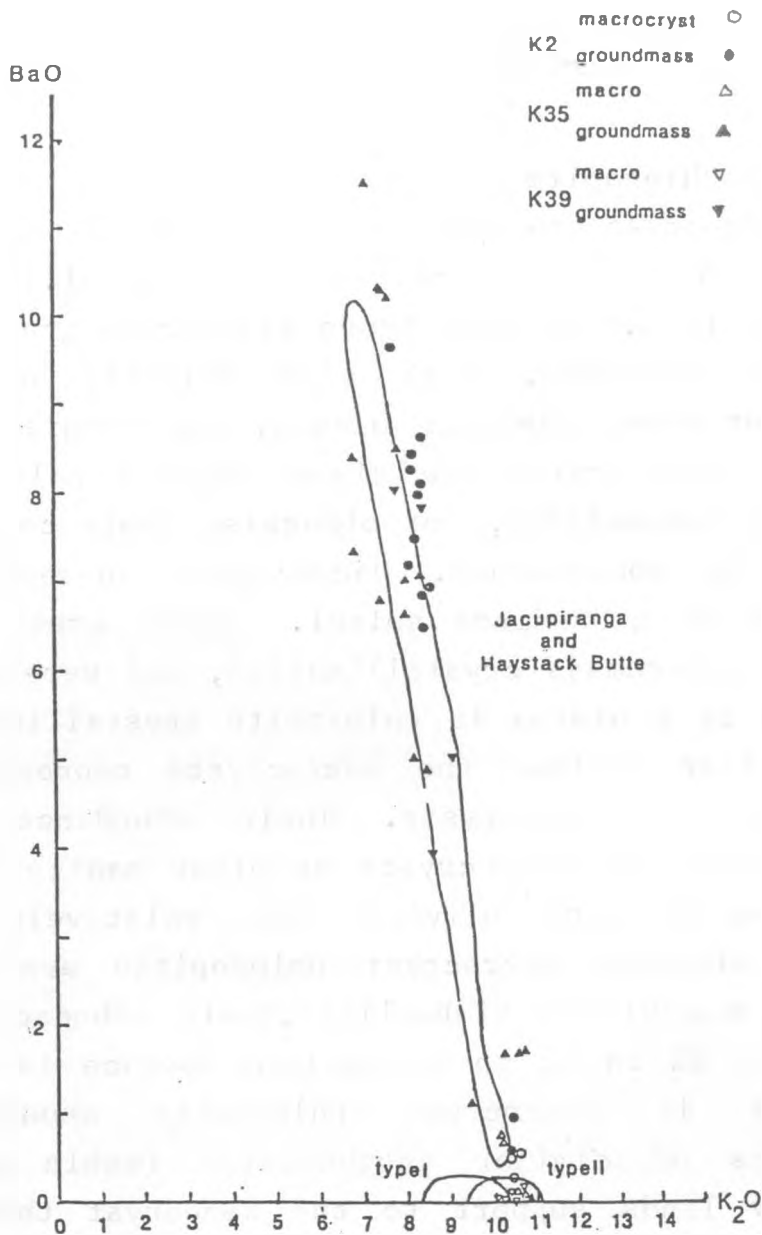


Figure 3.5. BaO v K_2O for phlogopites. Macrocrysts have low Ba, whereas groundmass phlogopites show Ba enrichment. The fields outlined are for high Ba phlogopites from the Jacupiranga carbonatite (Gaspar and Wyllie 1982) and Haystack Butte monticellite peridotite (Wendlandt 1976), and type I and type II kimberlite micas (Smith et al. 1978).

Groundmass Phlogopite

The groundmass phlogopites are of a composition not previously recorded in kimberlite (Smith et al 1978, Mitchell 1986) due to their extreme Ba enrichment. Groundmass phlogopites are very small (<0.1mm), pale or colourless equant grains, found abundantly in the fine

grained kimberlite matrix. These phlogopites usually contain microscopic ulvospinel and perovskite inclusions, indicating their origin in the later stages of crystallisation. Their composition is highly variable with BaO ranging from 0 to 11.5%. BaO is inversely correlated with K₂O (see fig 3.5) which varies from 6.5 to 10.5%. (BaO/K₂O=0-1.64) The grains are continuously zoned, from Ba rich cores, to low Ba rims, indicating a rapid depletion of Ba in the residual melt by phlogopite crystallisation. The groundmass phlogopites are distinctly low in Cr (<0.5%) and TiO₂ (0.5-2%, BaO/TiO₂=0-9.2) and can be clearly distinguished from the macrocryst phlogopites (fig 3.6).

Figure 3.7 is a plot of Al/Si vs Ba/K molar ratios. There is a broad trend of increasing Al/Si with increasing Ba/K. Wendlandt (1978) found a similar trend in the Ba-phlogopite from Haystack Butte, and interpreted it as a result of the substitution $Ba + Al \rightleftharpoons K + Si$. The replacement of K⁺ by Ba²⁺ in the interlayer site requires charge balance which is achieved by the substitution of Al³⁺ for Si⁴⁺ in tetrahedral sites.

Ba phlogopites have not previously been recorded from kimberlite (Mitchell 1986, Smith et al. 1978, Dawson and Smith 1975), though Arima et al. (1986) report BaO up to 4% in phlogopites found in xenoliths in kimberlite. These micas, though, are Cr-rich and are dissimilar to the groundmass phlogopites of K35. The Ba-rich phlogopites of K35, are however, similar in composition to those found in the Jacupiranga carbonatite (Gaspar and Wyllie 1982) and a 'monticellite peridotite' from Haystack Butte, Montana (Wendlandt 1976).

Fig 3.5 shows that the Ba fractionation trend found in the phlogopites from K35 is similar to that found in Jacupiranga and Haystack Butte, indicating that the late stage liquid from which the kimberlitic phlogopites

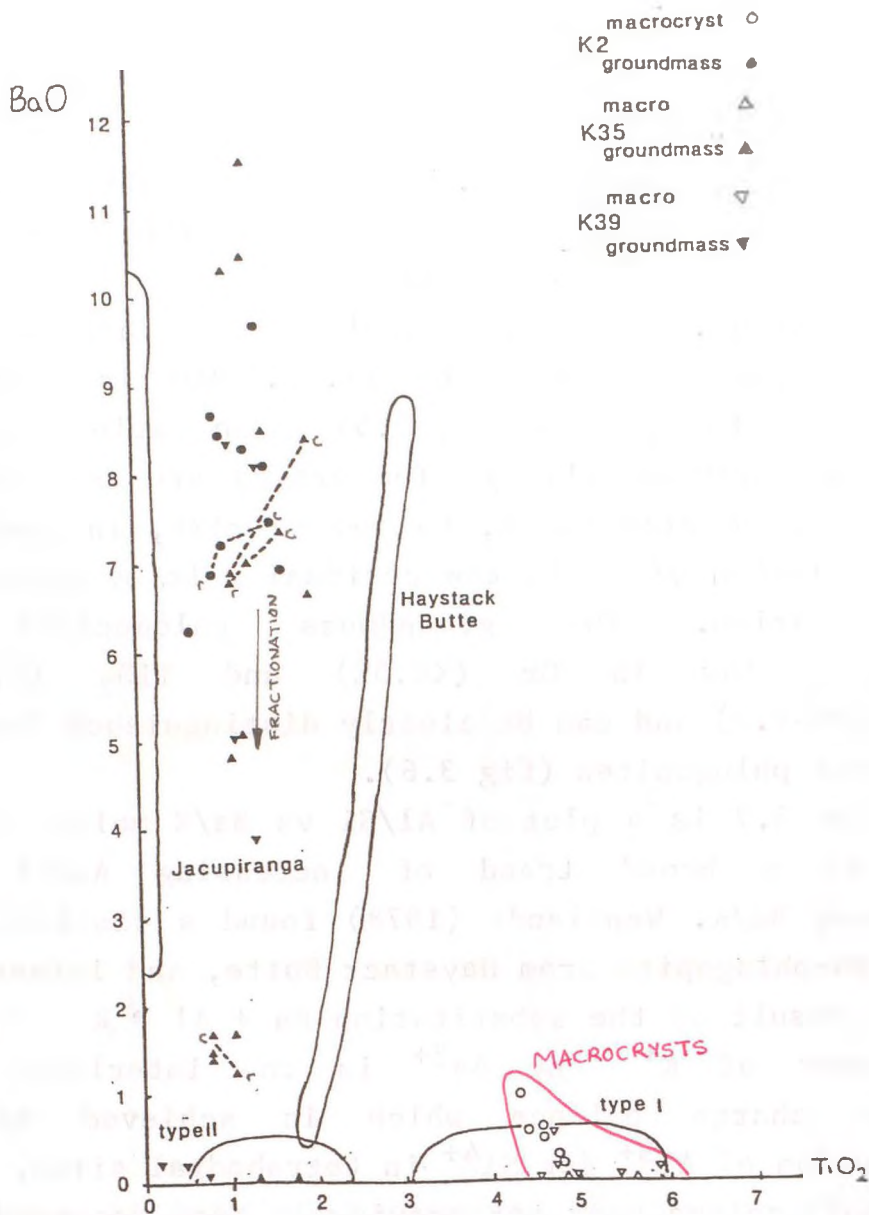


Figure 3.6. BaO v TiO_2 for macrocryst and groundmass phlogopites. Dotted lines join core and rim compositions. High Ba concentration gradients from core to rim in groundmass phlogopite indicates a rapid depletion of Ba from the melt.

crystallized was similar to that from which the carbonatitic phlogopites crystallized. The low Ba end of the fractionation trend coincides with the compositions quoted by Smith et al. (1978) for their type II kimberlite phlogopites. The type II phlogopites are abundant groundmass microphenocrysts with higher mg number, and lower TiO_2 , Cr_2O_3 and Al_2O_3 , than the type I phlogopites. Type II phlogopites have low BaO (<0.5%).

concentrations, in the phlogopites, and subsequent rapid reductions, indicate that Ba was partitioned into the phlogopite more readily than K, indicating that $D^{Ba} > D^K$.

The measurement of partition coefficients is beyond the scope of this work, but it can be roughly estimated by attempting to calculate the composition of the melt at the time of the onset of groundmass phlogopite crystallisation. For this calculation, it is necessary to use certain unconstrained assumptions:

- 1) The kimberlite acted as a closed system on a small scale (10cm) during crystallisation after emplacement.
- 2) The whole rock composition of a sample can be taken as that of a parental melt.
- 3) The order of crystallisation of different minerals is known - as determined from thin sections.
- 4) The proportion of different minerals in a thin section is representative of those in the rock.

Starting with the whole rock composition of K35, mineral compositions were subtracted, in the order of crystallisation, and in proportion to their abundance in the rock. The order of crystallisation is:

Cr-spinel
olivine
olivine + ilmenite
ilmenite
ulvospinel + perovskite
monticellite
phlogopite
calcite

The subtraction of 3% Cr-spinel, 45% olivine, 4% ilmenite, 11% ulvospinel, 3% perovskite and 10%

monticellite (total 76%) leaves a residual liquid that is depleted in Fe, Mg, Ti and Cr. As crystallisation proceeds, the liquid becomes progressively enriched in Si, Al, Ca, volatiles (H_2O and CO_2) and the incompatible elements Ba, Sr and K. Incompatible elements become compatible as soon as phases which host them start to crystallize (eg Nb, Ta and REEs in Perovskite). After about 76% fractionation, the calculated residual liquid is predicted to have a composition containing 35% SiO_2 , >25% volatiles and 10% CaO. BaO is now enriched to about 0.8%.

Phlogopite, monticellite and calcite crystallize from the residual liquid. The ratio of BaO in the Ba-phlogopites (8%) to the BaO in the estimated residual liquid (0.8%) is of the order of 10 to 1. This can only be taken as an order of magnitude estimation of the distribution coefficient of Ba in the phlogopite-fluid system, but it is consistent with the findings of Wendlandt (1978).

The behaviour of K is also important. Norry (pers comm.) suggests that in the high Ca-volatile residual fluid, K could complex to form the kalsilite molecule ($KAlSiO_4$) and effectively reducing its partition into phlogopite. Wendlandt (1978) suggests that because $D^{Ba} > D^K$, the Ba concentration in the phlogopite is simply a function of its abundance in the liquid.

Figure 3.6 indicates that at the onset of phlogopite crystallization, the Ba was rapidly exhausted in the liquid, resulting in the later fractionation of normal phlogopite. The unusual Ba enrichment could be a function of high Ba abundances initially in the liquid, and the effects of the $CaCO_3$ saturated residual liquid on the distribution coefficient of K in phlogopite. This is supported by the observation that lamproites, with high Ba and low $CaCO_3$ do not contain Ba-phlogopite (Nixon pers

comm.). The low Ti, Cr and Fe in these phlogopites is due to the depletion of these elements from the melt by previous spinel and ilmenite fractionation. It is predicted that a detailed search of other calcite kimberlites from other areas will also reveal the presence of Ba-phlogopite in the groundmass.

3.1.2 Whole Rock Geochemistry

The major element composition of the two samples of K35 are very similar (see table 3.1) despite the visible presence of more crustal xenoliths in K35/X than K35/M. The xenolith content is, however, very low, and appears not to have significantly affected the chemistry of the samples. The contamination index (CI) of Clement (1982) for K35/M and K35/X are 1.17 and 1.11 respectively. Clement (pers comm) states that a sample with $CI < 1.3$ is essentially fresh and uncontaminated.

For all major elements, K35 falls within the ranges quoted by Smith et al. (1985) for group I kimberlites, and in element-element plots (eg fig 4.10) can be seen to be a typical group I kimberlite. MgO, at 33%, is at the high end of the kimberlite range, an indication that relatively little fractionation has occurred.

The transition metal abundances in K35 plot within the 'basalt' field of Langmuir et al. (1977), with the exception of Cr and Ni which are enriched in the kimberlite (see fig.3.8). At 1700ppm Cr and 1300ppm Ni ($Ni/V=9.3$), these kimberlites are intermediate between basalts (Cr 300-400 Ni 400-500, $Ni/V=0.5-1.6$) and mantle peridotites (Cr 1500-7000, Ni 1500-2500, Fischer et al. 1969, Nixon et al. 1981, Erlank et al. 1987). Cr and Ni decrease with the fractionation of Cr-spinel and olivine. Vanadium was not detected in either the olivines or spinels, therefore Ni/V and Cr/V ratios can be used as

indicators of fractionation of these phases. Kimberlites have higher Ni, Cr, Ni/V and Cr/V than mid ocean ridge basalts (MORB), but similar abundances of the other transition metals. It is therefore suggested that these kimberlites record less olivine and spinel fractionation than MORB, implying that kimberlite can be regarded as a primitive melt.

K35 contains extremely high concentrations of incompatible trace elements, with steep REE patterns (fig 3.9). The two samples have almost identical compositions, indistinguishable within analytical error ($La/Nb = 0.66-0.68$, $La/Yb_N = 110-120$). The mantle normalized trace element abundances (fig 3.10) are similar to those of other kimberlites (Smith et al 1985, Mitchell 1986) from Southern Africa. The absolute abundances of the trace elements are quite high (La 183ppm, Nb 277ppm), though within the kimberlite range. The characteristic troughs at K and Sr are common to kimberlites. A full discussion of the significance of the geochemistry is deferred to chapter 4, where interkimberlite variations are considered. The important conclusion at this stage is that within the (admittedly limited) sampling, there is no detectable variation in whole rock chemistry beyond analytical error.

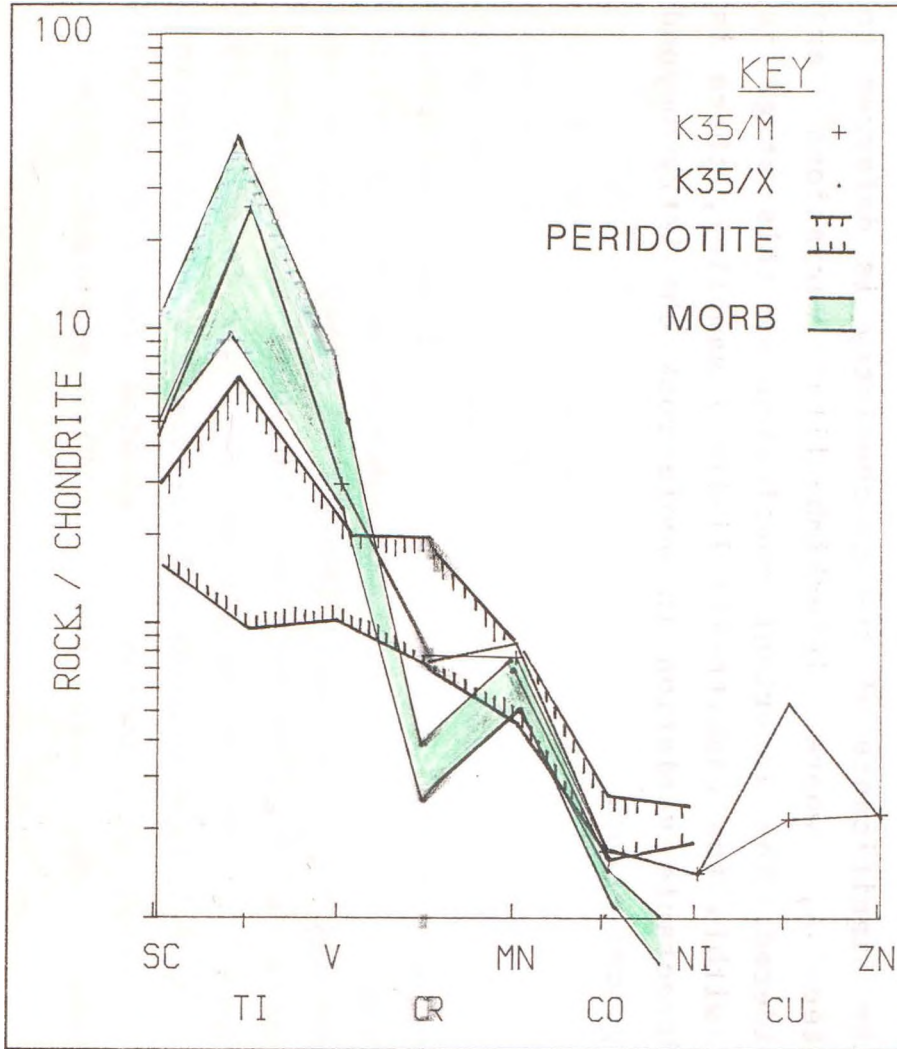


Figure 3.8: Chondrite normalised transition element plot for K35. MORB (Langmuir et al. 1977) and mantle peridotite (Fischer et al 1969, Nixon et al 1981) fields shown for comparison. Normalising values from Langmuir et al. (1977)

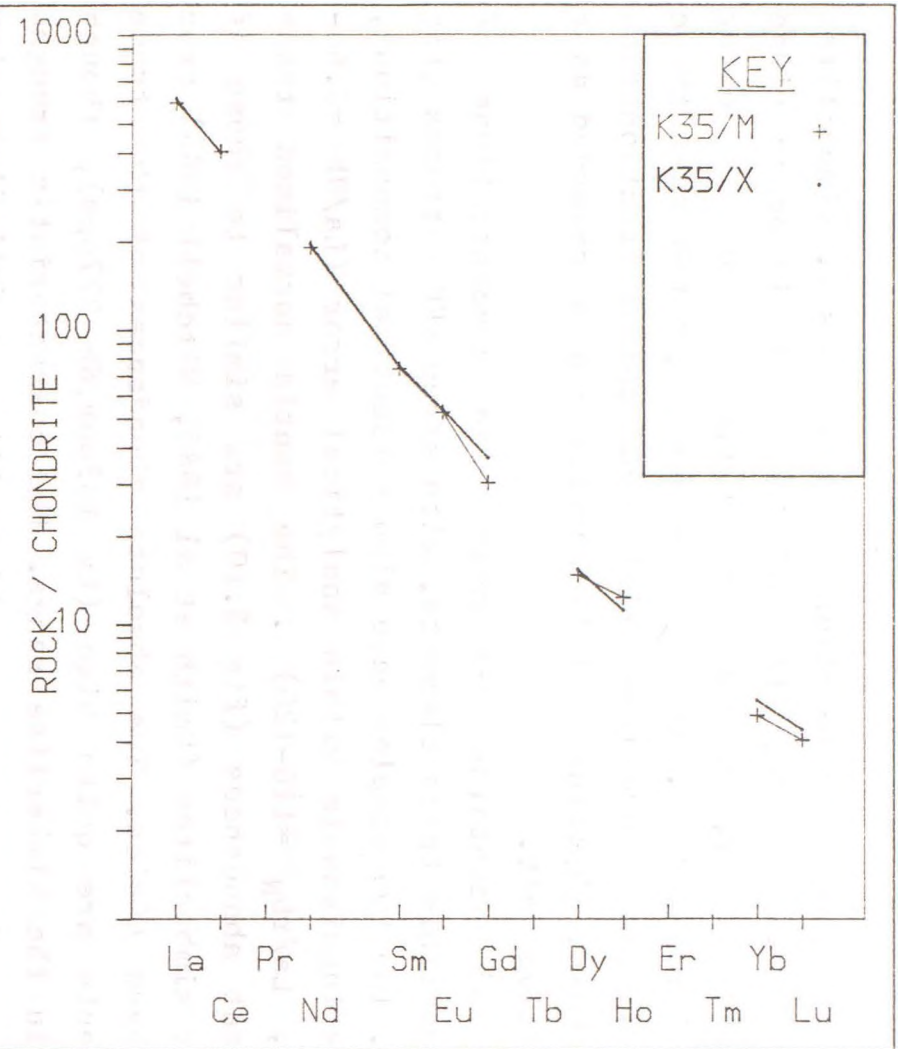


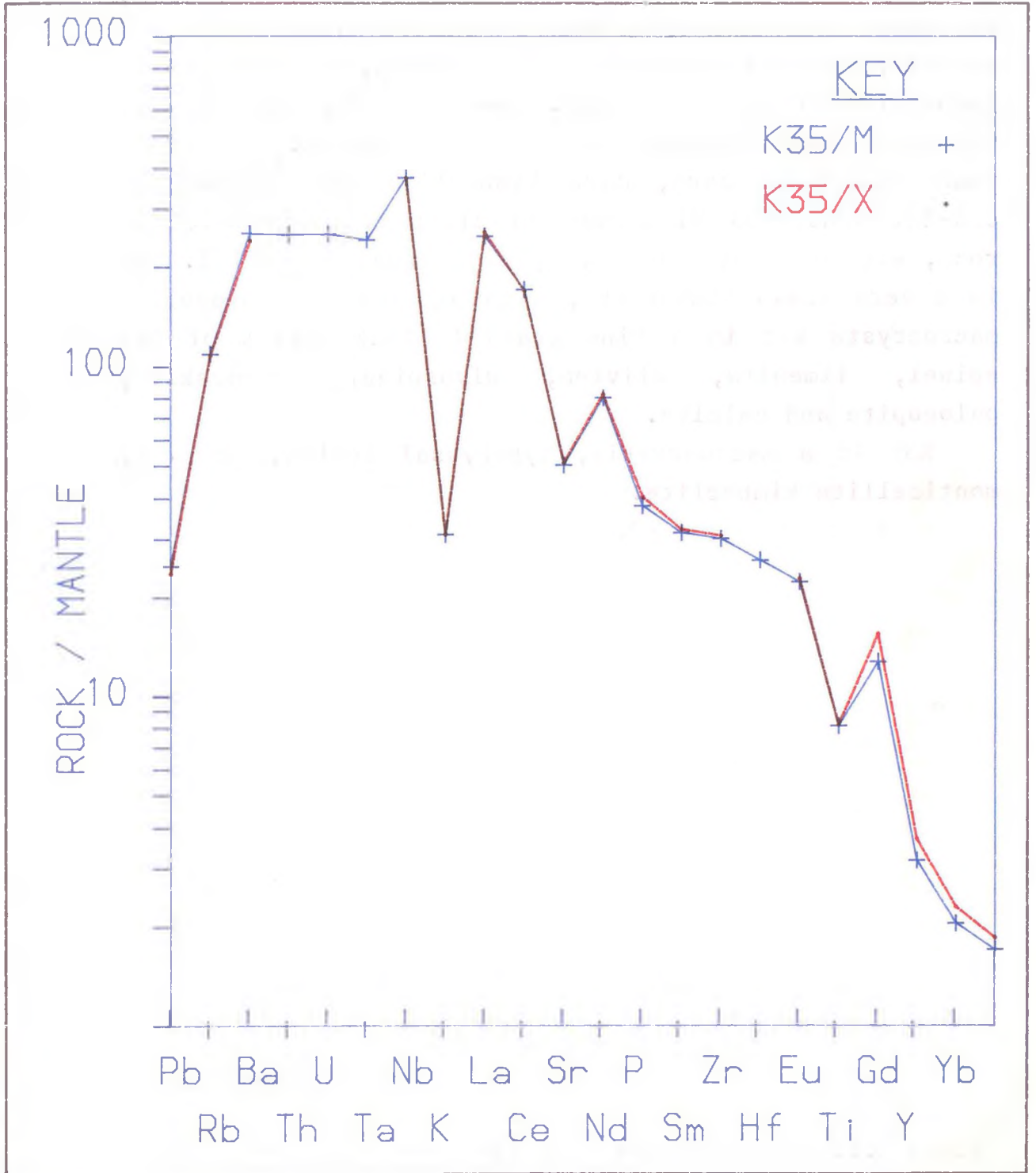
Figure 3.9: Chondrite normalised REE plot for K35. Normalising values from Boynton (1984).

TABLE 3.1: WHOLEROCK KIMBERLITE DATA

	33/K2/W1/M	K2/W1/X	K2/W2/M	K2/W2/X	K2/W3/M	K2/W3/X	K2/3/M	K2/3/X	36/K35/M	36/K35/X	K39/W/M	K39/W/X	K39/1/M
SiO2	33.92	32.95	30.39	29.98	29.73	29.51	31.25	30.99	33.86	32.29	33.46	32.27	31.02
TiO2	1.46	1.47	1.58	1.56	1.55	1.48	1.49	1.44	1.77	1.78	1.27	1.21	1.17
Al2O3	4.26	4.37	4.18	4.15	4.05	4.04	4.29	4.11	3.88	3.05	2.63	3.02	2.59
Fe2O3	8.27	8.27	8.99	8.85	8.56	8.32	8.15	8.01	10.48	10.22	9.98	9.61	9.27
MnO	0.16	0.18	0.17	0.17	0.17	0.19	0.16	0.18	0.17	0.19	0.18	0.19	0.16
MgO	21.93	20.69	23.64	22.65	22.75	21.41	21.73	20.14	30.67	30.30	33.45	29.69	31.69
CaO	14.60	14.39	15.93	16.15	16.42	15.88	15.45	15.84	8.64	8.83	7.04	8.74	8.88
Na2O	1.00	0.94	0.50	0.51	0.58	0.68	0.72	0.98	0.24	0.11	0.11	0.14	0.20
K2O	2.92	2.98	1.93	2.35	2.19	2.19	2.63	2.45	0.86	0.86	0.48	0.52	0.92
P2O5	1.43	1.47	1.30	1.28	1.22	1.21	1.48	1.37	0.80	0.85	1.01	0.99	0.99
L.O.I.	9.56	10.69	10.49	11.99	12.01	12.78	11.75	12.41	8.94	9.36	10.65	11.51	9.80
Cr	1240	1306	1355	1309	1344	1270	1256	1198	1787	1698	1787	1877	1977
Co	52	52	58	55	55	55	54	52	80	82	85	80	77
Ni	795	783	874	804	824	798	772	747	1352	1343	1379	1297	1313
Cu	40	77	39	34	31	68	37	78	25	62	18	47	18
V	359	353	228	201	219	214	279	226	145	145	131	146	138
Sc	38	32	42	37	40	40	37	39	28	25	22	27	30
Zn	74	74	77	78	72	75	74	76	79	77	80	80	81
Rb	146	160	103	126	132	133	140	137	71	70	32.4	40.3	61
Cs	3.6	-	2.15	-	-	-	4.02	-	1.63	-	0.42	-	1.44
Sr	1560	1629	2819	2050	2504	2480	1780	1915	1099	1115	1264	1400	1310
Y	18.5	16.5	16.3	18.6	18.3	18.7	18.9	18.7	15	17.4	18.2	16.1	18.3
Zr	232	250	240	244	237	251	236	252	350	357	278	283	272
Nb	286	290	300	297	301	291	291	285	277	276	300	293	291
Pb	8.54	8.65	8.29	8.02	6.91	7.91	7.72	8.54	5.20	5.13	6.32	6.11	5.59
Ba	2900	3099	3044	2805	2908	2952	2806	2903	1832	1736	1524	1601	2362
U	5.81	-	5.09	-	-	-	7.00	-	5.44	5.03	5.74	-	6.63
Th	27.7	(33)	30.9	(33)	(33)	(33)	28.7	(30)	23.2	(28)	26.2	(30)	25.5
Ta	9.13	-	10.1	-	-	-	9.37	-	10.2	-	10.5	-	9.68
Hf	5.05	-	5.31	-	-	-	5.26	-	8.31	-	6.55	-	6.13
La	204.7	177.2	189.5	190.7	179.4	179.5	176.2	173.6	182.6	187.7	191.4	193.7	193.6
Ce	302.7	301.1	319.1	311.1	302.9	297.4	294.5	289.9	325.5	322.1	344.7	347.5	341.0
Nd	109.8	109.4	113.2	110.0	107.3	106.8	105.8	102.7	113.9	116.7	124.0	123.0	121.6
Sm	14.0	13.8	14.26	14.23	13.87	13.91	13.82	13.16	14.33	14.66	15.93	15.53	15.75
Eu	3.758	3.688	3.848	3.780	3.676	4.093	4.00	3.511	3.840	3.926	4.454	4.068	4.089
Gd	9.170	7.754	7.873	9.380	9.217	9.203	9.088	8.888	7.80	9.461	10.01	8.313	10.11
Dy	4.989	4.968	4.983	4.962	4.880	4.885	4.897	4.877	4.723	4.927	5.071	5.046	5.110
Ho	0.810	0.940	0.930	0.819	0.805	0.830	0.835	0.808	0.884	0.800	0.846	0.939	0.833
Yb	1.375	1.327	1.350	1.350	1.323	1.465	1.435	1.387	1.024	1.148	1.164	1.171	1.150
Lu	0.172	0.171	0.165	0.180	0.178	0.184	0.189	0.195	0.130	0.141	0.148	0.149	0.144
C.I.	1.41	1.44	1.27	1.27	1.34	1.327	1.343	1.44	1.17	1.11	1.05	1.16	1.04
Ni/V	2.21	2.22	3.83	4.00	3.76	3.73	2.77	3.31	9.32	9.26	10.53	8.88	9.51
Ta/Th	0.330	-	0.327	-	-	0.326	-	-	0.440	-	0.401	-	0.380
La/Nb	0.715	0.611	0.632	0.642	0.596	0.617	0.606	0.609	0.659	0.680	0.638	0.661	0.665
(La/Yb) _N	100.4	90.03	94.64	97.20	91.42	82.60	82.78	84.33	120.2	110.2	110.9	111.5	113.5

	K39/1/X	36/K53/M	36/K53/X	33/K4	33/K5	33/K14	36/K43		33/K12	33/K13	36/K12	36/K16
SiO2	31.82	32.78	31.89	32.89	27.03	35.73	38.54	SiO2	31.12	27.84	29.21	29.06
TiO2	1.21	1.75	1.82	1.39	1.76	1.18	2.14	TiO2	3.14	1.55	1.71	2.58
Al2O3	3.04	3.13	3.08	3.16	2.13	6.46	5.43	Al2O3	4.18	2.27	2.15	2.22
Fe2O3	9.63	10.19	10.14	8.90	8.71	7.41	8.24	Fe2O3	12.73	8.17	9.31	8.98
MnO	0.19	0.17	0.19	0.19	0.17	0.15	0.15	MnO	0.19	0.16	0.17	0.19
MgO	29.75	32.48	30.04	26.47	25.37	15.59	21.18	MgO	24.22	26.73	29.65	26.23
CaO	9.49	8.85	8.99	8.39	11.93	10.61	6.09	CaO	10.02	11.73	9.57	11.90
Na2O	0.25	0.08	0.12	0.12	0.20	2.42	0.39	Na2O	0.15	0.03	0.10	0.11
K2O	0.99	0.94	0.88	0.83	0.38	1.73	1.67	K2O	0.41	0.99	0.43	0.17
P2O5	1.06	0.84	0.83	0.81	0.71	0.59	0.23	P2O5	1.04	0.63	0.47	0.99
L.O.I.	10.00	8.62	9.46	12.32	17.81	9.99	13.20	L.O.I.	11.62	16.95	17.22	16.69
Cr	1644	1972	1686	1609	1728	959	1185	Cr	1260	1751	1573	1453
Co	78	82	82	74	70	52	65	Co	87	71	78	77
Ni	1305	1327	1341	1278	1089	578	1054	Ni	871	1171	1261	1072
Cu	49	25	60	43	51	48	69	Cu	58	54	39	50
V	145	148	155	-	-	-	109	V	72	130	102	160
Sc	28	31	23	19.9	16.1	19.6	14.7	Sc	25	26	22	26
Zn	76	76	77	81	55	72	67	Zn	112	52	55	67
Rb	65	71	71	21.5	18.1	79	97	Rb	26	58	15	13
Cs	-	1.58	-	2.71	1.18	5.03	11.3	Cs	-	-	-	-
Sr	1365	1089	1110	805	922	806	496	Sr	679	881	607	897
Y	18.8	17.2	15	12	10	18	16	Y	16	10	11	15
Zr	286	343	354	169	274	190	151	Zr	221	169	251	280
Nb	295	274	274	253	169	186	108	Nb	196	173	145	203
Pb	5.91	5.37	5.24	6.65	-	7.29	9.90	Pb	-	-	-	-
Ba	2420	1967	1840	706	981	1642	922	Ba	1158	1145	1136	1302
U	-	5.44	-	4.60	5.79	4.22	1.45	U	-	-	-	-
Th	(30)	23.8	(16)	26.8	13.4	19.1	7.16	Th	(17)	(16)	(16)	-
Ta	-	10.4	-	8.57	8.76	6.23	6.99	Ta	-	-	-	-
Hf	-	7.91	-	4.00	6.83	4.42	3.95	Hf	-	-	-	-
La	201.9	182.7	172.8	153	102	116	58.7	La	(78)	(68)	(54)	(137)
Ce	357.0	321.2	316.2	283	186	230	106	Ce	(75)	(53)	(31)	(172)
Nd	127.8	116.5	110.7	101	72.4	83.3	41.4	Nd	(49)	(38)	(32)	(81)
Sm	16.02	14.64	13.99	14.0	10.6	11.0	6.25	C.I.	1.42	1.05	1.03	1.18
Eu	4.190	3.850	3.757	3.56	2.87	2.80	1.44	Ni/V	12.10	9.01	12.36	6.7
Gd	10.30	9.411	7.652	-	-	-	-					
Tb	-	-	-	1.00	0.85	1.04	0.62					
Dy	5.261	4.840	4.695	-	-	-	-					
Ho	0.854	0.787	0.871	1.11	-	-	-					
Yb	1.178	1.056	1.119	1.47	0.80	1.40	1.33					
Lu	0.156	0.136	0.138	0.22	-	0.25	0.20					
CI	1.10	1.17	1.10	1.286	1.124	2.34	1.81					
Ni/V	9.00	8.97	8.65	-	-	-	-					
Ta/Th	-	0.437	-	0.320	0.654	0.326	0.976	XRF	Si, Ti, Al, Fe, Mn, Mg, Ca, Na, K, P, Cr, Co, Ni, Cu, V, Sc			
La/Nb	0.684	0.667	0.631	0.605	0.604	0.624	0.543	ICP	Zn, Y, Zr, Nb, Ba			
(La/Yb) _N	115.5	116.6	104.1	70.17	85.96	55.86	29.75	INAA	La, Ce, Nd, Sm, Eu, Gd, Dy, Ho, Yb, Lu			
								ID	U, Th, Ta, Hf, Cs			
									Rb, Sr, U, Pb			
									REE and Th in brackets for XRF analyses			

Figure 3.10. Mantle normalised trace element plot for K35. Normalising values taken from Sun (1988).



3.2

36/K39 BERSEBA RESERVE 6

K39 is located on the Berseba reserve about 1km east of K35. It too is a small pipe some 200x100m in area, weathered to a blue-grey dust at the surface. Occasional severely altered xenoliths were present, including some (crustal) dolerite xenoliths. Four borehole samples were obtained from between 40 and 50m depths. The rock recovered is a hard, dark kimberlite with occasional crustal xenoliths dispersed in clusters throughout the rock, with concentrations varying between 5 and 15%. K39 is a very fresh kimberlite, with olivine and phlogopite macrocrysts set in a fine grained black matrix of Cr-spinel, ilmenite, olivine, ulvospinel, perovskite, phlogopite and calcite.

K39 is a macrocrystic, hypabyssal facies, group I, monticellite kimberlite.

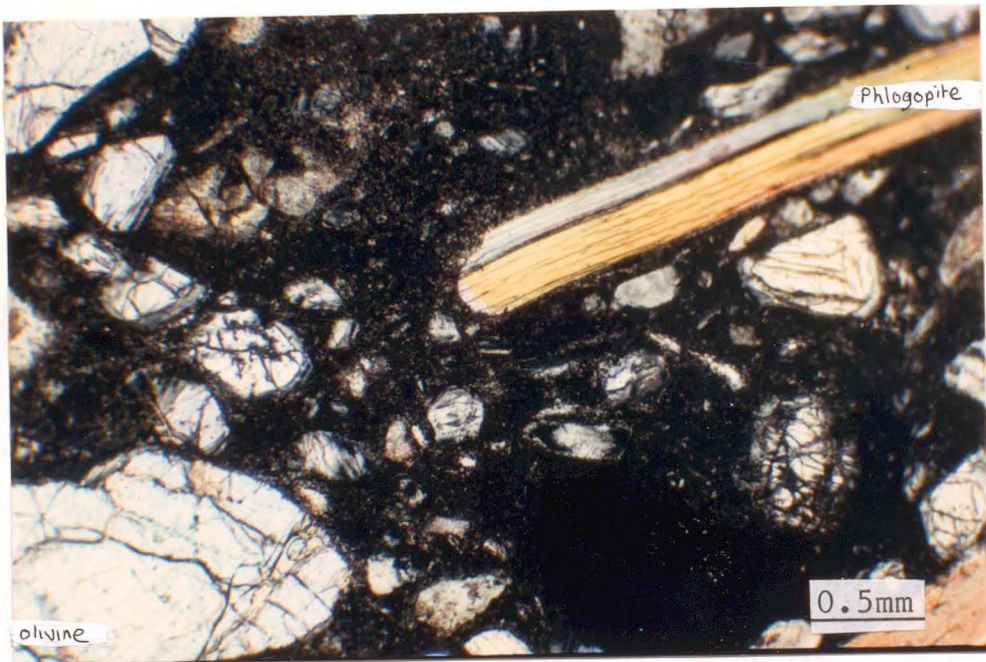


Plate 3.2: Photomicrograph of K39, showing olivine and phlogopite macrocrysts set in a fine dark spinel rich matrix



ETHOS

Boston Spa, Wetherby
West Yorkshire, LS23 7BQ
www.bl.uk

**PAGE MISSING IN
ORIGINAL**

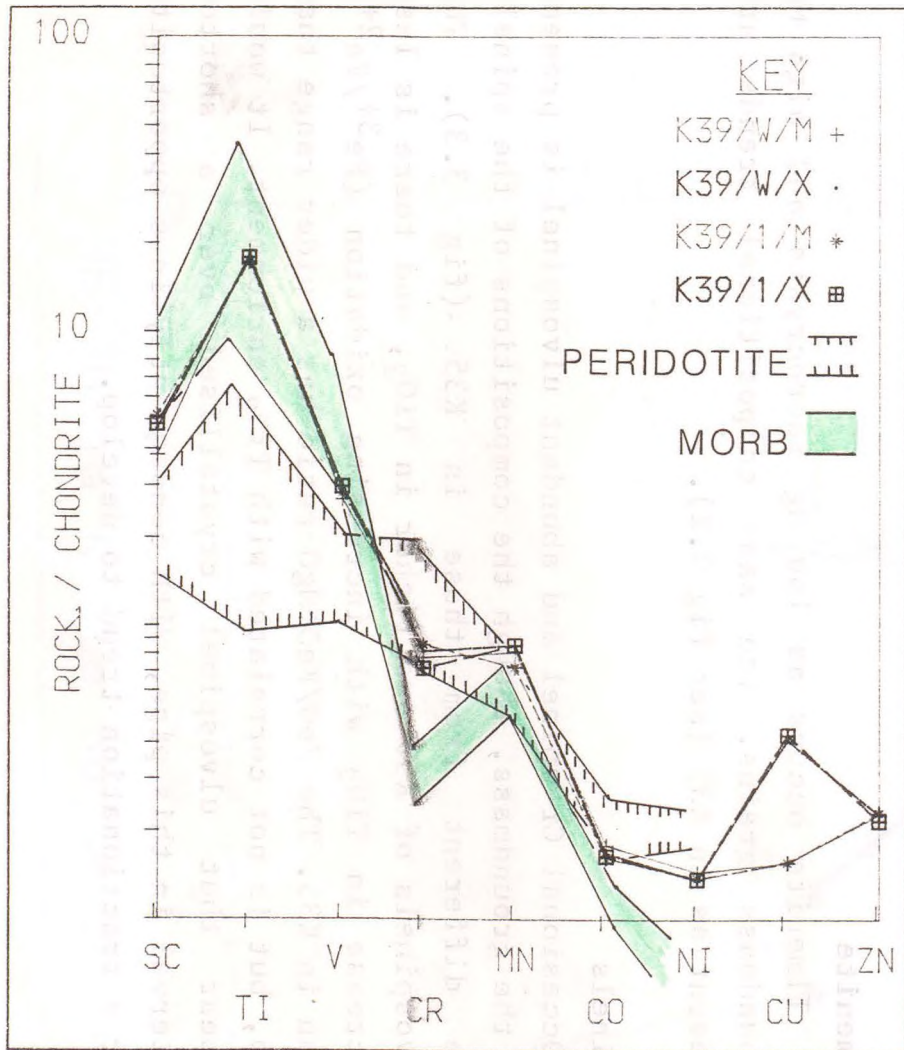


Figure 3.11: Chondrite normalized transition element plot for K39

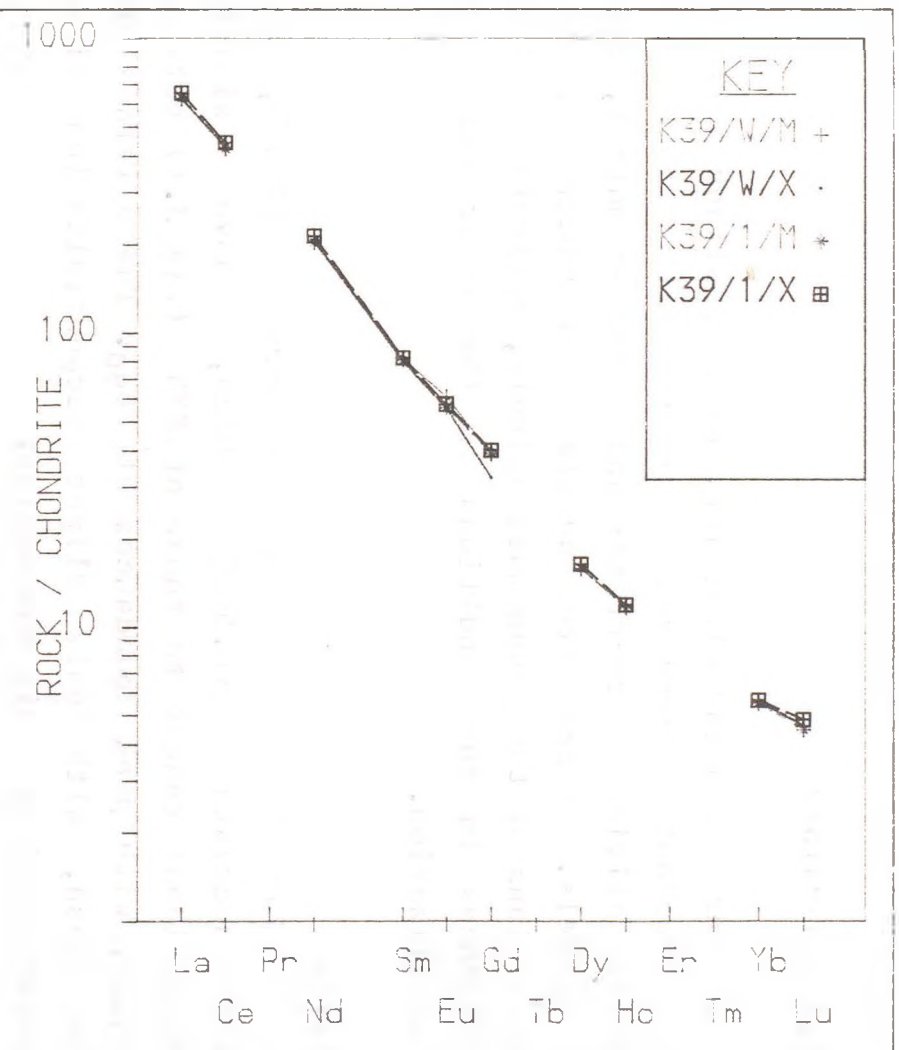


Figure 3.12: Chondrite normalized REE plot for K39.

3.2.1 Mineralogy

K39 has a similar mineralogy to K35, although it has more abundant macrocrystal mica; smaller but more abundant olivine macrocrysts; and a darker matrix, rich in spinels. There are subtle differences in the compositions of the groundmass spinels, reflecting slight differences in the conditions in the later stages of crystallization.

Olivine

Olivine is present as macrocrysts (<6mm), and microphenocrysts (<0.5mm) which, have similar compositional ranges to those of K35 (fig 3.1) between Fo₈₅₋₉₂, with peak abundances at Fo₉₀. The olivines are very fresh, with only slight serpentization along fractures and at grain boundaries.

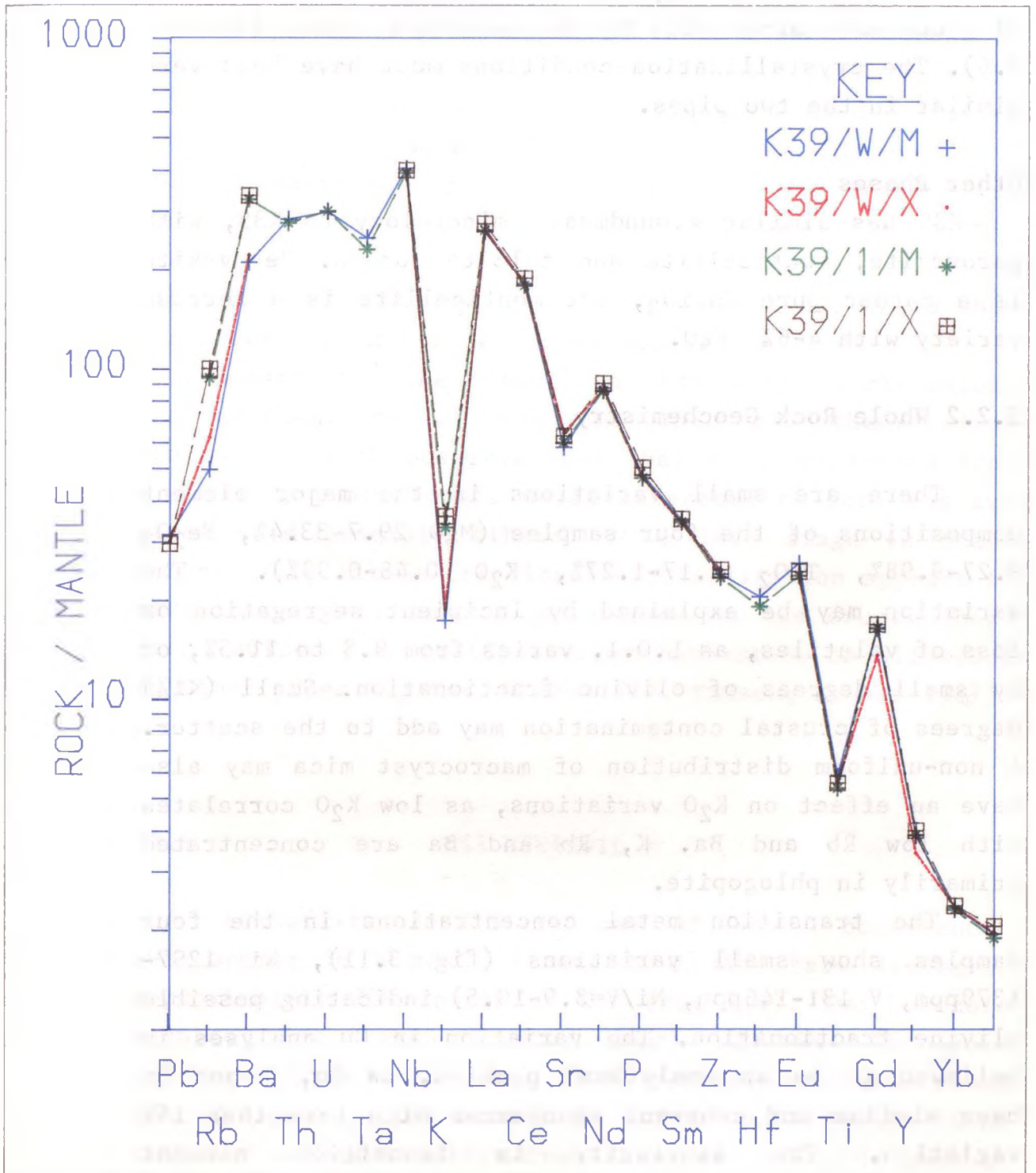
Ilmenite

Ilmenite occurs as low Mg macrocrysts and high Mg groundmass grains. The same compositional trends are present as in K35 (see fig 3.2).

Spinel

Occasional Cr-spinel and abundant ulvospinel is present in the groundmass, though the compositions of the spinels are different from those in K35 (fig 3.3). The ulvospinels of K39 are richer in TiO₂, and there is less decrease in TiO₂ with increasing oxidation (Fe³⁺/Fe²⁺) than in K35. The FeO/FeO+MgO ratio has a wider range than K35, but is not correlated with TiO₂ enrichment. It would appear that ulvospinel crystallised over a shorter interval in this pipe, with consequently less opportunity for a fractionation trend to develop.

Figure 3.13. Mantle normalised trace element plot for K39



Phlogopite

K39 differs from K35 in that it has more abundant macrocrystic micas. There are two types of mica present, as in K35; the high Ti, low Ba macrocrysts; and the low Ti groundmass micas with the Ba enrichment trend (see fig 3.6). The crystallization conditions must have been very similar in the two pipes.

Other Phases

K39 has similar groundmass mineralogy to K35, with perovskite, monticellite and calcite common. Perovskite is a rather pure CaTiO_3 , but monticellite is a ferroan variety with 4-6% FeO.

3.2.2 Whole Rock Geochemistry

There are small variations in the major element compositions of the four samples (MgO 29.7-33.4%, Fe_2O_3 9.27-9.98%, TiO_2 1.17-1.27%, K_2O 0.48-0.99%). The variation may be explained by incipient segregation or loss of volatiles, as L.O.I. varies from 9.8 to 11.5%, or by small degrees of olivine fractionation. Small (<1%) degrees of crustal contamination may add to the scatter. A non-uniform distribution of macrocryst mica may also have an effect on K_2O variations, as low K_2O correlates with low Rb and Ba. K, Rb and Ba are concentrated primarily in phlogopite.

The transition metal concentrations in the four samples show small variations (fig 3.11), Ni 1297-1379ppm, V 131-146ppm, Ni/V=8.9-10.5) indicating possible olivine fractionation. The variation in Cu analyses is believed to be an analytical problem, as Co, V and Sc have similar and coherent abundances with less than 15% variation. The similarity in transition element

abundances between K35 and K39, and in particular Ni, Cr, and Ti suggests that both magmas have been affected by the same amount (ie very little) of fractional crystallisation of olivine and spinels prior to emplacement.

K39 has similar incompatible trace element abundances to K35 (fig 3.13, La = 91-201ppm, La/Yb=111-115, La/Nb=0.64-0.68). All four samples have similar spidergram patterns to K35, with conspicuous troughs at K and Sr. Variations in REE, Nb, Ta, Th, and Zr are less than 4% between the four samples, which is within analytical error. The incompatible elements are very coherent with the exception of K, Rb and Ba, which show variations up to 50%, as noted above.

Considering the remarkable similarity in mineralogy and geochemistry of K39 and K35, and their close proximity, it is possible that they both originated from a common parental magma which separated to form the two pipes (and possibly others) at a late stage in their ascent. Very little fractional crystallisation appears to have taken place before emplacement in the crust. There is no evidence of multiple magma intrusions as witnessed in other pipes (eg Kao, Rolfe 1973, Finsch; Fraser 1987).

3.3 K53 RIETKUIL 7

Kimberlite 36/K53 is one of seven occurrences outcropping in a NE-SW lineation on the farm Rietkuil, approximately 75km north of K35 (fig 2.4). Two borehole samples were taken from a depth of 48m. The rock recovered is a hard, dark, fresh macrocrystic kimberlite containing up to 10% dark shale xenoliths. A great effort was made to use xenolith free material in K53/M, whereas

K53/X is known to contain a few percent shale. These variations are not reflected in Clements contamination index as K53/M has C.I.=1.17, whereas K53/X has C.I.=1.10 and lower SiO_2 , Al_2O_3 and K_2O (see table 3.1).

The kimberlite consists of abundant olivine macrocrysts and phenocrysts set in a fine grained groundmass of perovskite, ilmenite, spinel, monticellite, phlogopite and serpentine. Phlogopite macrocrysts are notably absent, and the groundmass phlogopite is much rarer than in K35. Groundmass spinels are common, and perovskite is particularly abundant. K53 is a hypabyssal facies, group I, macrocrystic, serpentine-monticellite-kimberlite.

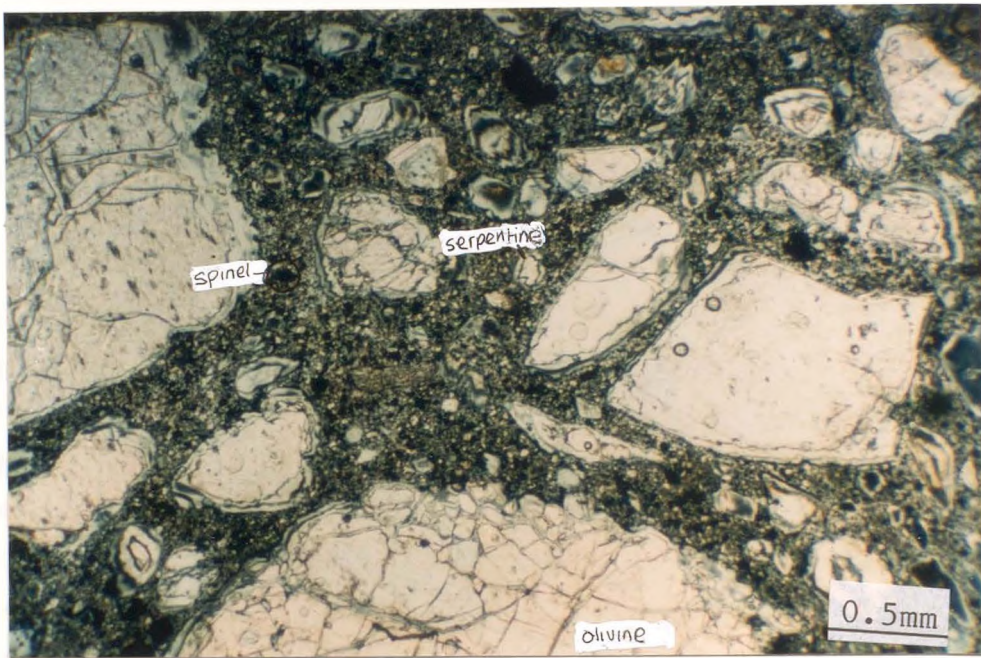


Plate 3.3. Photomicrograph of K53, showing large olivines, and a groundmass including spinels and serpentine

3.3.1 Mineralogy

The mineralogy of K53 is similar to that of K35. The same phases are present (except for the absence of macrocrystic phlogopite and the presence of serpentine)

in both pipes, though their abundances are different and their chemistry is subtly different.

Olivine

The olivine macrocrysts and phenocrysts in K53 have similar compositions to each other and to those of K35 (fig 3.1), with peak abundances at about Fo₉₀. Some olivines have serpentinised margins and fractures, but most are fresh.

Ilmenite

Ilmenite is not abundant in K53, but is present as the low Mg macrocryst and high Mg groundmass forms, as in K35.

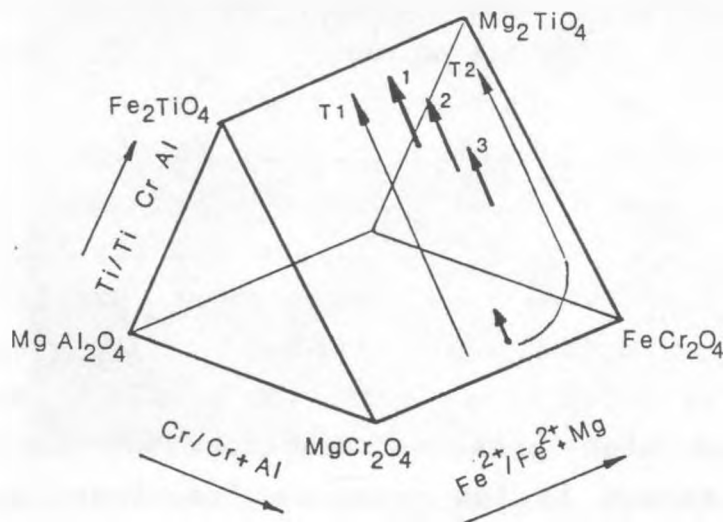
Spinel

Ulvospinel is the most common spinel type, with less abundant cr-spinel. The ulvospinels in K53 have distinctly different compositions to those in K35. The most noticeable difference in composition is the low TiO₂ contents (fig 3.3, 3.4). A TiO₂ enrichment trend is evident, as in K35, but occurs at higher FeO/(FeO+MgO) (fig 3.3). Mitchell (1986) postulates that parallel enrichment trends in spinels at different Fe/Mg (fig 3.14) are produced by a two stage evolution of the magma. The first stage is high pressure fractionation which raises Fe/Mg. The second is low pressure fractionation, during and after emplacement, which occurs at constant Fe/Mg, and results in TiO₂ enrichment, and ultimately to the formation of pure magnetite (the magnetite-ulvospinel trend, Mitchell 1986).

At first sight, it appears that these data support Mitchell's model of two stage fractionation, but a consideration of whole rock geochemistry (section 3.3.3) does not. The Ti content of the whole rock is remarkably

similar in both K35 and K53, indicating that early ilmenite fractionation has not removed Ti from the system. Equally, the similar Mg, Fe and Ni contents of the kimberlites are an argument against early olivine fractionation. The low Ti abundances in the spinels of K35 are balanced by a higher proportion of perovskite. The difference in Fe/Mg in the two sets of spinels still needs explanation. There are two possible explanations of the different mineralogies: 1) It is possible that more prolonged olivine crystallisation at low pressure increased the Fe/Mg ratio in the residual liquid, causing spinels to fractionate at higher Fe/Mg. 2) It is also possible that perovskite fractionation began earlier, perhaps due to higher Ca or lower CO₂/H₂O activity.

REDUCED SPINEL PRISM OF HAGGERTY(1976)



- | | | |
|----|----------------------------|-----------------|
| 1 | K35 K39 | } Mitchell 1986 |
| 2 | K2 | |
| 3 | K53 | |
| T1 | Magnesian Ulvospinel trend | |
| T2 | Titanomagnetite trend | |

figure 3.14 Spinel Prism showing compositional variations

It appears that magmas of the same bulk composition (see below) have crystallized slightly different mineral assemblages. Possible explanations are a difference in (1) pressure and temperature or (2) volatile composition at the time of crystallization. The presence of CO_2 in the melt has an effect on the activity of Ca, which in turn affects perovskite fractionation, and thus the partitioning of Ti. It is possible that (1) the samples of K53 crystallized at higher temperature and pressure than those of K35. As calcite is less stable at higher P and T, the Ca remained in the melt (not migrating into CaCO_3 segregations) and caused enhanced perovskite crystallization, which thus affected the TiO_2 content of the spinels. Alternatively (2), the $\text{CO}_2/\text{H}_2\text{O}$ ratio (not measured) was less in K53 than K35. The melt would therefore have less CaCO_3 , and more CaO, which would also cause enhanced perovskite fractionation.

It is not possible to prove the validity of either hypothesis, though the actions of one or both of them provide an explanation of the spinel compositions that is more consistent with the data than that of early high pressure fractionation. It is notable that calcite is much less abundant in K53, with serpentine present instead.

Phlogopite

Pale groundmass phlogopite is present, but not abundant. The Ba enrichment trend was found in these micas, although no micas were found with more than 3.7% BaO, perhaps due to the low calcite content of the rock (see section 3.1.2). Phlogopite macrocrysts are absent. The simplest explanation for this absence is that phlogopite macrocrysts are in fact xenocrysts and happen to be absent in this rock.. This could explain their variable presence in kimberlites of essentially the same

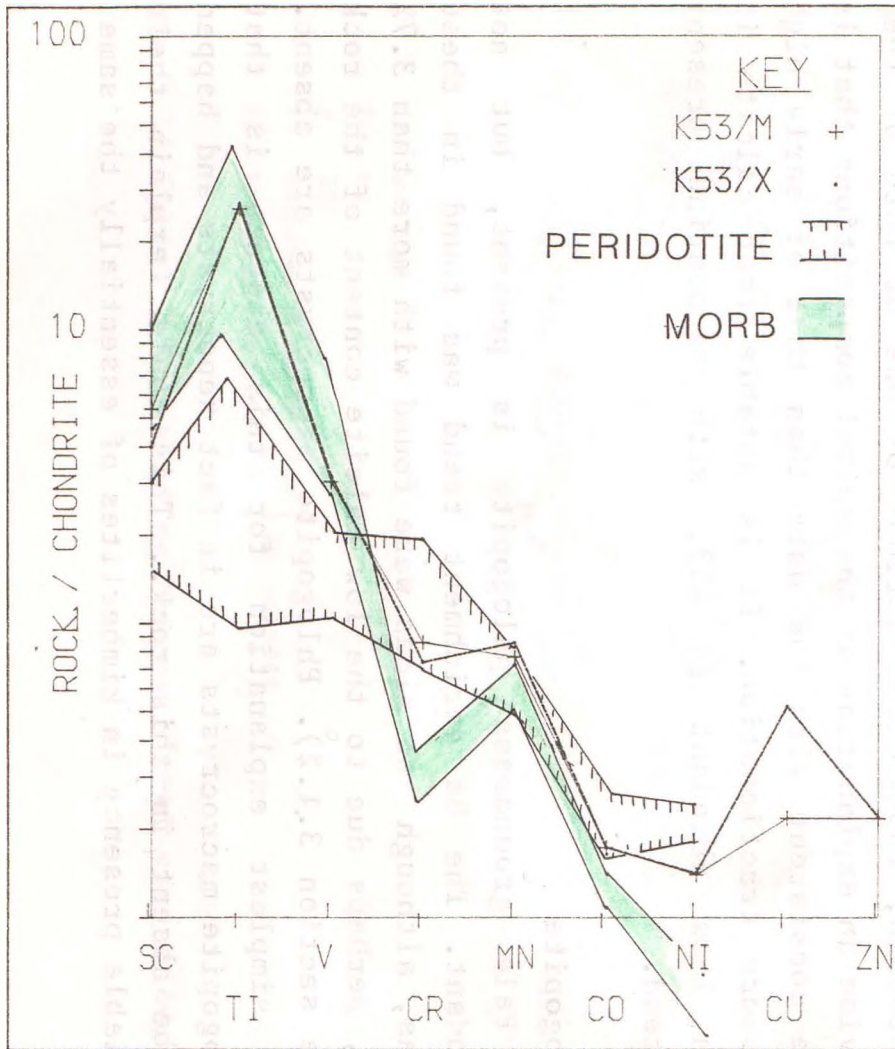


Figure 3.15: Chondrite normalised transition element plot for K53

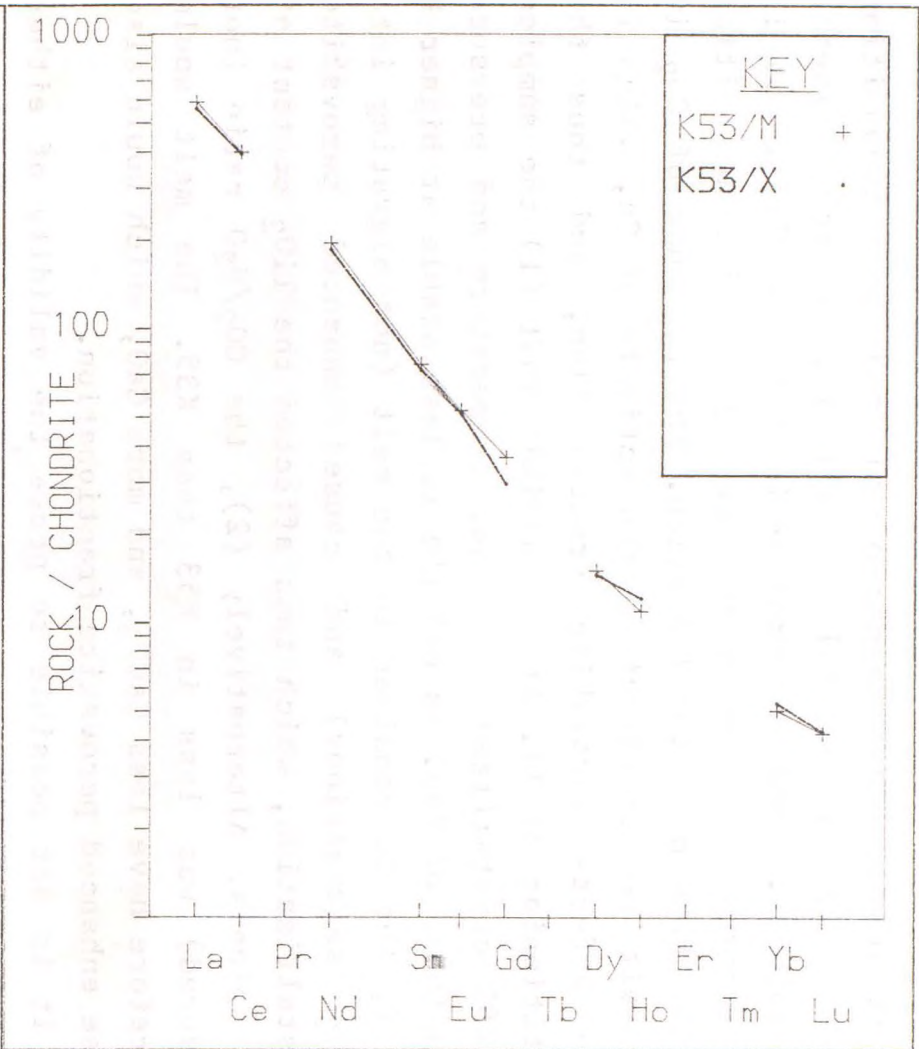
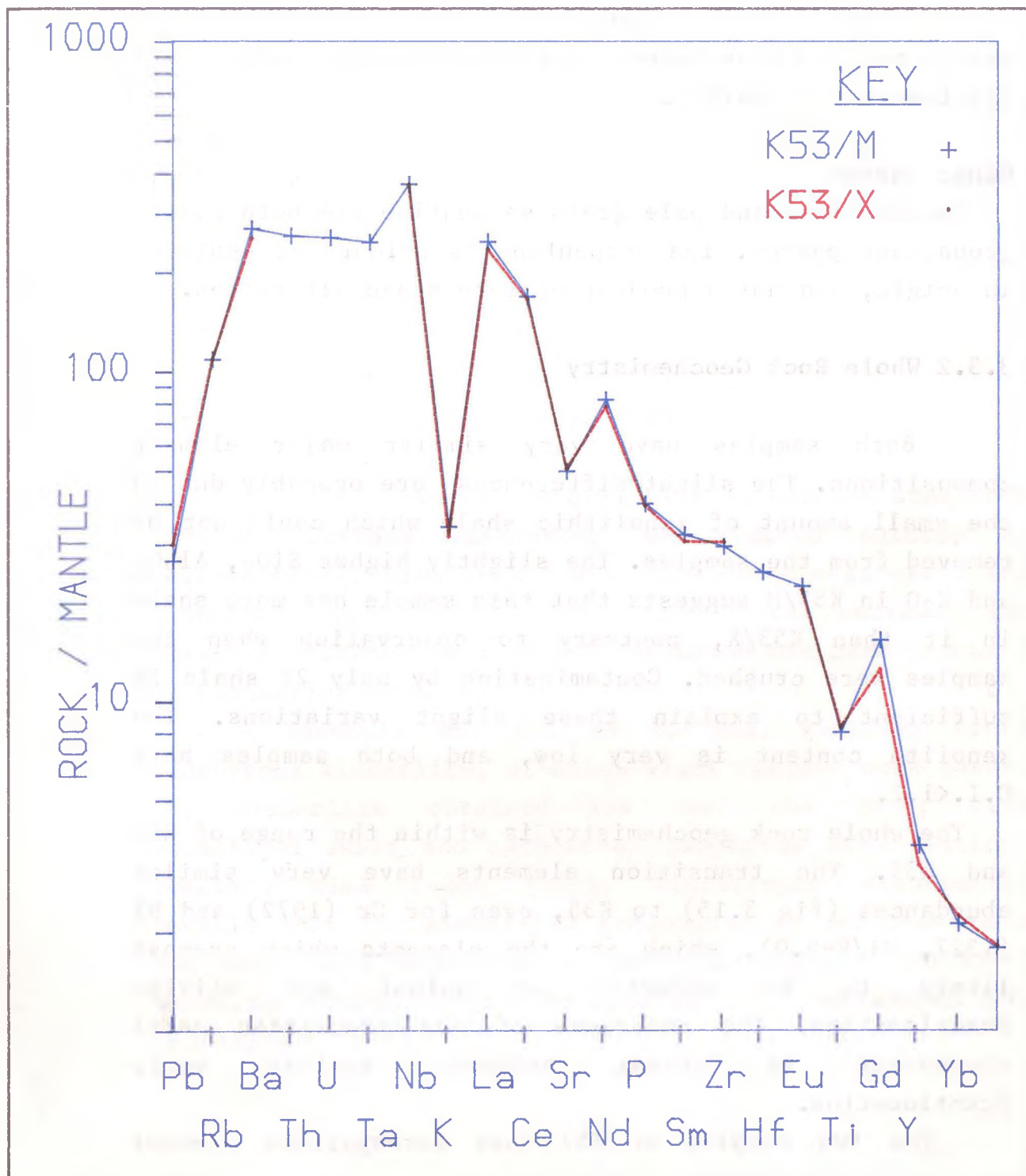


Figure 3.16: Chondrite normalised REE plot for K53.

Figure 3.17 Mantle normalised trace element plot for K53.



composition. It is not readily explained why, if they are phenocrysts, they should be absent in K53, present in K35, and abundant in K39.

Perovskite

Perovskite is abundant in K53, occurring as pseudocubic yellow/brown microphenocrysts which are relatively pure CaTiO_3 .

Other phases

Monticellite and pale green serpentine are both common groundmass phases. The serpentine is primary or deuteric in origin, and not a product of late stage alteration.

3.3.2 Whole Rock Geochemistry

Both samples have very similar major element compositions. The slight differences are probably due to the small amount of xenolithic shale which could not be removed from the samples. The slightly higher SiO_2 , Al_2O_3 and K_2O in K53/M suggests that this sample has more shale in it than K53/X, contrary to observation when the samples were crushed. Contamination by only 2% shale is sufficient to explain these slight variations. The xenolith content is very low, and both samples have C.I.<1.2.

The whole rock geochemistry is within the range of K35 and K39. The transition elements have very similar abundances (fig 3.15) to K35, even for Cr (1972) and Ni (1327, $\text{Ni/V}=9.0$), which are the elements which are most likely to be affected by spinel and olivine fractionation. The coherence of the transition metal abundances is strong evidence against early fractionation.

The two samples of K53 have incompatible element

abundances identical within error (fig 3.17). This is good evidence that the highly enriched kimberlite magma is not significantly affected by small amounts (<<5%) of crustal (xenolith) contamination. The mantle normalized plot (fig 3.17) again has the characteristic 'kimberlite' pattern with steep REE slopes (fig 3.16) and troughs at K and Sr.

Perhaps the most remarkable feature of the chemistry of K53 is its similarity to that of K35 and K39. The major element abundances are very similar, but the trace elements are identical within error ($La/Yb=116$, $La/Nb=0.67$). Interkimberlite variations are discussed more fully in chapter 4.

3.4

33/K2 ANIS KUBUB

Pipe 33/K2 is small and oval with an outcrop area some 100x75m. Surface weathering has reduced outcrop to characteristic blue/grey dust. Some small megacrysts and ultrabasic xenoliths can be found at the surface. Any possible evidence of multiple intrusion has been obscured by weathering effects.

A borehole was drilled to 80m, yielding fresh hypabyssal kimberlite, of which eight samples were taken. The kimberlite obtained was hard and dark, with occasional shale and carbonate xenoliths with distinct reaction rims 1-2mm thick. Microscopic examination reveals that the kimberlite groundmass is affected in a localised halo around each xenolith. The proportion of xenoliths varied between samples up to a maximum of 10% in sample K2/W1/X.

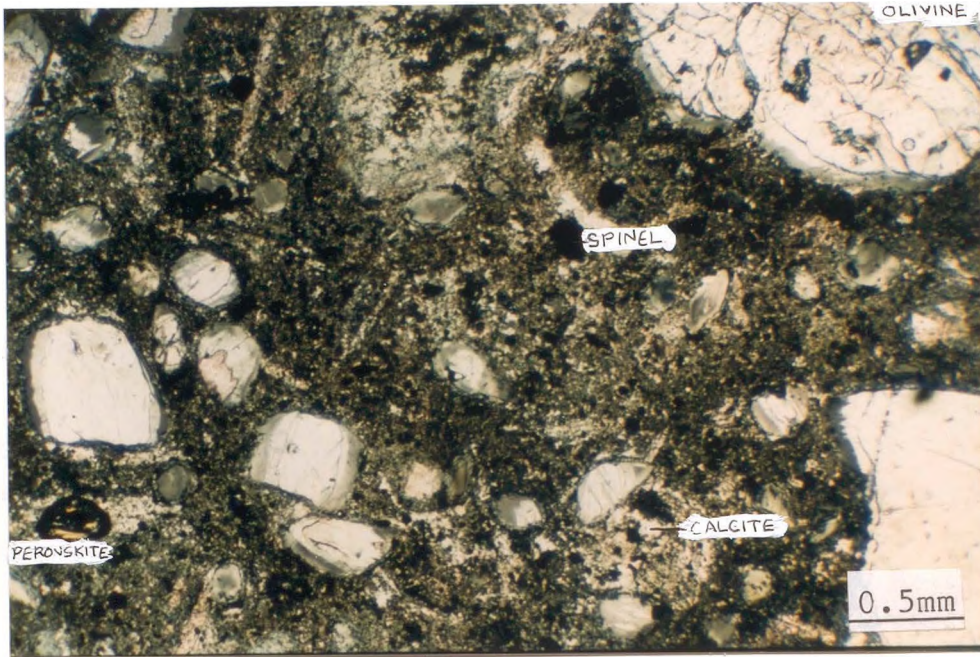


Plate 3.4 Photomicrograph of K2, showing fresh olivines in a matrix containing spinels, perovskite and calcite

The kimberlite consists of olivine and phlogopite macrocrysts set in a dark matrix of olivine microphenocrysts, Cr-spinel, ulvospinel, ilmenite, perovskite, phlogopite, primary calcite, apatite and monticellite. Rare pyroxene and garnet xenocrysts can be found. The rock is exceptionally fresh, with no evidence of alteration except very small patches of secondary calcite. K2 is a hypabyssal facies, macrocrystic, group I phlogopite-monticellite kimberlite.

3.4.1 Mineralogy

The mineralogy of K2 is similar to that of K35, but contains more phlogopite and much less olivine. Spinel has distinctive compositions and apatite is an important accessory mineral.

Olivine

Olivine, which makes up only 15% of the rock is present in two generations: a larger macrocryst type up to 1cm, with irregular shape and fractures, and a smaller (<2cm) subhedral phenocryst generation. The abundance of olivine is conspicuously lower than in the kimberlites described above. The macrocrysts and phenocrysts display the same compositional ranges (Fo₈₅₋₉₁) as the other pipes (fig 3.1). Most grains are unaltered, although some have been serpentinitised, especially along grain fractures.

Ilmenite

Ilmenite is not abundant in K2, but occurs in two chemical varieties, low Mg macrocrysts and high Mg groundmass grains.

Spinel

The spinels in K2 contain a higher proportion of Cr-spinel than the other pipes, though their compositions are similar. Ulvospinel is the common groundmass spinel type, which have compositions distinctive to the pipe. Fig 3.3 shows that the ulvospinels have a trend of increasing Ti at constant FeO/FeO+MgO, similar to the other pipes, but at compositions intermediate between K35 and K53. Using the arguments outlined previously, it is concluded that these compositions are a reflection of the chemical environment at the time of kimberlite emplacement rather than a result of early differentiation. Crystallization occurs over a similar Fe³⁺/Fe²⁺ range as the other pipes, but at intermediate levels of Ti partition into the spinels (fig 3.4).

Phlogopite

Phlogopite is also present in two generations: a larger, brown pleochroic macrocryst type, which is often deformed, and a smaller colourless generation in the groundmass. The groundmass type overgrows spinels poikilitically. The macrocrysts have a high Ti, low Ba composition similar to the type I phlogopites of Smith et al. (1978). The groundmass phlogopites are of the low Ti type with the Ba enrichment trend as described for K35 (section 3.1.2, fig 3.6).

Other Phases

The groundmass also contains perovskite, monticellite, calcite and apatite. The monticellite contains up to 10% FeO, which is a higher figure than any monticellite previously recorded (Mitchell 1986), but as monticellite is a phase rarely studied, no great importance is placed on this observation. Apatite is a rather common phase in the groundmass, more so than in the other kimberlites. It's presence is linked with higher levels of Ca and P in K2. It is a major host for Sr and the REEs (Mitchell 1986). Primary calcite occurs in patches in the groundmass, and is also a host for Sr.

3.4.2 Whole Rock Geochemistry

The eight samples of K2 have fairly uniform major element compositions (with the exception of K_2O and P_2O_5). These compositions, while within the ranges quoted by Smith et al (1985) for group I kimberlites, are distinctly different from those of the above described kimberlites. In particular, MgO (20%) is lower and CaO (30%) and Al_2O_3 (>4%) are higher. These figures may

reflect olivine fractionation (see chapter 4). Xenoliths were generally rare in the samples analysed, but the C.I. varies from 1.27 to 1.44. This is due to lower MgO because of olivine fractionation, rather than crustal contamination. This is supported by the low olivine abundances in thin section. It is not clear exactly when this fractionation occurred as it is possible (Clement pers comm) for 'apparent fractionation' to occur by flow differentiation during emplacement, yielding apparently aphanitic kimberlite.

Transition metal abundances support the inference of olivine and cr-spinel fractionation. There is a noticeable depletion of Ni (747-874, Ni/V=2.8-4) and Cr (1355-1198) relative to K35. Ni and Cr are more variable than Co, Sc, and V (see fig 3.18). This is evidence supporting the removal of olivine and cr-spinel at some stage.

Figure 3.20 shows the incompatible trace element normalised abundances. The REEs (La 173-204ppm, La/Yb=82-100 La/Nb=0.61-0.71), Nb (285-300ppm) and Th (27.7-30.9ppm) show little variation, although some other elements do. In particular, K, Rb, Ba, Sr and P show significant (up to 80%) variations.

The selective enrichment of these elements cannot be produced simply by the removal of olivine and cr-spinel from the system, as this would affect all incompatible elements hosted in the groundmass equally. The presence of greater modal phlogopite may cause increases in K and Rb, but would not cause 1000ppm (80%) variations ^{in Sr} between samples. Equally, higher modal apatite would not significantly increase the Sr and P₂O₅ content without affecting the REE abundances.

Conversely, higher modal apatite and groundmass phlogopite are probably a consequence of the enrichment in P, Sr, Rb, K and Ba. It appears that there is

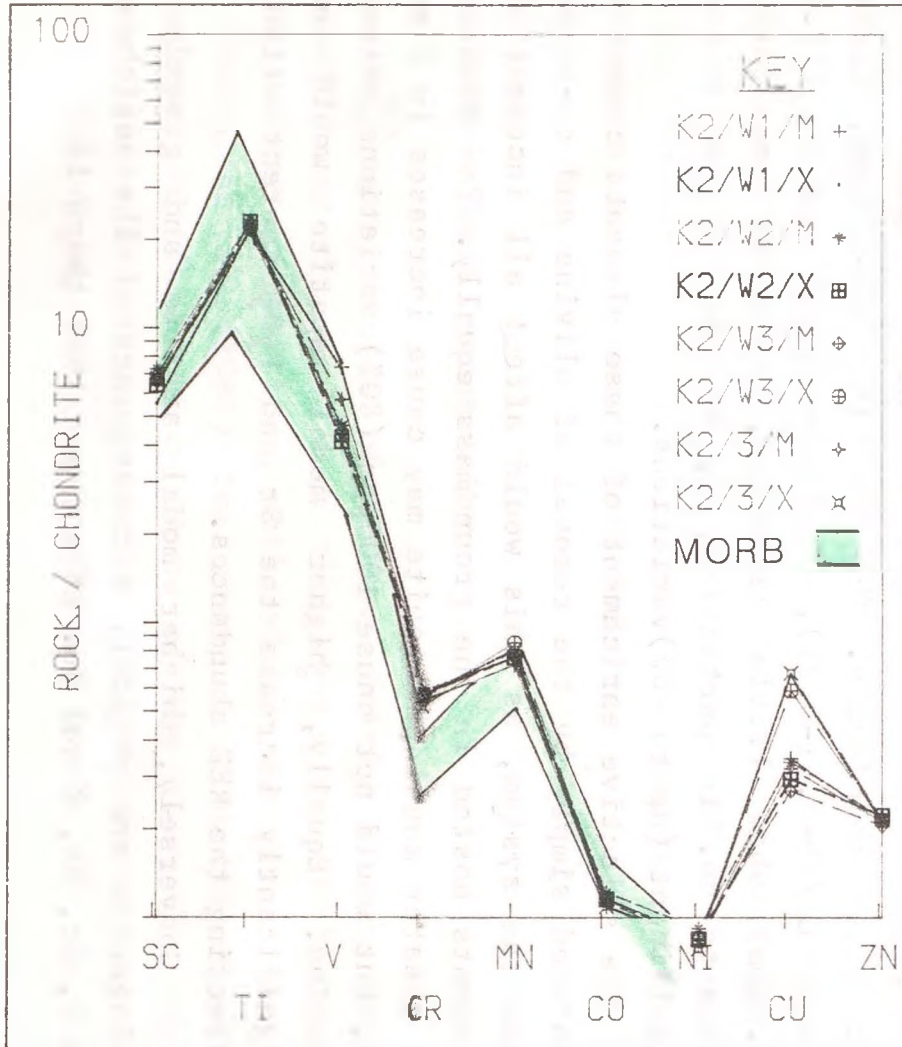


Figure 3.18: Chondrite normalised transition element pl for K2

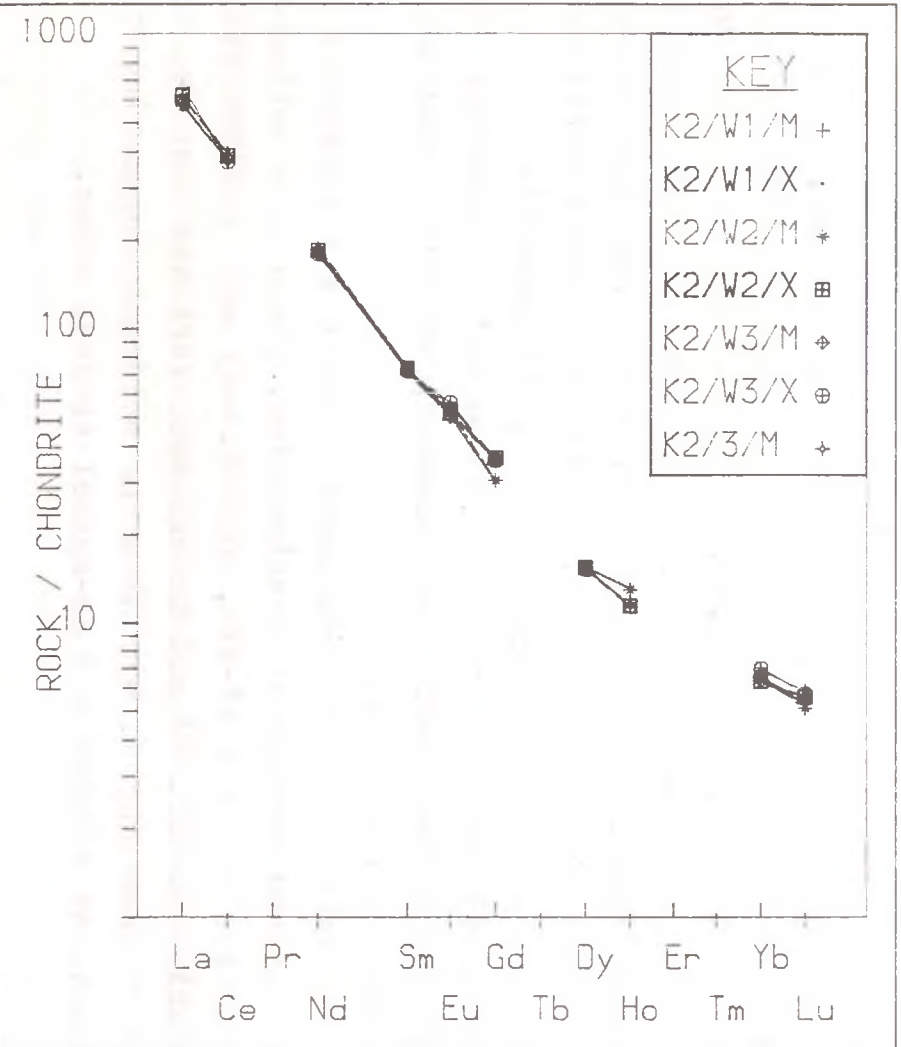


Figure 3.19: Chondrite normalised REE plot for K2.

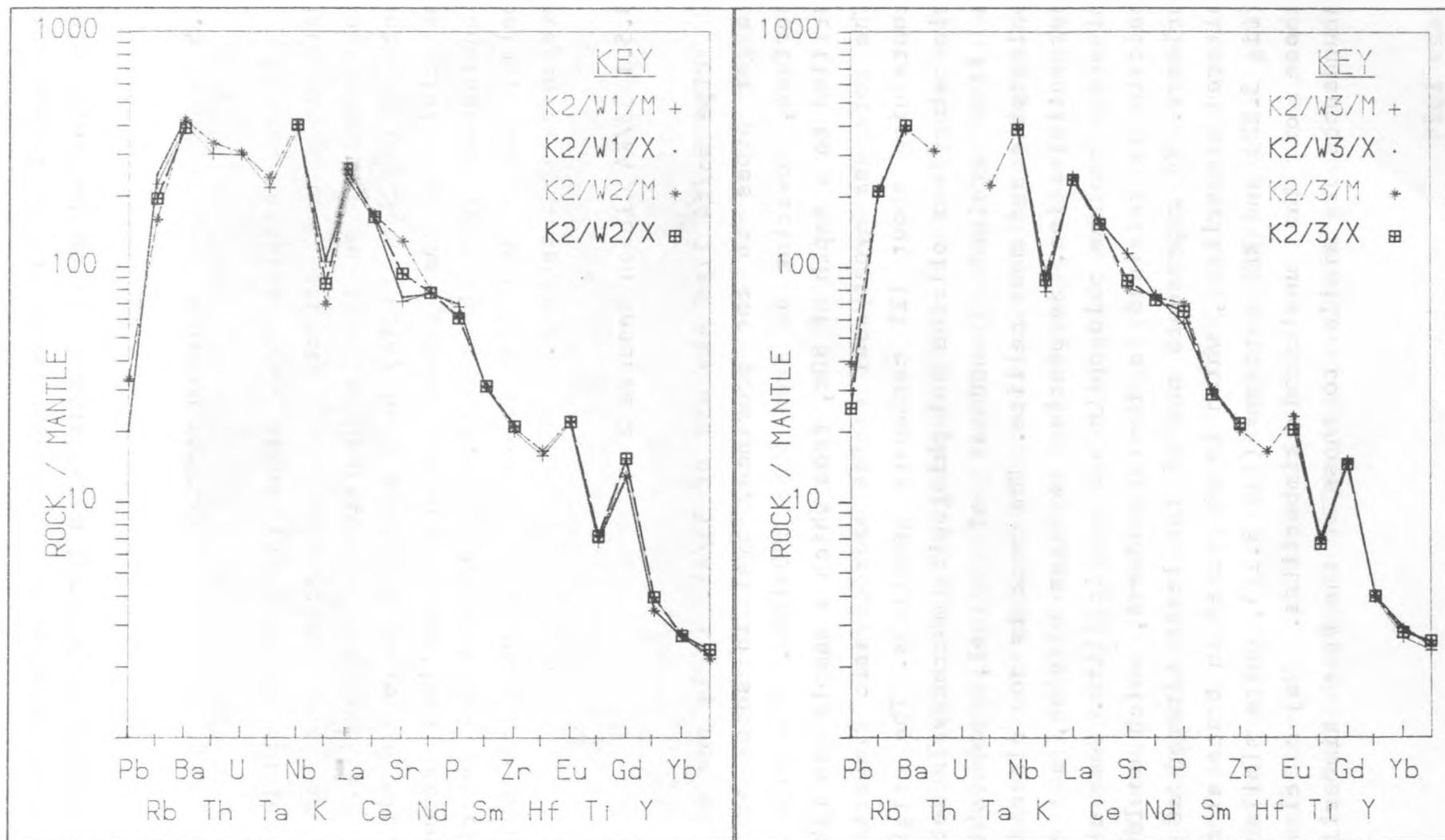


Figure 3.20: Mantle normalised trace element plots for K2

enrichment in certain trace elements, which is independent of the modal abundances of various minerals. This important point is considered further in chapter 4.

3.5 ALTERED SAMPLES

Altered samples from eight pipes were studied to determine the effects of weathering and crustal contamination on the geochemistry of kimberlite. Some authors (eg Jones 1984) have analysed obviously altered material from the surface and drawn sometimes erroneous conclusions from their data. The samples are described below, and a full discussion of alteration effects is presented in chapter 4.

3.5.1 33/K4 Gibeon Reserve 2

Pipe 33/K4 lies 4km WSW of 33/K2. It is one of the larger pipes in the province, oval in shape at the surface, covering an area some 300x100m. The pipe was drilled to a depth of 80m, from which a sample was taken. The core was hypabyssal facies macrocrystic kimberlite, containing about 12% carbonate xenoliths. The original mineralogy was olivine and phlogopite macrocrysts set in a fine grained groundmass of spinel, perovskite, phlogopite and monticellite. The rock is now altered by serpentinitisation. Serpentine replaces olivine, and clay minerals replace phlogopite and monticellite. Some clear calcite is retained in the groundmass, which could be primary. K4 represents one of the least altered of the altered kimberlites, which is reflected in trace element (fig 3.22) and REE patterns (fig 3.21), quite similar to those of the unaltered kimberlites. Major element abundances are similar to those of the fresh kimberlite,

though the volatile content has risen to 12.3%. This rock is taken as an example of incipient alteration, with little crustal contamination, (a conclusion supported by the relatively low C.I. of 1.29)

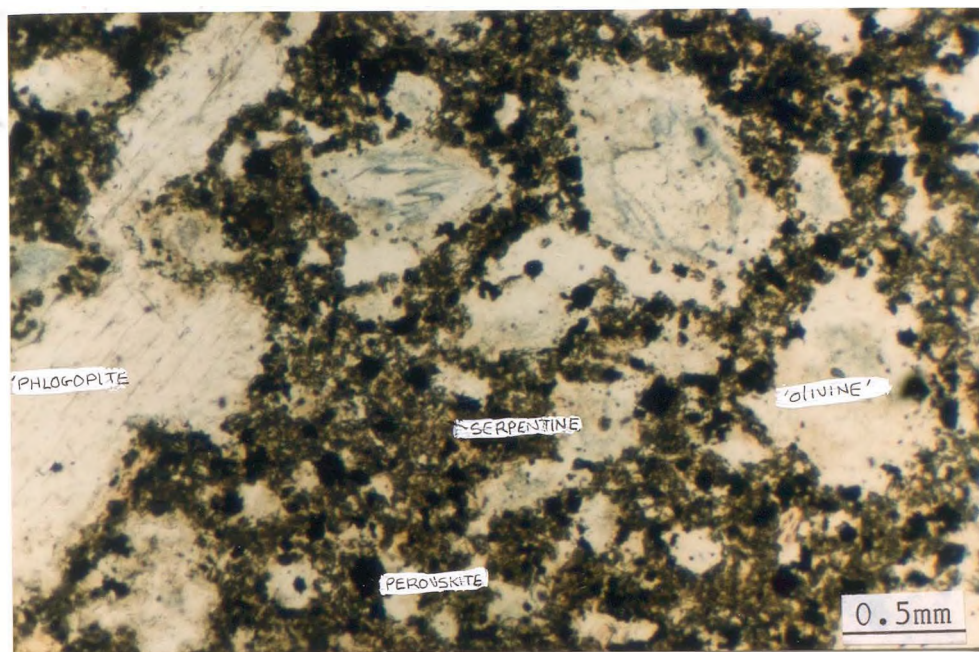


Plate 3.5. Photomicrograph of 33/K4, showing serpentinised olivines and phlogopites, in an altered, serpentinised groundmass.

3.5.2 33/K5 Zaris Sill

The Zaris Sill is located 120km west of the main Gibeon kimberlite province in the 'Zaris cluster'. One sample was obtained, which consisted of clay mineralised hypabyssal kimberlite. The kimberlite is relatively rich in macrocrystic phlogopite which has suffered partial alteration, mainly along cleavage planes. Olivines are serpentinised, and the groundmass has suffered extensive replacement by clay minerals. Calcite segregations appear to have recrystallised to coarse blocky sparite, but perovskite and spinels have survived unaltered. Any original phlogopite or monticellite in the groundmass has

been replaced by clay. Calcite veins are common cutting through the rock.

Xenoliths are not apparent. Despite the abundant phlogopite, the common occurrence of groundmass spinels indicate that this is a group I kimberlite. This rock represents a slightly higher degree of alteration than 33/K4. The contamination index is quite low, at C.I.=1.12, an indication of low crustal contamination.

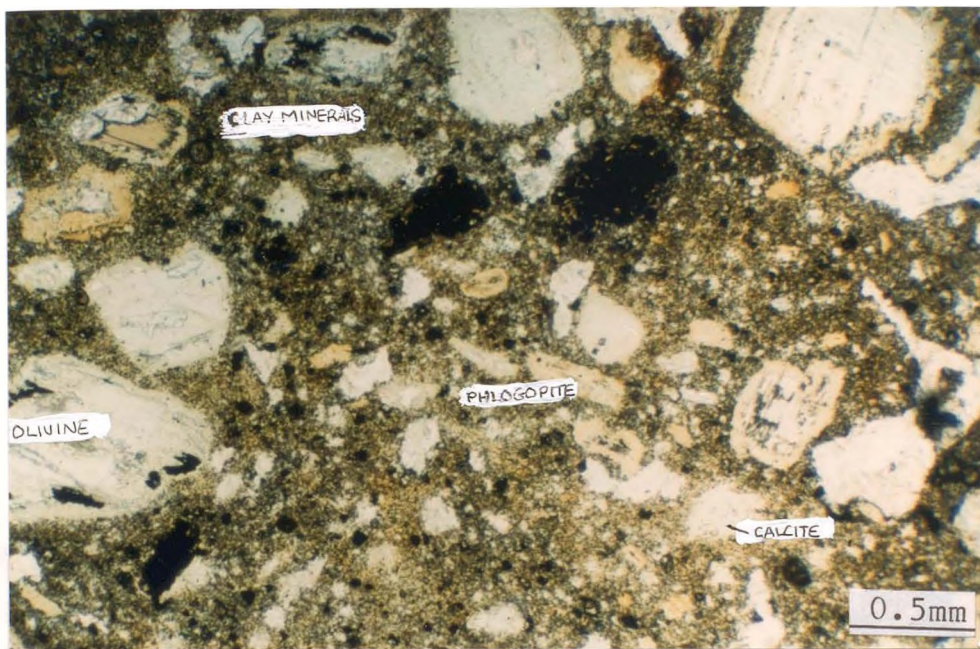


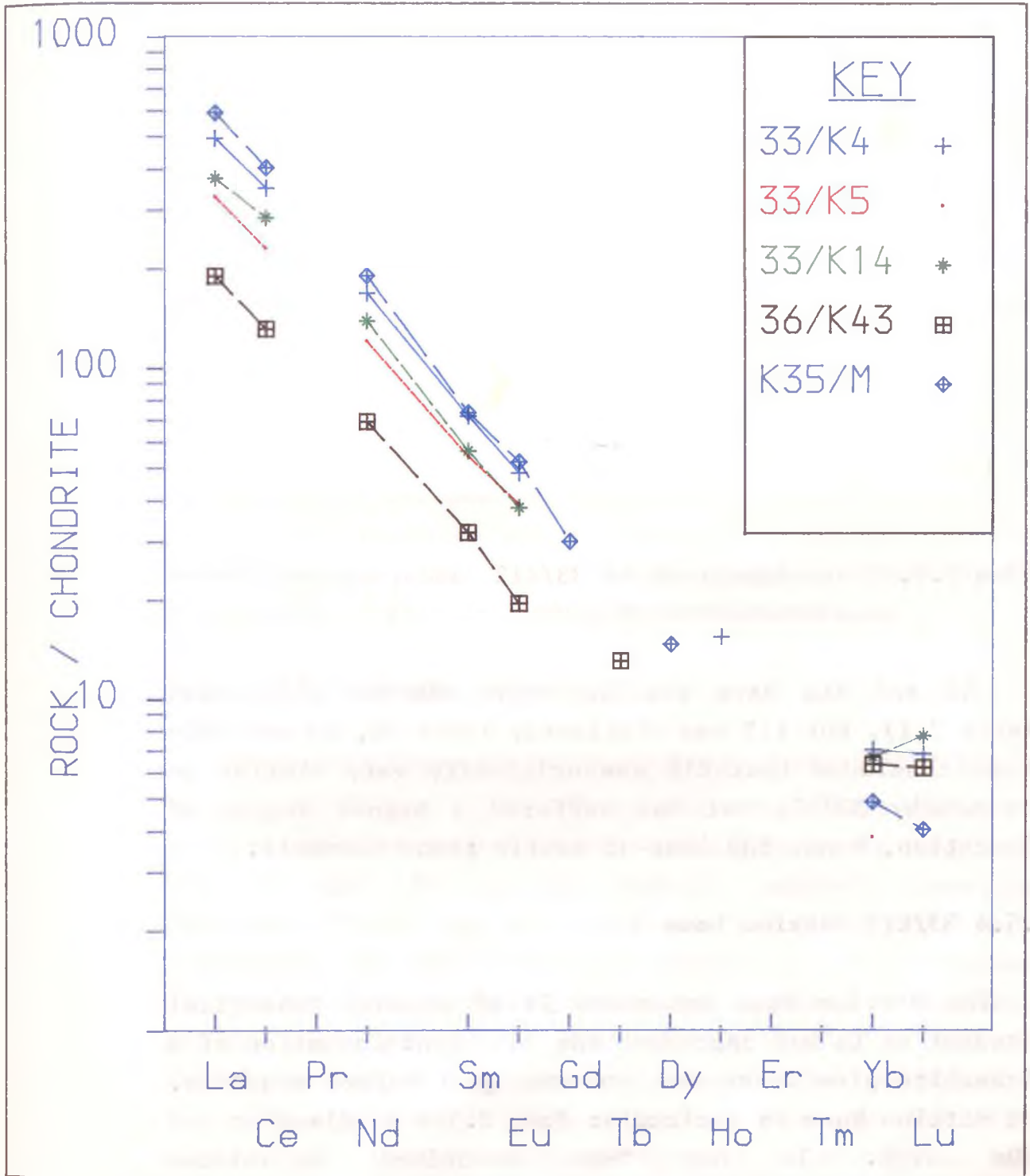
Plate 3.6. Photomicrograph of 33/K5, showing serpentinised olivines in a clay mineralised groundmass, which has secondary calcite patches

3.5.3 33/K12 Uitkoms 4

Kimberlite 33/K12 is a dyke in the Zaris cluster, 5km north of 33/K5. The rock is a hypabyssal macrocrystic kimberlite that has suffered extensive alteration, though there are no crustal xenoliths evident in the sample (hence C.I.=1.03).

The original mineralogy appears to be similar to 33/K5, but extensive chlorite and serpentine alteration has occurred. Large perovskites and spinels have survived, but olivine, phlogopite and (?)monticellite

Figure 3.21: REE plot for altered kimberlites, with K35 shown for comparison.



have been totally altered. From these petrographic observations it is expected that the whole rock chemistry should reflect more extensive alteration, with lower abundances of the more mobile elements.

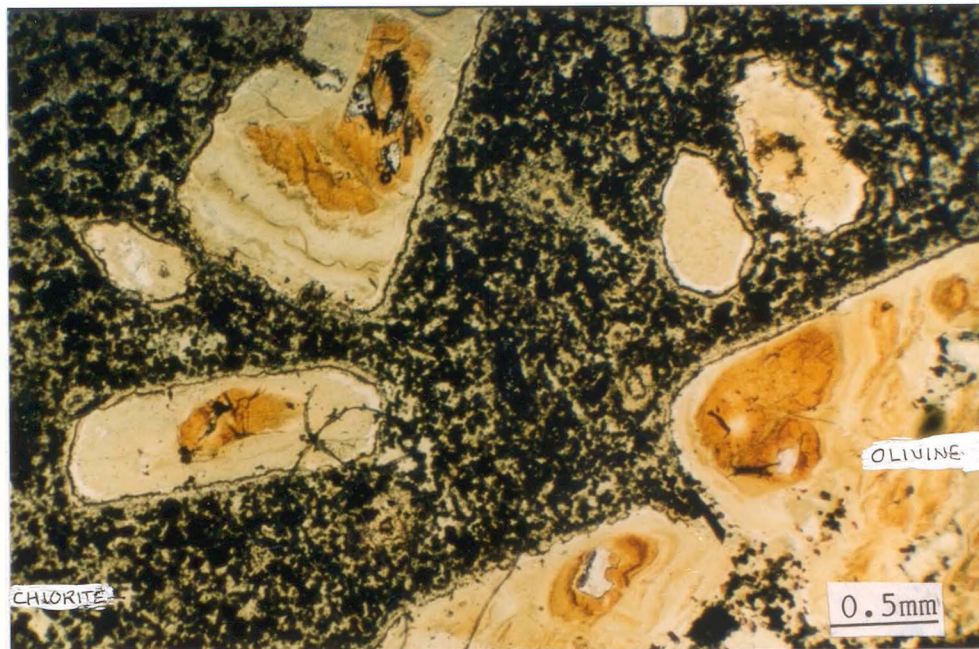


Plate 3.7. Photomicrograph of 33/K12, showing serpentinised olivines and a matrix of chlorite and spinels

K5 and K12 have similar major element abundances (table 3.1), but K12 has distinctly lower Rb, Sr and REEs. It is concluded that K12 was originally very similar to the nearby 33/K5, but has suffered a higher degree of alteration, hence the loss of mobile trace elements.

3.5.4 33/K13 Hatzium Dome

The Hatzium Dome occurrence is of unusual geological interest as it may represent the incipient formation of a kimberlite pipe which was arrested just before eruption. The Hatzium Dome is a circular dome 2.5km in diameter and 200m high. It has been described by Janse

(1964,1969,1975) and compared with the pseudovolcanic feature of Gross Brukkaros (see ch 6) which is a larger upwarped feature with a central crater of brecciated material associated with carbonatite magmatism. The Hatzium Dome consists of upwarped Nama sandstones with no evidence of fragmentation, though it is surrounded by annular faults. Two small (75cm wide) kimberlite dykes outcrop at the top of the dome.

The drill core recovered is altered aphanitic hypabyssal kimberlite. The kimberlite is petrologically similar to others examined, apart from it's aphanitic texture. This is perhaps a feature introduced during the later stages of emplacement as dyke material commonly contains fewer macrocrysts than adjoining pipes. The groundmass assemblage consists of spinels, perovskite, olivine, apatite, monticellite and calcite. Alteration has taken place in the form of calcite, chlorite and serpentine replacement.

Crustal xenoliths are not evident in the sample. This kimberlite therefore, is another example of altered, but not greatly crustally contaminated kimberlite.

3.5.5 33/K14 Gibeon Reserve 3

Kimberlite 33/K14 is located near the Fish River, between 33/K2 and 33/K4. Their close proximity favours a genetic relationship between these pipes, as suggested for K35 and K39 (section 3.2.3). Borehole core was recovered from 75m, but consisted of chlorite-altered hypabyssal kimberlite breccia containing 15% xenoliths. The rock had an original mineralogy similar to K2, with olivine and phlogopite macrocrysts, in a perovskite, spinel, phlogopite, calcite and monticellite groundmass.

The groundmass has suffered extensive chlorite alteration, though many phlogopite macrocrysts were

relatively fresh. The high xenolith content includes dolerite and shale fragments. The wholerock chemistry is therefore expected to be affected by both alteration and crustal contamination. This explains the C.I. of 2.34, and high K_2O contents despite relatively low concentrations of REEs and other incompatible trace elements. The transition elements are mostly unaffected by slight alteration as they are hosted by spinels which are relatively resistant to weathering. Ni, however, is quite low in K14, perhaps lost during the breakdown of olivine.

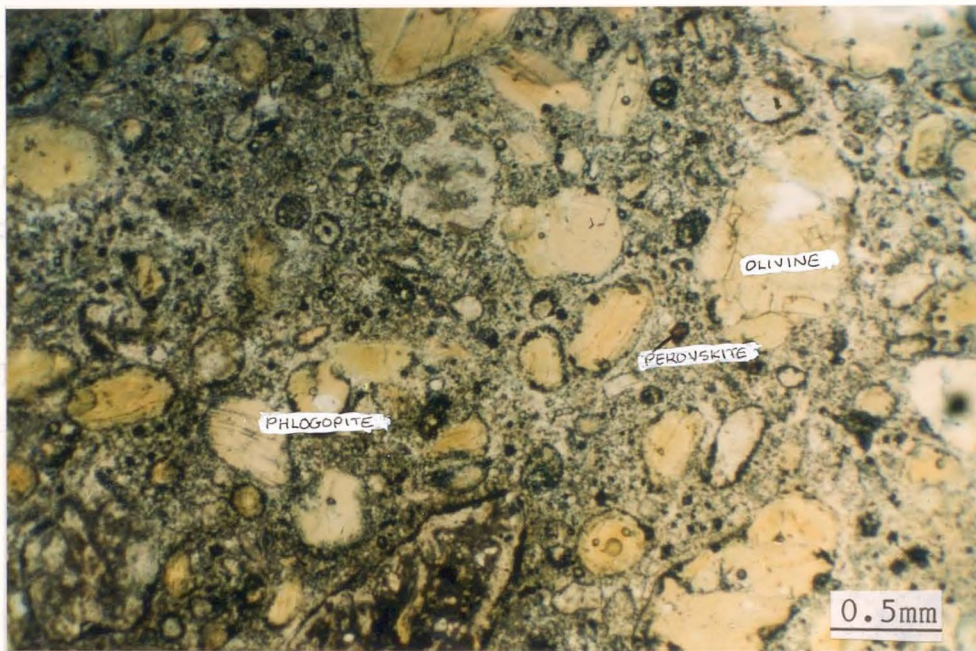


Plate 3.8. Photomicrograph of 33/K14, showing chlorite altered olivines, in a highly chloritised groundmass. Phlogopite is abundant

3.5.6 36/K12 Hanaus 2

Pipe 36/K12 is located in the middle of the Gibeon kimberlite province. It is oval in shape, covering an area of 120x100m at the surface. It is located 2.5km from the larger Hanaus 1 pipe which has multiple intrusions of kimberlite magma. Large megacrysts are common at Hanaus 1 (see ch 5) but unfortunately the pipe is of diatreme

facies at the surface. The nearby Hanaus 2 pipe yielded hypabyssal material, which unfortunately is altered.

The rock is a macrocrystic monticellite kimberlite with olivine and phlogopite macrocrysts set in a matrix of perovskite, spinel, calcite and apatite. Secondary calcite veins are common, and much of the groundmass is replaced by calcite and chlorite. Crustal xenoliths (10-20%) are common. This rock has suffered rather severe alteration, which is reflected in its relatively low concentrations of mobile trace elements and high volatile content (17.2%). A surprisingly high MgO content (29%) results in a C.I. of 1.03, which does not reflect the crustal xenolith content of the rock.

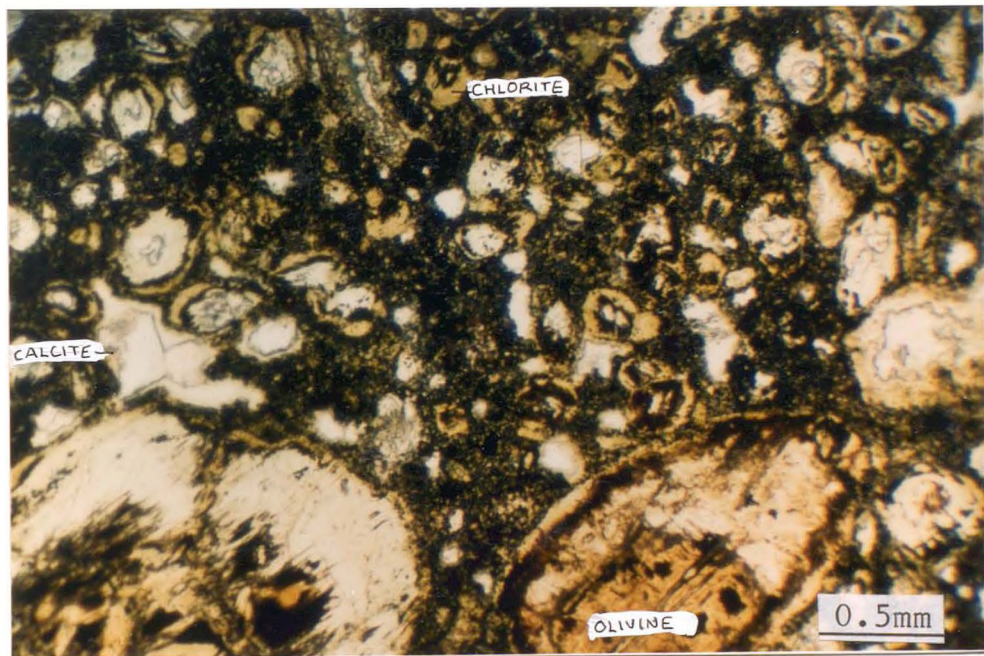


Plate 3.9. Photomicrograph of 36/K12, showing highly altered (chloritised) olivines, and a matrix altered to calcite and chlorite

3.5.7 36/K16 Deutsche Erde 1

Kimberlite 36/K16 is one of two pipes on the farm Deutsche Erde, from both of which megacrysts were recovered. It was therefore desirable to obtain fresh hypabyssal kimberlite from these pipes, to test the

theories of their cogenetic origin (see chapter 5). The larger pipe (36/K17) was of the diatreme facies, but K16 yielded hypabyssal kimberlite which unfortunately was severely altered.

The kimberlite is macrocrystic, containing some large partially chloritised phlogopites, and the matrix has been obliterated by calcite and chlorite replacement. Crustal xenoliths are present but not abundant.

The whole rock chemistry of this kimberlite reflects it's alteration: high volatile content (16.7%) and low mobile trace element concentrations relative to the fresh kimberlites.

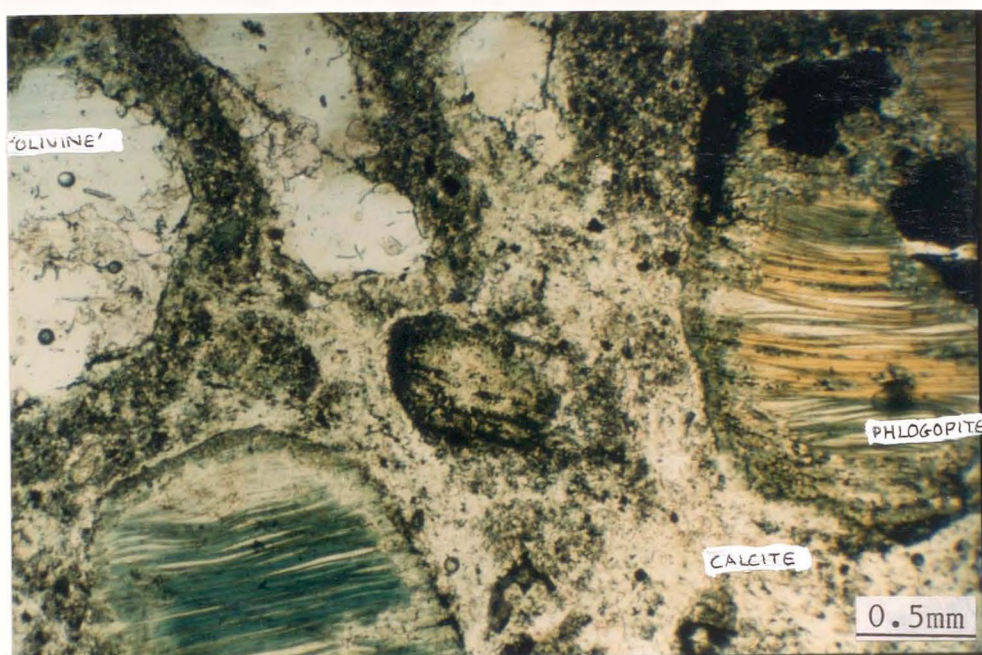


Plate 3.10. Photomicrograph of 36/K16, showing chloritised phlogopite and olivine macrocrysts, with a calcite replaced groundmass.

3.5.8 36/K43 Berseba Reserve 10

Pipe 36/K43 is situated some 7km NW of K35. They are both in the same cluster, so a combined study of K43 and K35 may be useful to demonstrate the effects of weathering on these kimberlites.

A borehole was drilled to 70m, and a sample was taken from a depth of 66m. The rock is altered hypabyssal facies macrocrystic kimberlite containing up to 12% shale and carbonate xenoliths. The original mineralogy was similar to K35, with olivine and phlogopite macrocrysts in a matrix of phlogopite, olivine, spinel, perovskite, calcite and possibly monticellite. The olivines are now completely serpentinitised, and the groundmass has been altered to serpentine and clay minerals. Patches of secondary calcite have the shape of calcite segregations, indicating a possible incipient segregatory texture in

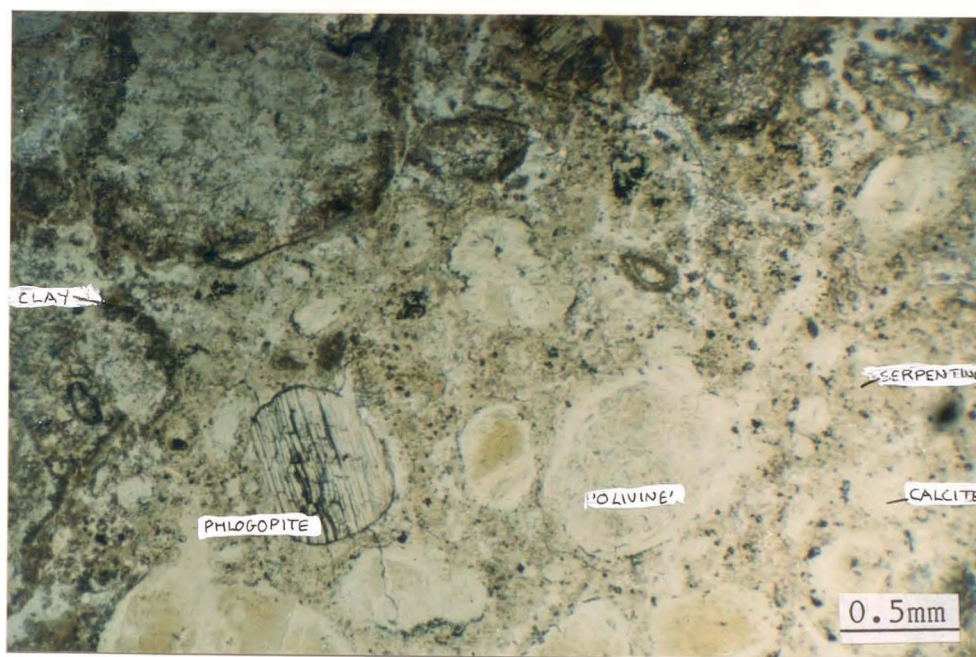


Plate 3.11. Photomicrograph of K43, showing - serpentinitised olivine and phlogopite macrocrysts set in a matrix of secondary calcite, clay and serpentine.

the original rock. Phlogopite macrocrysts are often still fresh, though calcite is common along cleavage planes.

K43 represents an incrementally higher degree of alteration than K4, K5 and K14 (above). This is reflected in it's wholerock geochemistry. The incompatible elements have lower abundances (fig 3.22) than the other pipes.

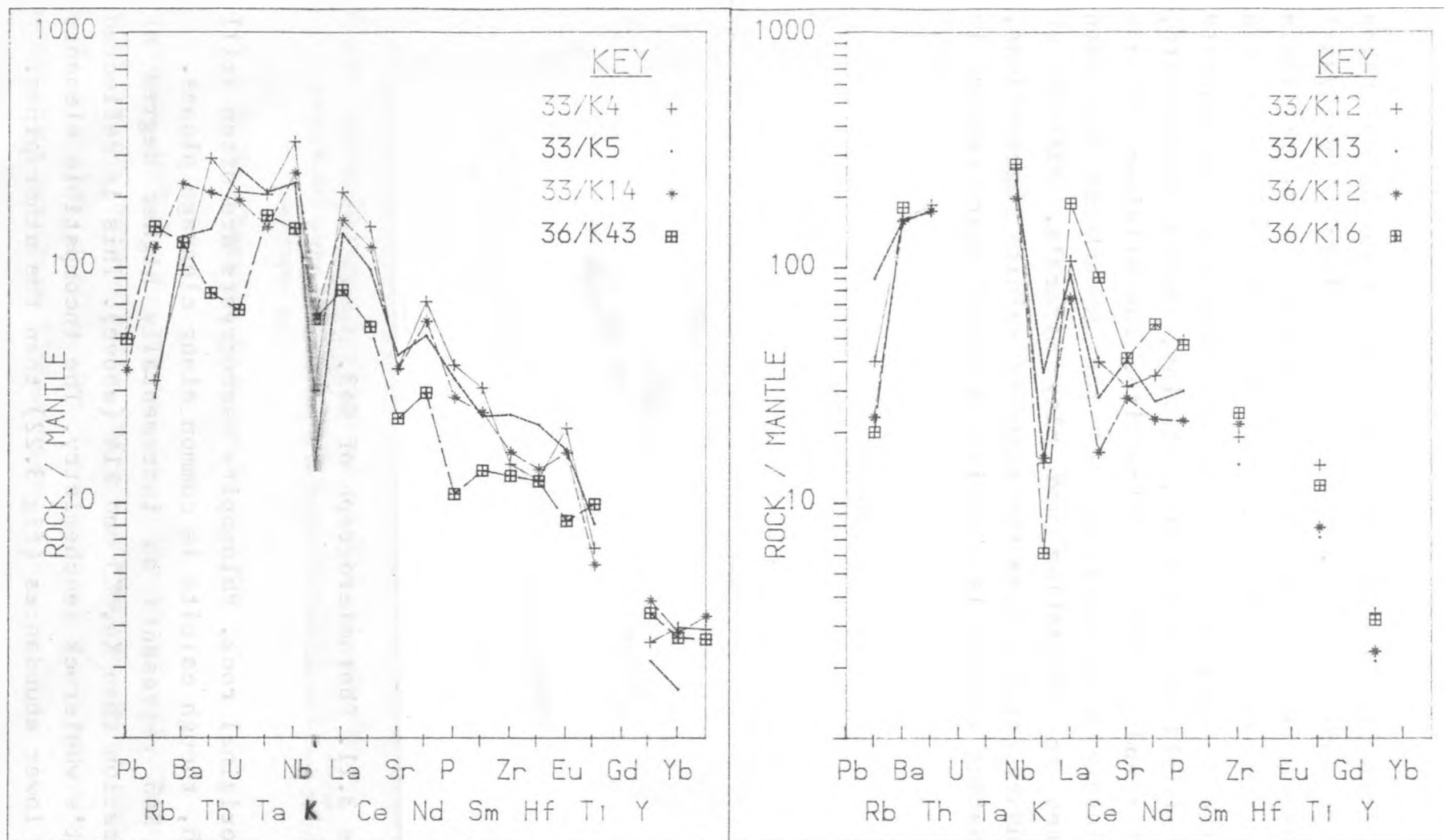


Figure 3.22: Mantle normalised trace element plots for altered kimberlites.

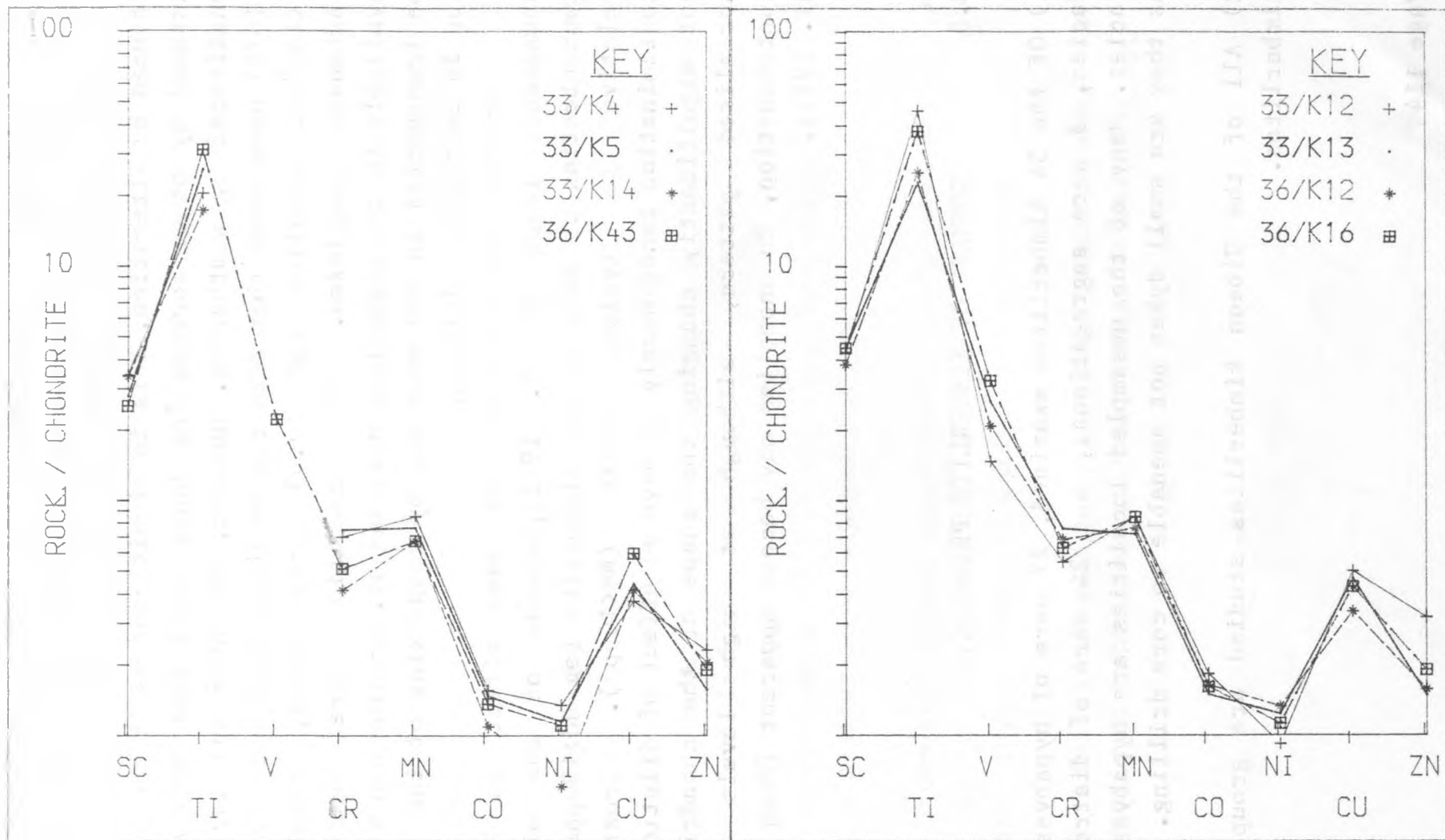


Figure 3.23: Chondrite normalised transition element plots for altered kimberlites.

Most noticeably the LREE concentrations in K43 are only a third of those in K35. Because the REE abundances are very similar in all the fresh kimberlites analysed, it is a logical assumption that the REE content of K43 has been reduced by alteration. This is significant as it has been assumed by other workers (eg Jones 1984) that REEs are unaffected by weathering. However, McLennan and Taylor (1979) have shown that REEs can be highly mobile in low T (<100°C), alkaline (pH >7.5) groundwaters, forming carbonate complexes. Such conditions are readily available in the kimberlite environment. Uranium can also be transported in the same way by complexing of the U⁶⁺ ion in carbonate solutions.

Crustal contamination has less affect on REE abundances (Fesq et al. 1975), because of the high concentration of REEs in the kimberlite (eg Nd>100ppm), relative to typical crust (Nd<10ppm). Crustal contamination tends merely to have an effect of dilution, not significantly changing the shape of the chondrite normalised pattern, although at high levels of contamination, Eu anomalies may become apparent (Fesq et al. 1975).

3.6 SUMMARY OF KIMBERLITE PETROLOGY

1) Of the 54 kimberlites examined, 27 were of hypabyssal facies, 3 were segregational, and 24 were of diatrema facies. Many of the unsampled localities are hypabyssal as they are small dykes not amenable to core drilling.

2) All of the Gibeon kimberlites studied are group I kimberlites.

- 3) Mineralogy is similar in all the kimberlites examined, consisting of olivine +/- phlogopite macrocrysts in a matrix of olivine, perovskite, spinel and monticellite +/- phlogopite, calcite, apatite and serpentine.
- 4) Most pipes consist of a single magmatic intrusion, with very little internal variation. Several large pipes (eg Hanaus 1) show evidence of multiple intrusion.
- 5) Of the four fresh kimberlites studied, three showed remarkable chemical and mineralogical similarities, with little evidence of fractionation, whereas 33/K2 appears to have undergone limited crystal fractionation.
- 6) Slight alteration can significantly affect the whole rock geochemistry, especially Rb, Ba, K, Sr and LREE contents.
- 7) Slight crustal contamination may have little effect on the trace element geochemistry.
- 8) Ba-phlogopite is produced in a late stage CaCO_3 rich magma similar to a carbonatite.
- 9) Groundmass spinel compositional variations may be due to differences in the chemical environment (P,T, $\text{CO}_2/\text{H}_2\text{O}$) rather than a result of earlier fractionation.
- 10) Olivine phenocrysts and macrocrysts have indistinguishable compositional ranges between Fo_{85-91} .

CHAPTER 4

INTERKIMBERLITE VARIATIONS

GEOCHEMISTRY AND PETROGENESIS

Whole rock chemical analyses of kimberlites record the combined effects of several components. The composition of the original/parental kimberlite magma depends on that of the asthenospheric source regions and the melting parameters (P,T, volatiles etc.). This parental composition may then be altered by interaction with the lithosphere, the entrainment of mantle xenoliths, crystal fractionation, crustal contamination and finally alteration (weathering). The effects of these processes have been identified using whole rock geochemistry.

The interpretation of the whole rock geochemistry is severely hampered by the problems inherent in the intrusive style (diatreme formation and devolatilisation), and multiple component nature of kimberlite. Mitchell (1986) categorically states that 'kimberlite whole rock compositions do not represent the compositions of the magmas from which they formed'. As a general comment on the literature this is undoubtedly true, but it is shown below that it is possible, when working on a set of closely related kimberlites to 'filter out' samples affected by contamination, alteration, and to some degree, fractionation. It is then possible to use trace element and isotope geochemistry to identify mantle source characteristics.

Most previous investigations of kimberlite geochemistry involve rather random sampling of unrelated intrusions (eg

Dawson 1980, Smith 1983). As a result, only the broadest conclusions could be drawn. Scott's (1979,1981) studies of the Holsteinborg kimberlite dykes are the only previous significant study of a group of closely related kimberlites. Scott demonstrates the effects of crystal fractionation of olivine plus minor chromite prior to emplacement.

The present study is, admittedly, limited by the unavoidable restrictions imposed by the early closedown of the drilling programme, and by the limited sampling possible within any particular pipe. However, because the kimberlites are closely related, significant conclusions may be drawn from interkimberlite variations.

4.1 FRACTIONATION

It was shown in chapter 3 that (within the limits of sampling) there was little chemical variation within pipes. Such small variations (eg K35/M and X) are difficult to interpret in terms of fractionation or contamination, because they are on the limits of realistic analytical precision, and can only be viewed as scatter. When all four fresh kimberlites (33/K2, 36/K35, 36/K39, 36/K53) are considered together (fig 4.1) it can be seen that there are indeed significant interkimberlite variations.

Fig 4.1 shows that K35, K39 and K53 have a restricted range of compositions (MgO 29-33%, SiO₂ 31-34%, CaO 7-10%) while 33/K2 is distinctly different, and more variable (MgO 20-24%, SiO₂ 30-35%, CaO 14-17%). There is no a priori reason to assume that K2 is genetically related to the other kimberlites, even though it is of approximately the same age. However, it is apparent from fig 4.1a,b,c,e that K2 lies on an olivine extraction line away from the other fresh kimberlites, such as K35. Fig. 4.1 d and f

reveal that a Cr and Fe bearing phase must also be fractionated to account for the slight discrepancy of Fe_2O_3 , and significant Cr depletion. This phase is Cr-spinel, the early forming spinel which is found as a microphenocryst in the kimberlite groundmass. Calculations from these variation diagrams indicate that the average K2 composition can be modelled by the fractionation of approximately 30% olivine plus 0.15% Cr-spinel from K35. There is no evidence that pyroxenes or garnet have fractionated from the magma (see chapter 5).

A consequence of olivine fractionation is an increase in the concentrations of incompatible trace elements. Nb, V and LREEs are incompatible in olivine and spinels. The fractionation of these phases should cause rising trace element concentrations with falling Ni, Cr and Mg. There is however no such rise in Nb, V and LREEs in K2 relative to K35 (fig 4.2). Indeed the LREE abundances are slightly lower in K2 (Nd 102-113ppm) than in K35 (Nd 113-116ppm). This is direct evidence that K35 cannot be a parental magma from which K2 has fractionated.

It is most likely that K2 does represent a relatively fractionated kimberlite, but it is not possible that K35 is the parental magma. The similarity in La/Nb and other trace element ratios of K2 and the other fresh kimberlites, do however, suggest close links between the two magma types (see section 4.5). The low modal abundance of olivine in K2 (chapter 3) supports the chemical evidence for olivine fractionation.

It is not possible to determine exactly when the fractionation occurred. There are two possibilities: 1) Olivine and spinel were gravitationally fractionated during ascent of the magma, prior to emplacement. 2) Olivine and spinel were separated from the liquid by flow differentiation as the magma was emplaced.

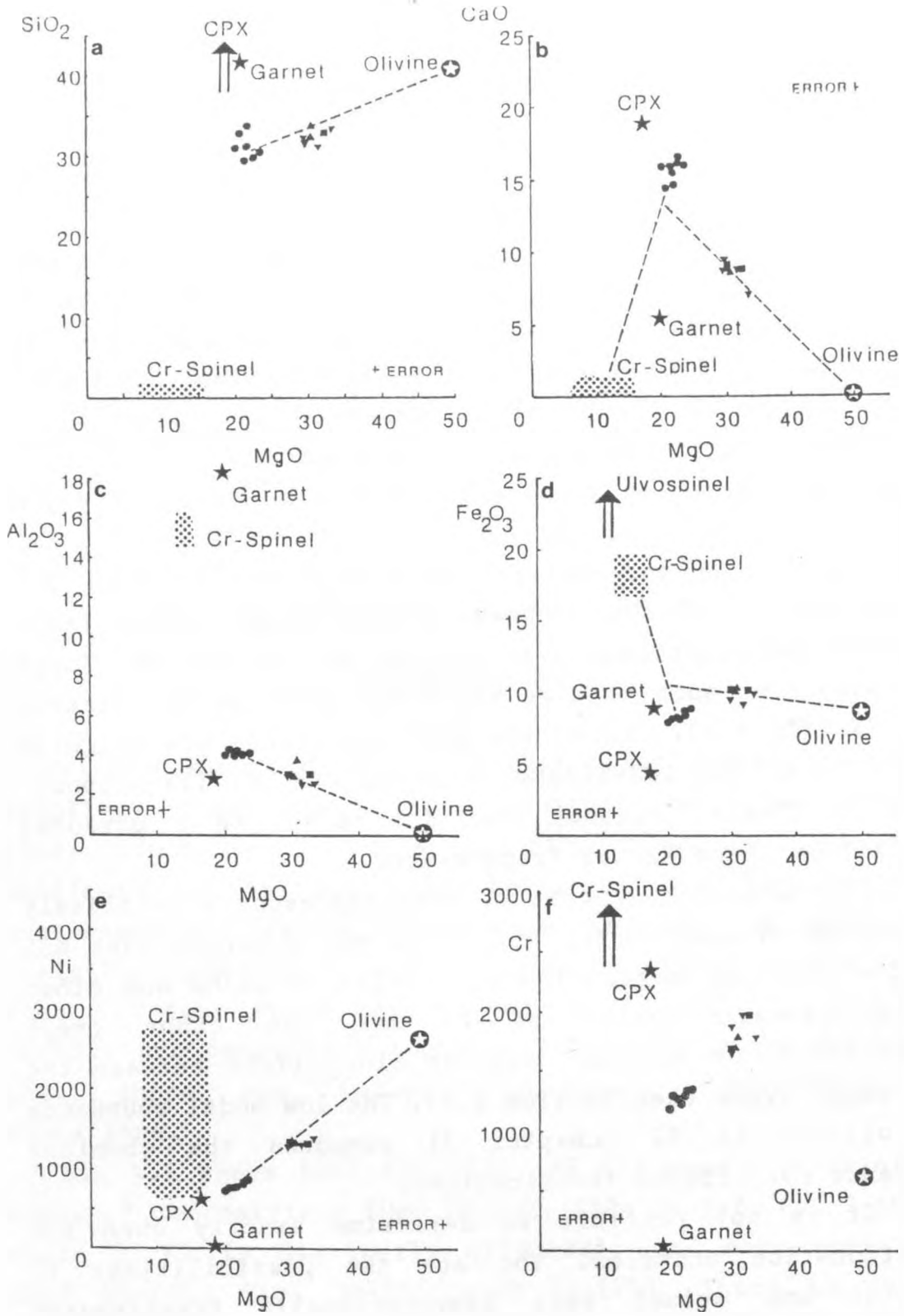


Fig 4.1. Major elements v MgO, showing evidence for 30% olivine plus minor chromite fractionation in K2, from a parental magma similar to K35, K39 and K53.
 K2● K35▲ K39▼ K53■

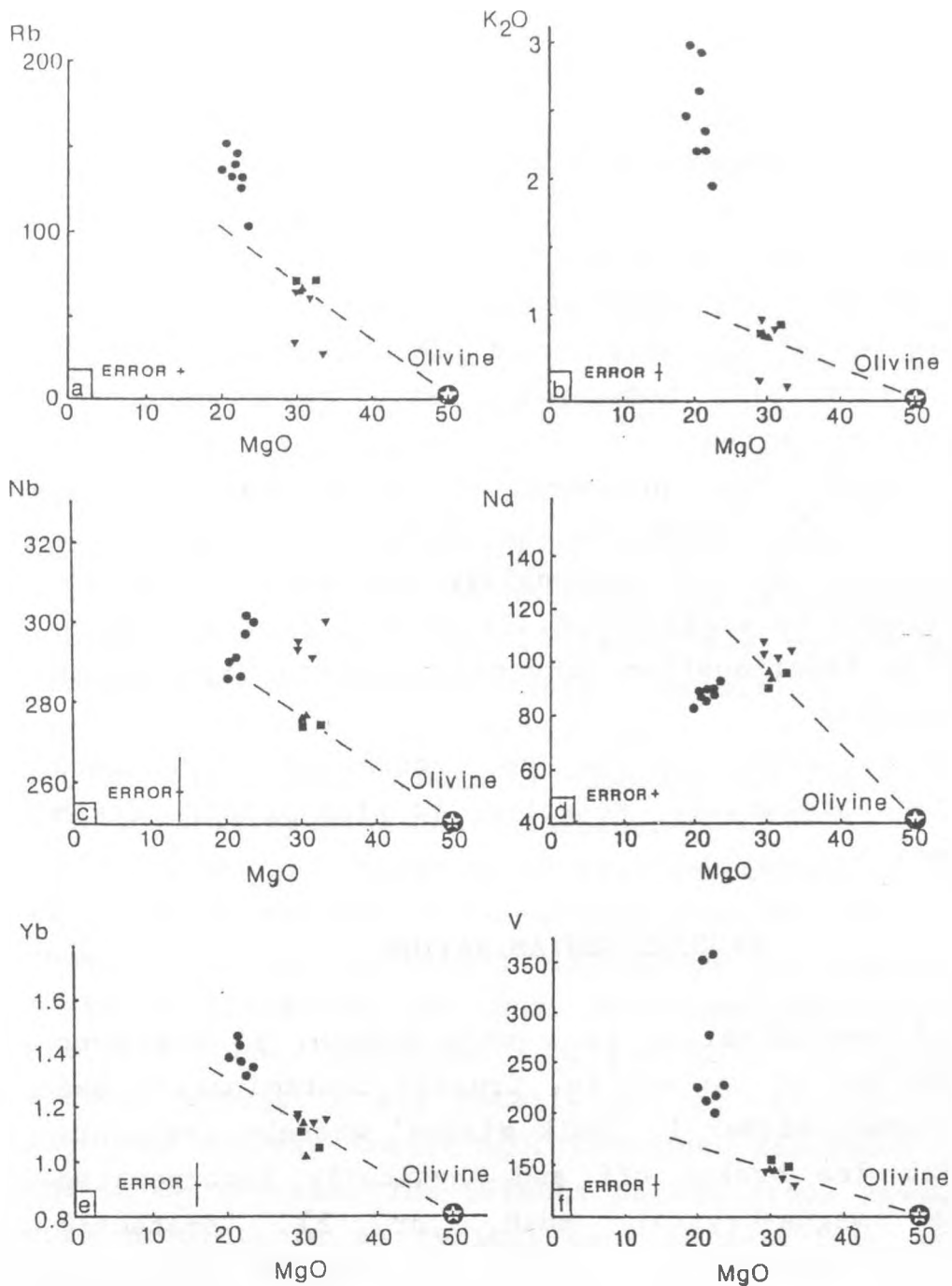


Fig 4.2. Trace elements v MgO, showing that trace element variations are decoupled from the effects of olivine fractionation. K and Rb are more enhanced than expected from fractionation, whereas Nd is decreased in K2 relative to K35. K2● K35▲ K39▼ K53■

Flow differentiation is commonly found in kimberlite dykes and sills (Dawson and Hawthorne 1973, Clement 1982, Mitchell 1986) . Scott (1979) concludes that olivine and spinel fractionation occurred in the Holsteinborg dykes during ascent when the magma was temporarily arrested.

The samples of K2 (which were taken from drill core) are all structurally homogeneous with no evidence of lamination or segregation, nor that they came from internal dykes. The presence of occasional crustal xenoliths in the magma is an indication that flow differentiation was not responsible for removing solids from the liquid on emplacement. It is therefore concluded that olivine fractionation occurred prior to emplacement near the surface.

In conclusion, K2 can be recognised as a more fractionated kimberlite relative to the other fresh kimberlites.

4.2

CRUSTAL CONTAMINATION

Crustal contamination is a very common, if not ever present feature of kimberlite. Crustal contamination can take two forms, either 1) 'bulk mixing' whereby fragments of wallrock are broken off and physically incorporated into the magma-crystal mush, or 2) 'anatectic assimilation' whereby the wall-rock, or fragments thereof, are melted by the kimberlite and cannot be observed petrographically.

In the kimberlites studied, crustal xenoliths were commonly found to have 'baked margins' 1-2mm thick, with relatively unaltered cores. The xenoliths appeared not to have melted in the magma. On a larger scale, it was observed in the field, and in the Wesselton Mine in Kimberley, that the kimberlite pipe-country rock contact is extremely sharp, with no evidence of contact

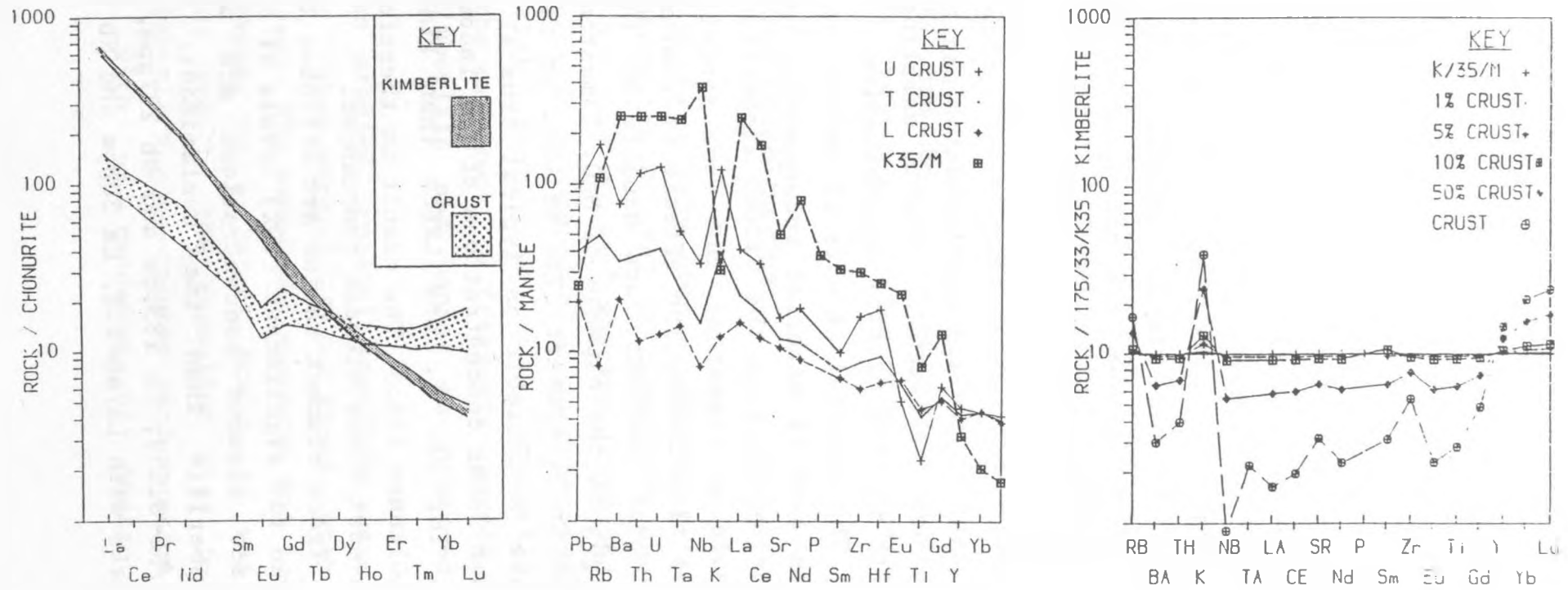
metamorphism

These observations indicate that the kimberlite is emplaced and cooled rapidly, with little opportunity to melt the country rocks. As a result, only very small rock fragments (1 or 2mm) are likely to be melted completely into the kimberlite melt. This is supported by McFadden's (1977) palaeomagnetic evidence that kimberlites may be emplaced at less than 400°C. It is concluded therefore, that in the samples studied, crustal contamination is produced by the bulk mixing of crustal fragments into the kimberlite. Melting of these xenoliths is minimal, and the actual magma composition is relatively unaffected, even though the whole rock sample composition may be. The extent of crustal contamination can therefore be estimated by hand specimen. Careful sampling can exclude samples with visible crustal contamination.

The chemical effects of crustal contamination depend on the type of material incorporated into the melt. Crustal contaminants in the Gibeon kimberlites are typically Nama shale or limestone, but Nama sandstone and Karoo basalt are also found. The effects of contamination on the major element chemistry are usually to increase the SiO_2 and Al_2O_3 at the expense of MgO . Limestone xenoliths increase the CaCO_3 content. The effects on the trace elements are more predictable as typical crustal materials have very much lower concentrations of the incompatible elements Nb, U, Th, Ba, P, and LREEs than kimberlite (Taylor and McClennan 1985). The result is therefore a dilution effect on most trace element abundances.

Trace element ratios are affected less than abundances, even for significant (10%) levels of contamination because trace element concentrations are much higher in the kimberlite than the contaminant. A kimberlite with $\text{La/Nb}=0.659$, La 183ppm and Nb 277ppm, contaminated by 10% shale with $\text{La/Nb}=1.2$, La 30ppm and Nb 25ppm, produces a

Figure 4.3. (a) REE composition of fresh kimberlites compared to average crust. (b) trace element composition of K35 compared to upper (U), total (T) and lower (L) crust. (c) effects of mixing various proportions of average crustal material with kimberlite K35. Crustal data from Taylor and McLennan (1985).



sample with $\text{La/Nb}=0.694$. Similarly, Nd and Sr isotope ratios are not greatly altered by small degrees of crustal contamination. The concentrations of K, Rb, Pb and the HREEs are, however, significantly increased by crustal contamination as these elements are concentrated in the crust in abundances greater than in kimberlite (Taylor and McClennan 1985).

Figure 4.3a and b show abundances of trace elements in the average crust (Taylor and McClennan 1985) relative to K35. Fig 4.3c is a trace element abundance diagram normalized to the kimberlite sample K35/M. It shows the average crustal composition, and the effects of 1, 5, 10 and 50% contamination of K35 by average crust. It can be seen that while the abundances of Ba, Th, Nb, U, Sr, P, Zr and the LREEs are reduced by crustal contamination, the abundances of Pb, Rb, K, Yb and Lu are significantly increased. Pb isotope systematics are therefore significantly affected by crustal contamination (especially the 207/204 ratio). Eu anomalies may be produced by large amounts of crustal contamination, but are unlikely to be detectable in samples in which xenoliths are not readily visible in hand specimen.

It is concluded that when samples are selected with little ($\ll 5\%$) or no visible crustal xenoliths, the trace element ratios and abundances are essentially unaltered by crustal contamination.

4.3 ALTERATION

Kimberlite is highly susceptible to low temperature alteration by groundwater interaction. Groundwaters dissolve olivine and groundmass minerals, precipitating a variety of secondary minerals (serpentine, calcite, chlorite and other clay minerals). This alteration is

accompanied by a loss in soluble (mobile) elements. Previous studies of the effects of alteration have concentrated on major element ratios, Mg/Si (Ilupin and Lutts 1971) and $(\text{SiO}_2 + \text{Al}_2\text{O}_3 + \text{Na}_2\text{O}) / (\text{MgO} + 2\text{K}_2\text{O})$ (Clement 1982) reflecting the ratio of clays and tectosilicates to olivine and phlogopite (see section 4.4). This study also aims to examine the effects of alteration on trace elements and isotope variations. Secondary alteration is distinguishable from the isochemical primary (deuteric) alteration often produced on emplacement. Deuteric alteration involves the hydrolysis of olivine to produce fine grained pseudomorphs of olivine, which are distinguishable from the fibrous overgrowths of secondary alteration (E Colgan pers comm).

The Gibeon kimberlites, being closely related, offer an opportunity to study the effects of various degrees of alteration on the whole rock geochemistry. Table 4.1 summarizes the alteration and crustal contamination styles in the 8 samples described in chapter 3. Alteration is progressive, with several identifiable levels:

- 1) Secondary serpentine alteration in the groundmass and along fractures in olivines. (33/K4, K13)
- 2) Clay (montmorillonite, illite etc) minerals and calcite in the groundmass, olivines almost completely replaced by serpentine/chlorite. Phlogopite macrocrysts partially altered, especially along cleavage planes. (33/K5, K12, K14, 36/K12)
- 3) Complete calcite/clay mineral replacement, olivines and phlogopite macrocrysts obliterated. (36/K16, K43)

TABLE 4.1

sample	groundmass alteration	olivine alteration	phlogopite alteration	crustal contamination
33/K13	serpentine & calcite	partial serpentine	phlogopite absent	minimal
33/K4	serpentine & calcite	partial serpentine	slight	minimal
33/K5	calcite & clay	serpentine & calcite	slight	minimal
33/K12	calcite & clay	serpentine 95%	phlogopite absent	minimal
33/K14	calcite & clay	chlorite 95%	slight	20%
36/K12	calcite + veins	serpentine	phlogopite absent	<5%
36/K43	severe calcite	obliterated calcite	severe calcite	35%
36/K16	severe calcite	obliterated calcite	chlorite	<10%

Figure 4.4 shows selected elements plotted against Nb. Nb was chosen as it shows only limited variation (274-301ppm) in the fresh samples. Fractionation tends to increase the Nb concentration (as Nb is an incompatible element), and crustal contamination to reduce it (as the

crust has relatively low Nb abundances). The small Nb variations in the fresh samples may reflect these processes. It can be seen that the altered samples (some of which also have significant crustal contamination) have highly variable Nb (108-253ppm). It is assumed that the altered samples originally plotted in, or close to, the field of fresh samples, before alteration and contamination. Vectors can then be drawn on element-element plots, from the fresh samples, through the altered samples, which reflect the effects of alteration, contamination and fractionation. Fig 4.4 demonstrates that while fractionation is clearly distinguishable from alteration; contamination often produces similar vectors.

Samples 33/K4, K5, K12, K13 and 36/K12 have variable alteration but little crustal contamination. These samples lie on an 'alteration vector' away from the fresh samples. 36/K16 has alteration plus a little (<10%) contamination, and 33/K14 and 36/K43 have major (>20%) crustal contamination, and are also altered.

In the SiO_2 vs Nb plot (fig 4.4a), K14 and K43 have increased SiO_2 relative to the fresh samples - a result of their added crustal contaminants. The altered samples, 33/K4, K5, K12, and K13 plot at lower SiO_2 - indicating that alteration has resulted in a loss of SiO_2 , through the breakdown of olivine, monticellite and phlogopite.

The CaO vs Nb plot (fig. 4.4b) shows the effects of fractionation as well as alteration and crustal contamination. Fractionation has caused CaO to rise in K2 (see section 4.1). Alteration causes a rise in CaO due to the precipitation of secondary calcite, and a reduction in Nb (due to dissolution and removal in groundwaters. Crustal contamination causes depletion in CaO and Nb.

Contamination and alteration are not distinguishable for Fe, as both produce a slight reduction in Fe_2O_3 with significant Nb depletion. Fractionation produces a slight

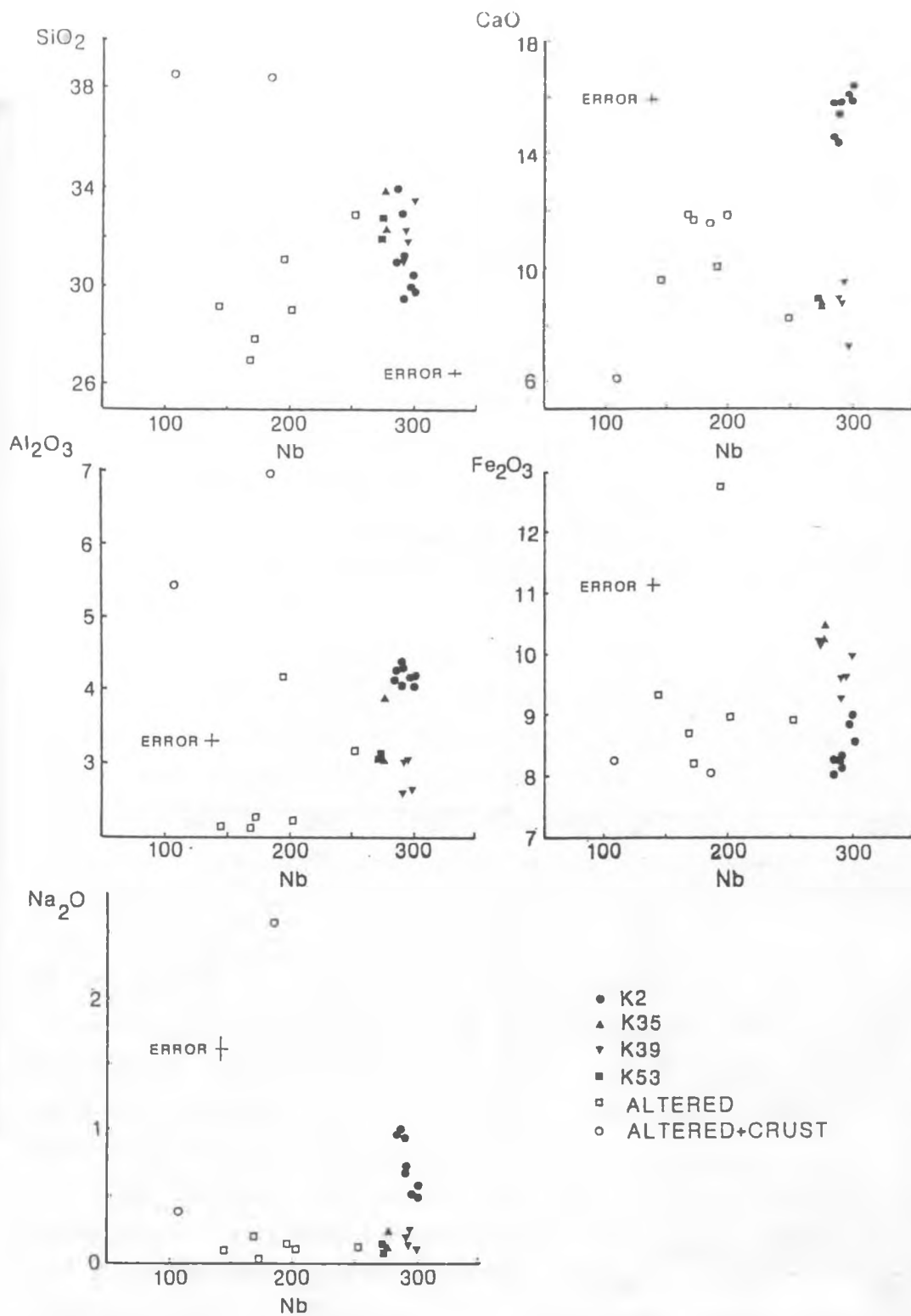


Fig 4.4. Major elements v Nb, showing altered samples and vectors for alteration, contamination and fractionation

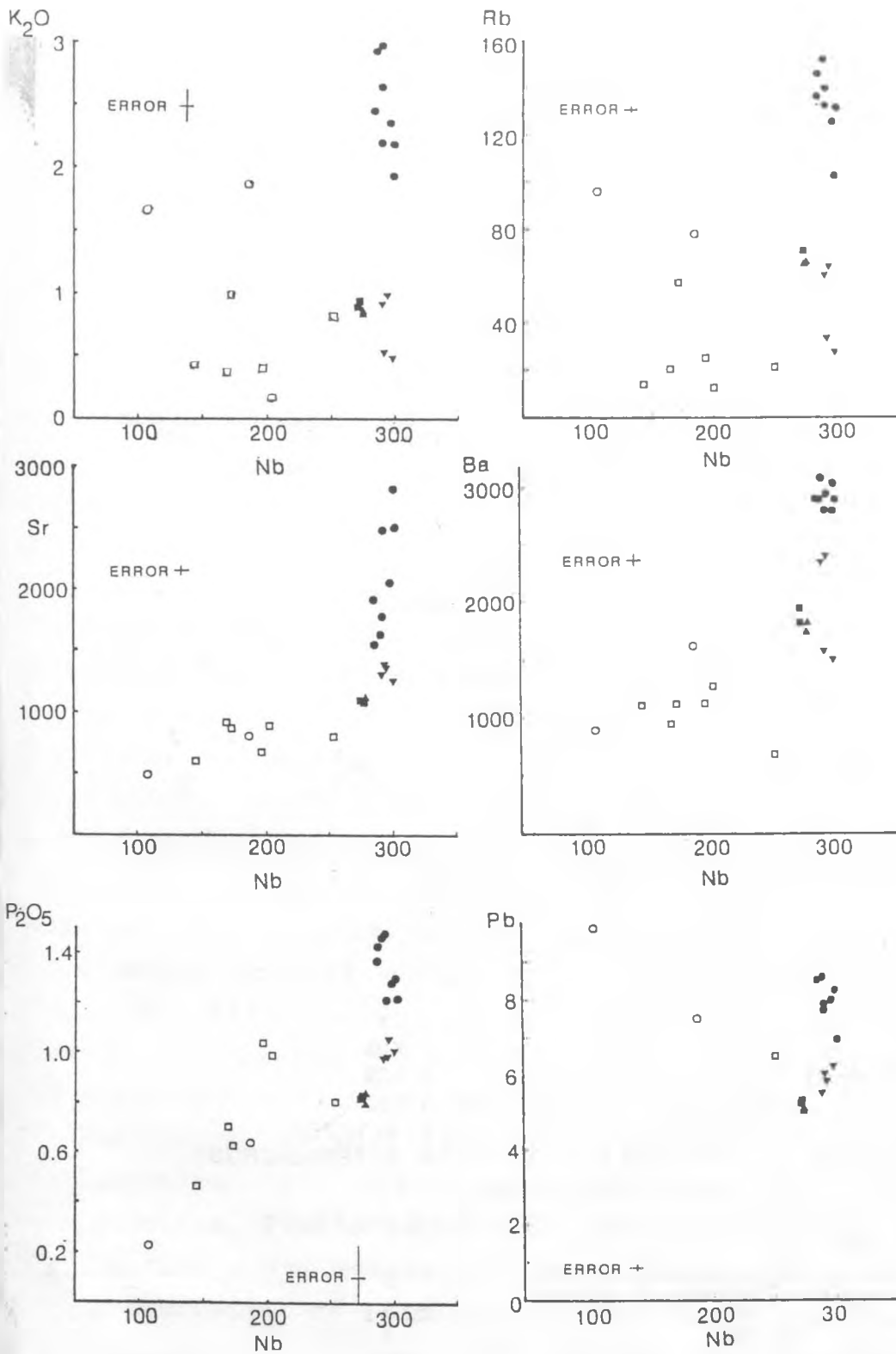


Fig 4.5. trace elements v Nb, showing trace element enrichment of K2 relative to K35. Also shown are altered samples and vectors for alteration, crustal contamination and fractionation ● K1 ▲ K35 ▼ K34 ■ K53 □ ALTERED ○ ALTERED + CRUST

depletion in Fe_2O_3 but a slight rise in Nb, and can therefore be identified.

It was suggested in sections 3.4.3 and 4.1 that the concentrations of Rb, Ba, K, Sr and P in 33/K2 were enhanced by a greater degree than could be produced by fractionation of olivine and chromite from K35. Fig 4.5 clearly shows that this enrichment is not due to either alteration or crustal contamination. Crustal contamination causes depletion in Ba, Sr and P, and enrichment in K, Rb, and Pb, while alteration depletes all of these elements as they are highly soluble in groundwaters. The contamination and alteration vectors are directed away from the enrichment in K2.

Of particular interest, is the effect of alteration on the REEs, as these are often considered to be immobile during low temperature alteration (eg Jones 1984). Fig 4.6 shows the fields for fresh and altered kimberlites. The altered samples have LREE abundances significantly lower than the fresh samples. Also shown is the field of Jones' (1984) data from 6 Gibeon kimberlites. Fig 4.7 shows that crustal contamination and alteration both have the effect of reducing La, Ce and Nd. The HREEs are increased by crustal contamination, and possibly alteration. This is explained by reference to fig. 4.3a, which shows that although kimberlite has massive LREE enrichment, average crust has higher HREE contents.

The unusual REE mobility may be explained by their solubility in alkali-carbonate solutions (see section 3.5.8). The Gibeon kimberlites, being calcite bearing, are perhaps more susceptible to REE loss than non-calcite kimberlites. It is concluded that the interpretation of REE and Nd isotope data from even slightly altered kimberlite samples must be undertaken with extreme caution.

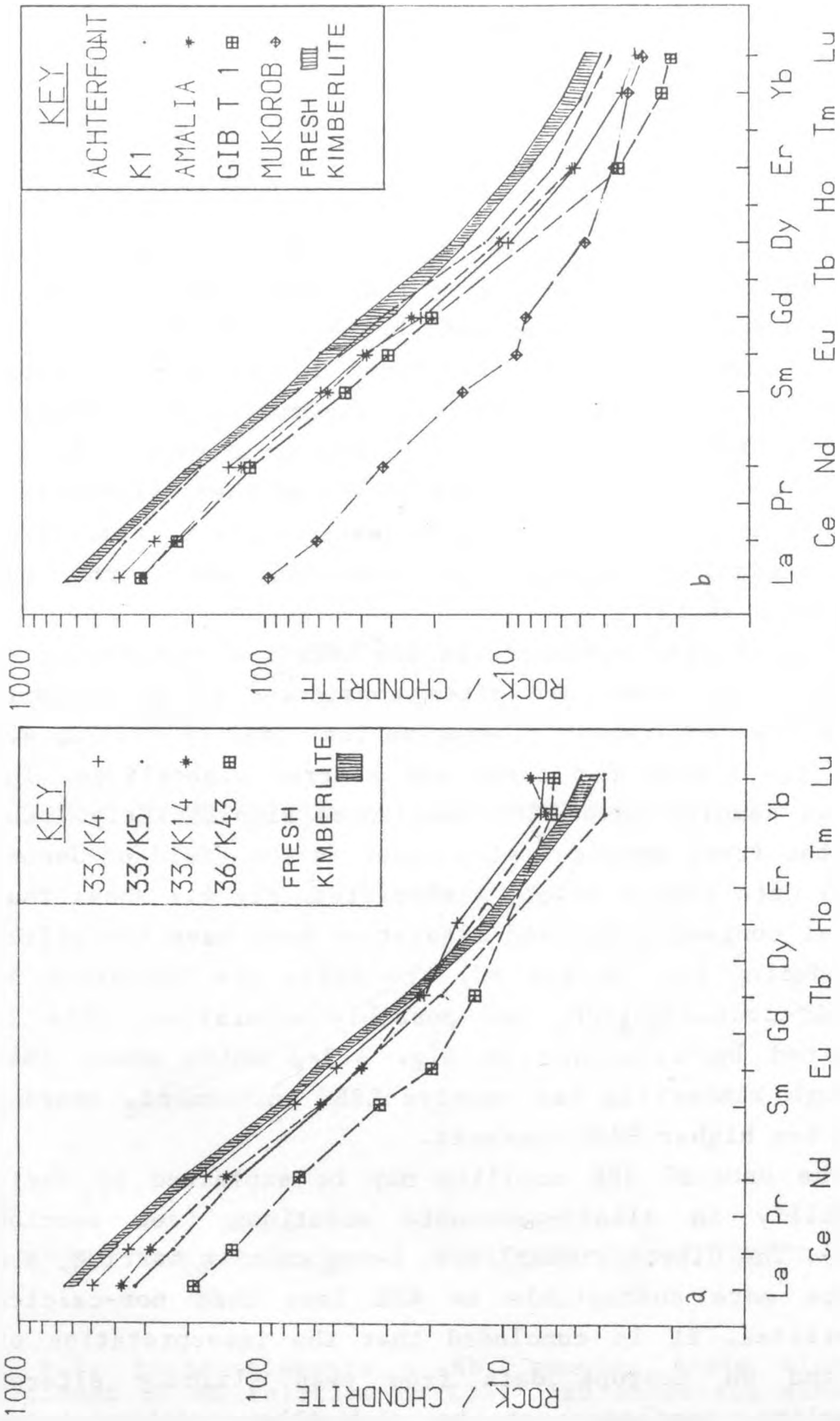


Fig 4.6. REE patterns of fresh kimberlites compared to altered kimberlites from (a) this work, (b) Jones (1984).

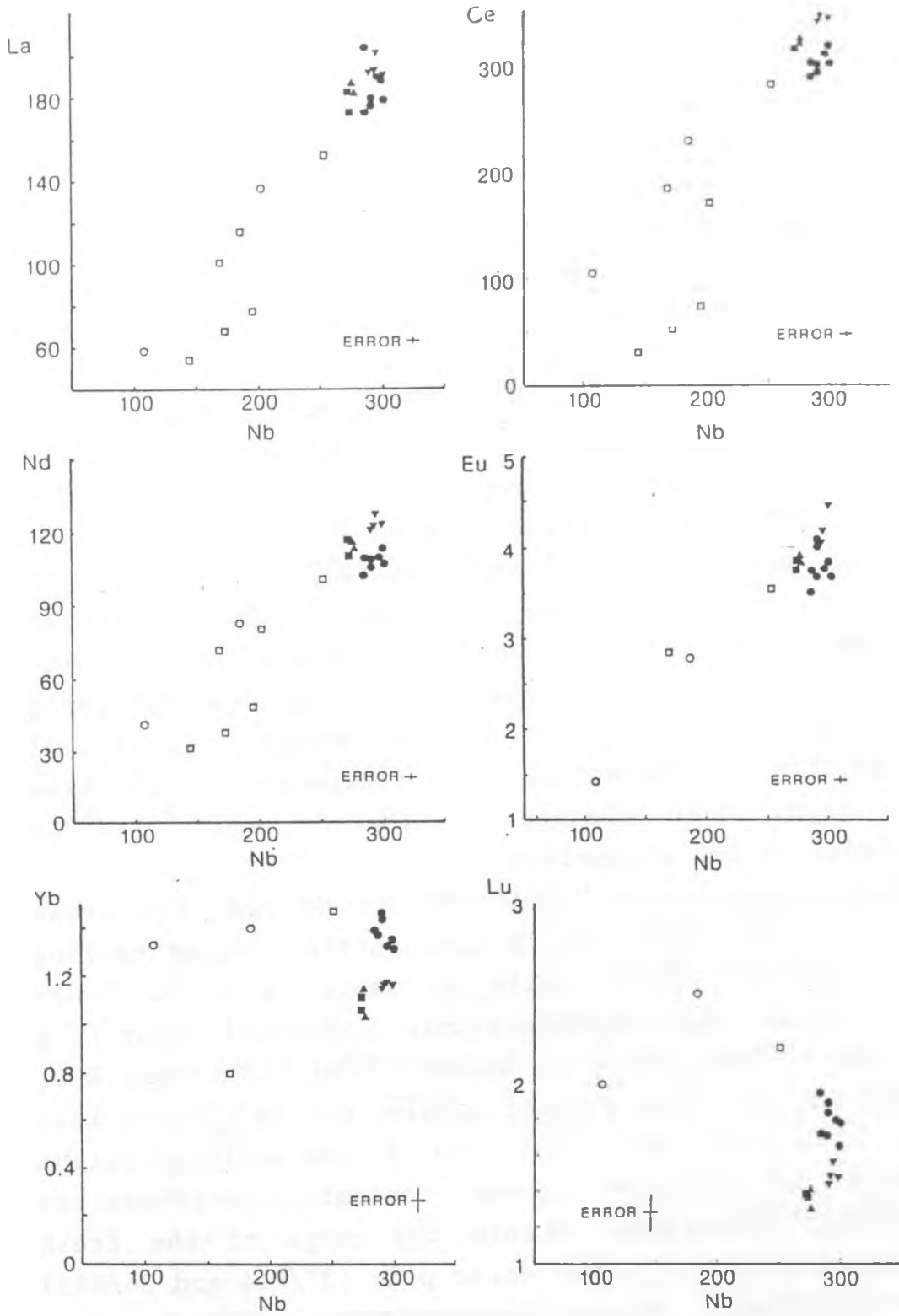


Fig 4.7. REEs v Nb for fresh and altered kimberlites showing decrease in LREE, and increase in HREE from alteration. Symbols as in Fig 4.5.

The Sr, Nd and Pb isotopic compositions of the kimberlites were analysed (see appendix 1) and age corrected to 70Ma (section 2.6.3). It is necessary to consider the effects of alteration and contamination on the kimberlite isotope systematics, as it is shown above that Sr, Nd and Pb are all affected by these processes. Fractionation has no effect on isotopic composition.

Figure 4.8a shows the $^{87}\text{Sr}/^{86}\text{Sr}$ initial ratio vs Sr concentration. The fresh samples K35, K39 and K53 cluster closely (0.7036-0.7039), but K2 has higher $^{87}\text{Sr}/^{86}\text{Sr}$ (0.7043-0.7053). The altered samples 33/K4, K5, K14, and K43 also have raised $^{87}\text{Sr}/^{86}\text{Sr}$ (0.7043-0.7081). The increase in $^{87}\text{Sr}/^{86}\text{Sr}$ in K2 is accompanied by an increase in Sr ppm relative to K35, whereas in the altered samples it is accompanied by a decrease in Sr. The more radiogenic Sr of K2 is not therefore a result of crustal contamination or alteration. Minor (serpentine) alteration causes significant changes in the Sr and $^{87}\text{Sr}/^{86}\text{Sr}$ composition of the kimberlite.

Figure 4.8b shows $^{143}\text{Nd}/^{144}\text{Nd}$ vs Nd ppm. The fresh kimberlites K35, K39 and K53 have initial ratios ranging from 0.512630-0.512693, while K2 ranges from 0.512663-0.512717. These ranges overlap within analytical error (fig 4.9), but K2 has generally higher $^{143}\text{Nd}/^{144}\text{Nd}$ than K35, K39 and K53. The four altered samples can be divided into 2 pairs. The first pair, 33/K4 and K5 have suffered slight alteration and negligible crustal contamination. These two have $^{143}\text{Nd}/^{144}\text{Nd}$ ratios within the range of the fresh kimberlites (fig 4.9). The second pair (33/K14 and 36/K43) have significant crustal contamination and are more severely altered. These have slightly lower $^{143}\text{Nd}/^{144}\text{Nd}$ (0.512595 and 0.512632) than the fresh samples. Alteration reduces Sm and Nd concentrations in the rock and may increase the Sm/Nd ratio. It is not known exactly when this alteration takes place, so the age correction of

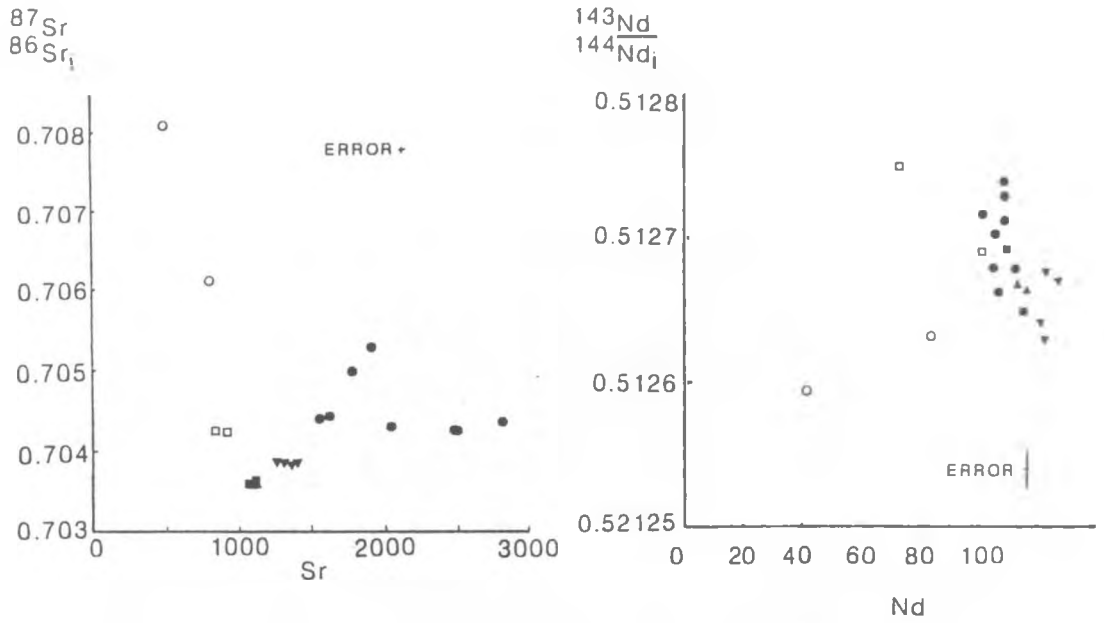
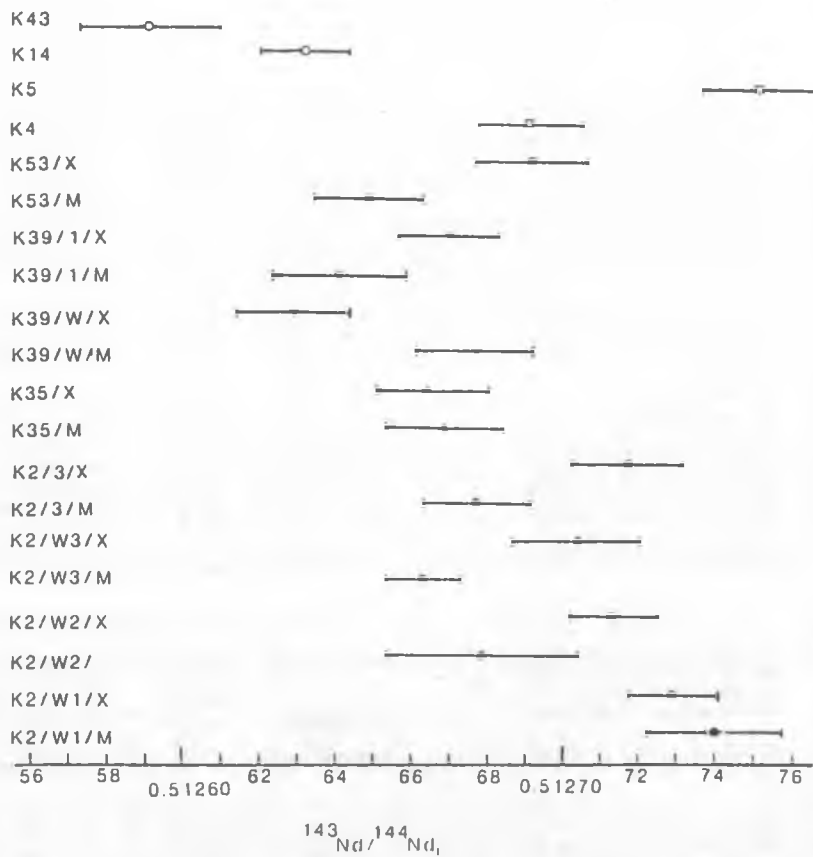


fig 4.8. (a) $^{87}\text{Sr}/^{86}\text{Sr}$ v Sr and (b) $^{143}\text{Nd}/^{144}\text{Nd}$ v Nd, showing effects of enrichment in K2 and alteration.

Fig 4.9. $^{143}\text{Nd}/^{144}\text{Nd}$ initial ratio variations with errors.



SYMBOLS AS IN FIG 4.6

TABLE 4.2 : Sr and Nd isotopic composition of kimberlites

SAMPLE	$^{87}\text{Rb}/^{86}\text{Sr}$	$^{87}\text{Sr}/^{86}\text{Sr}_m$	$^{87}\text{Sr}/^{86}\text{Sr}_i$	$\epsilon(\text{Sr})$	$^{147}\text{Sm}/^{144}\text{Nd}$	$^{143}\text{Nd}/^{144}\text{Nd}_m$	$^{143}\text{Nd}/^{144}\text{Nd}_i$	$\epsilon(\text{Nd})$
K2/W1/M	0.2797	0.704687+/-10	0.704418	-2.81	0.07709	0.512775+/-18	0.512740	3.71
K2/W1/X	0.2699	0.704714+/-8	0.704446	-2.41	0.07626	0.512764+/-12	0.512729	3.49
K2/W2/M	0.1057	0.704505+/-16	0.704400	-3.06	0.07616	0.512714+/-26	0.512679	2.52
K2/W2/X	0.1778	0.704507+/-12	0.704330	-4.06	0.07821	0.512749+/-12	0.512713	3.18
K2/W3/M	0.1525	0.704460+/-8	0.704308	-4.37	0.07815	0.512699+/-10	0.512663	2.21
K2/W3/X	0.1551	0.704457+/-12	0.704302	-4.45	0.07874	0.512740+/-17	0.512704	3.00
K2/3/M	0.2275	0.705247+/-12	0.705021	5.75	0.07897	0.512713+/-14	0.512679	2.52
K2/3/X	0.2069	0.705530+/-10	0.705324	10.05	0.07747	0.512753+/-15	0.512717	3.26
K35/W/M	0.1763	0.703801+/-10	0.703626	-14.3	0.07606	0.512703+/-16	0.512668	2.30
K35/W/X	0.1712	0.703803+/-10	0.703633	-13.95	0.07633	0.512665+/-16	0.512630	1.56
K39/W/M	0.0618	0.703993+/-10	0.703932	-9.70	0.07767	0.512713+/-16	0.512677	2.48
K39/W/X	0.0702	0.703981+/-10	0.703911	-10.00	0.07633	0.512665+/-18	0.512630	1.56
K39/1/M	0.1347	0.704034+/-10	0.703900	-10.16	0.07830	0.512677+/-18	0.512641	1.78
K39/1/X	0.1377	0.704008+/-10	0.703871	-10.57	0.07578	0.512705+/-13	0.512670	2.34
K53/W/M	0.1886	0.703827+/-10	0.703639	-13.86	0.07597	0.512684+/-15	0.512649	1.93
K53/W/X	0.1850	0.703851+/-16	0.703667	-13.46	0.07640	0.512728+/-15	0.512693	2.79
33/K4	0.0790	0.704455+/-10	0.704376	-3.4	0.08380	0.512729+/-14	0.512690	2.73
33/K5	0.0659	0.704358+/-10	0.704292	-4.59	0.08851	0.512792+/-15	0.512751	3.92
33/K14	0.2835	0.706432+/-10	0.706150	21.77	0.07983	0.512669+/-12	0.512632	1.60
36/K43	0.5659	0.708681+/-10	0.708118	49.70	0.07925	0.512631+/-19	0.512595	0.88

TABLE 4.3 : Pb isotopic composition of kimberlites

SAMPLE	U	Th	Pb	$^{206}\text{Pb}/^{204}\text{Pb}_m$	$^{207}\text{Pb}/^{204}\text{Pb}_m$	$^{208}\text{Pb}/^{204}\text{Pb}_m$	u	w	k	$^{206}\text{Pb}/^{204}\text{Pb}_i$	$^{207}\text{Pb}/^{204}\text{Pb}_i$	$^{208}\text{Pb}/^{204}\text{Pb}_i$
K2/W1/M	5.81	27.7	8.54	19.137+/-6	15.631+/-3	39.094+/-8	49.92	0.362	216.8	18.592	15.605	38.341
K2/W1/X			8.65	19.125+/-10	15.654+/-4	39.153+/-13						
K2/W2/M	5.09	30.9	8.29	19.226+/-5	15.645+/-4	39.267+/-10	52.80	0.383	250.1	18.649	15.618	38.399
K2/W2/X			8.02	19.184+/-8	15.636+/-4	39.143+/-10						
K2/W3/M			6.91	19.372+/-5	15.660+/-4	39.432+/-10						
K2/W3/X			7.91	19.336+/-6	15.646+/-5	39.357+/-12						
K2/3/M	7.00	28.7	7.72	19.323+/-5	15.651+/-4	39.354+/-11	59.03	0.428	250.1	18.678	15.620	38.486
K35/M	5.44	23.2	5.20	19.699+/-10	15.671+/-9	39.611+/-25	70.38	0.510	302.9	18.931	15.634	38.560
K35/X			5.13	19.825+/-11	15.625+/-9	39.624+/-22						
K39/W/M	5.74	26.2	6.32	19.767+/-6	15.689+/-2	39.832+/-6	68.85	0.499	282.4	19.015	15.653	38.852
K39/W/X			6.11	19.767+/-11	15.686+/-9	39.704+/-22						
K39/1/M	6.63	25.5	5.59	19.703+/-7	15.672+/-1	39.683+/-4	77.97	0.565	309.9	18.852	15.632	38.608
K39/1/X			5.91	19.314+/-8	15.719+/-7	39.427+/-21						
K53/M	5.62	23.8	5.37	19.778+/-11	15.665+/-9	39.697+/-24	68.86	0.499	301.4	19.026	15.629	38.651
K53/X			5.24	19.815+/-5	15.691+/-4	39.772+/-10						
33/K4	4.60	26.8	6.65	18.657+/-16	15.618+/-19	38.907+/-65	44.35	0.322	267.0	18.173	15.595	37.981
33/K14	4.22	19.1	7.29	18.972+/-11	15.719+/-9	39.218+/-22	37.48	0.272	175.3	18.563	15.700	38.610
36/K43	1.45	7.16	9.90	18.805+/-7	15.701+/-6	38.862+/-14	9.414	0.683	48.03	18.702	15.696	38.695

$$u = ^{238}\text{U}/^{204}\text{Pb} \quad w = ^{235}\text{U}/^{204}\text{Pb} \quad k = ^{232}\text{Th}/^{204}\text{Pb}$$

altered kimberlite therefore introduces further errors.

The slight alteration of 33/K4 and K5 has not produced a detectable alteration of the $^{143}\text{Nd}/^{144}\text{Nd}$ ratio, but the more severe alteration and contamination of 33/K14 and 36/K43 has produced a slight decrease in $^{143}\text{Nd}/^{144}\text{Nd}$. It is concluded therefore, that although the Nd isotope system is less susceptible to alteration than the Sr system, extreme caution is needed when interpreting Nd isotope data from kimberlites which are not fresh.

K2 has slightly lower Nd concentrations and higher $^{143}\text{Nd}/^{144}\text{Nd}$ than K35. This relationship is similar to that produced by alteration, but it has been shown from other lines of evidence (above) that alteration is not the cause of variation between K35 and K2.

Both U and Pb are soluble in aqueous solutions and are present in the crust in high concentrations. As a result, the Pb isotopic composition of kimberlite is susceptible to modification by alteration and crustal contamination processes. Fig 4.5d shows that the altered and contaminated samples have higher Pb concentrations than the fresh kimberlites, due to precipitation of Pb from groundwater solutions, and from crustal contamination.

The altered samples plot away from the fresh kimberlites on Pb isotope diagrams (fig 4.19), displaced to higher $^{207}\text{Pb}/^{204}\text{Pb}$ and $^{208}\text{Pb}/^{204}\text{Pb}$, but lower $^{206}\text{Pb}/^{204}\text{Pb}$.

4.4 COMMENT ON CLEMENT'S CONTAMINATION INDEX.

Clement's (1982) contamination index (CI) represents the ratio of clays and tectosilicates to olivine and phlogopite, and as such should reflect the effects of both alteration and contamination on kimberlite. The contamination index is also affected by fractionation, as the removal of olivine significantly reduces MgO, and

therefore increases the CI.

In this study, it was found that 33/K2 had CI=1.27-1.44, while K35, K39 and K53 had CI=1.04-1.17. This difference is in part due to fractionation in K2, causing Mg depletion, and in part due to K enrichment. The higher CI of K2 is neither due to crustal contamination nor alteration (section 4.1). It was also found that some altered samples with little contamination (33/K4, K5, K13, 36/K12, K16) had low CI (1.03-1.28) indicating that in some cases alteration does not significantly affect the contamination index. However, samples with high crustal contamination (33/K14, 36/K43) did have increased CIs (1.81-2.34) due to increased Si, Al and Na from shale contaminants.

It appears that for CI to be increased significantly above unity there must be major (>20%) crustal contamination, which is easily visible in hand specimen. Thus it is easier to see small degrees of contamination in hand specimen than to detect it's presence by the use of the CI.

In conclusion, the contamination index may be useful when examining data in the literature, when descriptions or samples are unavailable, but it was not useful in detecting small degrees of alteration or contamination in the Gibeon kimberlites.

4.5 CHEMICAL VARIATIONS IN THE GIBEON KIMBERLITES

This section examines the chemical variations between the four fresh, non-contaminated kimberlites 33/K2, 36/K35, K39 and K53. It was shown in section 4.1, 4.2 and 4.3 that kimberlite 33/K2 has a trace element composition which cannot be explained by crustal contamination, alteration or fractionation of a typical Gibeon kimberlite such as K35. It is argued that although K2

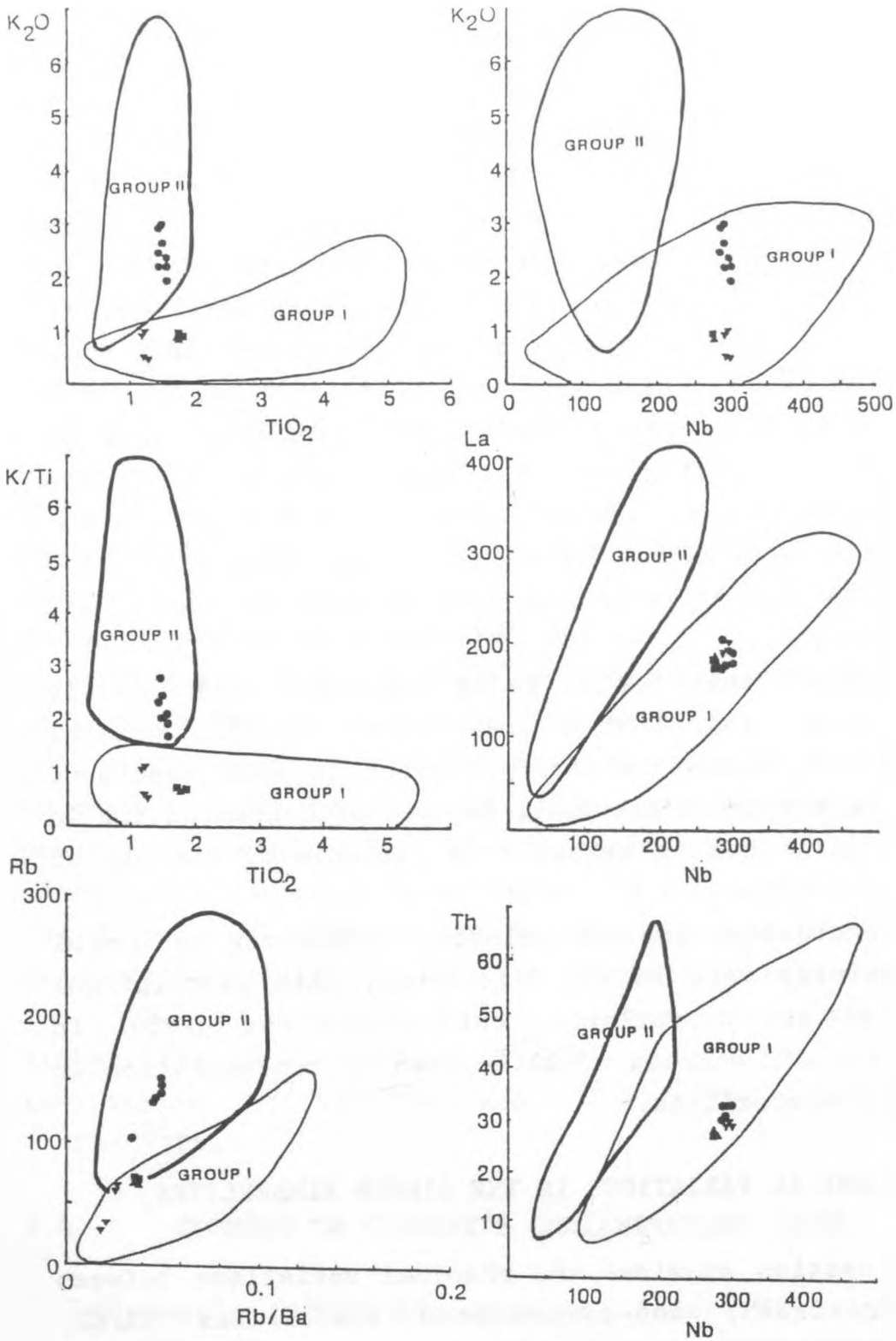
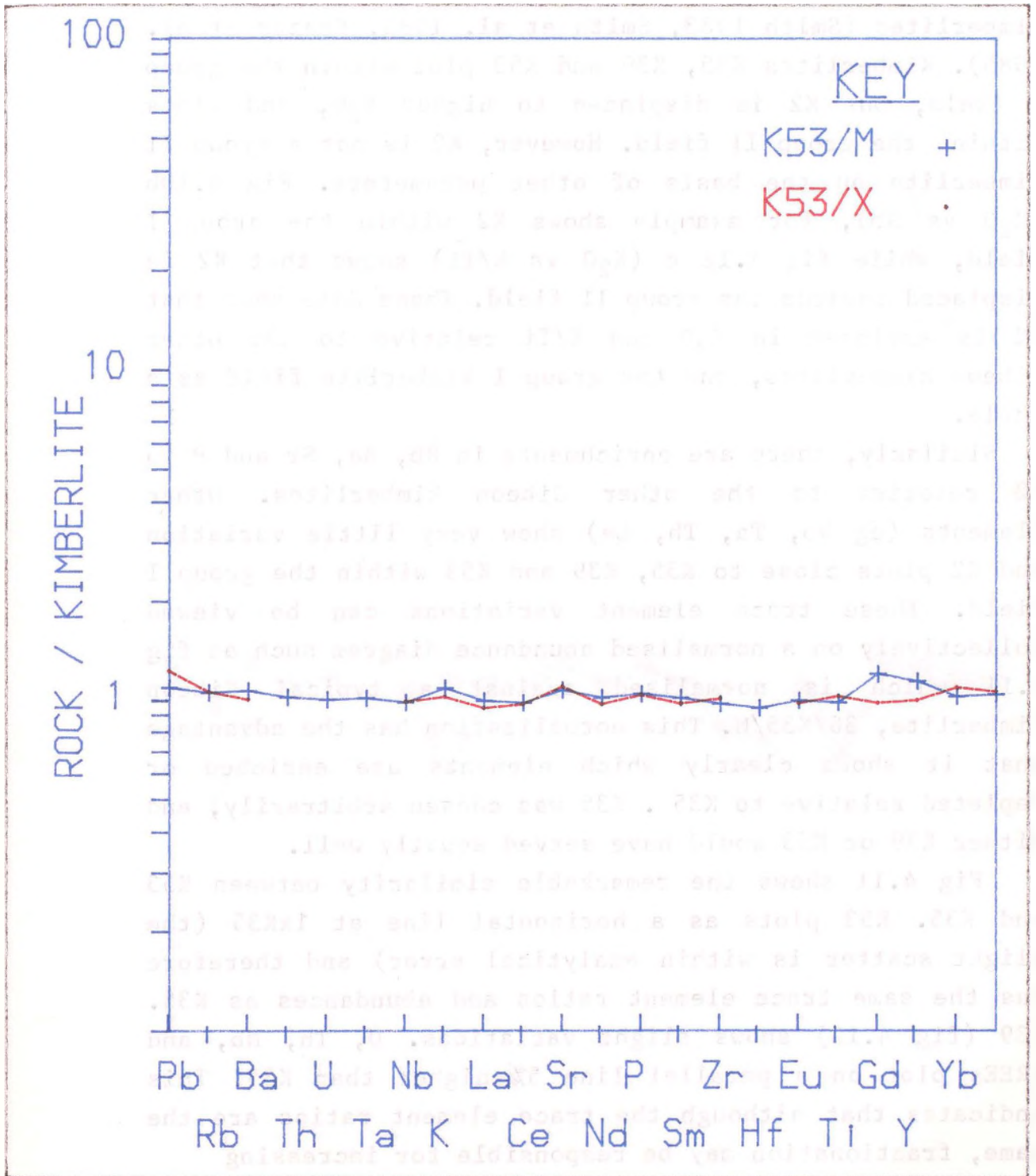


Fig 4.10. Trace element variations in the Gibeon kimberlites compared to group I and II kimberlites of Smith et al (1985). ● K2 ▲ K35 ▼ K39 ■ K53

Fig 4.11. Kimberlite-K35 normalised plot for K53



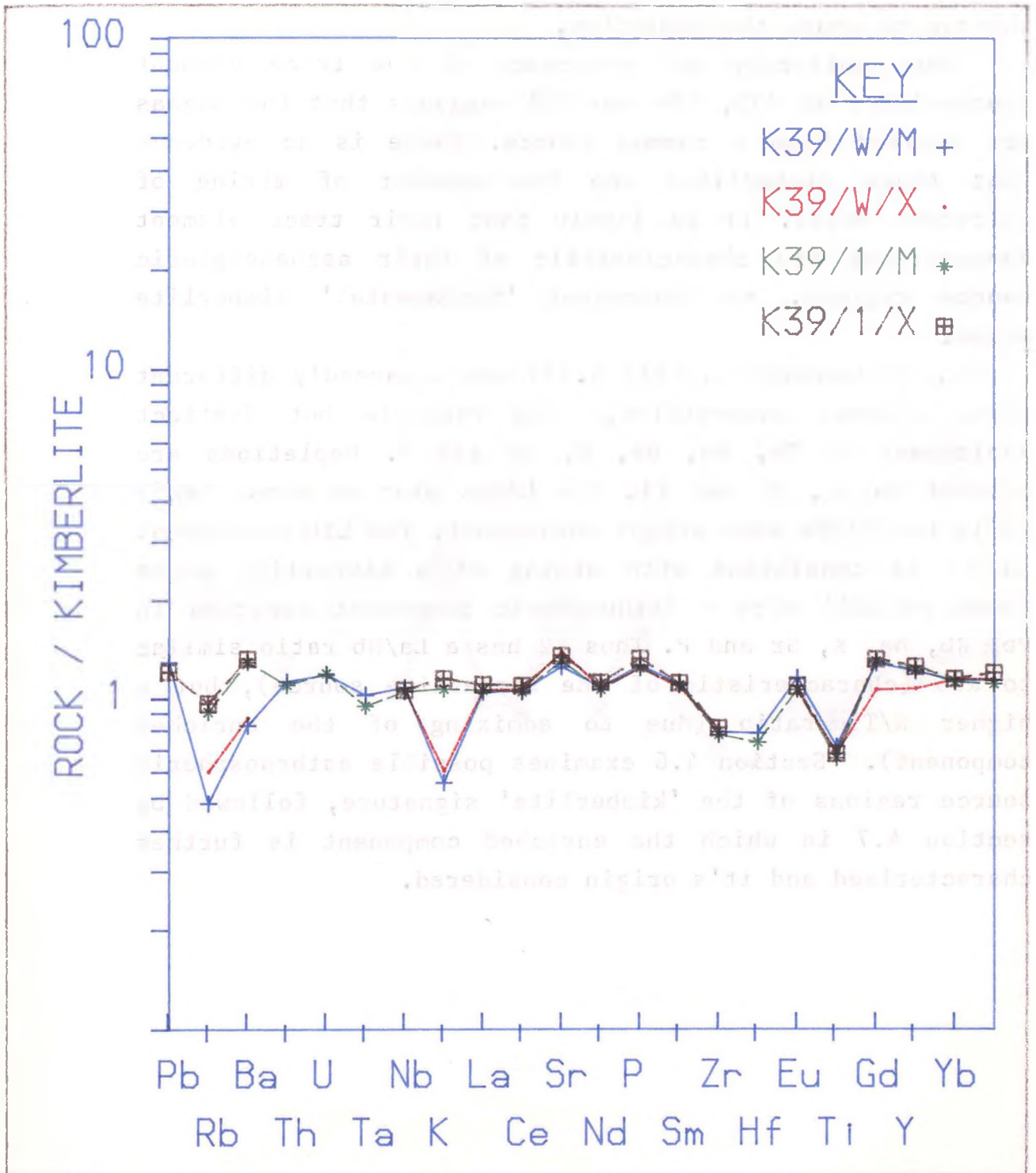
shows evidence of possible olivine and Cr-spinel fractionation (section 4.1), this fractionation is not responsible for its extreme trace element enrichment.

Figure 4.10a is a plot of K_2O vs TiO_2 , showing the Gibeon Kimberlites and the fields of other group I and II kimberlites (Smith 1983, Smith et al. 1985, Frazer et al. 1985). Kimberlites K35, K39 and K53 plot within the group I field, but K2 is displaced to higher K_2O , and plots within the group II field. However, K2 is not a group II kimberlite on the basis of other parameters. Fig 4.10b (K_2O vs Nb), for example shows K2 within the group I field, while fig 4.12 c (K_2O vs K/Ti) shows that K2 is displaced towards the group II field. These data show that K2 is enriched in K_2O and K/Ti relative to the other Gibeon kimberlites, and the group I kimberlite field as a whole.

Similarly, there are enrichments in Rb, Ba, Sr and P in K2 relative to the other Gibeon kimberlites. Other elements (eg Nb, Ta, Th, La) show very little variation and K2 plots close to K35, K39 and K53 within the group I field. These trace element variations can be viewed collectively on a normalised abundance diagram such as fig 4.11 which is normalised against a typical Gibeon kimberlite, 36/K35/M. This normalization has the advantage that it shows clearly which elements are enriched or depleted relative to K35. K35 was chosen arbitrarily, and either K39 or K53 would have served equally well.

Fig 4.11 shows the remarkable similarity between K53 and K35. K53 plots as a horizontal line at $1 \times K35$ (the slight scatter is within analytical error) and therefore has the same trace element ratios and abundances as K35. K39 (fig 4.12) shows slight variations. U, Th, Nb, and LREEs plot on a parallel line 5% higher than K35. This indicates that although the trace element ratios are the same, fractionation may be responsible for increasing

Fig 4.12. Kimberlite-K35 normalised plot for K39.

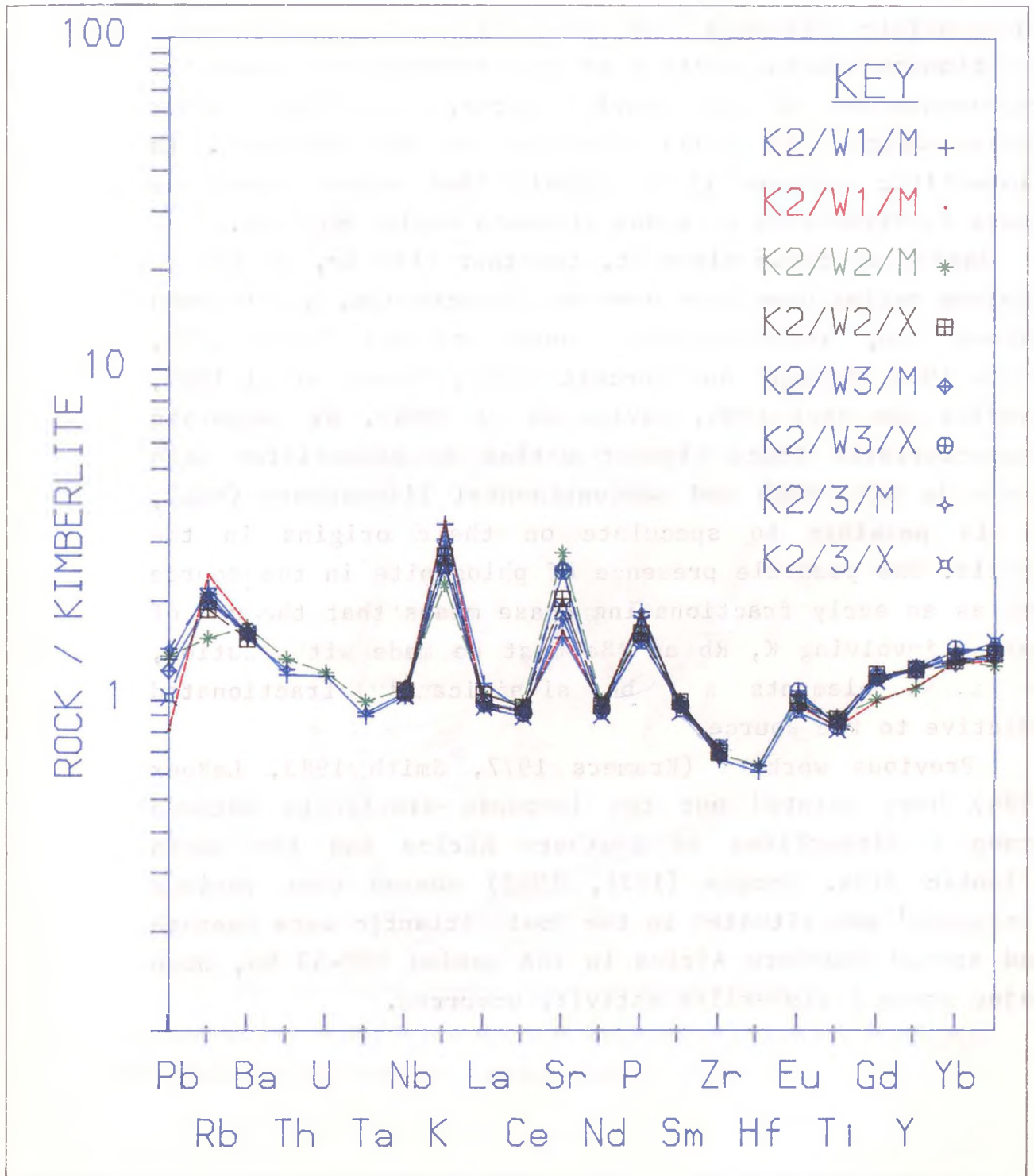


their abundance. However, with such small variations, such an interpretation is tentative. Ti, Hf and Zr are depleted in K39 relative to K35. This depletion is consistent with minor ilmenite and/or perovskite fractionation. Ilmenite crystallises before perovskite, and is the more likely of the two to cause the depletion.

The similarity and coherence of the trace element geochemistry of K35, K39 and K53 suggests that the magmas are derived from a common source. There is no evidence that these kimberlites are the product of mixing of different melts. It is likely that their trace element compositions are characteristic of their asthenospheric source regions, and represent 'fundamental' kimberlite magma.

K2, in comparison, (fig 4.13) has a markedly different trace element composition, with variable but distinct enrichment of Pb, Rb, Ba, K, Sr and P. Depletions are evident in Zr, Hf and Ti. The LREEs plot at about 1xK35 while the HREEs show slight enrichment. The LIL enrichment in K2 is consistent with mixing of a kimberlite magma (such as K35) with a lithospheric component enriched in Pb, Rb, Ba, K, Sr and P. Thus K2 has a La/Nb ratio similar to K35 (characteristic of the kimberlite source), but a higher K/Ti ratio (due to admixing of the enriched component). Section 4.6 examines possible asthenospheric source regions of the 'kimberlite' signature, followed by section 4.7 in which the enriched component is further characterised and it's origin considered.

Figure 4.13. Kimberlite-K35 normalised plot for K2.



In basaltic systems, the trace elements Rb, Ba, Th, U, K, Ta, Nb, and La have very low bulk distribution coefficients ($D < 0.1$). Ratios between these highly incompatible elements are generally not significantly fractionated during melting or fractionation and hence are representative of the mantle source, providing minor phases which host these elements are not involved. In kimberlitic systems it is likely that minor phases do cause fractionation of trace elements during melting.

Ratios of these elements, together with Sr, Nd and Pb isotope ratios have been used to characterize, and to some extent map, asthenospheric source regions (Hart 1984, White 1985, Allegre and Turcotte 1985, Weaver et al 1986, Zindler and Hart 1986, Davies et al 1988). By comparing characteristic trace element ratios in kimberlites with those in OIB, MORB and subcontinental lithosphere (SCL), it is possible to speculate on their origins in the mantle. The possible presence of phlogopite in the source and as an early fractionating phase means that the use of ratios involving K, Rb and Ba must be made with caution, as these elements may be significantly fractionated relative to the source.

Previous workers (Kramers 1977, Smith 1983, LeRoex 1986) have pointed out the isotopic similarity between group I kimberlites in Southern Africa and the South Atlantic OIBs. Morgan (1971, 1983) showed that various 'hotspots' now situated in the South Atlantic were beneath and around Southern Africa in the period 120-60 Ma, when major group I kimberlite activity occurred.

4.6.1 Location of OIB

Figure 4.14 shows the locations of several known ocean islands and seamounts in the South Atlantic, (namely Ascension, St Helena, Tristan da Cunha, Gough, Discovery, Vema, Shona and Bouvet) and their palaeo-tracks inferred from palaeo reconstructions of plate positions (Morgan 1983).

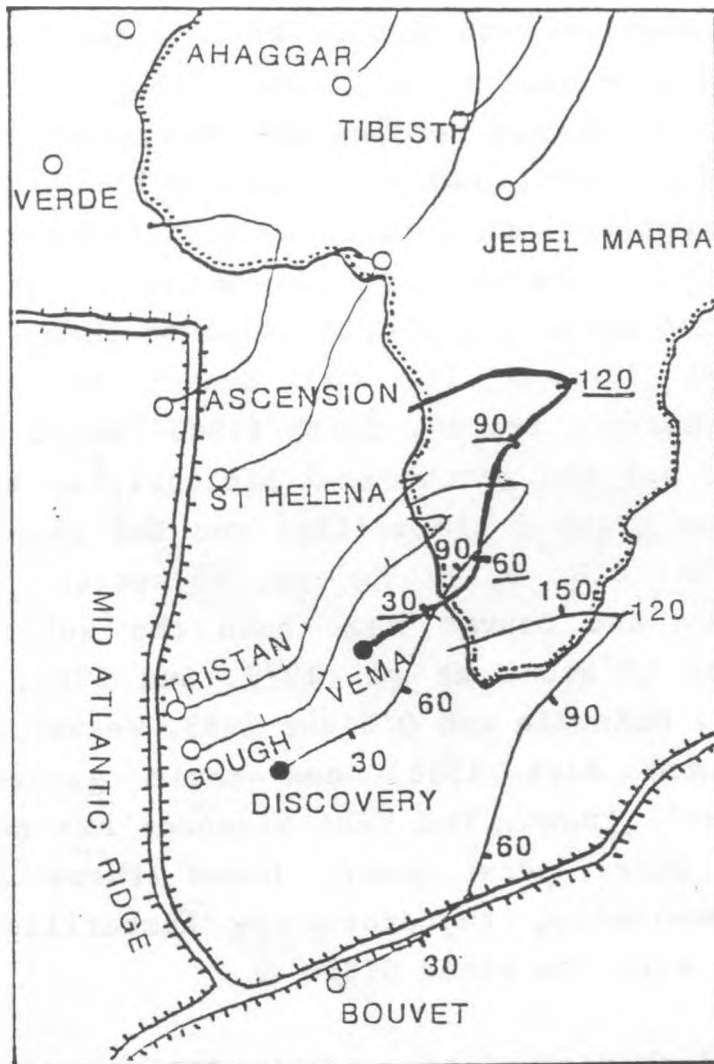


Figure 4.14. Location of OIB around the South Atlantic, and their palaeotraces, after Morgan (1983)

All of these hotspots have been located beneath Africa at some point during the last 150Ma. At 90Ma, the Discovery hotspot was located beneath central Namibia. By 60Ma, the Discovery hotspot had moved offshore, while the Vema hotspot was located beneath central Namibia. At 30Ma, Vema was located on coastal southern Namibia. All other hotspots were located away from Namibia at all times since 150Ma.

The Vema hotspot appears to coincide in time and space with the emplacement of the Gibeon kimberlites, and the Tertiary alkali volcanics of the Klinghardtts and Schwarzeberg. The Discovery hotspot was traversing central Namibia 30Ma before Vema, and may possibly be related to the Blue Hills monticellite peridotite (and other undated parakimberlites?) located in the Gibeon area.

The majority of group I kimberlites in southern Africa (erupted between 80 and 114 Ma) cannot be closely correlated with hotspot traces. Smith (1983) noted this, but also pointed out the geochemical similarities between the South African group I kimberlites and the basalts of Bouvet Island. The OIBs of St Helena, Ascension, Gough, Tristan Discovery and Bouvet have been the subject of extensive studies (O'Nions et al. 1977, Sun 1980, White and Hoffman 1982, McKenzie and O'Nions 1983, Weaver et al. 1986, Zindler and Hart 1986) and their geochemical signatures are well known. The Vema seamount has not yet been sampled (LeRoex pers comm), hence there is no chemical data available, therefore the kimberlites can only be compared with the other OIBs.

4.6.2 Geochemical characteristics of the OIBs

The South Atlantic islands display considerable inter-island variations in ratios of highly incompatible elements. Intra-island variations, although present, are relatively small, such that each island has distinctive

isotope and trace element characteristics.

Weaver et al. (1986) show that Ascension, Bouvet and St Helena have consistent trace element ratios (eg La/Nb, Ba/Nb, Ba/La, Ba/Th and Rb/Th). Tristan da Cunha and Gough are enriched in Ba relative to the other islands. For several trace element ratios, Gough and Tristan are clearly distinguishable from Bouvet, St Helena and Ascension. These differences can be illustrated on a mantle normalised abundance diagram (fig 4.15) or a trace element ratio-ratio plot (fig 4.16). Fig 4.15 shows the normalised abundances increasing from right (compatible) to left (incompatible), peaking at Nb, then decreasing for St Helena, Bouvet and Ascension. Gough and Tristan show distinct peaks at Ba. The Ba/Nb vs La/Nb plot (fig 4.16a) shows each island's distinct compositions, and the trend of increasing Ba/Nb and La/Nb in the Gough and Tristan lavas.

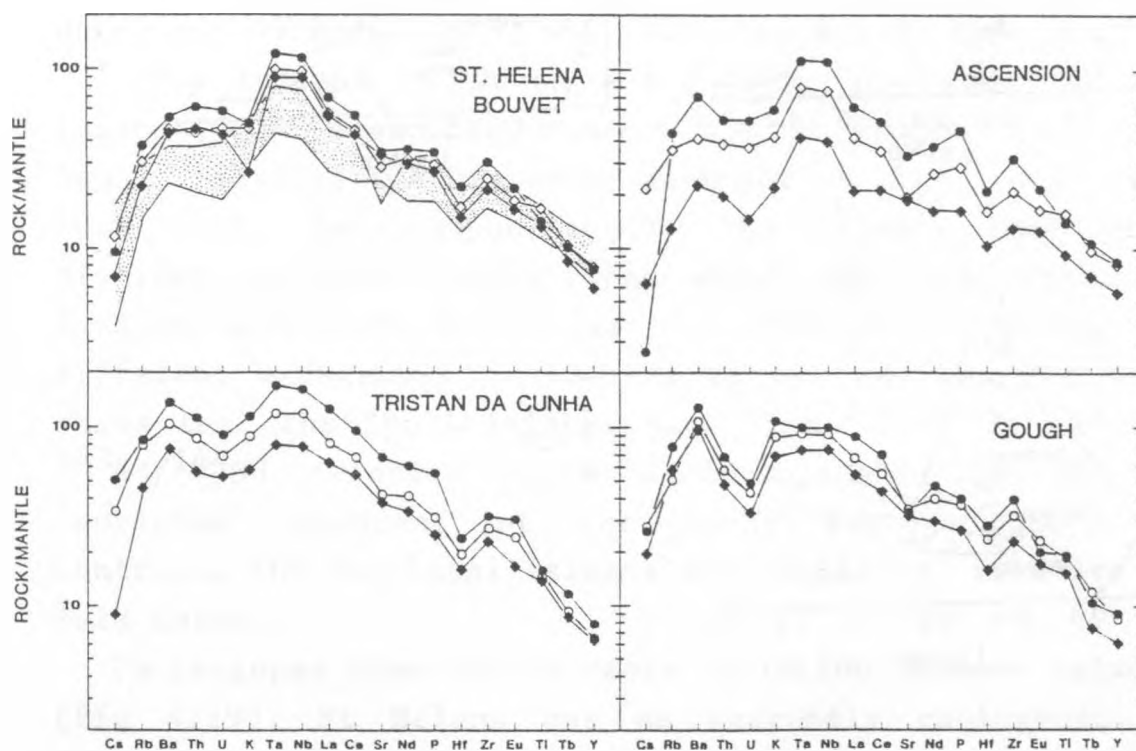


Figure 4.15. Mantle normalised trace element plots for South Atlantic OIB, from Weaver et al. (1986).

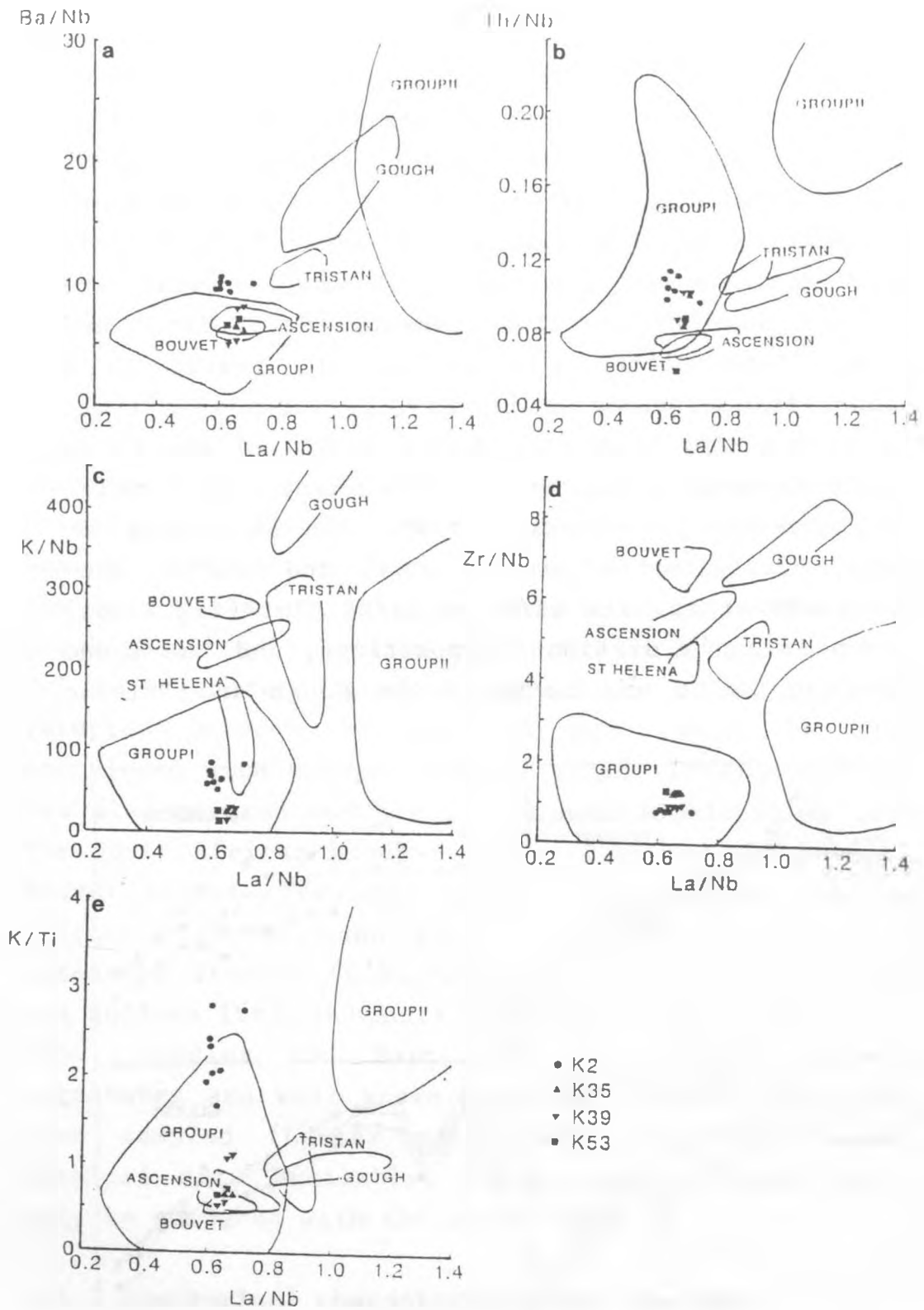


Fig 4.16. Incompatible element ratio plots for Gibeon kimberlites compared to South Atlantic OIB and group I and II kimberlites.

Dupre and Allegre (1983) and Weaver et al. (1986) interpret the trace element variations as the product of contamination of a typical OIB source with ancient pelagic sediments. Pb isotope data (Weaver et al 1986) indicate that this pelagic sediment is 1.5-2.0 Ga old. Allegre and Turcotte (1985) proposed that there may exist two end members, a 'primordial' source of essentially undifferentiated 'Bulk Earth' composition, and a second source derived from subducted oceanic lithosphere plus variable amounts of pelagic sediments. McKenzie and O'Nions (1983) suggested that delaminated subcontinental lithosphere could be an alternative source for the enriched component.

Hart (1984) showed that a number of OIBs located in a band in the southern hemisphere (between the Equator and 60°S) display similar enrichment features. This band (fig 4.17) is known as the 'Dupal Anomaly' (Hart 1984) after Dupre and Allegre (1983) who first noted it's existence.

The islands of Gough and Tristan are thus 'Dupal' islands, and Ascension, Bouvet and St Helena are 'non-Dupal' islands. The Discovery seamount is also 'Dupal' (Le Roex 1986, data unpublished). The islands each have distinct isotopic compositions which are interpreted by Zindler and Hart (1986) as the product of mixing of different end-member reservoirs in the mantle. Fig 4.18 shows that the Dupal islands have high $^{87}\text{Sr}/^{86}\text{Sr}$ and low $^{143}\text{Nd}/^{144}\text{Nd}$ relative to Bulk Earth, and lie in the 'enriched' quadrant of the Nd-Sr isotope plot. In contrast, the non-Dupal islands are 'depleted' relative to Bulk Earth.

Pb isotopes show considerable variation between islands (fig 4.19). St Helena has an extremely radiogenic Pb composition and plots close to the endmember HIMU source of Zindler and Hart (1986). Bouvet and Ascension have less radiogenic Pb than St Helena, and plot close to the

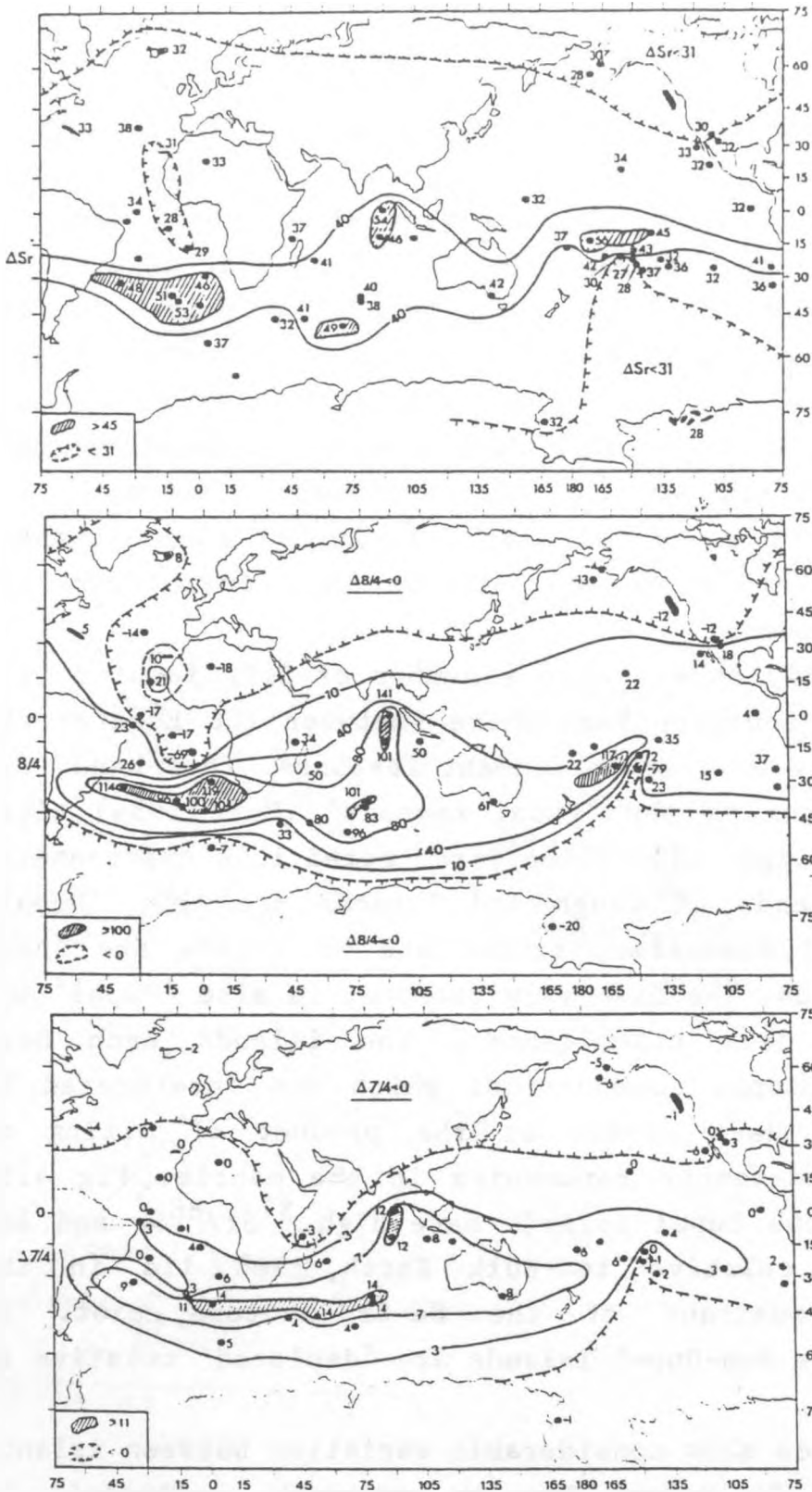


Figure 4.17. Dupal anomaly contours from Hart (1984). Figures refer to Sr, 8/4 and 7/4 deviations from reference values. See Hart (1984) for details. Note location of Namibia within Hart's Dupal zone.

northern hemisphere reference line (NHRL, Hart 1984). Gough lies at lower $^{206}\text{Pb}/^{204}\text{Pb}$ (18.5), but has elevated $^{207}\text{Pb}/^{204}\text{Pb}$ (15.6) above the NHRL. This ^{207}Pb enrichment indicates an ancient enrichment event (Sun 1980).

4.6.3 Comparison of Kimberlites and OIBs

Kimberlites have trace element concentrations significantly higher than OIBs, with steeper REE patterns. Such differences could be produced by different degrees of partial melting of similar source materials. Significant trace element fractionation may occur if minor phases have a controlling effect during melting. Ratios of markedly different elements (eg La/Yb) are not expected to be representative of source materials, though ratios of very similar elements (eg La/Nb) may be.

On the mantle normalised trace element plot (eg fig 3.10), kimberlites characteristically have a trough at K. This trough could be due to the retention of a K bearing phase in the source during melting. This phase is likely to be phlogopite. Phlogopite may also be involved in early fractionation, hence the presence of phlogopite macrocrysts in many kimberlites. Trace elements concentrated in phlogopite (K and Rb in particular) are therefore unlikely to be useful as an indicator of mantle source regions. Similarly, ilmenite, perovskite and zircon may have controlling effects on Ti, Hf and Zr. The use of trace element ratios as source region characterisers is therefore potentially misleading.

The potassium troughs are less common and less pronounced in alkali basalts, an indication that the potassium bearing phase (?phlogopite) has melted during basalt production. This is to be expected as basalts are produced by a higher degree of partial melting. The La/Nb ratio appears to be the most consistent ratio

amongst the Gibeon kimberlites, and is perhaps the best indicator of asthenospheric source characteristics. The Gibeon kimberlites have a limited La/Nb range (0.6-0.7) which is similar to those of the non-Dupal OIBs, Bouvet, St Helena and Ascension. K/Nb and Rb/Nb are lower in the kimberlites than in the OIBs (fig 4.16), perhaps because some phlogopite remains in the source during melting, which retains K and Rb in the source relative to Nb. K2 has higher and more variable Rb and K than K35, K39 and K53 (this variation is interpreted as a secondary enrichment in section 4.7). Ba/Nb ratios, like La/Nb ratios are similar in the Gibeon kimberlites to those in the non-Dupal OIBs (fig 4.16), suggesting that Ba, unlike K and Rb, is not retained preferentially in the asthenospheric source. This suggests that either Ba is hosted primarily in another phase (macrocryst phlogopites have low Ba concentrations) or residual phlogopite is not the cause of the low K and Rb in the kimberlites.

Measured Th/Nb ratios are somewhat variable (fig 4.16) in the kimberlites (possibly due to a higher degree of analytical error) and are slightly higher than (though within the range of) the Th/Nb ratios from Bouvet, Ascension and St Helena. The higher Th/Nb ratios could be due to a smaller degree of partial melting in the kimberlites than in the OIBs, and the greater incompatibility of Th than Nb. The ^{208}Pb compositions of the kimberlites do not support the alternative proposal that the kimberlite source has higher Th/Nb than the Bouvet source, as their $^{208}\text{Pb}/^{204}\text{Pb}$ initial ratios are very similar. It is therefore concluded that the slightly higher Th/Nb ratios of the kimberlites is due to Th being more incompatible than Nb, and Th/Nb fractionation occurring at very low degrees of partial melting.

Zr/Nb and Hf/Nb ratios show very little variation between kimberlites (fig 4.16). As K2 has similar Zr/Nb

and Hf/Nb to K35, K39 and K53, it is unlikely that either the fractionation or secondary trace element enrichment evident in K2 has significantly affected the Zr/Nb and Hf/Nb ratios. The Zr/Nb ratio of the kimberlite (~ 1) is much lower than that of the OIBs (>4). This can be attributed to the fact that Nb is more incompatible than Zr and Hf, and therefore fractionation of Zr and Hf relative to Nb occurs during partial melting. Zr/Nb, and Hf/Nb ratios are therefore of little use in comparing source regions.

The K/Ti ratio of K35, K39 and K53 is similar to that of Bouvet and Ascension. K2 has significantly higher K/Ti (fig 4.16). Both K and Ti appear to be depleted relative to the other trace elements in the kimberlites (fig 3.10), perhaps due to retention in a minor phase during partial melting. It may therefore be coincidence that the K/Ti ratio in K35 etc. falls within the range of Bouvet and Ascension. However, if K and Ti are both hosted primarily in the same phase, then the K/Ti ratio of that phase would characterize the K/Ti of the melt (and the source region). Thus if K and Ti are hosted primarily in phlogopite (or even mathiasite, the K-titanate), the retention of these two elements together may still result in K/Ti ratios that are characteristic of the source, even though K/Nb ratios are not.

Cautious interpretation of trace element ratios reveal that the Gibeon kimberlites appear to have asthenospheric source regions which are similar to the non-Dupal islands of the South Atlantic (Bouvet, Ascension and St Helena) The trace element data are not distinctive enough to correlate the Gibeon kimberlites with any particular island. Group I kimberlites in general show much larger variations in trace element ratios than the Gibeon kimberlites, such that no single ocean island source could represent all the South African kimberlites.

La/Yb and possibly also Zr/Nb and Th/Nb ratios may be used as a relative measure of degree of partial melting. High La/Yb and Th/Nb and low Zr/Nb are indicative of low degrees of partial melting. The Gibeon kimberlites have higher La/Yb and Th/Nb, and lower Zr/Nb than the non-Dupal OIBs, which (coupled with similar La/Nb and Ba/Nb) indicates that the kimberlites reflect lower degrees of partial melting of similar source materials.

K35 and K53 display little variation in La/Yb ($\text{La/Yb}_N=110-120$), Th/Nb (0.837-0.869) and Zr/Nb (1.25-1.29), which together with isotope ratios that are identical within error suggests that the two kimberlites were derived from an identical source by the same degree of partial melting, or that they are derived from the same batch of melt. K39 also has similar La/Yb and Th/Nb, but has lower Zr/Nb (0.93-0.97) than K35 and K53. The Zr and Hf depletion in K39 could be due to slight ilmenite fractionation. La/Yb and Th/Nb ratios are not significantly affected by slight olivine or ilmenite fractionation. Thus taken together, these ratios suggest that K39 was also produced by the same degree of partial melting as K35 and K53.

Kimberlite K2 is more difficult to interpret because it's composition appears to have been modified by a secondary trace element enrichment process. The La/Yb ratio is decreased by the addition of a component which has lower La/Yb than the kimberlite. This component has the effect of significantly enriching the HREE content of the rock. The La/Yb ratio, therefore, is not a useful indicator of the degree of melting in K2. Th/Nb (0.98) and Zr/Nb (0.82) are slightly higher and lower respectively in K2 than the other kimberlites, which may possibly indicate a lower degree of partial melting for K2. However, because of the small variations and high 'noise' in the data, such a conclusion cannot be rigorously maintained. Within the

limitations of the scatter of the data, it is concluded that the Gibeon kimberlites are all derived from very similar asthenospheric sources, by the same degree of partial melting.

Trace element ratios are subject to fractionation during partial melting but isotope ratios are not. A comparison of isotope ratios is therefore of interest. The Gibeon kimberlites were erupted 70+/-10 Ma ago, whereas the South Atlantic OIBs are less than 10Ma old (White and Hoffman 1982). The Epsilon notation (DePaulo and Wasserburg 1976) is therefore used to represent initial ratios (see appendix 1).

The Gibeon kimberlites have time integrated 'depleted' isotope characteristics ($\epsilon_{\text{Sr}}=-9.7$ to -14 , $\epsilon_{\text{Nd}}=1.56$ to 2.79) as have other group I kimberlites (fig 4.18). The Gibeon kimberlites plot close to Bouvet, but at slightly lower Nd. Fig 4.18 shows that the Gibeon kimberlites (and other group I kimberlites) have isotopic characteristics that are similar to non-Dupal OIBs, particularly Bouvet, but are not identical.

Pb isotopes cannot be measured relative to the Bulk Earth evolution as are Sr and Nd, because the Bulk Earth value is not known. The Gibeon kimberlites are age corrected to 70Ma using measured U/Pb ratios. It is not possible to age correct the OIBs in this way because the measured U/Pb ratios in the basalts is higher (Sun 1980) than in the source in which the Pb isotopes developed during the last 70Ma. The U/Pb ratios of the sources are not known precisely, but Sun (1980) has shown that OIBs have μ values ($^{238}\text{U}/^{204}\text{Pb}$) ranging from 10 to 30. Thus taking the maximum possible μ value of 30, it is calculated that the $^{206}\text{Pb}/^{204}\text{Pb}$ growth is only 0.3 in 70Ma. A more realistic μ value of 10-15 results in $^{206}\text{Pb}/^{204}\text{Pb}$ growth of 0.1-0.15. Thus the $^{206}\text{Pb}/^{204}\text{Pb}$ growth over 70Ma in the OIB source is very small compared

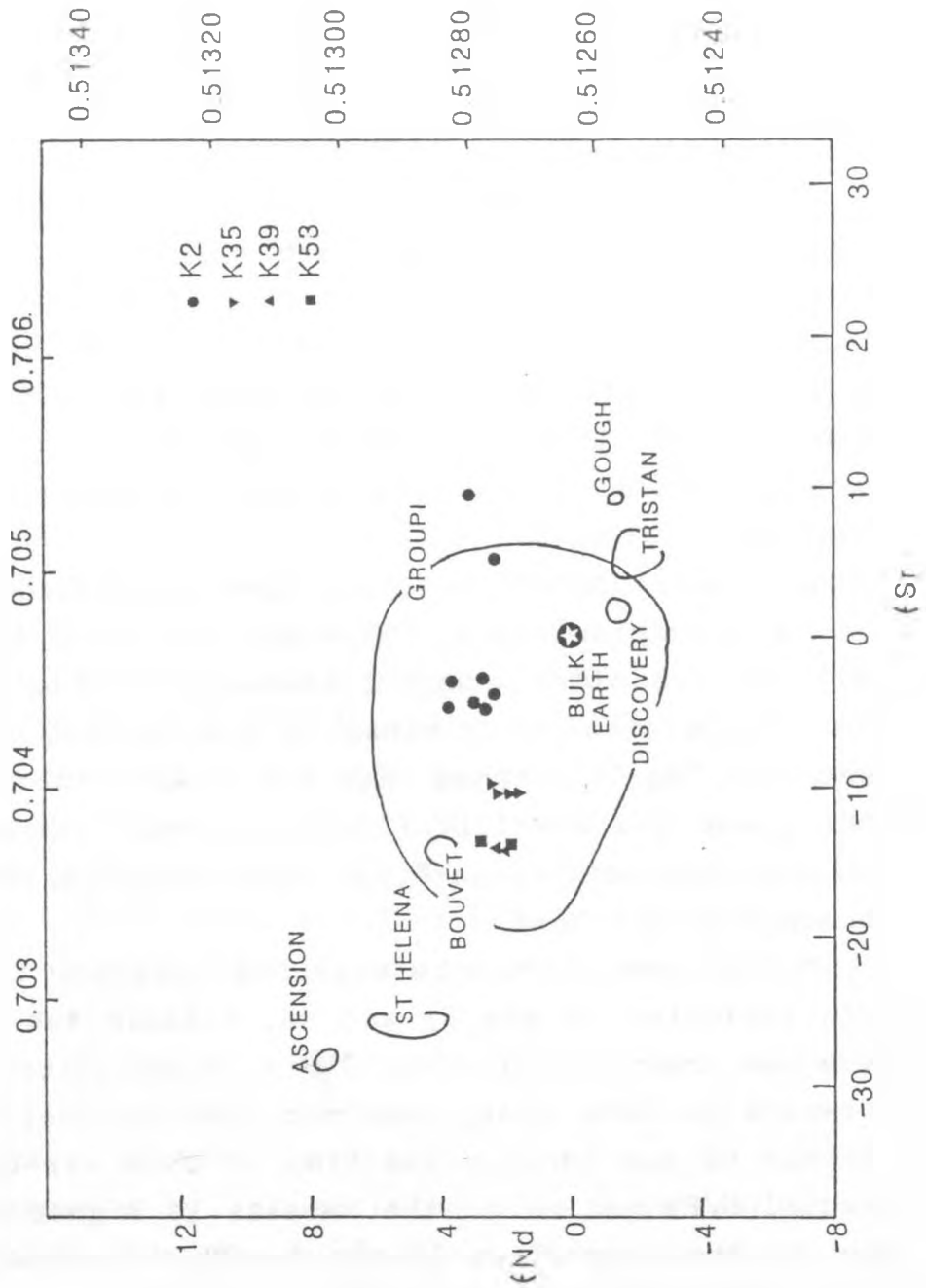


Figure 4.18. ϵ_{Nd} v ϵ_{Sr} for Gibeon kimberlites. Note that K2 is displaced to high ϵ_{Sr} compared to the other kimberlites which cluster close to Bouvet.

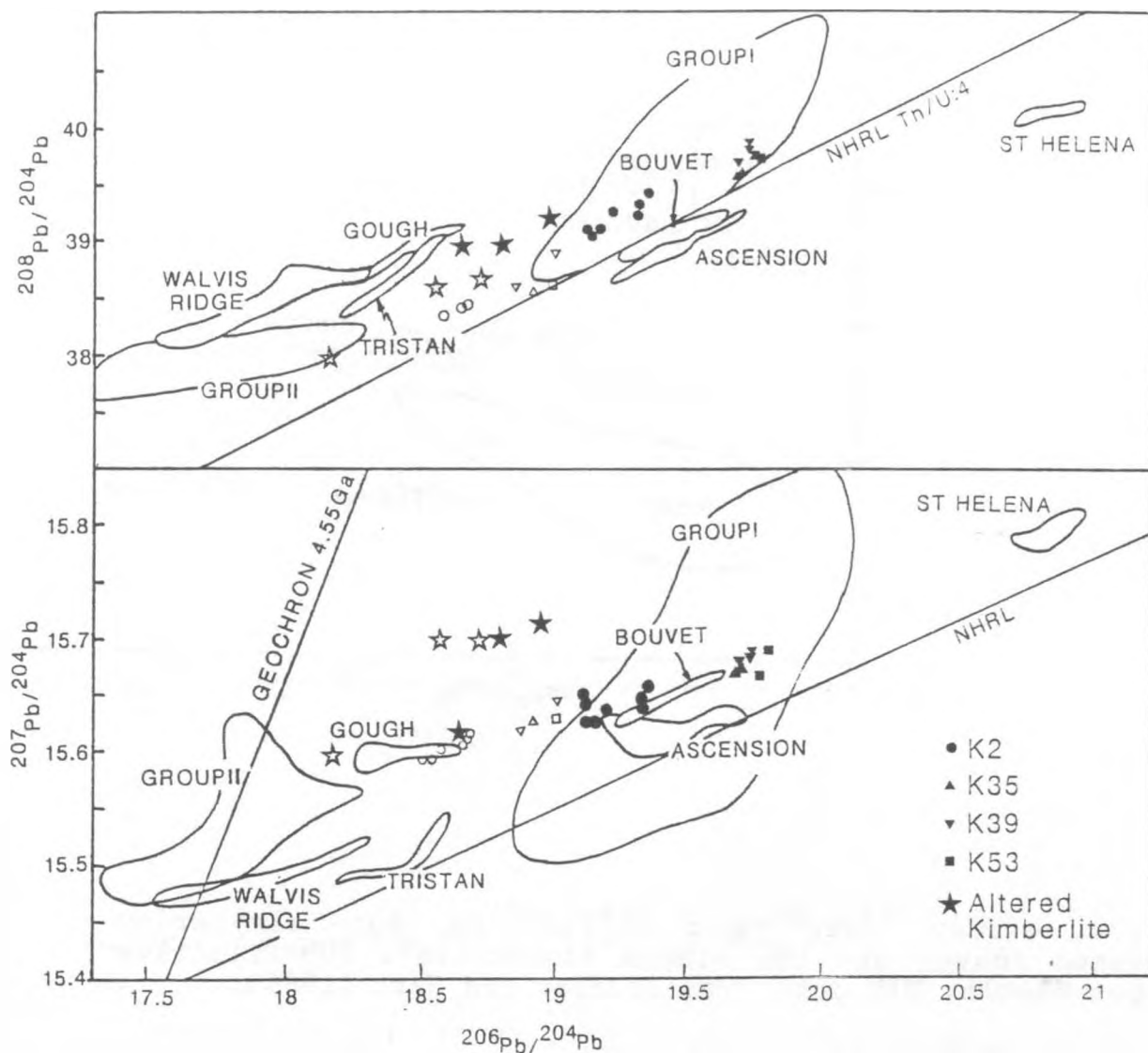


Fig 4.19. Pb isotope composition of the Gibeon kimberlites. Filled symbols represent measured (present day) ratios, open symbols, initial (70Ma) ratios. The kimberlites plot close to Bouvet. Altered samples are displaced to high 7/4 and 8/4. See text for discussion. OIB data from Zindler and Hart (1986)

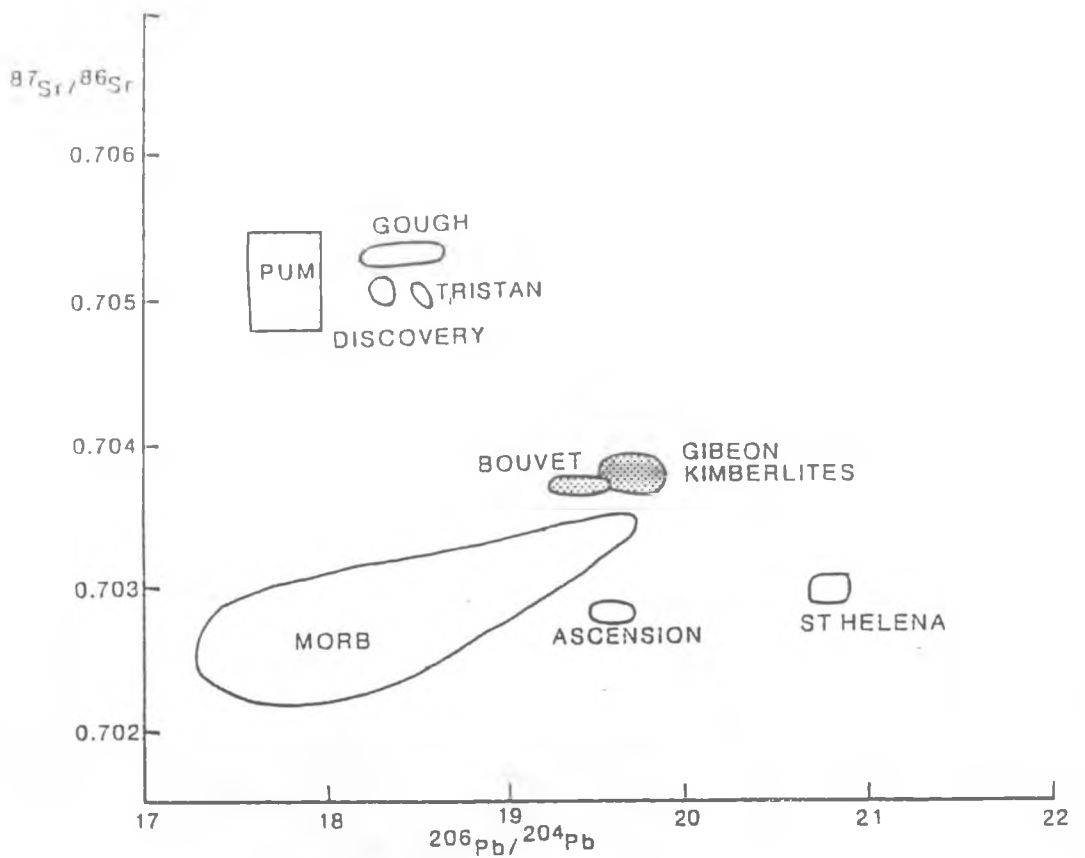


Figure 4.20a. $^{87}\text{Sr}/^{86}\text{Sr}$ v $^{206}\text{Pb}/^{204}\text{Pb}$. Note similarity between Bouvet and the Gibeon kimberlites. PUM=Primitive upper Mantle. OIB data from Zindler and Hart (1986).

to the $^{206}\text{Pb}/^{204}\text{Pb}$ variations between islands. The kimberlites, in contrast have u values of 49 to 78, producing changes of 0.54 to 0.85 in the $^{206}\text{Pb}/^{204}\text{Pb}$ ratio over 70Ma. ^{235}U and ^{232}Th have shorter half-lives than ^{238}U , and most of the ^{235}U and ^{232}Th originally in the earth has now decayed away. As a result, the relative growth of ^{207}Pb and ^{208}Pb in the last 70Ma are small compared to the growth of ^{206}Pb .

The Pb isotope variation between ocean island sources is large compared to the change in composition over 70Ma, so kimberlite initial ratios can be compared with present day (=initial) ratios of OIBs.

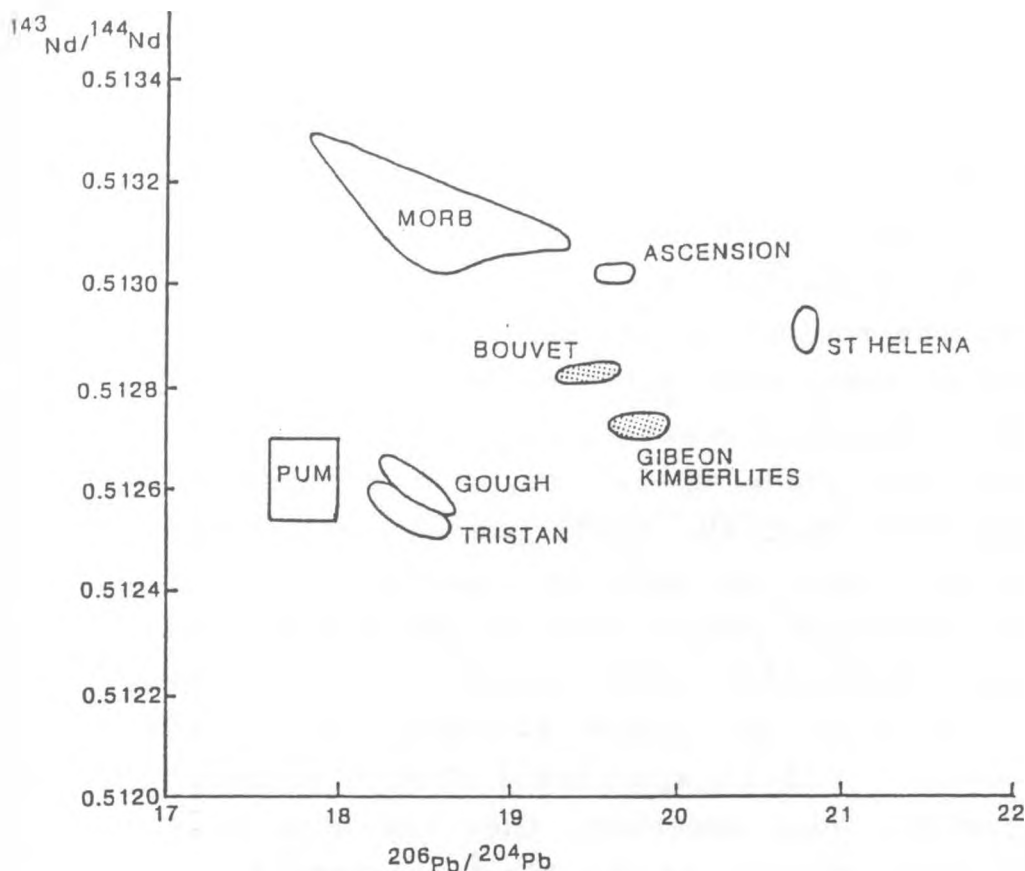


Figure 4.20b. $^{143}\text{Nd}/^{144}\text{Nd}$ v $^{206}\text{Pb}/^{204}\text{Pb}$.

Kimberlite and OIB Pb initial ratios are plotted in fig 4.19. The Gibeon kimberlites plot in a close cluster ($^{206}\text{Pb}/^{204}\text{Pb}=18.85-19.02$; $^{207}\text{Pb}/^{204}\text{Pb}=15.63-15.65$; $^{208}\text{Pb}/^{204}\text{Pb}=38.56-38.85$) within the group I field, and close to Bouvet and Ascension. The kimberlites have slightly lower initial $^{206}\text{Pb}/^{204}\text{Pb}$ than the present day Bouvet, but similar $^{207}\text{Pb}/^{204}\text{Pb}$ and slightly lower $^{208}\text{Pb}/^{204}\text{Pb}$. St Helena has much higher $^{206}\text{Pb}/^{204}\text{Pb}$, $^{207}\text{Pb}/^{204}\text{Pb}$ and $^{208}\text{Pb}/^{204}\text{Pb}$ than the Gibeon kimberlites, whilst the Dupal islands of Gough and Tristan have much less radiogenic Pb. Fig 4.20a (Sr-Pb) and 4.20b (Nd-Pb) show that the Gibeon kimberlites can best be correlated with the Bouvet OIB source.

In conclusion, the Gibeon kimberlites (K35, K39 and K53) show a restricted range of trace element and isotope compositions which reflect their origins in a source region similar to that of Bouvet. The variation in K2 cannot simply be explained as a variation in the asthenospheric source region, as the more radiogenic Sr of K2 requires a time integrated Rb/Sr enrichment which is unfeasible in the convectively mixing asthenosphere.

The kimberlites are produced by very low degrees of partial melting, such that the partition of some trace elements (eg K, Rb) into the melt is controlled by the presence of low abundance phases such as phlogopite. In the case of basalt production these phases are likely to melt completely so that the trace elements behave as incompatible elements. It is speculated that if samples are obtained from the Vema seamount, they may show non-Dupal characteristics, similar to the Gibeon kimberlites.

Hart (1984) extrapolated contours of the 'Dupal Anomaly' through Namibia (fig 4.17) and Vema. The kimberlite data indicate that non-Dupal type magma source exists beneath Southern Africa, and therefore that the Dupal anomaly does not exist as a broad continuous belt around the southern hemisphere.

4.7 THE TRACE ELEMENT COMPOSITION OF K2

The trace element composition of kimberlite 33/K2 can be interpreted as the product of the mixing of a kimberlite magma (of the same composition as K35, K39 and K53) and a component enriched in the trace elements K, Rb, Ba, Pb, Sr and P (section 4.5). The composition and amount of this component is not known. A closer examination of the difference between the K2 samples and K35 (which can be taken as a typical and representative Gibeon kimberlite) reveals more about the character of this

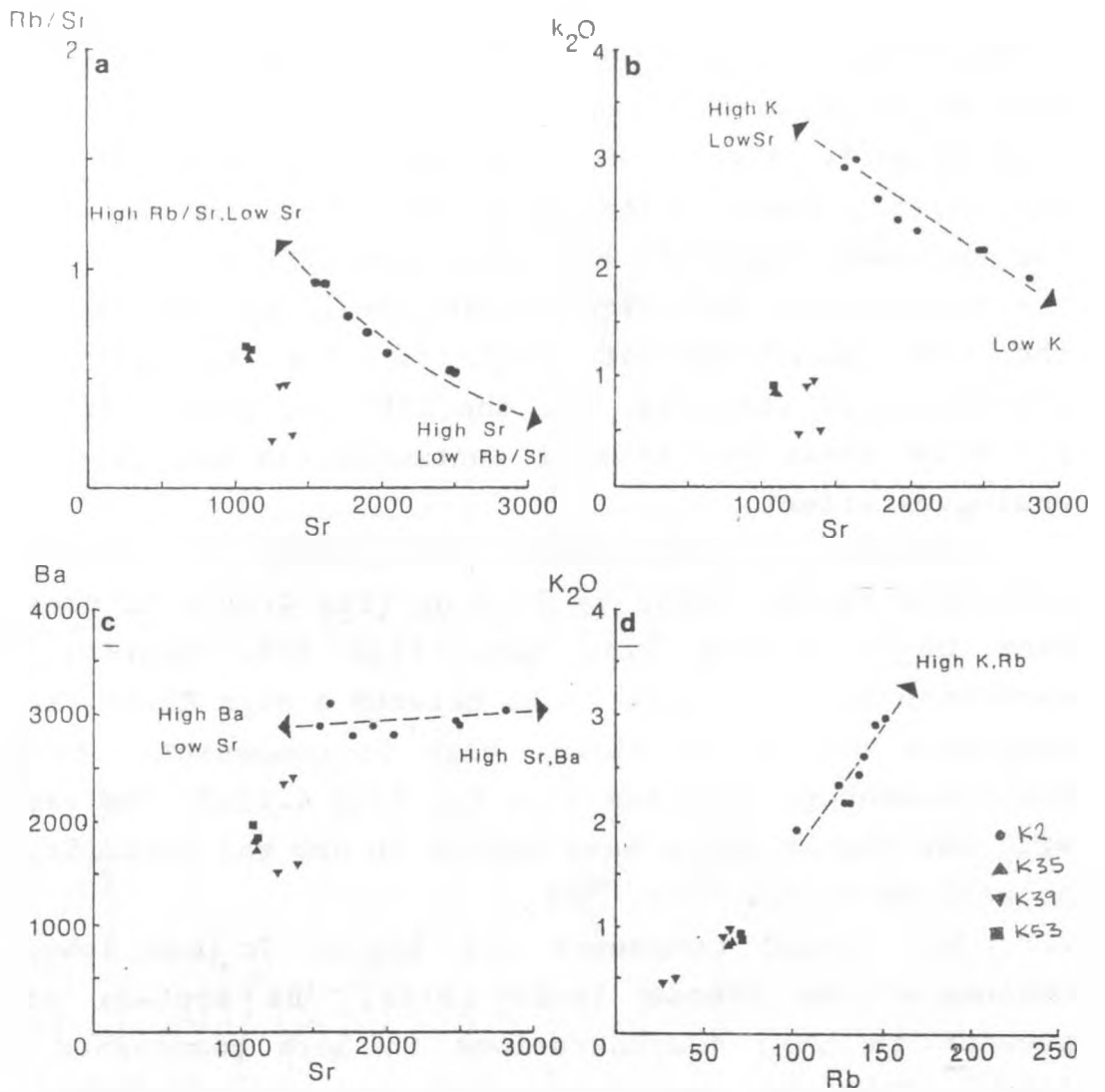


Figure 4.21. Trace element plots showing the nature of the enrichment in K2. (a) K2 forms a mixing trend between a high Rb/Sr, low Sr component and a low Rb/Sr, high Sr component. (b), (c) and (d) show that the High Rb/Sr component has high K, Rb and Ba and the low Rb/Sr component has low K and Rb, but high Ba.

component. This information is then compared to known mantle and crustal materials in order to constrain the possible origins of the enriched component.

Relative to K35, K2 has increased K/Ti, K/Ba, Rb/Ba, K/Nb, and Sr/Nd, and decreased U/Pb and La/Yb. There is also an increase in $^{87}\text{Sr}/^{86}\text{Sr}$ and Sr ppm, but little change in $^{143}\text{Nd}/^{144}\text{Nd}$ and Nd ppm. There is a decrease in

$^{206}\text{Pb}/^{204}\text{Pb}$, $^{207}\text{Pb}/^{204}\text{Pb}$, $^{208}\text{Pb}/^{204}\text{Pb}$ and U/Pb, together with an increase in Pb ppm. K2 has slightly lower LREE and significantly higher HREE contents than K35 (figs 4.2, 4.7, 4.13). These differences can be easily modelled if the enriched component has much less LREE enrichment than the kimberlite, but significant levels of REE such that the low abundance of HREE in the kimberlite are significantly enriched, but the LREE are hardly affected. Fig 4.3a shows how crustal contamination can produce an analogous effect.

A problem in this simple mixing model is revealed by reference to the Rb/Sr vs Sr plot (fig 4.21): K2 does not plot on a mixing line away from K35. Instead, the variation in K2 appears to be between a high Rb/Sr, low Sr component and a low Rb/Sr, high Sr component. The high Rb/Sr component also has high K_2O (fig 4.21b). The samples with the higher Rb/Sr have higher Rb ppm and lower Sr ppm, as well as higher $^{87}\text{Sr}/^{86}\text{Sr}$.

The second component has higher Sr and lower Rb concentrations (hence lower Rb/Sr). Ba appears to be present in high concentrations in both components (fig 4.21c). These two components could be two phases which are melted into the kimberlite, first the high Rb/Sr phase, then the high Sr phase.

As a first approximation of the composition of the enriched component(s), the composition of K35 is subtracted from the average of the eight K2 samples. This 'additional component' (K2^*) is plotted on a kimberlite normalised diagram (fig 4.22d). K2^* has a very distinctive pattern on the kimberlite normalised diagram. It has peaks at Pb, Rb, Ba, K, Sr and P, and troughs at Nb, Ta, La, Ce Nd and Sm. Clearly, bulk assimilation of average crustal materials (fig 4.22a) or Etendeka flood basalts (fig 4.22b) would not cause the enrichment patterns found in K2. Mantle peridotites generally have low concentrations

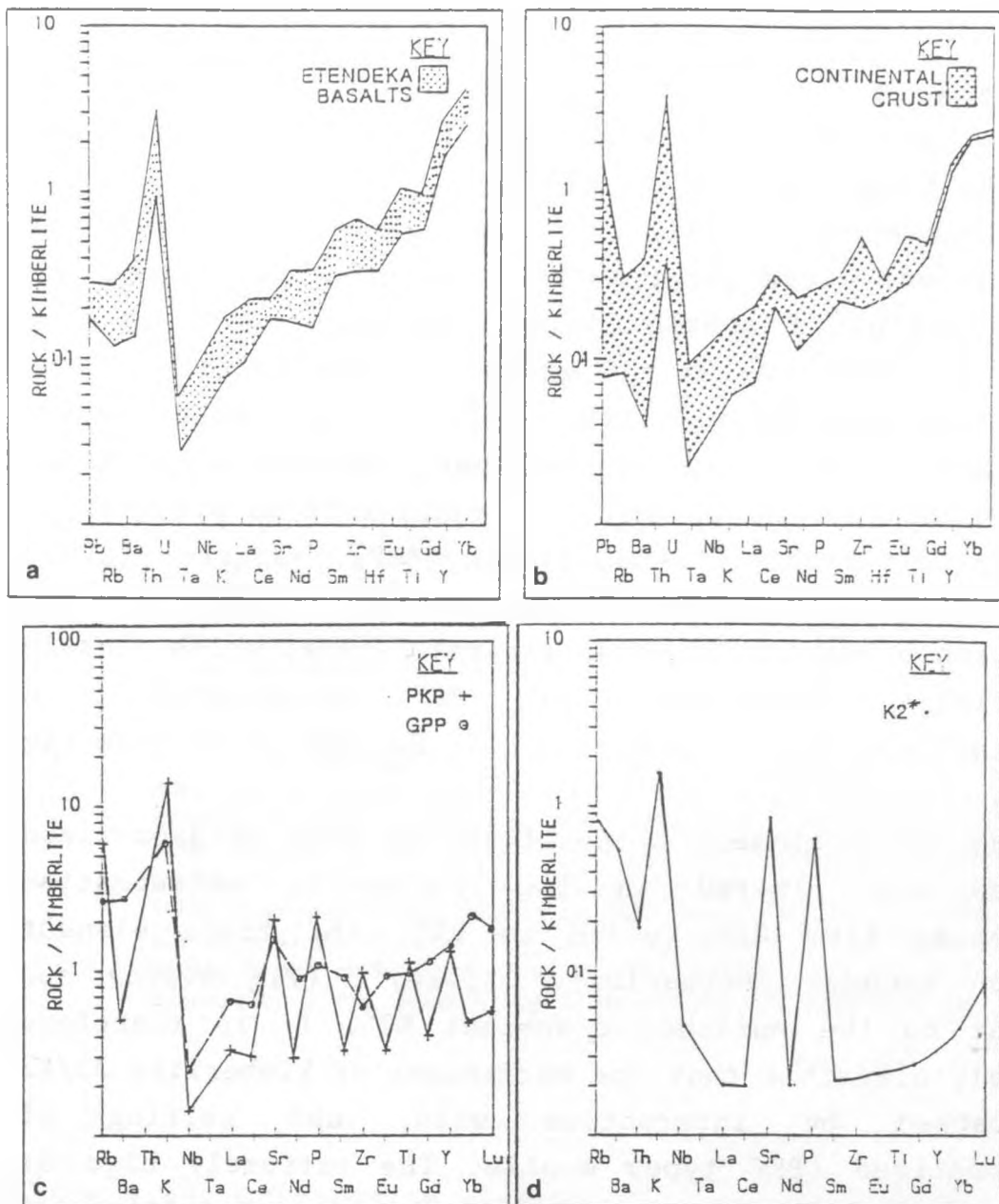


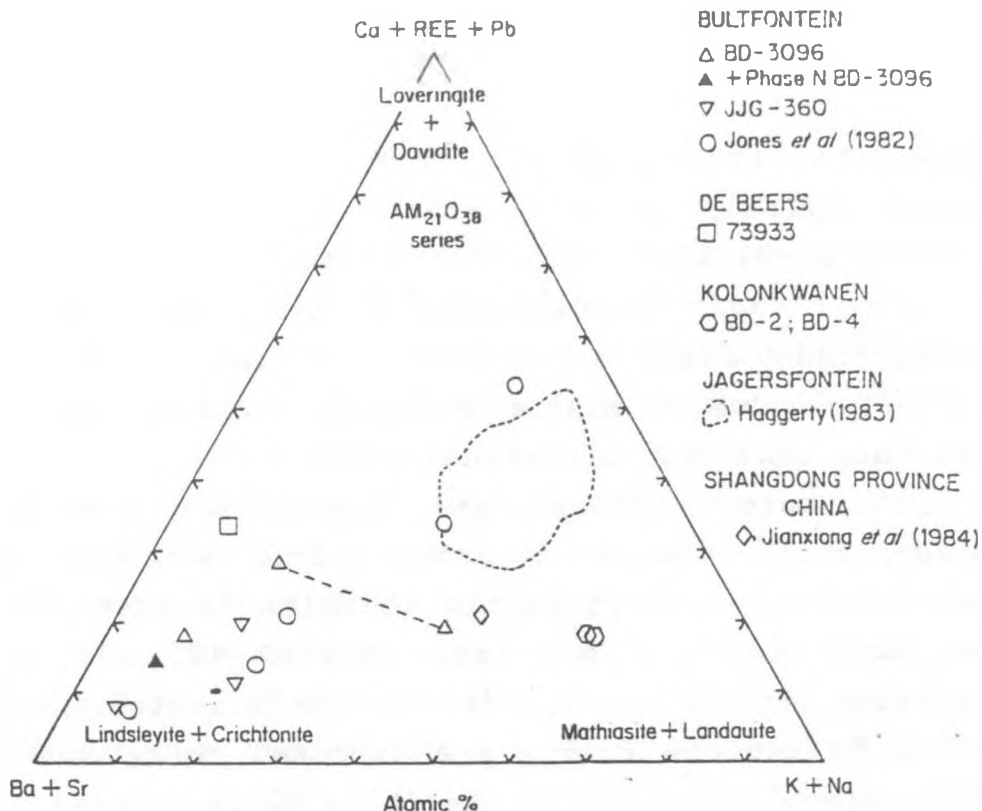
Figure 4.22. Kimberlite normalised trace element plots for various crustal and mantle materials. (a) and (b) shows that crustal and basaltic patterns are not similar to the enriched component $K2^*$ (d). Enrichment of peridotites by metasomatism produces PKP mantle which bears resemblance to $K2^*$, with increased Rb, Ba, K, Sr and P relative to Nb and REEs. Data from Taylor and McClelland (1985), Erlank et al (1984) and Erlank et al. (1987).

of incompatible trace elements (Nixon 1987). Metasomatised peridotites, however, are greatly enriched in incompatible elements (Lloyd and Bailey 1975).

Erlank et al. (1987) show how a suite of peridotites from Kimberley are progressively enriched (metasomatised) by the influx of mantle fluids. Metasomatism of garnet-peridotite (GP) causes the growth of phlogopite, forming garnet-phlogopite-peridotite (GPP). As metasomatism progresses, garnet is reacted out, forming phlogopite-peridotite (PP) and ultimately K-richterite is produced in phlogopite-K-richterite-peridotite (PKP). Haggerty (1983, 1986) has found that metasomatism also results in the formation of exotic Ti-oxide minerals (LIMA) which contain significant quantities of Ba (Lindsleyite), K (Mathiasite), Sr (Crichtonite), Ca, Na, REE or Pb (see fig 4.23).

The trace element compositions of some metasomatised nodules are plotted in fig 4.22c. As metasomatism progresses from GPP to PP to PKP, the trace element pattern becomes increasingly 'spikey', (fig 4.22c) and similar to the enriched component K2*. It is therefore entirely plausible that the enrichment of kimberlite 33/K2 is caused by interaction with, and melting of metasomatised (PKP type) mantle. The extremely high Sr enrichment could be plausibly explained by melting of crichtonite, the Sr-Ti-oxide found in PKP metasomatised nodules. Such an explanation fits the enrichment characteristics of K2. The two components (high Rb/Sr and high Sr) identified in fig 4.21 can therefore be explained by phlogopite + K-richterite melting to provide Rb, K and Ba (the high Rb/Sr component) whilst crichtonite/lindsleyite provide Sr and Ba (the high Sr component).

Isotopic constraints support this explanation, as the high Rb/Sr enrichment in K2 is matched by high $^{87}\text{Sr}/^{86}\text{Sr}$.



A large cation (A-formula site) plot of crichtonite minerals in the $AM_{21}O_{38}$ (M = small cations) series. Minerals characteristic of metasomatized harzburgites (PKP) are lindsleyite (Ba) and mathiasite (K), but solid solutions of other members are also present. The compilation is taken from Haggerty *et al.* (1983), with additional data for lindsleyite coexisting with phase N (Haggerty *et al.*, 1986) in sample BD3096 from Bultfontein (Table IIIb), and mathiasite from a kimberlite in the Shandong Province, China (Jianxiang *et al.*, 1984). Note that lindsleyite and mathiasite are both present in BD3096, and that the mathiasite composition is very similar in large cations to mathiasite from Shandong.

Figure 4.23. Crichtonite minerals from Haggerty (1987).

Erlank *et al.* (1987) present Sr isotope data for PKP nodules from Kimberley which have $^{87}\text{Sr}/^{86}\text{Sr} > 0.706$, as has the enriched component in K2. The Sr isotope composition of K2 can be expected to be severely affected by a high $^{87}\text{Sr}/^{86}\text{Sr}$ component, as 30-60% of it's Sr is derived from this enriched component.

The Nd isotope composition of K2, in contrast, is hardly affected by the enriched component. This is because the Nd concentration is much lower in the PKP than the

kimberlite. Erlank et al. (1987) present data for the sample AJE168, a PKP which has 5.5ppm Nd, with $^{143}\text{Nd}/^{144}\text{Nd}=0.51248$, compared to K35/M which has 114ppm Nd, with $^{143}\text{Nd}/^{144}\text{Nd}=0.512664$. K2 has 103-113ppm Nd, with $^{143}\text{Nd}/^{144}\text{Nd}=0.51266 - 0.51274$. The variation in $^{143}\text{Nd}/^{144}\text{Nd}$ due to mixing with the enriched component is less than realistic analytical error.

Pb isotope ratios also support the proposal that metasomatised mantle is the source of the enriched component. K2 is enriched in Pb which is less radiogenic than that in K35, and lies between K35 and some PKP xenoliths (Erlank et al. 1987) on Pb-Pb isotope plots (fig 4.19). Pb isotope ratios are expected to be modified by this process as 30-50% of the Pb in K2 is derived from the enriched source.

It is concluded that the trace element geochemical variations in K2 can be explained by the mixing of kimberlite (represented by K35) and a component derived by the melting of phlogopite, K-richterite and possibly crichtonite from PKP type metasomatised mantle. Such an explanation, although it fits the data, is speculative and cannot be proved. Efforts were made to identify LIMA minerals, but none were found. Similarly, no PKP nodules were found in the field.

4.8 COMPARISON WITH KIMBERLITES FROM OTHER AREAS

The Gibeon kimberlites have a restricted range of compositions which lie within the broader field of group I kimberlites defined by Smith et al. (1985). Even when sampling has excluded the effects of crustal contamination and alteration; the effects of degree of partial melting, interaction with enriched lithosphere, entrainment of peridotite xenoliths and fractionation may all combine to produce the final kimberlite composition. Most trace

element ratios can be modified by these processes, and may not reflect mantle source characteristics. The least affected ratio appears to be La/Nb, which is therefore the most reliable source rock indicator.

K35 appears to be a kimberlite whose composition reflects its source characteristics. Fractionation is negligible, peridotite xenoliths were avoided in sampling and there is no evidence of fractionation or interaction with the lithosphere. These processes can be represented on trace element abundance diagrams normalised to K35/M. Fractionation produces an increase in trace element abundances without affecting ratios (apart from elements compatible in the fractionating phases). A decrease in degree of partial melting also produces an increase in trace element levels, but the most compatible elements are increased slightly more than the compatible elements. Admixture of bulk peridotite tends to lower the trace element abundances. Interaction with enriched lithosphere (as in K2) produces characteristic 'spikes' at particular elements.

Plotting the compositions of kimberlites from other provinces on K35 normalised plots is more instructive than using simple trace element ratio-ratio plots. Most trace element ratios in kimberlites are not characteristic of their source regions, due to the controlling effects of minor phases on many incompatible elements during very small degrees of partial melting or fractionation.

Fig 4.24 presents the composition of several on-craton group I kimberlites, normalised to K35/M (data taken from Smith et al. 1985). These kimberlites all have trace element compositions distinctly different from K35. The shape of the patterns reveal indications of the evolution of the kimberlites. The Jwaneng kimberlite is a large diamond bearing pipe in Botswana. Jwaneng is remarkably

Figure 4.24. K35-normalised trace element plot for cratonic (group IA) kimberlites, from Smith et al (1985).

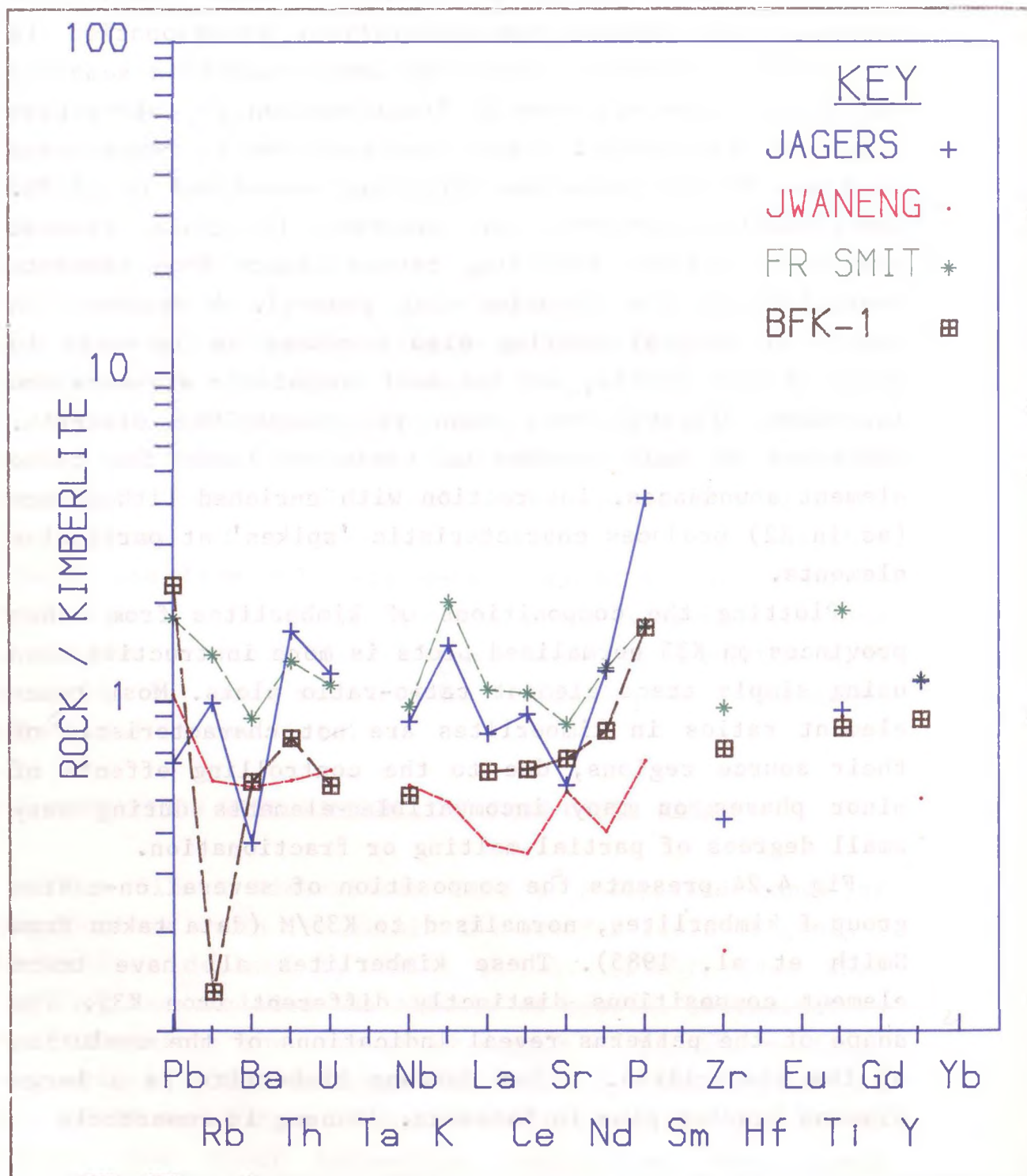
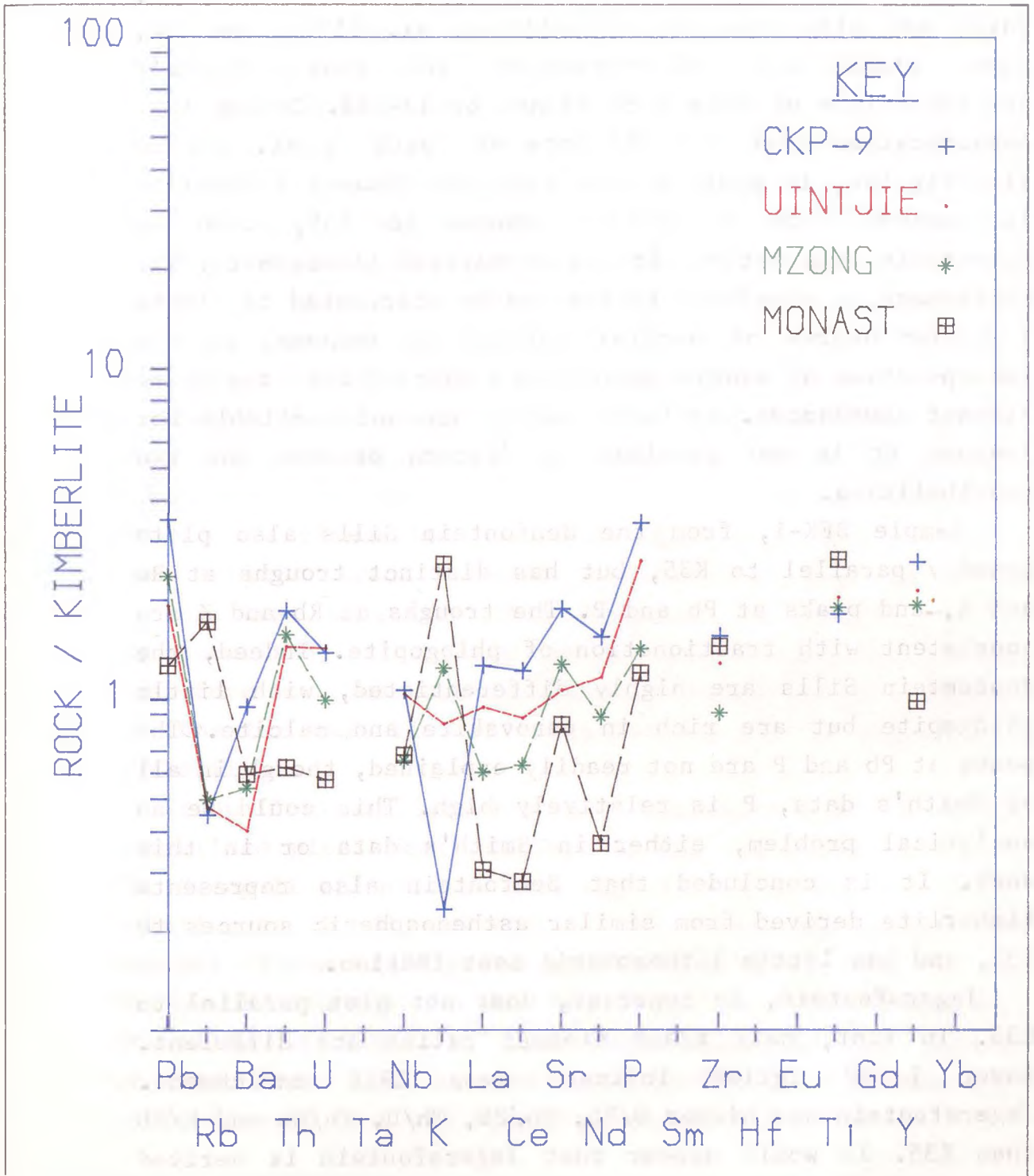


Figure 4.25. K35-normalised trace element plot for off-craton (group IB) kimberlites, from Smith et al. (1985).



similar to K35, plotting parallel to K35 but at lower abundance levels. Jwaneng has lower La/Nb than K35, but similar ratios of Rb, Ba, Th, U, K, Nb and Sr. Smith et al. (1985) measured La, Ce and Nd by XRF. ICP determinations of REE by Fraser (1987) on sample Finsch B, which was also measured by Smith et al. (1985) by XRF, show significant discrepancies in that Fraser's determinations of REEs were higher by 13-24%. Taking into consideration that the REE data of Smith et al. may be slightly low, it would appear that the Jwaneng kimberlite is derived from a similar source to K35, with no detectable interaction with metasomatised lithosphere. The difference in abundance levels can be attributed to either a higher degree of partial melting in Jwaneng, or the incorporation of mantle peridotites which dilute the trace element abundances. As La/Yb ratios are not available for Jwaneng it is not possible to discern between the two possibilities.

Sample BFK-1, from the Benfontein Sills also plots broadly parallel to K35, but has distinct troughs at Rb and K, and peaks at Pb and P. The troughs at Rb and K are consistent with fractionation of phlogopite. Indeed, the Benfontein Sills are highly differentiated, with little phlogopite but are rich in perovskite and calcite. The peaks at Pb and P are not readily explained, though in all of Smith's data, P is relatively high. This could be an analytical problem, either in Smith's data or in this work. It is concluded that Benfontein also represents kimberlite derived from similar asthenospheric sources to K35, and has little lithospheric contribution.

Jagersfontein, in contrast, does not plot parallel to K35. In fact, most trace element ratios are different. Lower La/Nd ratios indicate less LREE enrichment. Jagersfontein has higher U/Pb, Th/Pb, Th/U, Th/Nb and K/Nb than K35. It would appear that Jagersfontein is derived

from mantle sources different to K35, and by a higher degree of melting.

Despite the differences between these kimberlites, in broad terms there are significant similarities in the abundance levels and ratios of trace elements in on-craton kimberlites.

Off-craton group I kimberlites (fig 4.25) tend to bear less similarity to K35. Despite the erratic spikes and troughs in fig 4.25, there appears to be a general slope down to the left (ie there is less enrichment in incompatible elements relative to compatibles.) La/Nd ratios are also less than in K35. The trace element ratios of these kimberlites appear to be more affected by fractionation and lithospheric interaction than K35, hence the highly variable trace element ratios.

Rb and K are severely depleted in sample CKP-9 from a sill in Botswana (an indication of phlogopite fractionation), but are enriched in Monastery, probably due to the glimmerite xenoliths observed in the samples. The erratic trace element patterns of the group I kimberlites suggests that limited interaction with metasomatised lithosphere is a common feature. It is therefore not possible to identify asthenospheric source regions for most kimberlites as easily as for the Gibeon kimberlites.

Group II kimberlites are quite distinctive on the K35/M normalised plot. Most distinctive are the peaks at K and Pb. Group II kimberlites have high levels of Pb, Rb, Ba, K relative to Th, Nb and REEs. The Finsch kimberlite for example (Fraser 1987), has high levels of Pb, Rb, Ba, K, Sr and P relative to Th, Nb, REEs, Zr, Hf, Ti and Y. Attention is drawn to this observation as the Finsch pattern bears an interesting similarity to that of kimberlite K2 from the Gibeon province (fig 4.27).

Figure 4.26 K35-normalised plot for group II kimberlites, from Smith et al. (1985) and Fraser et al. (1985).

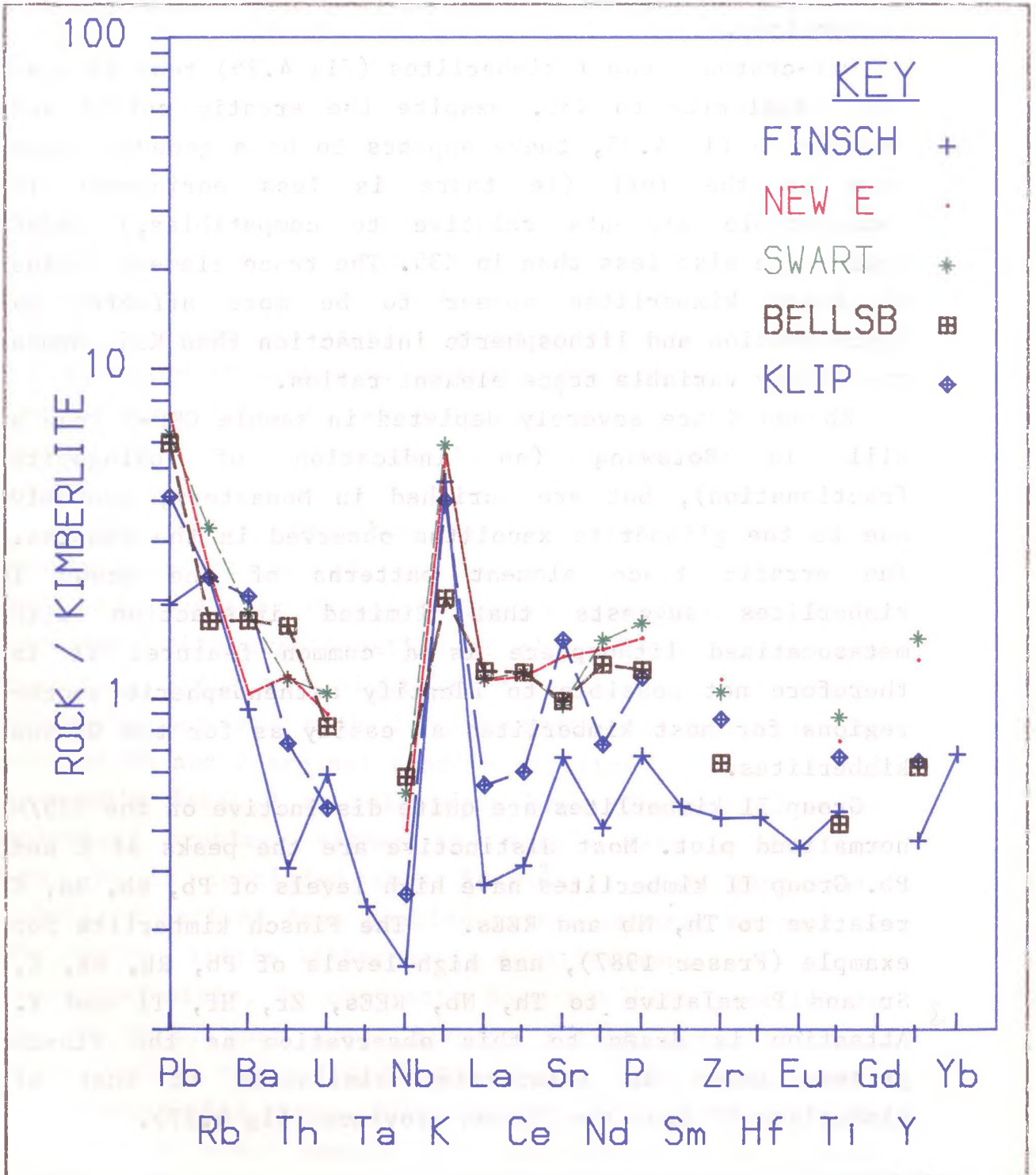
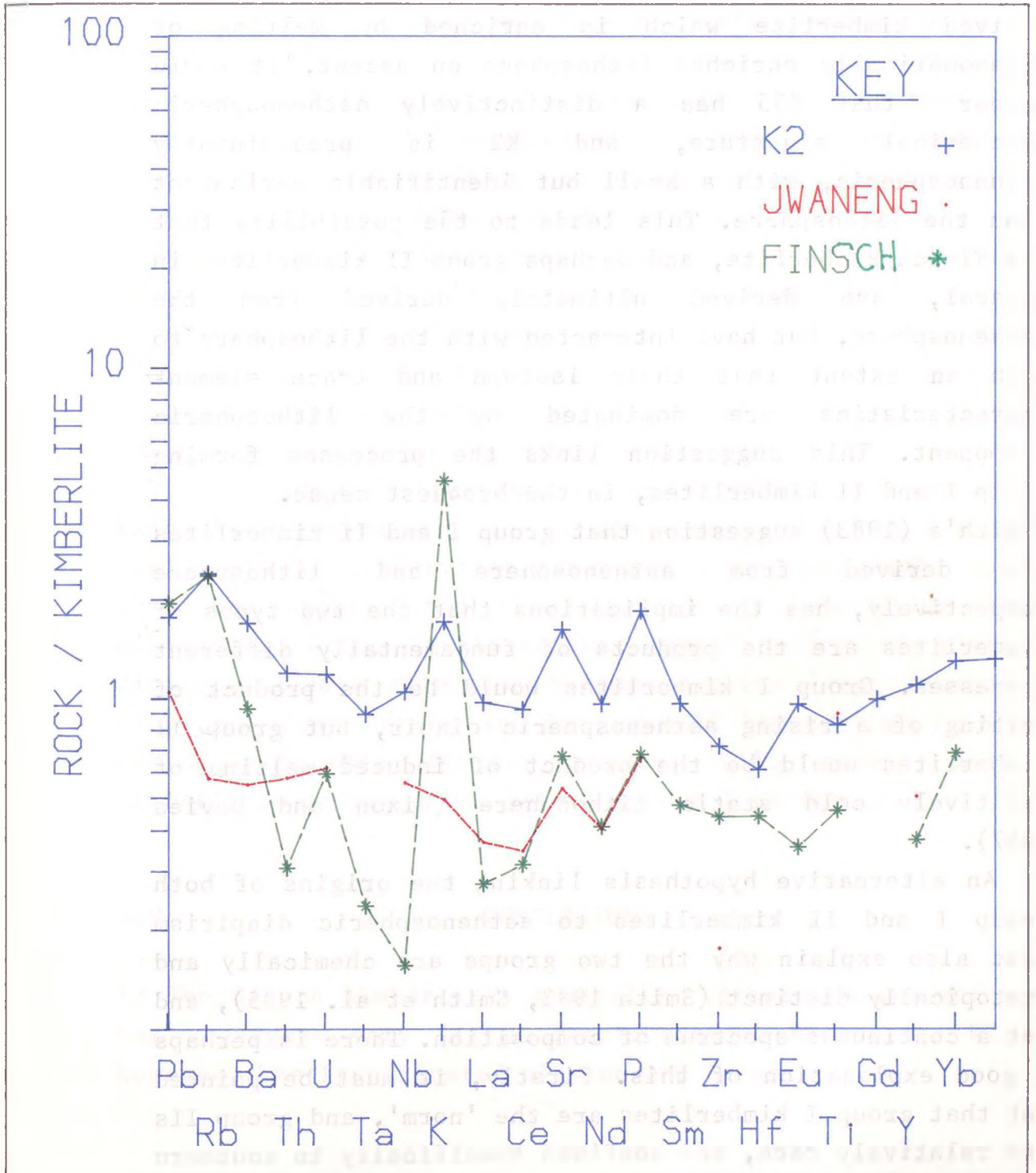


Figure 4.27. K35-normalised plot comparing K2 with Finsch (group II) and Jwaneng (group I). Note that K2 and Finsch both have peaks at Pb, Rb, K, Sr and P.



Fraser (1987) concluded that the trace element enrichment patterns evident in group II kimberlites are due to prior enrichment of lithospheric mantle source regions, by incompatible element rich hydrous fluids. It was suggested above that K2 is an asthenospherically derived kimberlite which is enriched by melting of metasomatically enriched lithosphere on ascent. It would appear that K35 has a distinctively asthenospheric geochemical signature, and K2 is predominantly asthenospheric, with a small but identifiable enrichment from the lithosphere. This leads to the possibility that the Finsch kimberlite, and perhaps group II kimberlites in general, are derived ultimately derived from the asthenosphere, but have interacted with the lithosphere to such an extent that their isotope and trace element characteristics are dominated by the lithospheric component. This suggestion links the processes forming group I and II kimberlites, in the broadest sense.

Smith's (1983) suggestion that group I and II kimberlites are derived from asthenosphere and lithosphere respectively, has the implications that the two types of kimberlites are the products of fundamentally different processes. Group I kimberlites would be the product of melting of a rising asthenospheric diapir, but group II kimberlites would be the product of induced melting of relatively cold static lithosphere (Nixon and Davies 1987).

An alternative hypothesis linking the origins of both group I and II kimberlites to asthenospheric diapirism must also explain why the two groups are chemically and isotopically distinct (Smith 1983, Smith et al. 1985), and not a continuous spectrum of composition. There is perhaps a good explanation of this. Firstly, it must be pointed out that group I kimberlites are the 'norm', and group IIs are relatively rare, and confined specifically to southern

Africa (Skinner 1986). Secondly, although known group I kimberlites range in age from 1600Ma (Kuruman) to 50Ma (Tanzania), group II kimberlites are restricted to the period between 200Ma (Dokolwayo) and 114Ma (Eendekuil). Thus group II kimberlites are restricted in both time and space. They would therefore appear to represent a special case. It is perhaps no coincidence that the time during which group II kimberlites are erupted is contemporaneous with the breakup of Gondwanaland. The Indian Ocean formed when continental rifting occurred on the south-east African coast at 190Ma, and the Atlantic Ocean formed on the south-west African coast during rifting at 120Ma. Major basaltic volcanism occurred in southern Africa (the Karoo) during this time, and numerous hotspots were in the vicinity of South Africa. Group II kimberlites are therefore not only restricted in time and space, but they coincide with a major tectono-thermal event.

This connection is (surprisingly) rarely mentioned by kimberlite geologists. It is the opinion of the author that group II kimberlites represent a special event, and that the broad two fold division of kimberlite is misleading. Group II kimberlites appear to have received disproportionate attention because several large diamond mines in South Africa are in group II kimberlite. It is anticipated that further studies will reveal more kimberlites intermediate between group I and group II.

4.9

CONCLUSIONS

1) The Gibeon kimberlites generally represent magma which has undergone very little fractionation. Kimberlite K2, however, has fractionated olivine and Cr-spinel.

2) Small amounts (<5%) of crustal contamination have little effect on trace element and isotope ratios.

3) Kimberlites are extremely susceptible to alteration. Slight groundmass alteration can seriously affect trace element compositions.

4) LREEs are highly mobile during groundwater alteration of calcite kimberlite. Even slight alteration affects isotope ratios, especially those of Sr and Pb, but also Nd.

5) The Gibeon kimberlites K35, K39 and K53 have a restricted range of trace element and isotope composition which can be interpreted as the product of partial melting of non-Dupal OIB type mantle.

6) Kimberlite K2 shows evidence of mixing of a kimberlite magma with trace element enriched lithosphere comparable to PKP type metasomatised nodules.

7) Group I kimberlites are predominantly asthenospherically derived melts from OIB type sources. Group II kimberlites may be derived from similar magmas which have undergone extensive assimilation of enriched lithospheric melts due to exceptional thermal conditions prevalent during continental breakup of Gondwanaland.

CHAPTER 5

THE KIMBERLITE - MEGACRYST RELATIONSHIP

5.1

INTRODUCTION

Kimberlites often contain large (>1cm) single crystals of garnet, diopside, orthopyroxene, ilmenite, and less frequently, phlogopite and zircon known as megacrysts or discrete nodules (Nixon and Boyd 1973). Despite numerous studies, the origin of megacrysts and their relationship with the host kimberlite are still uncertain. The fundamental question is whether megacrysts are phenocrysts or xenocrysts.

The large size (up to 20 cm) of individual crystals, their chemical homogeneity and generally undeformed nature of the megacrysts lead Nixon and Boyd (1973) to conclude that they formed in a liquid over long periods of time. P,T estimations (Nixon and Boyd (1973), Gurney et al. (1979), Harte and Gurney (1981), Hops et al. (1986)) indicate that they formed over a large temperature range (1400-1000°C) but at relatively constant pressure (about 50 kbar, i.e. at the base of the lithosphere). Although individual crystals are homogenous, suites of crystals from the same pipe show marked variation in composition with highly variable Mg/Fe ratios.

Fe/Mg and Ca/Mg enrichment correlate with decreasing temperature, which is interpreted as evidence that the megacrysts crystallised from an evolving magma (Nixon and Boyd (1973), Gurney et al. (1979), Harte and Gurney (1981)). Wyllie (1986) proposed that megacrysts could be produced by the interaction of a melt from asthenospheric peridotite with lithospheric harzburgite. He suggests that such a melt, ponded at the base of the lithosphere, would

be above its solidus temperature, and have no tendency to crystallise, and could therefore exist for long periods of time. The melt would, however, chemically interact with depleted harzburgite in the lithosphere, forming the megacryst suite over long periods of time. Megacrysts would then represent some kind of mantle pegmatite, which may be disrupted by erupting kimberlite and carried to the surface as xenoliths.

Nixon and Boyd (1973) and Pasteris et al. (1980) alternatively proposed that the megacrysts are produced by crystal fractionation of a magma body in the low velocity zone (LVZ) at depths of 150-200km. Disruption of this crystal-liquid mush by a carbonatitic melt derived from deeper in the asthenosphere, and subsequent mixing of the two liquids, is suggested as the origin of the kimberlite. Nixon and Boyd (1973) therefore regard kimberlite as a hybrid melt, with megacrysts being phenocrysts to the silicate melt component.

Gurney et al. (1979), Harte and Gurney (1981) and Jones (1984), in contrast suggested that megacrysts are cumulates from a rising diapiric melt, which has a decreasing temperature gradient from centre to margin. In this model, megacrysts are early stage phenocrysts from kimberlite, or from the melt which evolved to become kimberlite.

It has proved to be difficult to validate any of these arguments. Element partition coefficients vary not only with pressure and temperature but also with the chemical composition of the melt. As a result, the choice of partition coefficients cannot be tightly constrained, and hence the composition of the parental melt is difficult to determine. Irving and Frey (1978) show that variations in REE partition coefficients are highly dependent upon composition, but are similar in alkali basalts and kimberlites. The effect of the presence of carbonates on

these coefficients is not well known, but the presence of CO₂ affects the stability fields of the various megacryst phases (Olafsson and Eggler 1983). Jones (1987) argued, from REE evidence, that megacrysts were fractionated from a liquid of alkali basalt composition, which subsequently evolved to a kimberlite liquid. This conclusion, however, is in direct contradiction to major element evidence: fractionation of Mg rich pyroxenes, garnet and olivine from a basaltic liquid clearly cannot produce a kimberlite melt with 30% MgO. Schulze (1985, 1987) suggested that the parental liquid was kimberlitic because (1) kimberlitic inclusions had been found in some megacrysts (Schulze 1985), and (2) the bulk major element composition of the megacryst suite is highly magnesian and similar to kimberlite. A kimberlitic parental melt would also seem likely in the light of experimental work (Wyllie 1980, Brey 1978, Brey et al. 1983) which predicts that silicate melts produced at 50kbar or more are likely to be highly magnesian, and that basaltic compositions can only be produced at much shallower depths.

It is argued in chapters 3 and 4 that the Gibeon kimberlites are direct products of mantle melting, which have risen to the surface with little fractionation. If kimberlites in general are direct mantle melts, and not hybrids produced by mixing of melts, then isotope evidence should provide a conclusive answer to whether megacrysts are phenocrysts or xenocrysts. However, it appears (section 4.8) that many kimberlites have had their original geochemical characteristics altered by interaction with the lithosphere. The Gibeon kimberlites, some of which are unaffected by lithospheric interaction, represent a good opportunity to test the kimberlite-megacryst relationship with the use of Pb, Sr and Nd isotopes.

Several workers have previously used isotope evidence

to address this problem. Kramers (1977, 1981) analysed several megacrysts which had similar, but slightly different isotopic compositions to the few kimberlites that had then been analysed. Unfortunately the megacrysts and kimberlites were not from the same intrusions. Basu and Tatsumoto (1980) found that a megacryst from Mukorob (Gibeon Province) had a slightly higher $^{143}\text{Nd}/^{144}\text{Nd}$ than other South African kimberlites. Smith (1983) provided a more extensive study of several megacrysts which indicated that megacrysts are not in isotopic equilibrium with the group I kimberlite field. These studies all have the drawback that the megacryst composition is compared to the group I field, and not specifically to the composition of the host kimberlite from which the megacryst was collected.

South African kimberlites and South Atlantic OIB tend to have relatively small variations in Nd and Sr isotopes compared with Pb isotope variations. Pb isotope analysis of megacrysts and host kimberlites therefore offer a more promising opportunity to distinguish between the kimberlite and megacryst sources.

5.2

SAMPLES

The primary objective of this study is to determine whether megacrysts are xenocrysts or phenocrysts. Ideally megacrysts and whole-rock kimberlite samples examined should be taken from the same locality. In practise it was found that the largest kimberlite pipes yield the most abundant, largest and freshest megacrysts. Unfortunately, these kimberlites were of the TKB facies, and therefore unsuitable for isotope analysis. None of the megacrysts obtained from the dykes and smaller pipes yielded enough material which was fresh enough for isotope analysis.

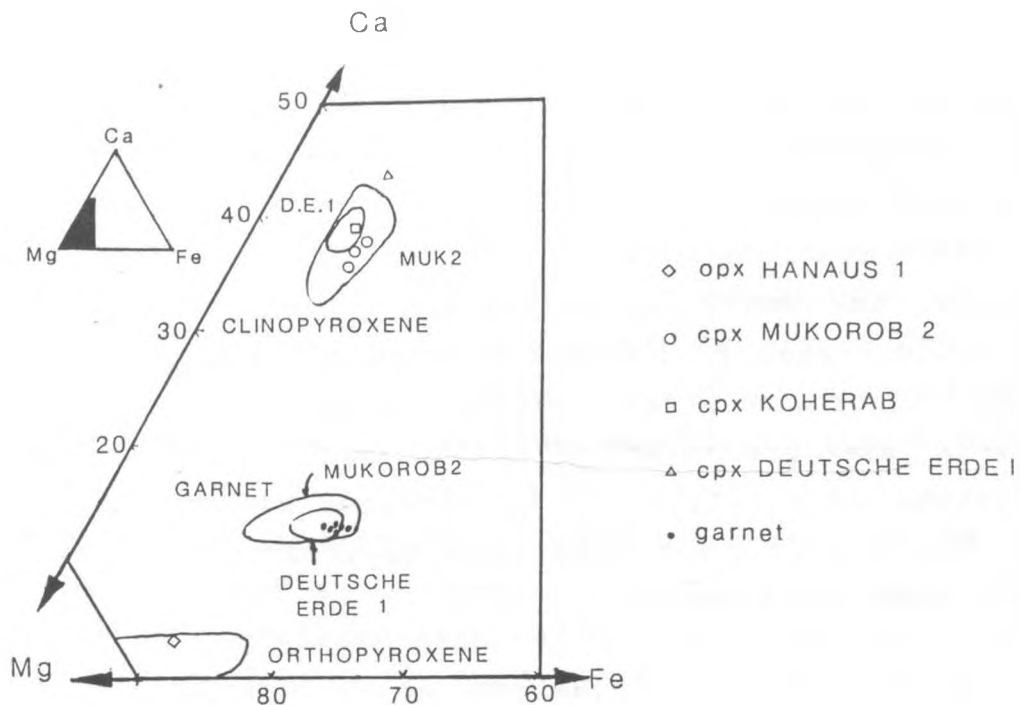


Figure 5.1. Ca-Mg-Fe plot for megacrysts, showing that the samples analysed in this study are comparable in composition to others from the Gibeon province. For comparison, the fields of Gibeon megacrysts from Mitchell (1987) are shown.

The megacrysts analysed were selected because they provided the best ultrapure separates. Five diopside, one enstatite and six garnet megacrysts of the Cr-poor suite from seven pipes were analysed (table 5.1). No Cr-rich megacrysts have been reported from the Gibeon province and none were found in this study. The megacryst samples were prepared (see appendix 1) by crushing and hand-picking. The best samples were selected for analysis. These were exhaustively hand-picked again immersed in pure ethanol, which reduces surface reflections so that the grain can be seen more clearly. In this way it is possible to ensure that each grain was totally free from alteration, cracks or inclusions.

Extreme care was taken in sample preparation as megacrysts are susceptible to contamination of their

isotopic systematics from two potential sources. Firstly, surface weathering can alter parent-daughter and isotope ratios, and secondly, as the kimberlite magma has much higher concentrations of U, Pb, Rb, Sr, Sm and Nd than the megacrysts, any small inclusions of magma, or cracks in grains could seriously affect the measured isotope ratios.

The major and trace element compositions of the megacrysts are presented in table 5.2. Major element compositions were determined by electron microprobe, and U, Pb, Rb, Ba, Sr, and REEs were determined by isotope dilution mass spectrometry.

TABLE 5.1
MEGACRYST SAMPLE LIST

LOCALITY		SAMPLE	Sr	Nd	Pb	REE
Hanaus I	36/K11	OPX2		*	*	
	36/K11	GT 1		*		*
Diamantkop	36/K13	GT 6		*		*
Deutsche Erde I	36/K16	GT 4		*		*
Deutsche Erde II	36/K17	CPX4	*	*	*	*
Koherab	36/K15	CPX1	*		*	
	36/K15	GT 3		*		*
Vipersdorf	37/K3	GT 5		*		*
Mukorob II	37/K6	CPX3		*	*	*
	37/K6	CPX6	*	*	*	*
	37/K6	CPX5		*	*	*
	37/K6	GT 2		*		*

The megacrysts studied were generally from different kimberlites, but three diopsides and one garnet from 37/K6 (Mukorob 2) were analysed. The compositions of the megacrysts from Mukorob 2 fall within the ranges determined by Mitchell (1987) for suites of Cr-poor

megacrysts from that pipe (fig 5.1). Also, a garnet from 36/K16 (Deutsche Erde 1) falls within Mitchell's (1987) range for that pipe. The other megacrysts have similar compositions to the above. The megacrysts studied are therefore typical megacrysts from the Gibeon province.

The diopside samples display a range in $\text{Ca}/(\text{Ca} + \text{Mg})$ which is interpreted (eg Schulze 1987) as the result of fractionation from an evolving liquid. $\text{Ca}/(\text{Ca} + \text{Mg})$ is relatively low in high temperature megacrysts but increases with fractionation and falling temperature, and thus can be used as a temperature index (Schulze 1987). Cr_2O_3 often correlates with $\text{Ca}/(\text{Ca} + \text{Mg})$ (eg Jakob 1977), but in the five diopside samples studied there is no such correlation. Trace element concentrations show considerable variations between samples (table 5.2), but do not show good correlations with $\text{Ca}/(\text{Ca} + \text{Mg})$, indicating that the megacrysts have not crystallised in a single closed fractionation system.

These data support Mitchell's (1987) conclusions that there were several distinct magma systems fractionating contemporaneously, resulting in each pipe having its own distinguishable megacryst suite. Mitchell (1987) suggested that kimberlite eruption could mix together two or more megacryst batches, which could explain why the three megacrysts from Mukorob 2 appear not to be cogenetic.

The garnet megacrysts also show compositional variations, with a range in $\text{Mg}/(\text{Mg} + \text{Fe})$ (table 5.1). The $\text{Mg}/(\text{Mg} + \text{Fe})$ variations have been interpreted (eg Schulze 1987) as the result of fractional crystallisation of an evolving magma. The six garnet samples also display a range in Cr, Ti and trace elements, but do not show good correlations with $\text{Mg}/(\text{Mg} + \text{Fe})$. The lack of correlation between $\text{Mg}/(\text{Mg} + \text{Fe})$ and trace element concentrations is evidence that the megacrysts are not derived from a single fractionating system. Thus it is concluded (in agreement

with Mitchell's (1987) observations) that the megacrysts from different pipes are not cogenetic, but are derived from distinct evolving magma batches. This evidence supports the Harte and Gurney (1981) model of crystallisation in which megacrysts crystallise in small apophyses on the margins of a rising diapir, and are subsequently disrupted by the erupting kimberlite.

TABLE 5.2

COMPOSITION OF GARNET MEGACRYSTS

	GT 1	GT 2	GT 3	GT 4	GT 5	GT 6
SiO ₂	42.11	41.98	41.82	41.35	41.66	42.04
TiO ₂	0.81	0.62	0.74	1.06	0.84	0.90
Al ₂ O ₃	21.95	22.62	21.55	21.34	21.71	21.92
Cr ₂ O ₃	1.22	0.50	1.34	1.36	1.42	0.92
Fe ₂ O ₃	1.21	1.00	1.52	1.41	1.04	1.38
FeO	8.23	8.89	1.43	8.27	8.09	8.05
MnO	0.25	0.35	0.33	0.27	0.28	0.26
MgO	19.60	19.10	19.87	19.29	19.37	19.79
CaO	5.14	5.07	5.27	5.25	5.26	5.13
Total	100.23	99.66	99.65	99.63	99.57	100.45
Ca/Ca+Mg	0.160	0.165	0.162	0.168	0.163	0.155
Mg/Fe+Mg	0.789	0.775	0.800	0.780	0.793	0.790
Rb	0.0441	0.2652	0.1406	0.0298	0.0537	0.737
Sr	0.773	-	3.182	-	1.515	5.377
La	-	0.384	0.013	0.039	0.054	0.060
Ce	-	1.047	0.049	0.221	0.353	0.366
Nd	3.774	1.978	0.161	1.113	1.476	1.413
Sm	3.541	1.737	0.155	1.003	1.389	1.285
Eu	1.990	0.975	0.084	0.536	0.769	0.638
Gd	8.666	4.391	0.391	2.337	3.338	3.726
Dy	-	-	0.704	4.473	7.061	5.670
Er	11.896	5.883	0.492	2.900	4.535	3.821
Yb	10.559	5.5877	0.472	2.692	4.411	3.696
Lu	-	-	0.072	-	0.739	0.546

COMPOSITION OF CLINOPYROXENES AND ORTHOPYROXENE

	CPX 1	OPX 2	CPX 3	CPX 4	CPX 5*	CPX 6
SiO ₂	53.95	55.96	53.71	54.69	53.90	53.27
TiO ₂	0.44	0.29	0.44	0.21	0.46	0.60
Al ₂ O ₃	2.94	2.36	3.35	0.702	3.72	3.65
Cr ₂ O ₃	0.83	0.27	0.62	0.312	0.38	0.13
FeO	4.13	0.29	4.21	4.75	4.82	5.46
MnO	0.09	0.14	0.15	0.09	0.11	0.14
MgO	18.09	32.0	17.74	16.84	18.86	17.50
CaO	18.00	1.34	17.61	21.03	16.07	17.08
NaO	1.30	0.33	1.29	1.07	1.25	1.35
NiO	0.09	0.08	0.09	0.04	0.06	0.10
Total	99.89	100.07	99.28	99.80	99.67	99.34
Ca/Ca+Mg	0.421	0.030	0.417	0.472	0.386	0.412
Mg/Fe+Mg	0.885	0.886	0.882	0.863	0.875	0.851
Rb	0.199	0.255	0.194	0.305	0.065	0.192
Sr	260			170	79	87.7
U	0.0969	0.0163	0.0685	0.0966	0.0983	0.0185
Pb	0.4525	0.0226	0.0440	0.3007	0.2745	0.1867
La			1.561	2.489	1.96	1.980
Ce			5.170	9.207	8.20	8.323
Nd			4.375	9.076	5.4	5.508
Sm			1.106	2.321	1.34	1.401
Eu			0.357	0.743	0.49	0.517
Gd			0.823	1.978		1.045
Dy			0.616	1.124		0.801
Tb					0.24	
Er			0.204	0.337		0.275
Yb			0.121	0.165	0.24	0.154
Lu			0.013	0.018	0.036	0.019
Hf					0.62	
Sc					19.4	
Co					40	
Cr					2420	

*REE analysed by INAA

5.3.1 Pb Isotopes

The Pb isotopic composition of the six pyroxene megacrysts (analysed by G. Davies) is shown in table 5.4 and fig 5.2. There is considerable variation in Pb (0.1867-0.4525ppm) and U (0.0163-0.0983) resulting in a large range in u-values (4.47-22.85). The megacrysts display a large range of initial (=70 Ma) Pb isotopic compositions which do not correlate with μ -values. It is possible that the mild leaching procedure used during analysis (see appendix 1) could slightly reduce the U/Pb ratios, but this effect would be too small to account for the range in isotope ratios.

It is clear from fig 5.2 that the megacrysts are not in isotopic equilibrium with the compositional range determined for the Gibeon kimberlites. Sample CPX3 from Mukorob 2 has similar initial Pb ratios to the kimberlites K35, K39 and K53, but the other megacrysts have less radiogenic Pb. Also, the three megacrysts from Mukorob 2 (CPX3, CPX5 and CPX6) have distinctly different Pb isotopic compositions and are therefore not in isotopic equilibrium with each other.

The isotopic compositions of the host kimberlites of these megacrysts could not be measured because the kimberlite had suffered severe alteration. It can only be assumed that the host kimberlites were derived from similar sources to the fresh kimberlites (which showed a restricted compositional range). It was shown in chapters 3 and 4 that the Pb isotopic composition of the fresh kimberlites K35, K39 and K53 represent those of their source regions, and that they have not been modified on ascent (as in the case of K2). The megacrysts are not in isotopic equilibrium with the kimberlites and therefore cannot be phenocrysts formed in the kimberlite magma.

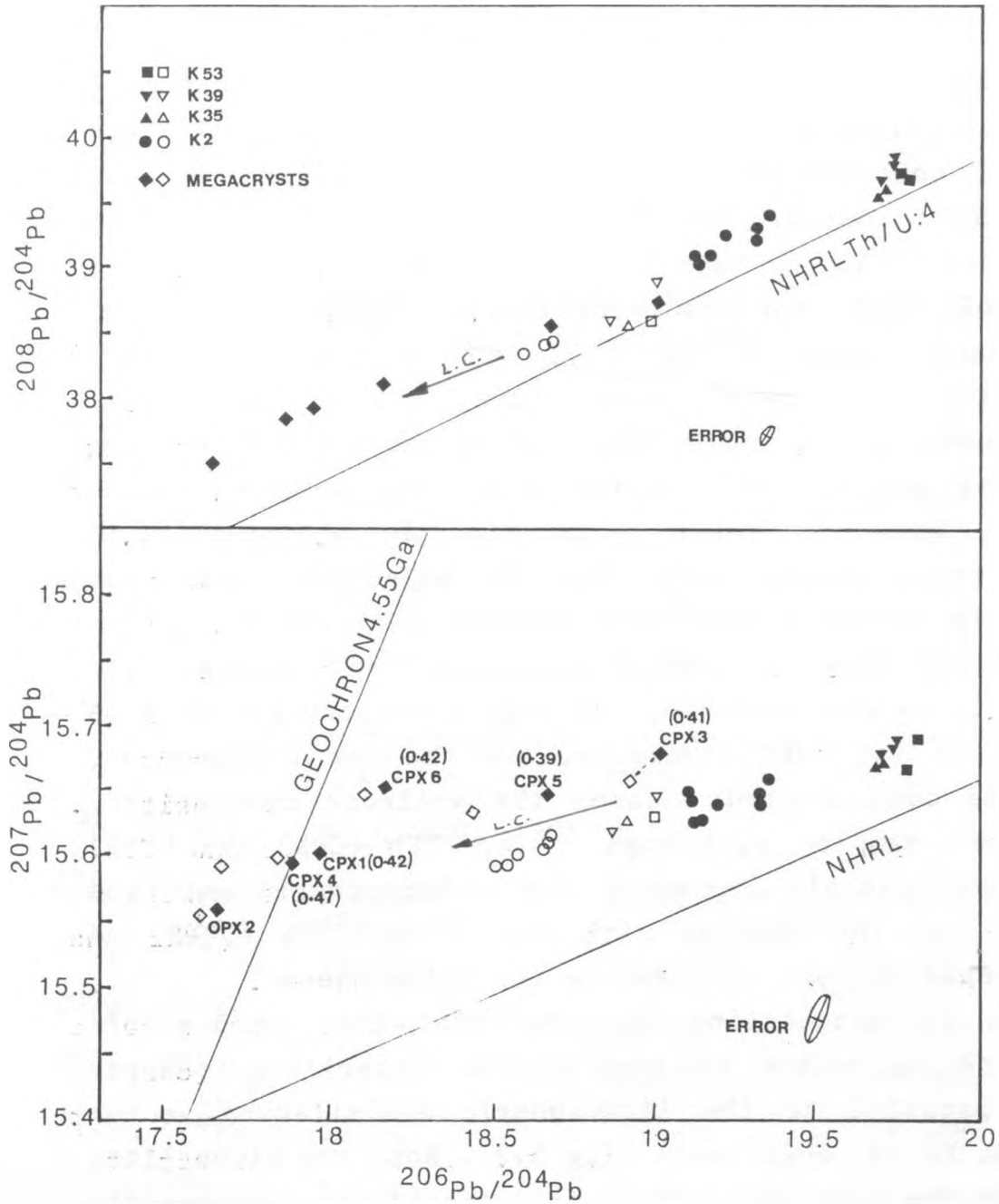


Figure 5.2. Pb isotopic composition of Gibeon megacrysts and kimberlites. Open symbols = initial (70Ma) ratio, closed symbols = measured ratios. Also shown are vectors, L.C., indicating the effects of lithospheric contamination on the megacrysts and kimberlites. Error ellipse represents the 1.3% per mass unit fractionation correction applied to measured ratios. Figures in brackets are Ca/(Ca+Mg) ratios

The Pb isotopic compositions of the megacrysts shows a broad correlation with $\text{Ca}/(\text{Ca}+\text{Mg})$ suggesting that the isotopic composition of the magma was changing as the magma fractionated. The samples with high $^{206}\text{Pb}/^{204}\text{Pb}$ (CPX3 and CPX5) have low $\text{Ca}/(\text{Ca}+\text{Mg})$ suggesting a relatively high temperature origin. In contrast, CPX1 and CPX4 have lower $^{206}\text{Pb}/^{204}\text{Pb}$, and higher $\text{Ca}/(\text{Ca}+\text{Mg})$ suggesting a lower temperature origin. A clear relationship would not be expected as the samples are from different pipes, and crystallised from separate magma batches, but the broad correlation is significant. A simple fractionation model for the megacrysts would not result in isotopic variation between megacrysts, but an assimilation-fractional-crystallisation (AFC) model could do so. In an AFC scenario, the high T megacrysts would be closest to the melt endmember, and the low T megacrysts would be contaminated towards the wallrock composition. Thus the samples with high $^{206}\text{Pb}/^{204}\text{Pb}$ (CPX3 and CPX5) would most closely represent the asthenospheric melt end member, and the samples with low $^{206}\text{Pb}/^{204}\text{Pb}$ (OPX2 and CPX4) would be most affected by the lithosphere.

It is interesting to note that the lithospheric contamination vector assigned to the kimberlites (chapter 4) is parallel to the lithospheric assimilation vector apparent in the megacrysts (fig 5.2). Both the kimberlites (K2) and the megacrysts which are affected by lithospheric interaction are displaced higher above the NHRL (ie that they have relatively radiogenic $^{207}\text{Pb}/^{204}\text{Pb}$ compared to $^{206}\text{Pb}/^{204}\text{Pb}$), which is a characteristic of old (lithospheric) Pb and of the Dupal signature.

TABLE 5.4

Pb Isotope Composition of Pyroxene Megacrysts

	CPX1	OPX2	CPX3
$^{238}\text{U}/^{204}\text{Pb}$	13.413	4.471	10.016
$^{235}\text{U}/^{204}\text{Pb}$	0.0973	0.0324	0.0726
$^{206}\text{Pb}/^{204}\text{Pb}_m$	17.964	17.651	19.024
$^{207}\text{Pb}/^{204}\text{Pb}_m$	15.600	15.559	15.669
$^{208}\text{Pb}/^{204}\text{Pb}_m$	37.909	37.518	38.750
$^{206}\text{Pb}/^{204}\text{Pb}_i$	17.817	17.602	18.915
$^{207}\text{Pb}/^{204}\text{Pb}_i$	15.593	15.557	15.664
<hr/>			
	CPX4	CPX5	CPX6
$^{238}\text{U}/^{204}\text{Pb}$	20.079	22.854	6.245
$^{235}\text{U}/^{204}\text{Pb}$	0.1456	0.166	0.453
$^{206}\text{Pb}/^{204}\text{Pb}_m$	17.886	18.680	18.170
$^{207}\text{Pb}/^{204}\text{Pb}_m$	15.597	15.648	15.650
$^{208}\text{Pb}/^{204}\text{Pb}_m$	37.835	38.515	38.106
$^{206}\text{Pb}/^{204}\text{Pb}_i$	17.667	18.430	18.102
$^{207}\text{Pb}/^{204}\text{Pb}_i$	15.587	15.636	15.647

5.3.2 Nd Isotopes

The Nd isotopic composition of 6 garnet and 4 diopside megacrysts are presented in table 5.5. As with Pb, the Nd isotopes display a range of initial ratios which overlaps, but does not coincide with that of the kimberlites (fig 5.3). This indicates isotopic disequilibrium at the time of kimberlite emplacement.

The isotopic growth curves of the megacrysts and kimberlite are plotted in fig 5.4. Interestingly, 4 garnet and 3 CPX growth curves intersect at 0.51273 ± 2 and 78 ± 9 Ma (which is the approximate age of kimberlite emplacement). It would appear then, that at the time of kimberlite emplacement, some, but not all, of the megacrysts were in isotopic equilibrium, with a Nd isotopic composition slightly, but distinctly, different from the kimberlite.

The Nd isotope data may have age significance regarding the formation age of the megacrysts. There are two possible interpretations:

- 1) The intersection of the garnet and CPX Nd growth curves at 78 ± 9 Ma represents the formation age of the megacrysts. This age is coincident with or slightly older than the 70 ± 10 Ma ages determined for the kimberlites in chapter 2.
- 2) The megacrysts existed for some unknown length of time, in the mantle, before entrainment in the kimberlite, and the Nd isotope ratios were continuously re-equilibrated by diffusion. Isotopic divergence occurred when the megacrysts were erupted to the surface and cooled below their blocking temperatures.

The former hypothesis is favoured because the megacrysts were collected from pipes up to 65km apart, and it is considered unfeasible that isotopic equilibrium could be maintained over such distances, especially as the three CPX megacrysts from Mukorob 2 have not maintained isotopic equilibrium. However there is no reason to suppose that the megacrysts are cogenetic. The megacrysts whose growth curves do not intersect at 78 ± 9 Ma may be the products of magmas whose compositions are being modified by an AFC process, as suggested above for Pb isotopes. The evidence for an AFC process is not clear in the Nd isotope system as the isotopic variations are

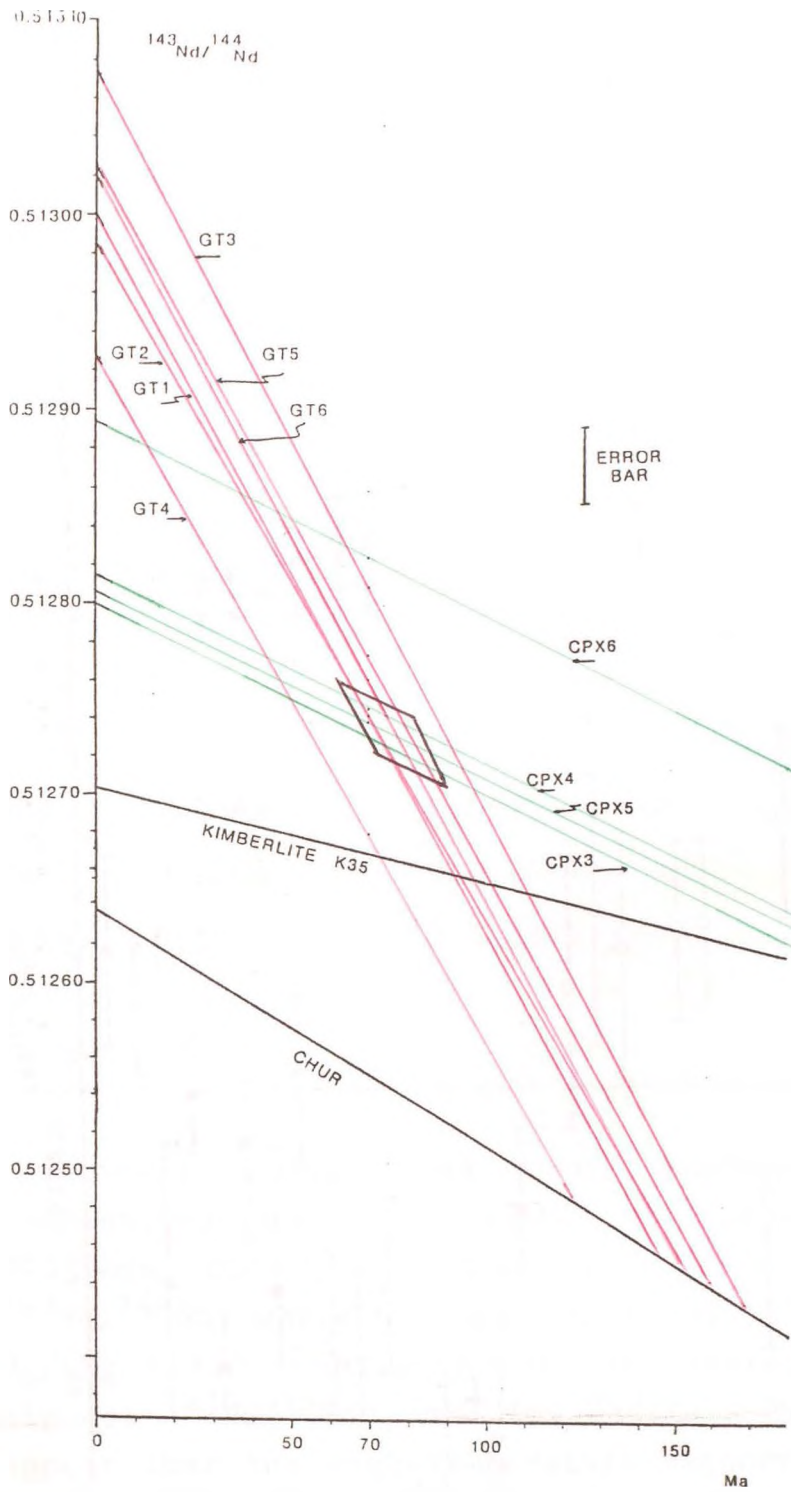


Figure 5.4. Nd growth curves for pyroxene and garnet megacrysts, kimberlite K35 (representative of the Gibeon kimberlites) and the chondritic uniform reservoir (CHUR). 2σ analytical error bar is shown.

Figure 5.3. Nd isotopic composition of Gibeon kimberlites and megacrysts at 70Ma, with 2 σ analytical errors.

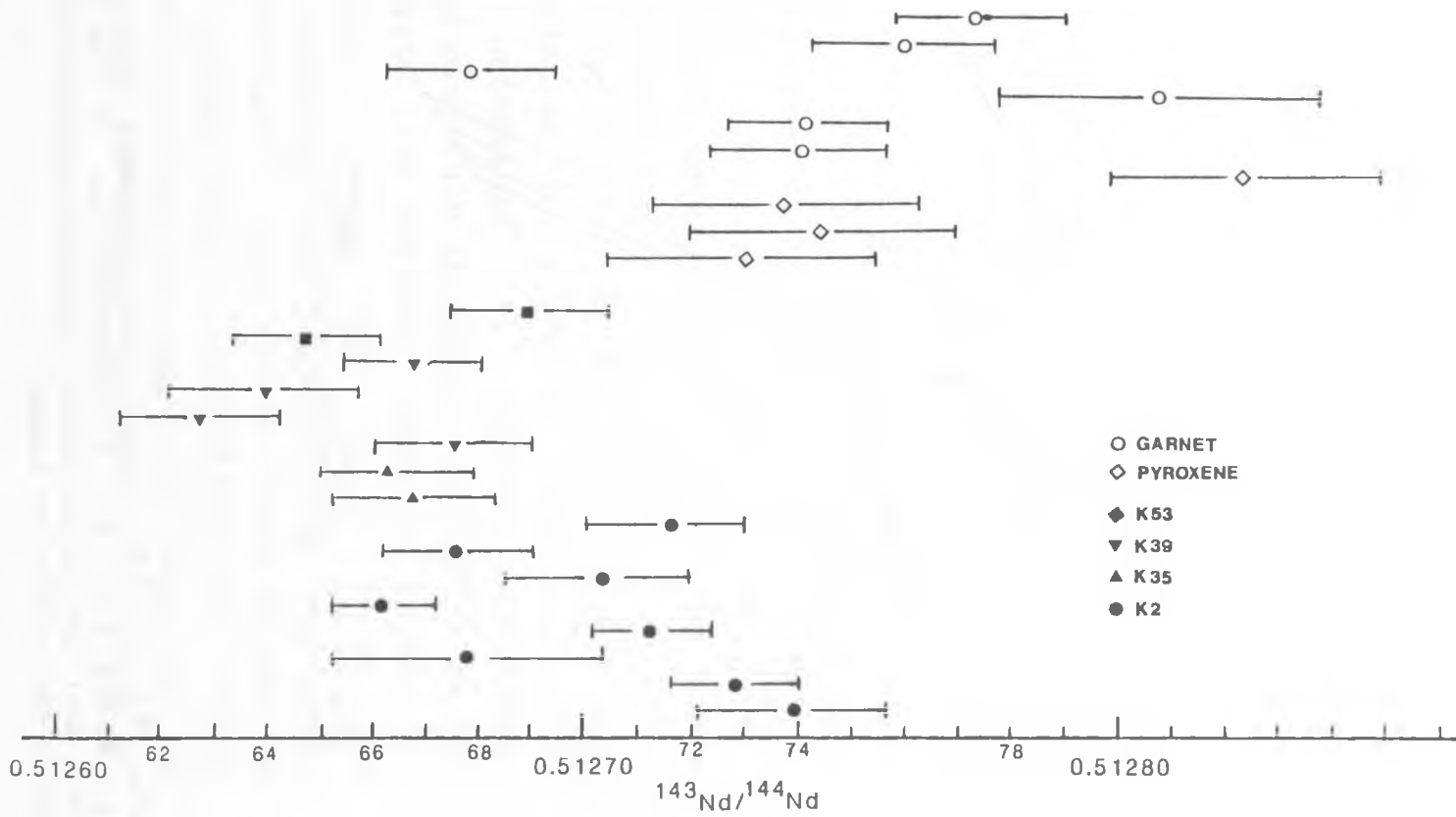


TABLE 5.5

Nd Isotopic Composition of Megacrysts

	$^{147}\text{Sm}/^{144}\text{Nd}$	$^{143}\text{Nd}/^{144}\text{Nd}_m$	$^{143}\text{Nd}/^{144}\text{Nd}_i$	Nd
GT 1	0.5673	0.513001+/-17	0.512741	3.74
GT 2	0.5308	0.512985+/-15	0.512742	3.74
GT 3	0.5821	0.513075+/-30	0.512808	5.03
GT 4	0.5448	0.512929+/-16	0.512679	2.52
GT 5	0.5690	0.513021+/-17	0.512760	4.10
GT 6	0.5496	0.513025+/-18	0.512773	4.35
CPX2		0.512891+/-30		
CPX3	0.1528	0.512801+/-30	0.512731	3.53
CPX4	0.1546	0.512816+/-30	0.512745	3.81
CPX5	0.1500	0.512807+/-30	0.512738	3.67
CPX6	0.1538	0.512895+/-30	0.512824	5.35

relatively small, and most samples have isotopic compositions which are within analytical error. However GT3 has the highest Mg/(Mg + Fe) (T) and highest $^{143}\text{Nd}/^{144}\text{Nd}$, while GT4 has the lowest $^{143}\text{Nd}/^{144}\text{Nd}$, and low Mg/(Mg + Fe). Similarly, of the pyroxenes, CPX6 has the highest $^{143}\text{Nd}/^{144}\text{Nd}$, and low Ca/(Ca + Mg). Thus it would appear that the high temperature megacrysts represent the least contaminated, and the low temperature megacrysts the most contaminated melt. This data tentatively supports an AFC model involving a depleted asthenospheric melt interacting with an enriched lithospheric wallrock.

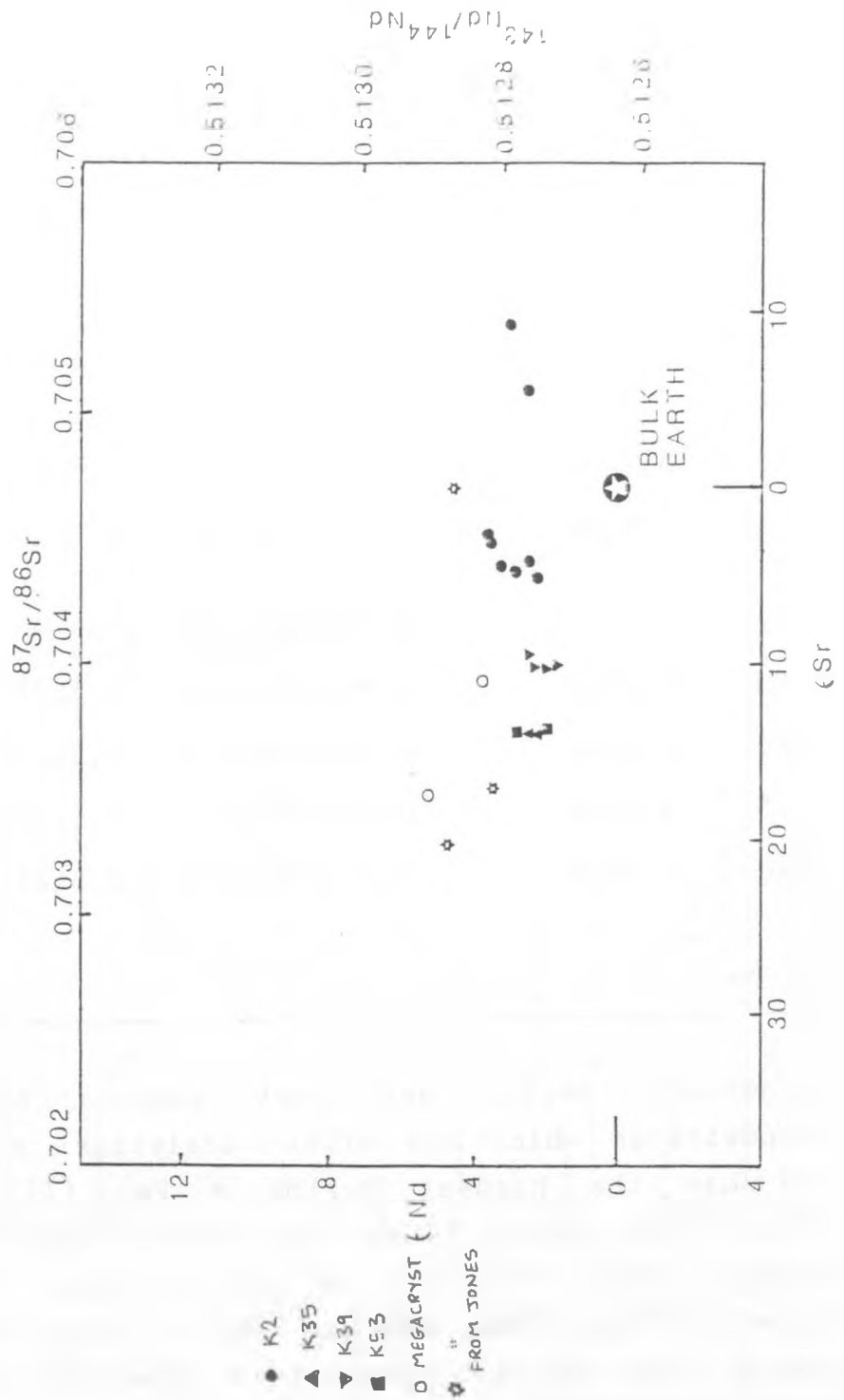


Figure 5.5. ϵ_{Nd} v ϵ_{Sr} diagram for Gibeon kimberlites and megacrysts. Also shown are three garnets from Jones (1983)

5.3.3 Sr Isotopes

Sr isotope analysis of the megacrysts was largely unsuccessful due to laboratory problems, but three precision analyses were obtained. Two of these (CPX1, CPX4) had initial ratios in the range of the Gibeon kimberlites, but CPX6 had a lower initial ratio (0.703372 ± 40 , $\epsilon_{\text{Sr}} = -17.6$), which correlated with its high Nd initial ratio (0.512824 ± 30 , $\epsilon_{\text{Nd}} = 5.35$). This megacryst is therefore clearly not in isotopic equilibrium with the Gibeon kimberlite field (see fig 5.5).

Three garnet megacrysts analysed by Jones (1984) are also plotted on fig 5.5. Two of these have similar compositions to CPX6 ($\epsilon_{\text{Sr}} = -17$, $\epsilon_{\text{Nd}} = 3.5$; $\epsilon_{\text{Sr}} = -20$, $\epsilon_{\text{Nd}} = 4.8$) while the third has much more radiogenic Sr ($\epsilon_{\text{Sr}} = -3$), but similar Nd ($\epsilon_{\text{Nd}} = 4.7$). It is considered possible that the latter sample may have suffered to some degree from contamination/alteration.

These data indicate that the megacrysts are derived from variable and depleted sources which are not in isotopic equilibrium with the host kimberlites. Furthermore, the Sr isotope data support the AFC hypothesis developed above. CPX6 (high ϵ_{Nd} , low ϵ_{Sr}) has low $\text{Ca}/(\text{Ca} + \text{Mg})$ (high T) relative to CPX1 and CPX4 which have higher ϵ_{Sr} and higher $\text{Ca}/(\text{Ca} + \text{Mg})$.

The combined Pb, Sr and Nd isotope data tentatively support the hypothesis that the megacrysts crystallised from an evolving asthenospheric magma which was assimilating enriched lithospheric wallrock. The isotopic composition of the asthenospheric parental magma cannot be defined, but would appear to have radiogenic Pb, perhaps similar to the kimberlites, but more depleted Sr and Nd. The lithospheric component has enriched Sr and Nd, but

relatively non-radiogenic Pb, with high $^{207}\text{Pb}/^{204}\text{Pb}$ relative to $^{206}\text{Pb}/^{204}\text{Pb}$.

TABLE 5.6

Sr Isotopic Composition of Megacrysts				
	$^{87}\text{Rb}/^{86}\text{Sr}$	$^{87}\text{Sr}/^{86}\text{Sr}_m$	$^{87}\text{Sr}/^{86}\text{Sr}_i$	Sr
CPX1	0.00221	0.703914+/-36	0.703912	-9.99
CPX4	0.00518	0.703857+/-28	0.703852	-10.84
CPX6	0.00632	0.703379+/-40	0.703372	-17.65

5.4

DISCUSSION

The isotope data presented above is good evidence that the megacrysts were not in isotopic equilibrium with the host kimberlite at the time of emplacement, and therefore are not phenocrysts. The megacrysts do, however, appear to have formed at approximately the same time as, or shortly before, the kimberlite which is possible evidence for a genetic relationship.

Jones (1984, 1987) suggested that megacrysts are phenocrysts from a protokimberlite, which subsequently evolved to kimberlite by an AFC process involving fractionation of megacrysts and subsequent lithospheric assimilation. The Pb isotope data negate this possibility as the kimberlite and high temperature megacrysts both have radiogenic Pb ($^{206}\text{Pb}/^{204}\text{Pb} > 18.5$) and the lithospheric contaminant has unradiogenic Pb ($^{206}\text{Pb}/^{204}\text{Pb} < 18$). Jones' model would require the kimberlite to have unradiogenic Pb. However, the megacrysts do show evidence (above) of derivation from parental magmas evolving

through AFC processes, but the kimberlite is neither the parent nor the daughter product of this process. The megacrysts are therefore xenocrysts to the kimberlite,

There are several other lines of inquiry which support this conclusion.

1) The megacryst suites investigated by Nixon and Boyd (1973), Harte and Gurney (1981) and Mitchell (1986,1987) indicate that megacrysts are produced by fractionation from an evolving liquid. If the kimberlite is the liquid from which the megacrysts crystallised, it would be expected that a suite of kimberlites would plot on an evolution trend on element-element plots. The Gibeon kimberlites show no such trend. Although K2 appears to have fractionated olivine, there is no evidence that it has fractionated garnet or pyroxenes (chapter 4). Also, the other kimberlites (K35, K39 and K53) show almost no evidence of fractionation at all, and have remarkably similar compositions. This consistency in composition is evidence against early fractionation from the kimberlite magma.

2) The high levels of transition metals in the kimberlites (chapter 3) are further evidence against megacryst fractionation: Sc, V and Mn would be depleted by ilmenite fractionation, but are present at consistent levels in all the kimberlites (figs 3.8, 3.11, 3.15, 3.18).

3) Ilmenite megacrysts have been found (Haggerty et al. 1979, Pasteris et al 1980, Boctor and Boyd 1980 and Mitchell 1986) to have rim compositions distinctly richer in MgO than their homogeneous core composition. This is interpreted as the result of reaction between the megacryst and the kimberlite, precipitating an overgrowth of MgO rich ilmenite. This is evidence that megacrysts are not in equilibrium with the kimberlite, and is a further possible indication that they are xenocrysts.

Despite the above arguments, a genetic relationship

between kimberlite and megacrysts cannot be totally ruled out. This is because of the ubiquitous occurrence of megacrysts in kimberlite (Nixon, Mitchell, Skinner pers comm) and their apparently contemporaneous formation ages (this work and Jones 87).

The combined Pb, Nd and Sr data presented above correlate broadly with $Ca/(Ca+Mg)$ and $Mg/(Fe+Mg)$ (which are indices of temperature and fractionation) An AFC model is proposed to account for the isotopic and geochemical variations between the megacrysts. The parental melt is asthenospheric, geochemically similar to OIB type magmas with relatively radiogenic Pb (also similar to the Gibeon kimberlites) and depleted Sr and Nd (more depleted than the Gibeon kimberlites). As the magma cools and crystallises the megacryst suite, it becomes enriched in Ca and Fe relative to Mg. Also, assimilation of lithospheric wallrock occurs, so that the isotopic composition of the melt progressively changes towards that of the wallrock. The wallrock has less radiogenic Pb, but high $^{207}Pb/^{204}Pb$ relative to $^{206}Pb/^{204}Pb$, and enriched Sr and Nd. The resulting megacryst suite then falls on a mixing line between the two mantle components. The scale of the magma batches must be small relative to the diapir as each kimberlite pipe appears to have it's own distinctive batch of megacrysts.

The data and model presented here is compatible with the model of Harte and Gurney (1981) in which megacrysts crystallised from melts formed at the edge of a mantle diapir. Small peripheral batches of melt could then interact with their lithospheric wallrocks. A kimberlite melt subsequently produced by the same diapir could then disrupt the megacrysts and transport them to the surface. The melt parental to the megacrysts could thus be distinct from the kimberlite, so that the two are not cogenetic in the strictest sense, but are still related to the same

igneous event.

The data is also compatible with the model of Wyllie (1986) in which megacrysts are produced by the reaction of an asthenospheric melt with lithospheric harzburgite, at the base of the lithosphere. The kimberlite may then be totally unrelated to the megacryst forming event.

5.5

CONCLUSIONS

- 1) A xenocrystic origin for megacrysts is preferred because the megacrysts are not in isotopic equilibrium with the kimberlite.
- 2) The range in isotopic composition of the megacrysts (especially Pb) is interpreted as the product of mixing of depleted (asthenospheric melt) and enriched (lithospheric wallrock) components in an AFC process.
- 3) The kimberlite has an isotopic composition distinct from that of the asthenospheric melt parental to the megacrysts.
- 4) It is not possible to distinguish between the models of (1) Wyllie (1986) whereby an asthenospheric melt ponded at the base of the lithosphere reacts with harzburgite, or (2) that of Egglar et al. (1979) and Harte and Gurney (1981) whereby megacrysts form from small isolated melts at the margins of a rising diapir which subsequently produces the kimberlite.

CHAPTER 6

ASSOCIATED ALKALINE ROCKS

6.1

INTRODUCTION

In Namibia, there exists a NE-SW lineament of alkali igneous intrusions extending from the Gibeon kimberlite province (70+/-10 Ma) to the Schwarzeberg nephelinite (30 Ma) (see fig 2.1). One of the aims of this project was to investigate this lineament to test the hypothesis that the rocks could be related to a 'hot-spot' trace moving east to west across Namibia. The different rock types could then possibly be the products of melting at progressively shallower depths as the hot spot source (? asthenospheric diapir) impinged upon progressively thinner lithosphere as the African plate moved eastwards relative to the hotspot as the Atlantic Ocean opened.

Unfortunately, due to the highly altered state of almost all of the intrusions, coupled with the early closedown of the drilling programme, it was not possible to obtain any samples suitable for geochemical analysis, apart from at two localities: (1) Gross Brukkaros and The Blue Hills monticellite peridotite, and (2) the Schwarzeberg nephelinite. The Blue Hills monticellite peridotite (116 Ma, section 2.6.2) lies within the Gibeon kimberlite province (fig 2.4), but predates the kimberlites by 45+/-10 Ma. It appears to have been intruded at about the time the Discovery hotspot was beneath the area. The Schwarzeberg nephelinite (30 Ma) was emplaced at the time when the Vema hotspot was beneath

it's location (see section 4.6.1). The Gibeon kimberlites (70+/-10 Ma) were emplaced when the Vema hotspot was beneath the Gibeon area.

6.2 GROSS BRUKKAROS AND THE BLUE HILLS

6.2.1 location

Gross Brukkaros is situated on the southern margin of the Gibeon kimberlite province (fig 2.4), and is described in detail by Janse (1969). It is a large (8km diameter, 600m high) eroded pseudo-volcanic feature, comprising a large central vent surrounded by small satellite vents and radial dykes. The main vent consists of up-domed Nama sediments which have collapsed into a central caldera-like crater, together with inward dipping fine grained clastic sediments derived from the Nama sequence by phreatomagmatic explosion (Lorenz pers comm). The centre of the crater consists of a fine grained microbreccia. No igneous rocks are found in the main vent (Janse 1969), only brecciated country rock sediments. Janse (1975) believes Gross Brukkaros to be an incipient carbonatite volcano which was arrested during formation.

Around the main vent are numerous small satellite vents forming domes, consisting of coarse country rock breccia and calcite cement, with calcite veins. Long thin micaceous carbonatite dykes radiate up to 6km away from Gross Brukkaros.

The Blue Hills are a line of low flat topped hills on the southern slopes of Gross Brukkaros (plate 6.1) which are topped by a 1m thick calcite layer. The Blue Hills monticellite peridotite (described by Janse 1971) is possibly a sill which is exposed in several places beneath the calcrete. It is a dark blue porphyritic silicate rock, quite distinct from the carbonatites of the Gross

Brukkaros complex. The peridotite lies within the area of the radial dykes and satellite vents, but appears to post date the formation of the main vent.

Janse (1971) suggested that the monticellite peridotite represents a degassed portion of a kimberlite magma (the carbonatite representing the volatiles), and hence genetically linked the Gross Brukkaros and Blue Hills occurrences with the nearby Gibeon kimberlites. Alternatively, the monticellite peridotite could be totally independent (genetically) of the carbonatite, and it's composition explained in terms of melting parameters differing from those of the kimberlites.

Samples were taken from the monticellite peridotite and carbonatite dykes to test these alternative hypotheses and to investigate the geochemical nature of the sources of these unusual rocks.

6.2.2 Samples

PK2/A15. Monticellite Peridotite.

The rock is dark blue in hand specimen, with olivine phenocrysts and nodular aggregates of magnesian-ulvospinel set in a fine grained groundmass. No mantle or crustal xenoliths were seen at the outcrop.

The **olivine** phenocrysts (25%) are large fresh subhedral to euhedral grains up to 2mm. They display a limited compositional range, Fo_{90-94} , which is similar to, but slightly more magnesian than the kimberlitic olivines (chapter 3). Olivine also occurs as microphenocrysts in the groundmass.

Perovskite is present as pale brown slightly glassy euhedral microphenocrysts with high relief. Some grains show twinning, most are isotropic but some have anomolous blue interference colours.

Phlogopite occurs in the groundmass as pale laths which

enclose inclusions of magnetite and monticellite. The phlogopites are not enriched in Ba, as are the kimberlite groundmass phlogopites (chapter 3).

Magnesian ulvospinel is a common groundmass phase occurring as small (<0.1mm) subhedral grains, and also as nodular aggregates up to 1cm across. They are poor in Ti relative to the spinels in the kimberlites (fig 6.1), and have higher $FeO/(MgO + FeO)$ ratios. They also have relatively high Fe^{3+}/Fe^{2+} ratios (fig 6.2).

The rest of the groundmass consists of **monticellite** and nepheline. Monticellite is colourless with low birefringence and moderate relief forming slightly turbid granular patches. Nepheline forms larger interstitial grains, sometimes enclosing monticellite. It can be distinguished by it's cleavages and less granular appearance.

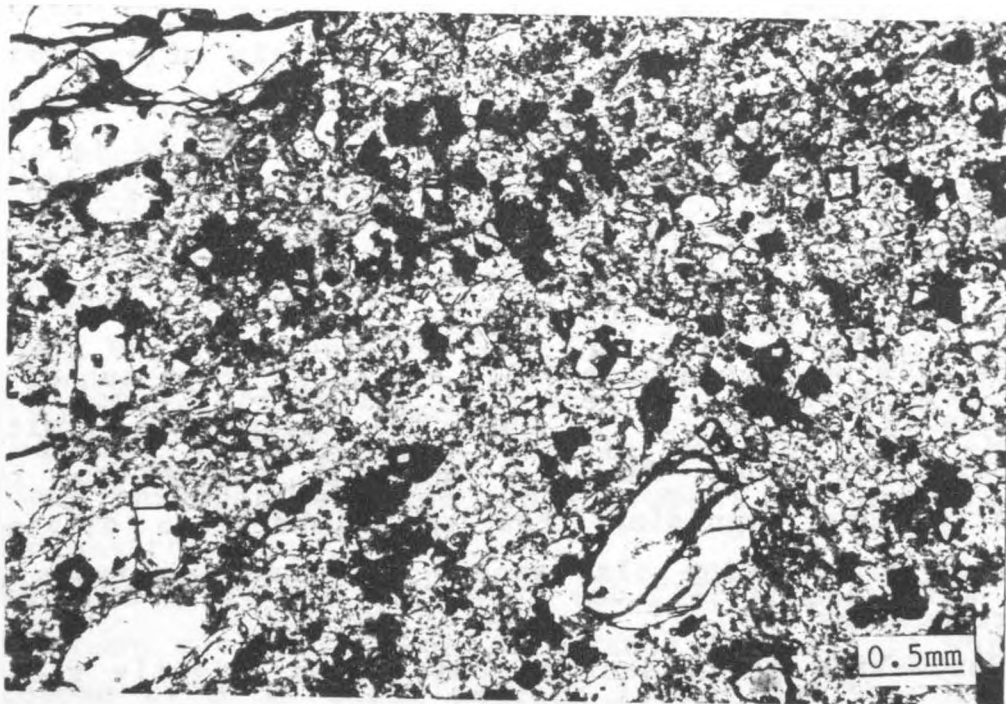


Plate 6.1 Photomicrograph of PK2/A15

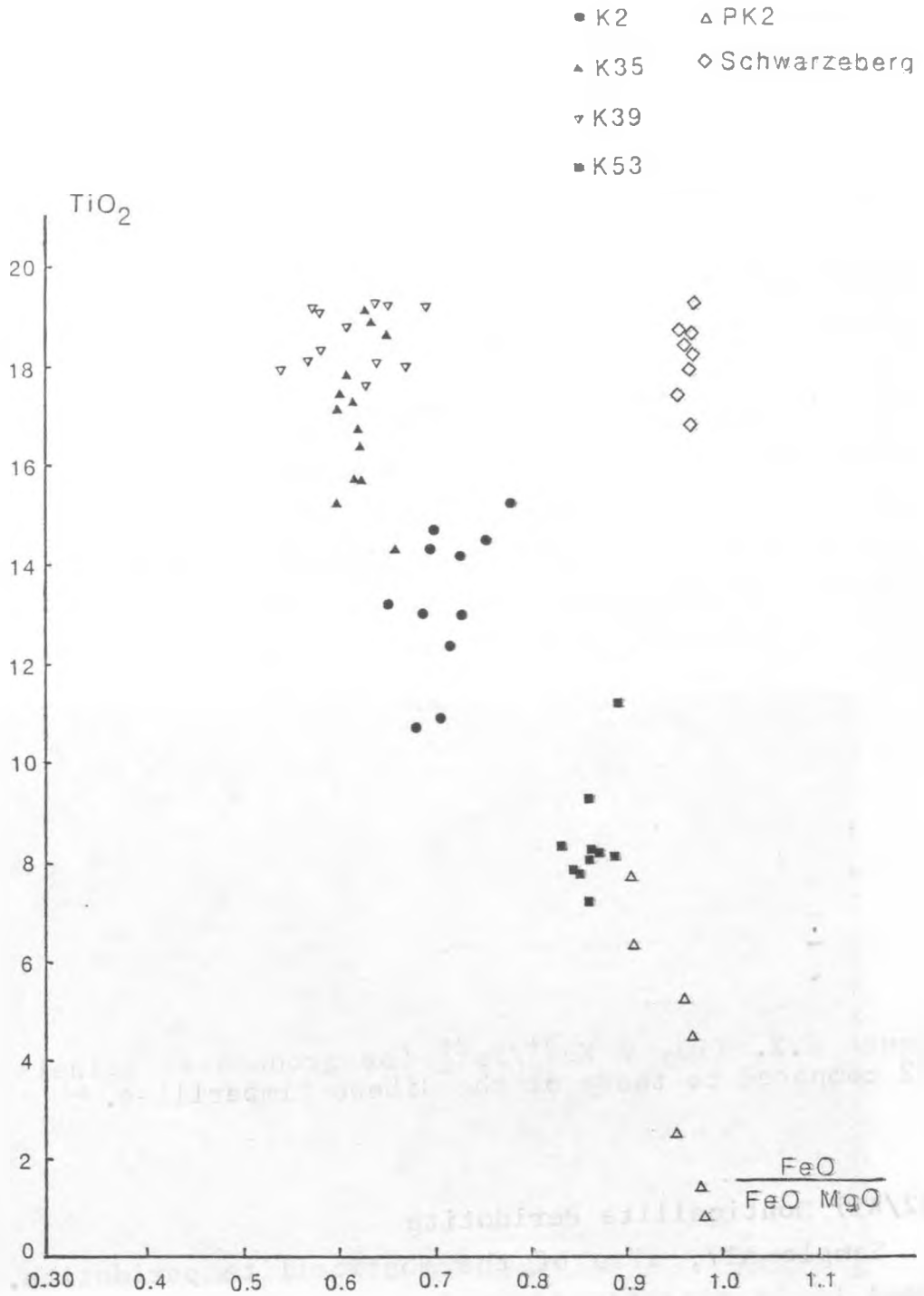


Figure 6.1. TiO_2 v $\frac{\text{FeO}}{\text{FeO} + \text{MgO}}$ for groundmass spinels from PK2 and Schwarzeberg compared to those of the Gibeon kimberlites.

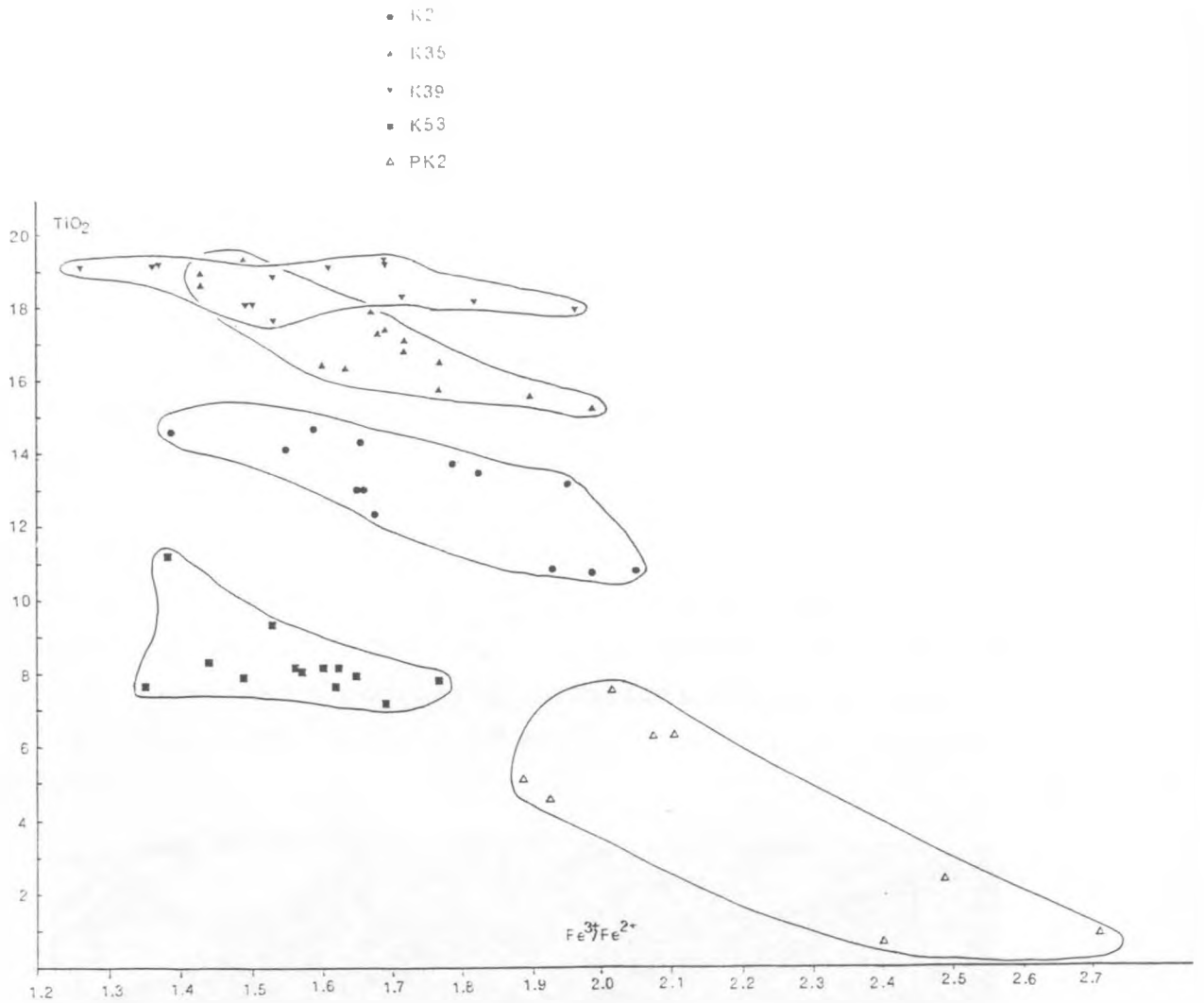


Figure 6.2. TiO_2 v $\text{Fe}^{3+}/\text{Fe}^{2+}$ for groundmass spinels from PK2 compared to those of the Gibeon kimberlites.

PK2/A17 Monticellite Peridotite

Sample A17, also of the monticellite peridotite, was found to be slightly altered on microscopic examination. The original mineralogy was the same as sample A15, but the olivines are now replaced by serpentine and secondary calcite replaces monticellite in the groundmass. The sample was analysed to test the effects of slight alteration on the rock. It was found that the alteration had disrupted the trace element composition and isotope systematics. Several other samples of the monticellite

peridotite were found to be more severely altered, and it was considered not useful to analyse them.

PK1/A20 Carbonatite

A20 is a sample of a carbonatite dyke located 2km south of the Blue Hills, and 6km south of the rim of Gross Brukkaros. The dyke is no more than 25cm wide, but can be traced for 2km. The carbonatite consists principally of calcite (55%), and phlogopite (40%) with minor magnetite (4%) and rare aegirine. Much of the originally blocky calcite has been replaced by a fine grained secondary calcite which is stained brown. Occasionally, brown calcite also occurs as pseudomorphs after olivine.

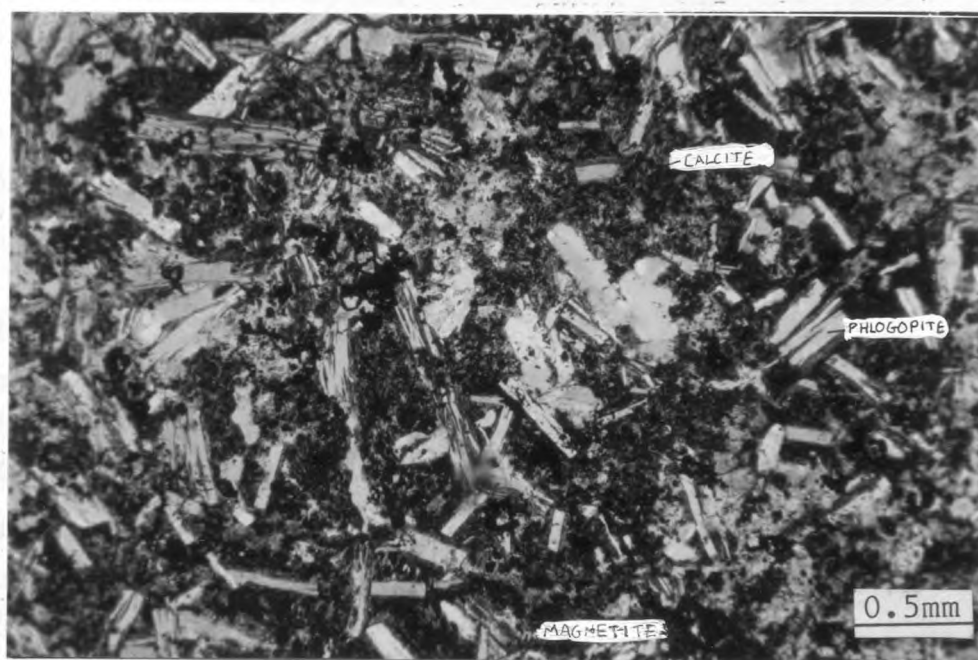


Plate 6.2. Photomicrograph of A20, showing phlogopite laths set in a turbid brown calcite matrix.

6.2.3 Genesis of monticellite peridotite by partial melting of carbonated peridotite?

Experimental Work

One of the major problems limiting the understanding of kimberlite petrology is the lack of knowledge of melting parameters at depth in the mantle. Experimental studies by Brey (1978), Brey et al. (1983), Olafsson and Eggler (1983) and Wyllie (1979, 1980, 1984, 1986) show broad agreement that kimberlite and related melts are produced by small degree partial melting of peridotite in the presence of volatiles, namely CO₂ and H₂O. The precise composition of the melt depends not only on the bulk composition of the source rock, but also on the temperature, pressure and volatile composition. For small degree partial melts, the solidus phases, in particular H₂O (phlogopite/amphibole) and CO₂ (dolomite/magnesite) bearing phases present during melting have a great influence on the composition of the initial melt.

Experimental determination of subsolidus reactions in the system peridotite-H₂O-CO₂, and hence stability fields (Wyllie 1979, Brey et al. 1983, Olafsson and Eggler 1983) disagree in detail, which has important consequences regarding magmagenesis. The effects of CO₂ and carbonate phases have dramatic effects on the peridotite solidus (Wyllie 1980). With increasing pressure the mantle solidus temperature increases (fig 6.3). Suddenly at about 25-28kbar* (Wyllie 1980), there is an increase in the solubility of CO₂ in the melt, and the solidus temperature falls by about 200°C, until at about 28kbar* the carbonation reaction:



* depending on CO₂/H₂O ratios

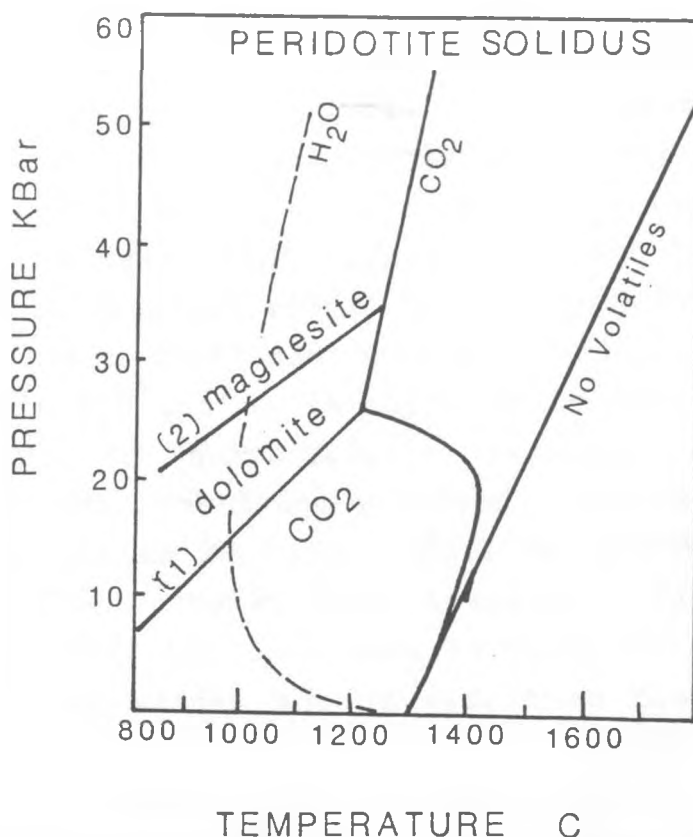


Figure 6.3. schematic representation of the peridotite solidus in the presence of CO_2 , H_2O and of the dry solidus after Wyllie (1977). Precise locations of reactions (1) and (2) and the solidii are uncertain as they vary with $\text{CO}_2/\text{H}_2\text{O}$ ratios, and experimental work to date has not shown good agreement.

occurs which reduces the CO_2 content of the melt as dolomite becomes stable. There is then a pressure interval during which dolomite is the stable carbonate phase, followed at higher pressures by magnesite. Of particular importance is the location of the subsolidus reaction:



because magnesite and dolomite both buffer CO_2 , but have different effects on the composition of the melt produced.

Dolomite buffering causes eutectic melting to produce liquids with constant MgO/CaO (about 1.3) over a range of pressures and degree of partial melting (Brey 1978).

Increasing $(\text{CaO} + \text{MgO})/\text{SiO}_2$ can be caused by increasing the CO_2 content in the source, decreasing the degree of partial melting or increasing the depth of origin.

When magnesite is the stable phase, the melts produced have MgO/CaO 3-4 times higher than melts produced in the presence of dolomite (Brey 1978). Kimberlites are produced by melting in the magnesite stability field (Brey 1978) while melilitites are produced in the dolomite stability field. The accurate determination of the dolomite-magnesite reaction therefore provides a constraint on the depth of melting of kimberlites and melilitites. Kushiro et al. (1975) estimated that reaction (2) above takes place at 50 ± 3 kbar between 1000 and 1200 °C, such that dolomite could be stable at the mantle solidus from 25-50kbar (75-150km).

However, Brey and Green (1976), Brey et al (1983) and Olafsson and Eggler (1983) find that dolomite is stable on the solidus only to about 32kbar, above which magnesite is stable. Dolomite is present on the solidus only between 80 and 110km, and magnesite is present at >110km. Brey (1978) considers that melilitites are produced by melting in the dolomite stability zone, which therefore restricts them to generation between 80 and 110km. Low CaO , Al_2O_3 melts (ie kimberlites) are produced in the magnesite stability field. The inclusion of megacrysts with equilibration pressures of 50kbar (Harte and Gurney 1981 etc.), diamonds (Boyd and Gurney 1986) and high temperature sheared nodules (Nixon and Boyd 1973) indicate an origin of kimberlite at depths in excess of 150km. Clearly kimberlites and melilitites are produced by melting at different depths.

Using the methods of Brey (1978), it is possible to compare the depth of origin, and degree of partial melting (F) of the monticellite peridotite with that of the Gibeon kimberlites. The use of trace element and isotope data can

be used to compare mantle source regions. Brey (1978) used a series of qualitative indicators to compare mantle melting conditions for several suites of melilitites, as summarised below:

MgO/CaO = 1-1.3		indicates buffered melting in the dolomite stability field
MgO/CaO = approx 4-5		indicates melting in the magnesite stability field
(CaO+MgO)/SiO ₂	α	CO ₂ and Pressure
	α	1/degree of partial melt (F)
CaO/Al ₂ O ₃	α	CO ₂ and F
CaO/Na ₂ O	α	CO ₂ and F
K ₂ O	α	1/F
P ₂ O ₅	α	1/F

Wholerock composition of PK2/A15

The major element ratios of sample PK2/A15 are compared in table 6.1 with a Gibeon kimberlite, K35/M and the Saltpetrekop melilitite (from Brey 1978). K35/M has MgO/CaO=3.6 which, as with other kimberlites, indicates melting in the magnesite stability field. A15 has MgO/CaO=0.9, which is just slightly lower than the 1-1.3 suggested by Brey (1978) to indicate CO₂ buffering by dolomite during melting.

PK2/A15 has (CaO + MgO)/SiO₂=1.28, which is extremely high and an indication that the melt is very primitive. Brey (1978) noted that the monticellite peridotite was the most primitive rock known to him. Increased (CaO + MgO)/SiO₂ can be produced by either increasing CO₂ during melting, or melting to a lower degree of partial melt (F), or melting deeper. The MgO/CaO ratio is evidence against melting at greater depths than the kimberlite. CaO/Al₂O₃ and CaO/Na₂O are both increased by increasing CO₂ or by increasing F. PK2/A15 has lower CaO/Al₂O₃ than K35, but

higher $\text{CaO}/\text{Na}_2\text{O}$, which is conflicting evidence and therefore inconclusive. K_2O and P_2O_5 are expected to increase with decreasing F . PK2/A15 has higher K_2O but lower P_2O_5 than the kimberlite, which is at first sight conflicting evidence. However, as K may not be behaving as an incompatible element because of the possible involvement of phlogopite as a residual phase during melting, a higher degree of buffered eutectic melting may increase K_2O (until phlogopite is exhausted in the source) and reduce P_2O_5 . However P_2O_5 could be reduced by retention of apatite in the source during melting. PK2/A15 has lower $(\text{La}/\text{Yb})_N$ than K35 which could either indicate higher F , or be a result of residual apatite.

Overall, the simplest interpretation of these data suggest that PK2/A15 is produced by a higher degree of partial melting, at shallower depths (in the dolomite stability field) in the presence of more CO_2 than the kimberlite. An alternative explanation is possible if apatite is present as a residual phase, affecting REEs and P, such that it is not possible to constrain the relative degree of partial melting or CO_2 abundance. The REE abundances do not appear to show removal of middle REEs, as would be the case if apatite was involved, so the simpler explanation of increased degree of partial melting is preferred.

Relative to the Saltpetrekop melilitite, PK2/A15 has higher $(\text{CaO} + \text{MgO})/\text{SiO}_2$, $\text{CaO}/\text{Na}_2\text{O}$, K_2O and P_2O_5 , and lower $\text{CaO}/\text{Al}_2\text{O}_3$, which together indicate that PK2/A15 was produced by a lower degree of partial melting at higher CO_2 contents.

TABLE 6.2

	PK2/A15	PK2/A17	PK1/A20	A44	A45	A73	A74	A4	PK48	PK55	PK62
SiO2	26.86	26.74	8.21	39.81	39.74	40.07	39.98	0.13	46.49	44.86	39.31
TiO2	3.20	2.72	0.93	2.42	2.42	2.40	2.39	0.01	3.35	2.22	4.18
Al2O3	5.14	3.78	1.31	11.66	11.82	11.82	11.70	0.01	14.44	15.46	7.45
Fe2O3	15.21	11.43	9.53	11.28	11.14	11.30	11.22	0.91	15.21	11.02	14.41
MnO	0.31	0.20	0.30	0.21	0.21	0.21	0.21	0.46	0.21	0.21	0.23
MgO	16.00	14.75	12.37	10.89	10.79	10.40	10.70	0.38	5.35	6.00	8.90
CaO	18.33	14.50	28.53	16.22	15.64	16.47	16.03	56.08	7.84	9.87	14.72
Na2O	0.08	0.39	0.16	2.77	3.08	2.63	2.88	0.10	2.68	2.88	0.31
K2O	2.45	2.88	0.12	1.70	1.53	1.40	1.82	0.03	1.19	1.39	1.63
P2O5	0.25	0.94	1.38	1.18	1.20	1.17	1.18	0.14	0.56	0.60	0.89
L.O.I.	10.73	20.11	36.18	1.77	1.74	1.89	1.83	42.80	1.78	5.59	0.49
Cr	472	547	75	384	390	393	414	-	60	241	236
Co	56	51	31	39	44	42	43	-	57	45	52
Ni	190	268	58	150	158	153	163	10	49	80	112
Cu	30	86	63	77	71	89	70	6	28	54	145
V	162	337	116	264	250	249	243	43	273	221	306
Sc	52	32	59	43	41	42	41	93	33	35	26
Zn	121	93	141	96	90	89	90	223	125	206	100
Rb	39	122	4	48	46	32	45	4	89	19	-
Cs	0.64	3.46	-	0.36	-	0.37	-	-	1.33	-	3.82
Sr	503	602	1315	1530	1480	1770	1445	1475	362	590	1463
Y	37.7	21.8	33.2	29.3	28.6	27.8	27.0	67.7	39.8	25.5	34
Zr	512	323	429	262	270	254	248	12	293	234	228
Nb	249	165	267	203	199	205	198	62	27	48	202
Pb	3.85	6.01	-	3.20	3.40	3.18	-	-	-	-	-
Ba	163	1963	2468	1063	1097	1088	1068	1030	578	971	2678
U	6.2	4.05	-	6.24	-	6.19	-	-	-	-	4.55
Th	20.5	36.9	(33)	12.2	-	11.7	-	-	3.06	-	14.8
Ta	11.3	7.58	-	8.81	-	8.90	-	-	1.79	-	10.9
Hf	12.2	6.78	-	5.61	-	5.30	-	-	7.47	-	8.80
La	179.4	94.17	258.6	123.6	120.2	115.9	113.1	815	36.15	37.90	122
Ce	354.9	172.6	490.4	228.0	220.6	209.2	206.6	2297	75.01	73.02	232
Nd	146.7	73.66	194.7	96.76	93.64	88.06	85.57	896	45.41	37.56	107
Sm	22.08	10.42	27.84	14.26	14.12	13.48	13.06	131	9.432	6.749	17.1
Eu	5.25	2.86	7.059	4.28	4.15	4.348	3.910	29.72	2.835	2.215	4.81
Gd	14.22	6.96	16.17	9.691	9.351	8.989	8.870	59.22	8.090	5.341	10.5
Dy	10.13	5.72	9.60	7.722	7.565	7.141	6.960	27.70	8.535	5.615	7.55
Yb	2.827	1.600	2.610	2.447	2.333	2.403	2.266	3.298	4.311	2.862	1.90
Lu	0.369	0.305	0.415	0.322	0.315	0.316	0.290	3.298	0.612	0.399	0.33
Ni/V	1.17	0.795	0.500	0.568	0.632	0.614	0.671	0.233	0.179	0.362	0.366
Ta/Th	0.720	0.205	-	0.722	-	0.761	-	-	0.585	-	0.736
La/Nb	0.8192	0.5707	0.9685	1.0131	1.0186	0.5654	0.5712	13.14	1.339	0.7896	0.604
(La/Yb) _N	42.8	39.7	66.8	34.1	34.7	32.52	33.65	166.6	5.653	8.928	43.3

A44, A45, A73, A74: Schwarzeberg Nephelinite; A4 Carbonatite, Dikke Willem; PK48, PK55 dolerite, PK62 melilitite Grunau

TABLE 6.3

SAMPLE	AGE	$^{147}\text{Sm}/^{144}\text{Nd}$	$^{143}\text{Nd}/^{144}\text{Nd}_m$	$^{143}\text{Nd}/^{144}\text{Nd}_i$	ϵNd	$^{87}\text{Rb}/^{86}\text{Sr}$	$^{87}\text{Sr}/^{86}\text{Sr}_m$	$^{87}\text{Sr}/^{86}\text{Sr}_i$	ϵSr
PK2/A15	116	0.09100	0.512673+/-49	0.512604	2.25	0.2242	0.704081+/-14	0.703711	-12.06
PK2/A17+	116	0.08552	0.512639+/-24	0.512574	1.62	0.5862	0.705938+/-10	0.704971	5.83
PK1/A20*	7116*	0.0864	0.512665+/-27	0.512599	2.11	0.0088	0.705154+/-10	0.705140	8.23
A44	30	0.08910	0.512804+/-23	0.512786	3.60	0.0907	0.703728+/-10	0.703689	-13.8
A45	30	0.09116	0.512757+/-15	0.512739	2.68	0.0899	0.703808+/-10	0.703770	-12.7
A73	30	0.09255	0.512779+/-12	0.512761	3.11	0.0523	0.703893+/-10	0.703871	-11.3
A74	30	0.09227	0.512745+/-15	0.512727	2.45	0.0901	0.703794+/-12	0.703755	-12.9
A4	730*	0.08857	0.512737+/-32	0.512720	2.31	0.0078	0.703216+/-14	0.703213	-20.6
PK48+	520	0.1256	0.512410+/-30	0.511982	0.24	0.7122	0.720905+/-12	0.715626	164
PK55+	520					0.0932	0.707109+/-10	0.706419	33.3
PK62+	520					0.0830	0.708249+/-10	0.707634	50.6

SAMPLE	U	Th	Pb	$^{206}\text{Pb}/^{204}\text{Pb}_m$	$^{207}\text{Pb}/^{204}\text{Pb}_m$	$^{208}\text{Pb}/^{204}\text{Pb}_m$	u	w	k	$^{206}\text{Pb}/^{204}\text{Pb}_i$	$^{207}\text{Pb}/^{204}\text{Pb}_i$	$^{208}\text{Pb}/^{204}\text{Pb}_i$
PK2/A15	6.2	20.5	3.85	20.789+/-10	15.790+/-16	40.615+/-53	108.7	0.789	371	18.815	15.694	38.476
PK2/A17+	4.05	36.9	6.01	19.290+/-12	15.649+/-10	39.331+/-26	43.84	0.318	413	18.494	15.610	36.955
A44	6.24	12.2	3.20	20.181+/-3	15.743+/-4	39.900+/-3	129	0.939	261	19.570	15.715	39.511
A45			3.44	20.201+/-20	15.724+/-29	39.796+/-72						
A73	6.19	11.7	3.18	20.213+/-2	15.724+/-5	39.686+/-26	128.9	0.935	252	19.612	15.696	39.312
A74			3.52	20.271+/-7	15.746+/-5	39.936+/-14						
A4				21.055+/-5	15.886+/-4	40.330+/-11						
PK48+				18.677+/-6	15.672+/-5	38.853+/-14						
PK55+				18.890+/-7	15.585+/-7	38.082+/-18						
PK62+				21.664+/-8	15.825+/-11	41.181+/-23						
PK62+				21.653+/-7	15.821+/-6	41.150+/-15						

$$u = ^{238}\text{U}/^{204}\text{Pb} \quad w = ^{235}\text{U}/^{204}\text{Pb} \quad k = ^{232}\text{Th}/^{204}\text{Pb}$$

+ altered samples

* age of intrusion was not determined but initial ratios were calculated at these ages for comparison with PK2 and A44 etc.

TABLE 6.1

	K35	PK2/A15	Saltpetrekop	implication for A15 relative to K35
MgO/CaO	3.55	0.87	1.13	shallower melting
$\frac{(\text{CaO}+\text{MgO})}{\text{SiO}_2}$	1.16	1.28	0.99	higher CO ₂ or lower F
CaO/Al ₂ O ₃	2.23	1.20	2.22	lower CO ₂ or F
CaO/Na ₂ O	36	229	7.5	higher CO ₂ or F
K ₂ O	0.86	2.45	1.5	?higher F
P ₂ O ₅	0.80	0.25	1.9	higher F or ?apatite retention
(La/Yb) _N	120	41		higher F

The trace element composition of PK2/A15 is very similar to that of the Gibeon kimberlites. On a chondrite normalised plot (fig 6.4), the relative elemental abundances increase from right (most compatible) to left (most incompatible) peaking at Nb, then decreasing to Pb. The K trough, characteristic of kimberlites, is present but relatively small. There are large troughs at Sr and P, which could be due to retention by apatite in the source. There is no evidence in favour of apatite fractionation, as it is a late forming mineral which has not been identified in this rock. Ba is noticeably low in A15, but the reason for this is not clear.

Figure 6.4. Chondrite normalised trace element plot for Blue Hills samples (A15 and A17) and a Gross Brukarros Carbonatite (A20).

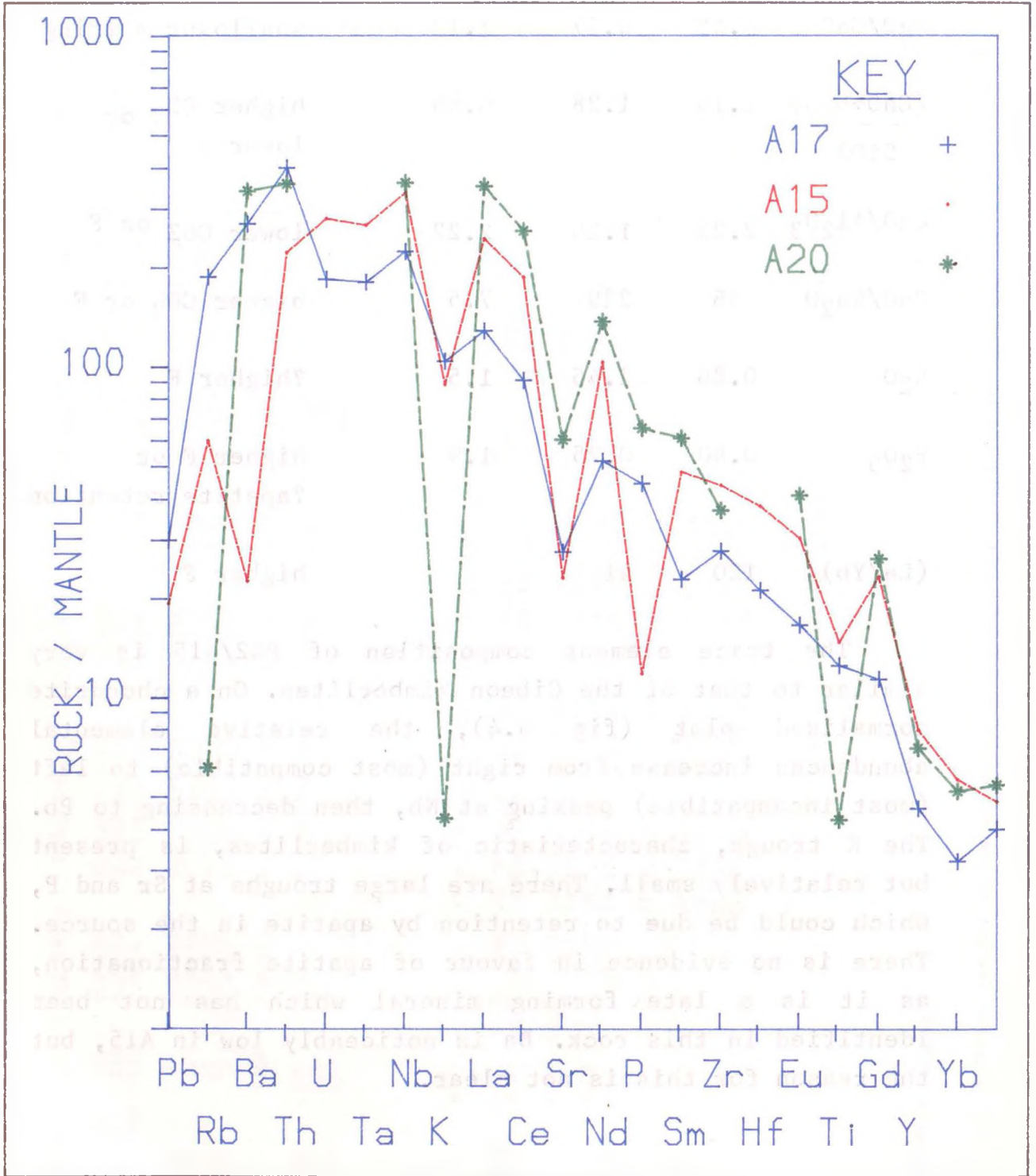
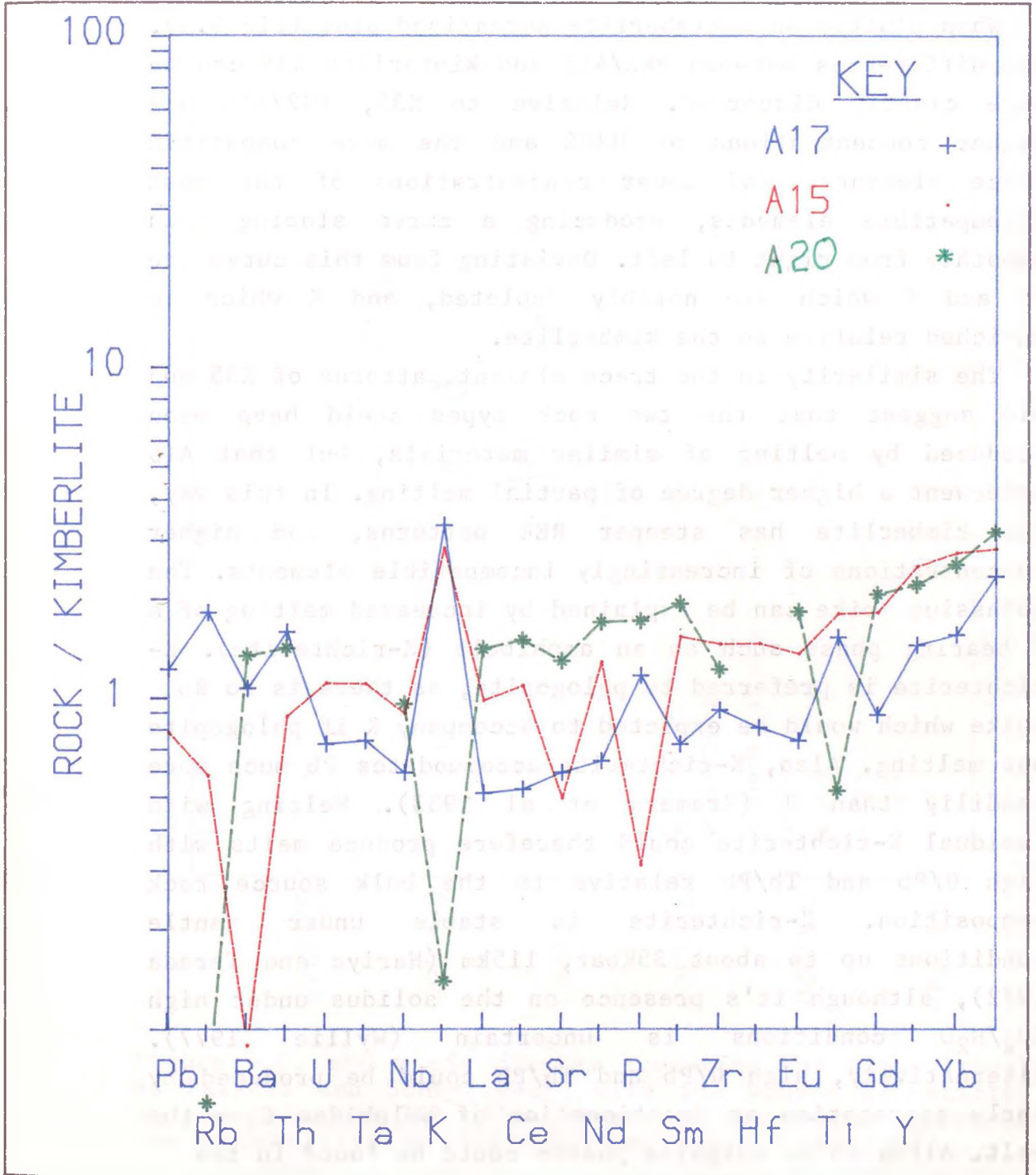


Figure 6.5 K35-normalised plot for A15, A17 and A20.



Sample PK2/A17, which has suffered from alteration has generally lower concentrations of trace elements due to their dissolution in, and removal by, groundwaters. PK2/A17 does however have high concentrations of Pb, Rb, Ba and Th relative to A15.

When plotted on a kimberlite normalised plot (fig 6.5), the differences between PK2/A15 and kimberlite K35 can be more clearly discerned. Relative to K35, PK2/A15 has higher concentrations of HREE and the more compatible trace elements, and lower concentrations of the most incompatible elements, producing a curve sloping down smoothly from right to left. Deviating from this curve are Sr and P which are notably depleted, and K which is enriched relative to the kimberlite.

The similarity in the trace element patterns of K35 and A15 suggest that the two rock types could have been produced by melting of similar materials, but that A15 underwent a higher degree of partial melting. In this way, the kimberlite has steeper REE patterns, and higher concentrations of increasingly incompatible elements. The potassium spike can be explained by increased melting of a K bearing phase such as an amphibole (K-richterite). K-richterite is preferred to phlogopite, as there is no Rb spike which would be expected to accompany K if phlogopite was melting. Also, K-richterite accommodates Pb much more readily than U (Kramers et al 1983). Melting with residual K-richterite could therefore produce melts with high U/Pb and Th/Pb relative to the bulk source rock composition. K-richterite is stable under mantle conditions up to about 35Kbar, 115km (Hariya and Terada 1972), although it's presence on the solidus under high CO₂/H₂O conditions is uncertain (Wyllie 1977). Alternatively, high U/Pb and Th/Pb could be produced by early segregation or fractionation of sulphides from the melt. Although no sulphide phases could be found in the

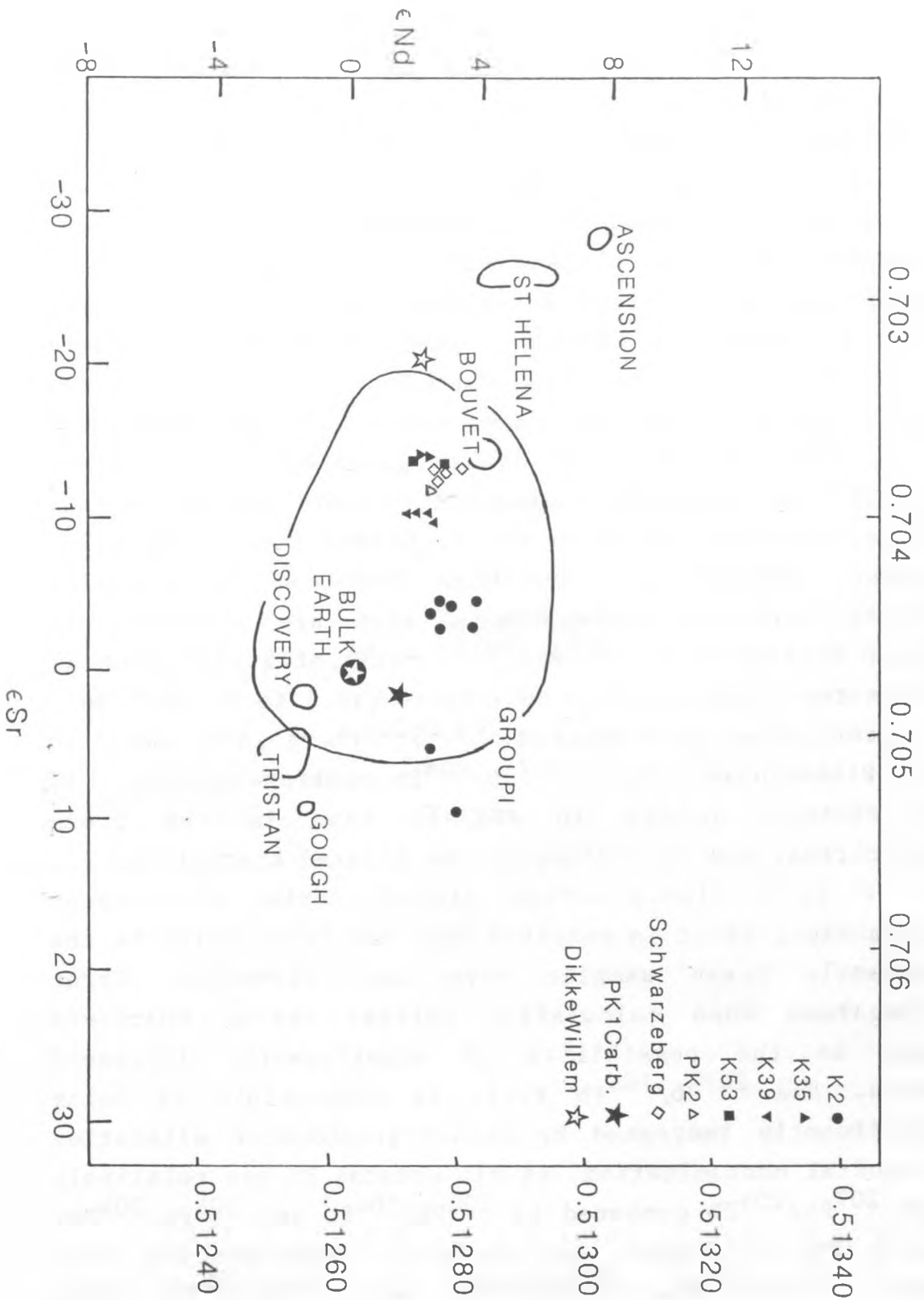


Figure 6.6. ϵ_{Nd} v ϵ_{Sr} diagram comparing the compositions of PK2/A15 and Schwarzeberg with the Gibeon kimberlites and S. Atlantic OIB. Also shown are the compositions of the carbonatites A4 (Dikke Willem) and A20 (altered).

rock, PK2/A15 does have anomalously low Ni/V and Cr/V which may be a result of sulphide fractionation.

Further evidence that PK2/A15 is derived from a similar source to the kimberlites is provided by Sr, Nd and Pb isotopes. PK2/A15 plots very close to the Gibeon kimberlites on the time integrated ϵSr vs ϵNd plot (fig 6.6), at $\epsilon\text{Sr}=-12.1$, $\epsilon\text{Nd}=3.44$, compared to the kimberlite field at $\epsilon\text{Sr}=-9.7$ to -14 , $\epsilon\text{Nd}=1.6$ to 2.8 . The altered sample PK2/A17, and the carbonatite A20 both have much higher $^{87}\text{Sr}/^{86}\text{Sr}$ which is due to groundwater alteration. PK2/A15 has extremely radiogenic present day Pb isotope ratios, plotting close to the St Helena field (fig 6.7). However, PK2/A15 also has high U/Pb and Th/Pb ratios (higher than the kimberlites). When age corrected to 116Ma, PK2/A15 has a $^{206}\text{Pb}/^{204}\text{Pb}$ ratio of 18.81 which is within the range of the kimberlites (18.8 to 19 at 70Ma). Similarly, the age corrected $^{208}\text{Pb}/^{204}\text{Pb}$ ratio is close to the kimberlites. The $^{207}\text{Pb}/^{204}\text{Pb}$ ratio however, is significantly higher in PK2/A15 than in the fresh kimberlites, and is similar to the altered kimberlites.

U is a highly mobile element during groundwater interaction, so it is possible that the U/Pb ratios in the apparently fresh samples have been disturbed. Error propagation when calculating initial ratios therefore leads to the possibility of significantly increased errors. The $^{207}\text{Pb}/^{204}\text{Pb}$ ratio is susceptible to being significantly increased by either groundwater alteration or crustal contamination, as old crustal Pb has relatively high $^{207}\text{Pb}/^{204}\text{Pb}$ compared to $^{206}\text{Pb}/^{204}\text{Pb}$ and $^{208}\text{Pb}/^{204}\text{Pb}$. Sample PK2/A17, which has suffered alteration has much lower $^{206}\text{Pb}/^{204}\text{Pb}$, $^{207}\text{Pb}/^{204}\text{Pb}$ and $^{208}\text{Pb}/^{204}\text{Pb}$ than PK2/A15, indicating that alteration is not the cause of the high $^{207}\text{Pb}/^{204}\text{Pb}$ in PK2/A15. It is therefore concluded that the high $^{207}\text{Pb}/^{204}\text{Pb}$ of PK2/A15 is either a characteristic of the source or a result of crustal

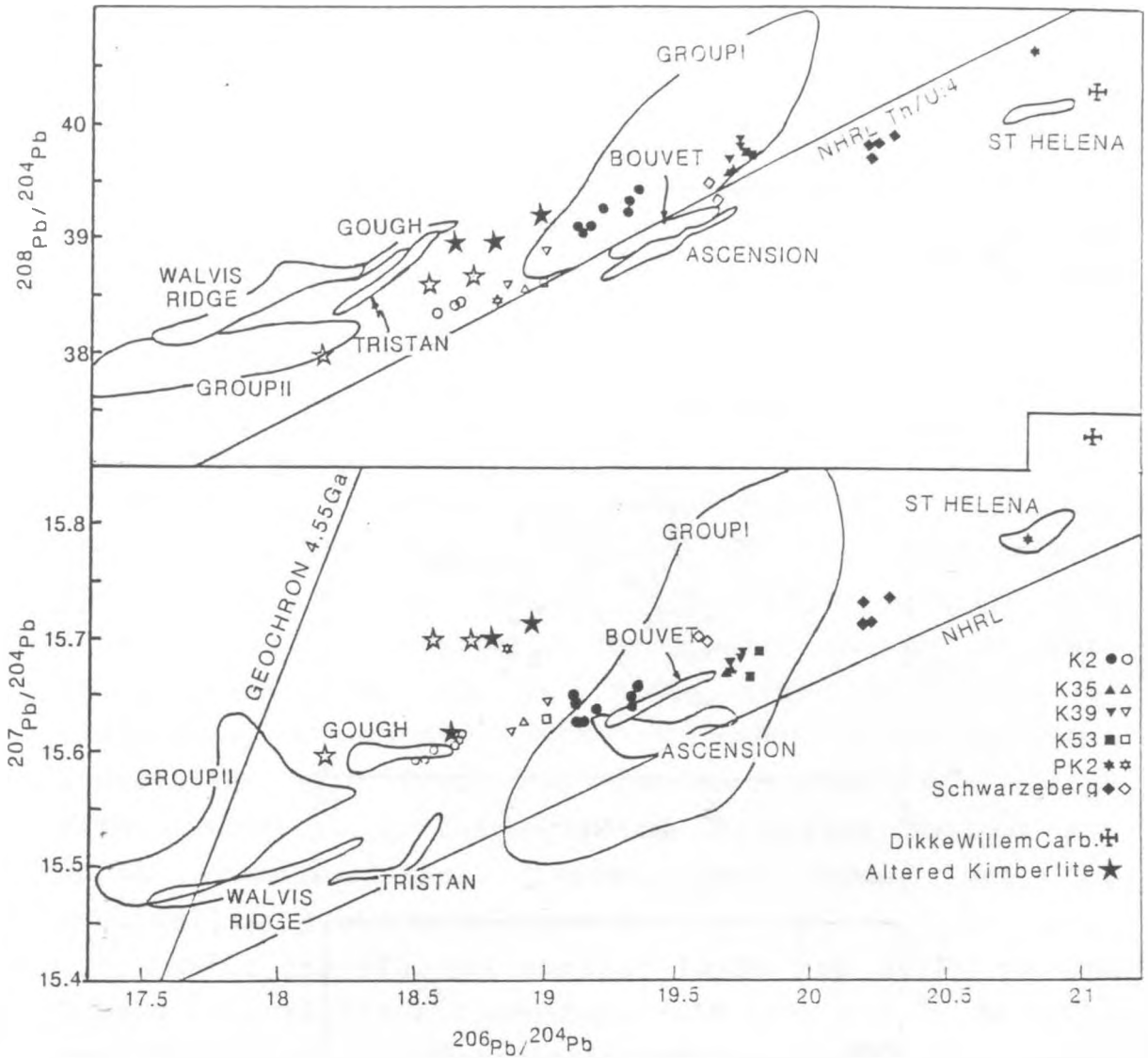


Figure 6.7. Pb isotope diagram comparing present day (solid symbols) and initial (open symbols) ratios of PK2/A15 and Schwarzeberg with the Gibeon kimberlites and S. Atlantic OIB. Note that at 116Ma, OIB are likely to have $^{206}\text{Pb}/^{204}\text{Pb}$ about 0.2-0.4 lower than at present, so that PK2 has an initial $^{206}\text{Pb}/^{204}\text{Pb}$ similar to Bouvet.

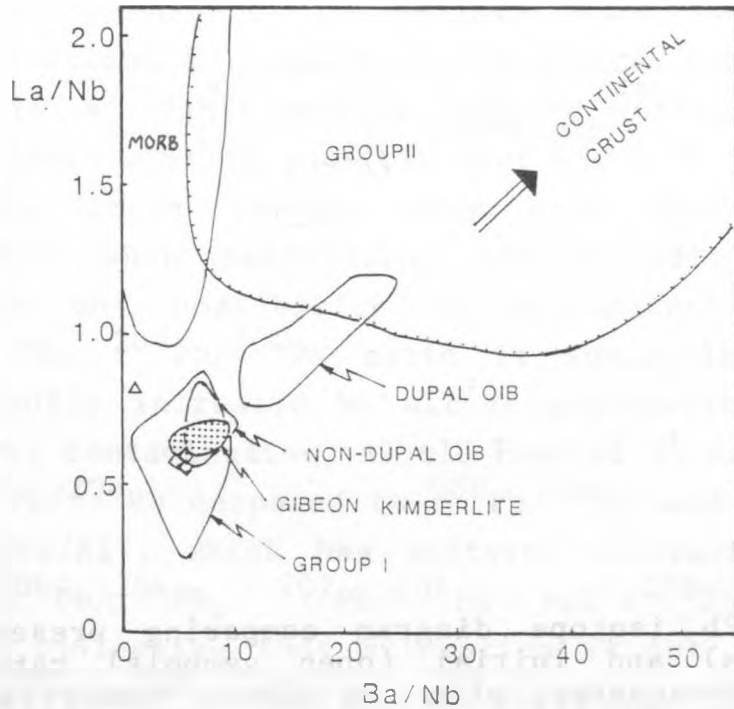
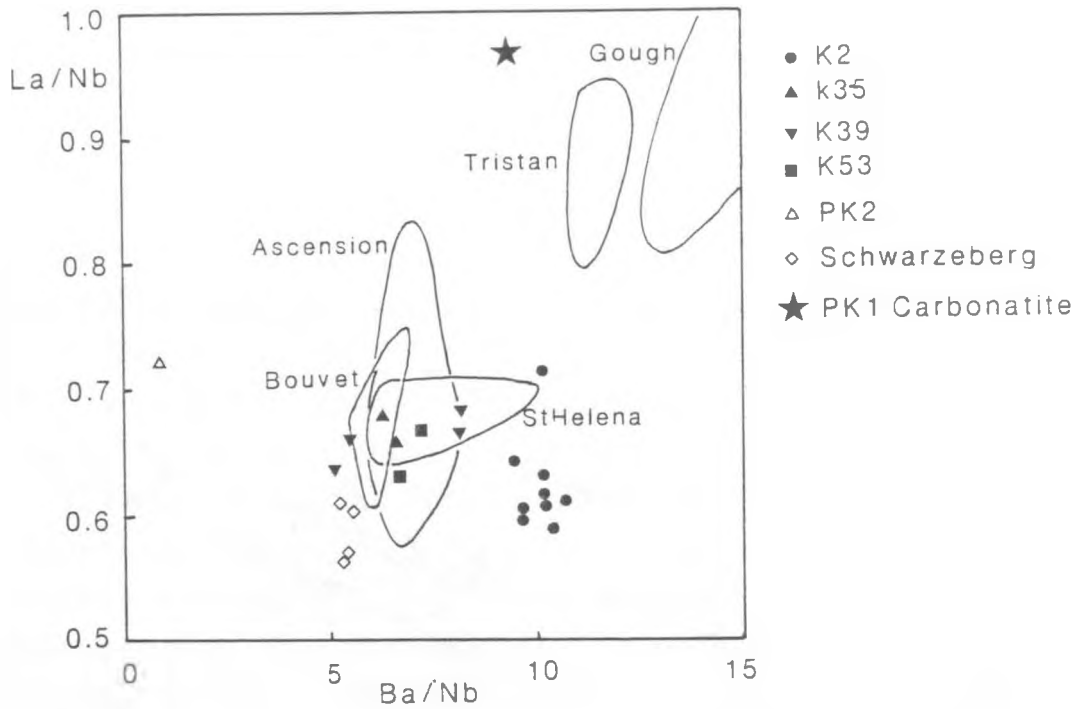


Figure 6.8. La/Nb v Ba/Nb plot showing similarity between PK2, Schwarzeberg, Gibeon kimberlites and non-Dupal OIB, in contrast to Dupal OIB, MORB and the continental crust.

contamination. The high $^{206}\text{Pb}/^{204}\text{Pb}$ and $^{208}\text{Pb}/^{204}\text{Pb}$ are primarily due to very high U/Pb and Th/Pb in PK2/A15, which are possibly produced by melting with residual K-richterite. It is therefore quite feasible that PK2 and the kimberlites were produced from isotopically and geochemically, though not mineralogically, equivalent source materials.

Mantle source regions

Trace element and isotope ratios point to a similarity in the mantle source regions of the monticellite peridotite and the Gibeon kimberlites, despite the apparent 45Ma difference in their ages (chapter 2). This is surprising as the two magma types appear to be temporally associated with different hotspots, the kimberlites with Vema, and the monticellite peridotite with Discovery. Furthermore, the Discovery hotspot has Dupal characteristics (LeRoex pers comm.) and the monticellite peridotite has not.

Sample PK2/A15 has similar La/Nb and Ba/Nb to the Gibeon kimberlites and non-Dupal OIB (fig 6.8). Low Ba/La and Ba/Nb are characteristic of non-Dupal OIB. Also, PK2/A15 has low ϵSr , similar to Bouvet, and the Gibeon kimberlites, but not Discovery. The high $^{206}\text{Pb}/^{204}\text{Pb}$ and $^{208}\text{Pb}/^{204}\text{Pb}$ initial ratios of PK2/A15 are also closer to Bouvet (at 116Ma) than to the Dupal islands. Only the raised $^{207}\text{Pb}/^{204}\text{Pb}$ (which is possibly due to crustal contamination) is reminiscent of a Dupal signature.

It is concluded that the monticellite peridotite could feasibly be produced by small degree partial melting of a non-Dupal type asthenospheric source rock, in the presence of CO_2 , in the dolomite, K-richterite stability field (at a depth of about 80-100km). Relative to the Gibeon kimberlites, the rock was derived by a higher degree of partial melting, at shallower depth, in an environment

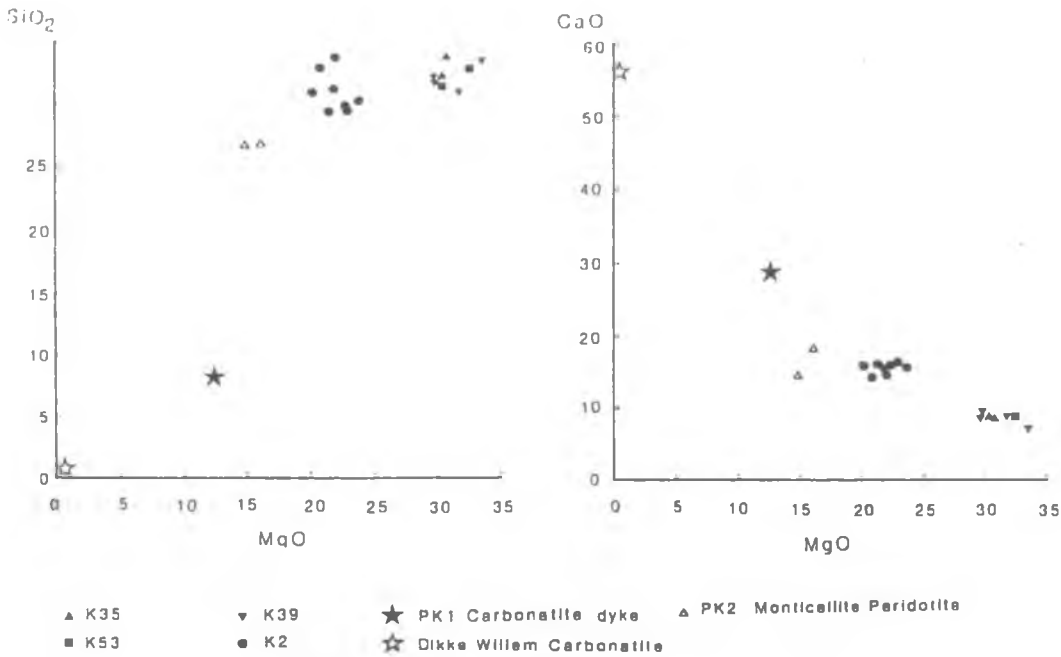


Figure 6.9. SiO₂ and CaO v MgO, showing the composition of PK2 relative to kimberlite and carbonatite.

richer in CO₂. The spatial association of the carbonatite is not thought to be due to a genetic relationship. Instead, the carbonatite is thought to be a separate mantle product, produced by incipient melting of carbonated peridotite (Wyllie 1979). The monticellite peridotite may have ascended through a zone of weakness produced by the carbonatite eruption.

6.2.4 Derivation by kimberlite devolatilisation

Janse (1971) suggested that the monticellite peridotite PK2 could be produced by desegregation of kimberlite into volatile (ie carbonatite) and magmatic (monticellite peridotite) portions. This was suggested on the basis that the Gibeon kimberlites appeared to have trace element concentrations intermediate between carbonatite and monticellite peridotite.

This suggestion is considered to be untenable for the following reasons:

1) The major element compositions of the monticellite

peridotite and carbonatite are not conjugates which could be mixed together in any proportions to produce kimberlite. Figure 6.9 shows that the monticellite peridotite and carbonatites both have lower MgO and SiO₂ than kimberlite, and higher CaO. A desegregation of kimberlite, producing a carbonatite would have to yield a residual magma that was richer in MgO and SiO₂, and poorer in CaO than the kimberlite. Janse's (1971) data, as well as that presented here show this point.

2) The trace element compositions of the monticellite-peridotite, and carbonatite could not be mixed together to produce kimberlite. Figure 6.5 shows that both PK2/A15 and the carbonatite PK1/A20 have higher concentrations of REE (Nd-Lu) and Zr than the kimberlite K35, and therefore are not conjugates which could be mixed together to produce kimberlite.

3) PK2/A15 has 10.7 % loss on ignition which is comparable to the kimberlites. Devolatilisation would reduce the volatile content.

4) The early olivine phenocrysts are of a different composition (Fo₉₄) to those found in kimberlites (Fo₉₀).

5) No magnesiochromites were found in the monticellite peridotite, but they are a common early microphenocryst phase in the kimberlites.

6) No megacrysts were found in the monticellite peridotite.

6.3 THE SCHWARZEBERG NEPHELINITE

The Schwarzeberg nephelinite is a very fine grained, hard dark grey rock containing no visible mantle or crustal xenoliths. Four exceptionally fresh samples were analysed. The four samples were petrographically identical, consisting of augite microphenocrysts set in a groundmass of augite, nepheline, magnetite and biotite.

Occasional resorbed olivine and orthopyroxene macrocrysts are present, and it is not clear whether they are xenocrysts or early phenocrysts.

6.3.1 Mineralogy

Zoned **titanaugite** (25%) occurs as euhedral to subhedral phenocrysts (up to 2mm) which show strong pleochroism from pale brown to pale green/yellow. Some grains appear to have been resorbed slightly. Augite is also a major constituent of the groundmass (20%), occurring as abundant laths (0.1-0.4mm).

Nepheline is a major groundmass phase (30%) occurring as small equant grains (<0.2mm) interstitially between the augites, forming a granular texture.

Titanomagnetite (10%) occurs as equant grains in the groundmass (<0.1mm) and also as inclusions within groundmass augites.

Biotite (1%) occurs rarely in the groundmass in tiny interstitial patches.

Extremely rare microscopic grains of a **Pb-Sb-sulphide** phase, probably galena, were found in the groundmass.

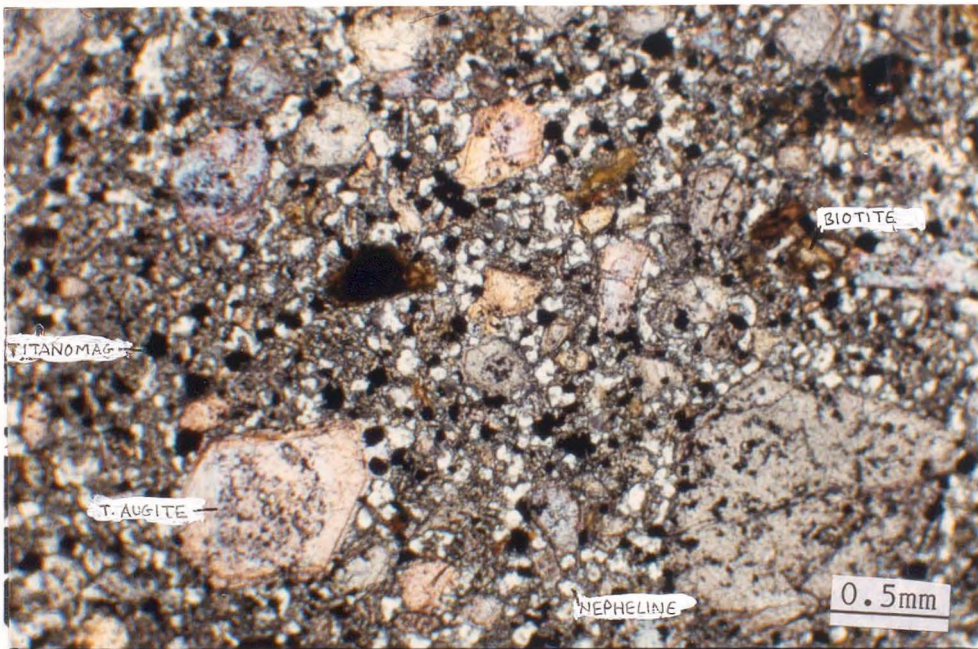


plate 6.3. Photomicrograph of Schwarzeberg nephelinite, showing titanite phenocrysts, and a groundmass of nepheline titanomagnetite and biotite

6.3.2 Petrogenesis

Eggler (1978) showed that nephelinite could be produced as an initial melt by melting over a range of depths in the mantle. In volatile rich conditions, nephelinite could be produced as shallow as 50km, while melilitite is produced between 80 and 100km. Increased degree of melting, or melting at shallower depths produces alkali basalts, and ultimately, tholeiitic basalts.

The composition of the initial melt depends heavily on the composition of the vapour present. In H₂O rich conditions, the melt is SiO₂ rich, but with increasing CO₂/(CO₂+H₂O), the melt becomes increasingly undersaturated in SiO₂ (Wyllie 1977). Mysen and Boetcher (1975) suggested that nephelinite would be produced when CO₂/(CO₂+H₂O)=0.8. Wyllie (1977) proposed that the CO₂/H₂O ratio of the melt is a reflection of the relative proportions of carbonate to phlogopite (or amphibole) present in the source, although at depths shallower than about 80km, CO₂ is present as a free vapour phase not as dolomite.

Thus the degree of silica saturation is controlled by three main factors: 1) depth of melting, SiO₂ decreases with depth, 2) degree of melting, SiO₂ increases with higher degree of melt, and 3) vapour composition, SiO₂ decreases with increased CO₂/H₂O.

Wedepohl and Muramatsu (1979) showed that kimberlites, nephelinites, alkali basalts and tholeiitic basalts formed a continuous spectrum of trace element compositions which they regarded as a result of increasing degree of partial melting from kimberlite to tholeiite. Eggler (1978) pointed out that the spectrum kimberlite-nephelinite-alkali basalt could reflect, to a large extent, the depth in the mantle to which a diapir rose before the magma segregated from the source.

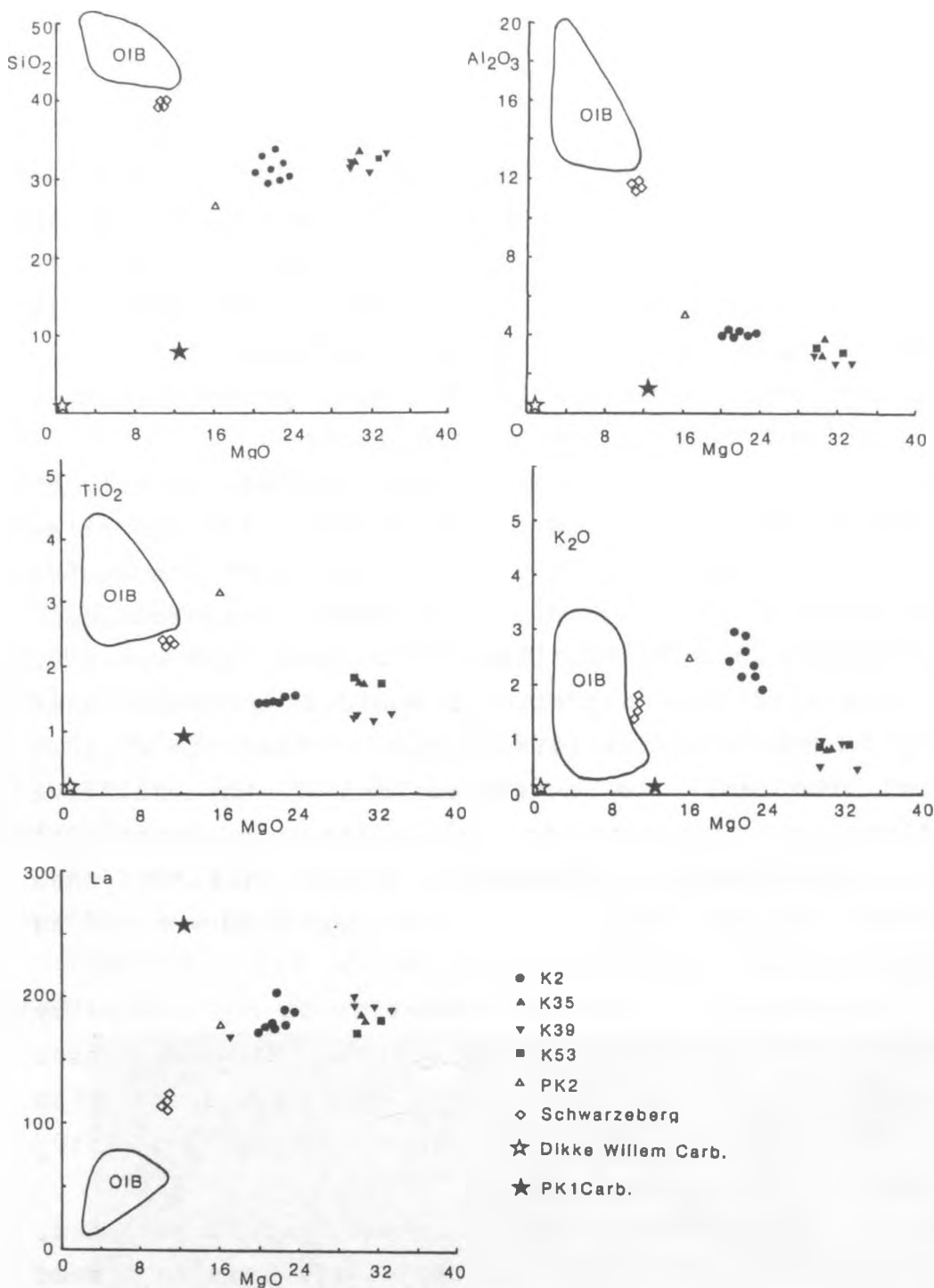


Figure 6.10. Harker diagrams showing the composition of the schwarzeberg nephelinite intermediate between OIB and Gibeon kimberlite.

The Schwarzeberg nephelinite has a MgO/CaO ratio of 0.7, which is significantly lower than the 1-1.3 found in melilitites (Brey 1978). This is an indication that the nephelinite did not melt in an environment buffered by dolomite, and hence was formed at <80km. The (CaO+MgO)/SiO₂ ratio of 0.66 is intermediate between alkali basalt and kimberlite, and reflects the higher SiO₂ in the nephelinite relative to kimberlite. The rock is undersaturated with respect to SiO₂ (hence the nepheline) which indicates high CO₂/H₂O in the source. On element-element plots, the nephelinite consistently plots between kimberlite and alkali basalt (fig 6.10).

The four nephelinite samples show very little compositional variation. The rock is predominantly fine grained and appears to be a primitive melt which has undergone little fractionation. The trace element composition shows similarities with the Gibeon kimberlites. On a chondrite normalised plot (fig 6.11) the relative elemental abundances increase from right to left, peaking at Nb-Ta, then decreasing to Pb. The nephelinite has small troughs at K and Sr, but these are very much less pronounced than in the kimberlite, indicating less retention of these elements in the source during melting. Relative to K35, the nephelinite has lower concentrations of LREE and LIL elements, but higher concentrations of HREE, K and Sr. The kimberlite has steeper REE patterns than the nephelinite, indicating that the nephelinite underwent higher degrees of partial melting. Pb concentrations are significantly lower in the nephelinite, relative to K35, resulting in higher U/Pb ratios. It is quite possible that early sulphide segregation/fractionation (rare Pb sulphides were found in the groundmass) provided a sink for Pb, hence increasing U/Pb ratios in the remaining silicate melt.

The nephelinite has very similar La/Nb (0.6) and Ba/Nb

(5.2) ratios to the Gibeon kimberlites (and Bouvet), an indication of their non-Dupal type signature and similarity to the Bouvet source.

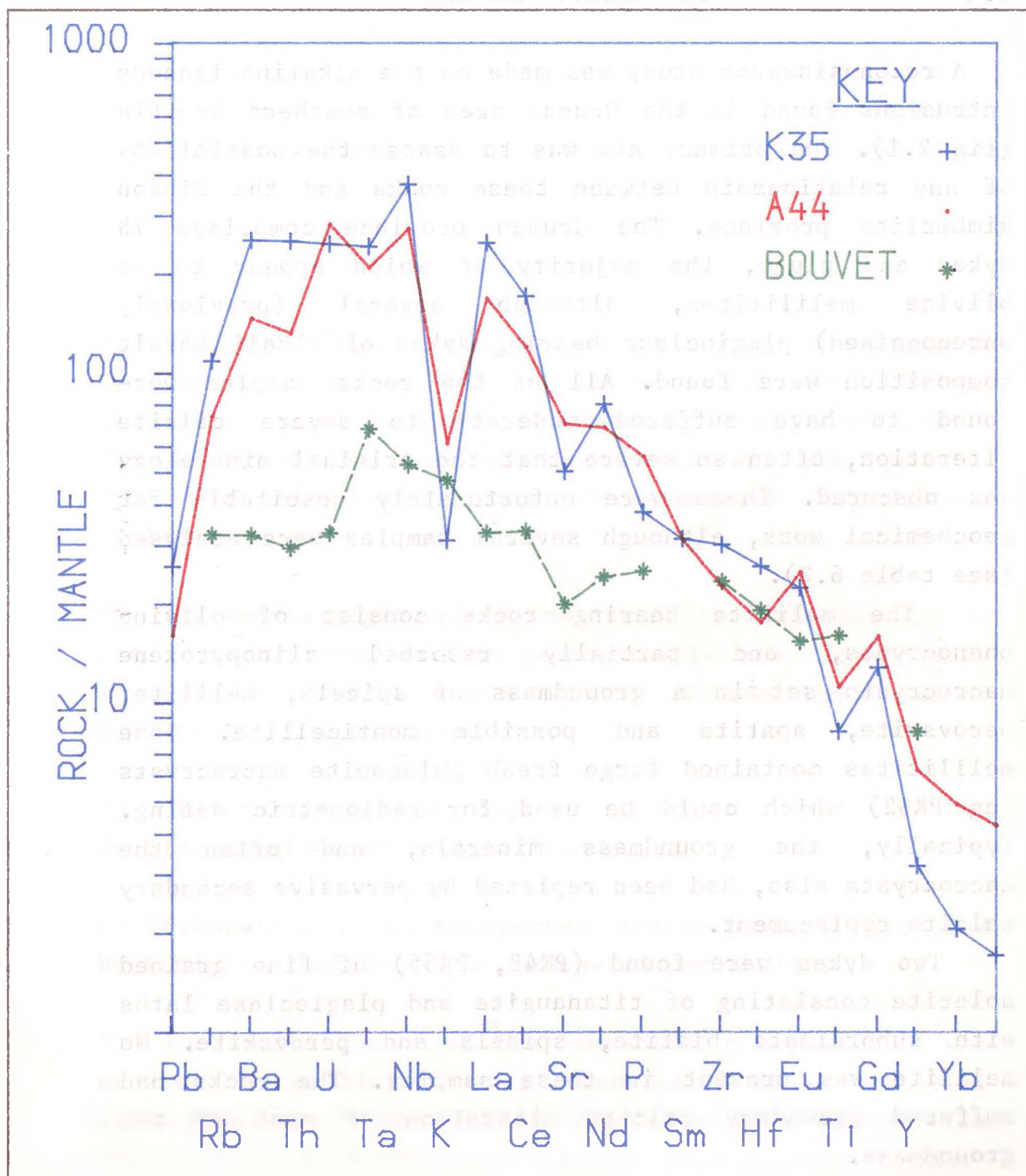
6.3.3 Source regions

The Schwarzeberg nephelinite is 30Ma old (chapter 2), 40Ma younger than the Gibeon kimberlites. On the time integrated ϵ_{Sr} vs ϵ_{Nd} plot (fig 6.6) the nephelinite plots at $\epsilon_{\text{Sr}}=-12.2$ to -13.8 , and $\epsilon_{\text{Nd}}=2.45$ to 3.6 , which is within the field of the Gibeon kimberlites, indicating that both rock types were derived from similar, slightly depleted, asthenospheric source materials.

Present day Pb isotope ratios are more radiogenic than the Gibeon kimberlites. On the $^{207}\text{Pb}/^{204}\text{Pb}$ vs $^{206}\text{Pb}/^{204}\text{Pb}$ plot (fig 6.7), the nephelinite plots between Bouvet and St Helena, slightly above the NHRL. The high U/Pb ($\mu=130$) in the nephelinite has produced significant $^{206}\text{Pb}/^{204}\text{Pb}$ growth in 30Ma. When age corrected to 30Ma, the nephelinite has $^{206}\text{Pb}/^{204}\text{Pb}=19.57$ to 19.60 (within the Bouvet range) and $^{207}\text{Pb}/^{204}\text{Pb}=15.70$ to 15.71 (slightly more radiogenic than Bouvet). The nephelinite has lower Th/U (2) than the kimberlites (4), which is reflected in the $^{208}\text{Pb}/^{204}\text{Pb}$ ratio (fig 6.7). The present day nephelinite plots below the NHRL on the $^{208}\text{Pb}/^{204}\text{Pb}$ vs $^{206}\text{Pb}/^{204}\text{Pb}$, but above above it at 30Ma, because of the relatively rapid growth of ^{206}Pb .

Despite the problems of age correction, it appears that the nephelinite is derived from an asthenospheric source similar to Bouvet and the Gibeon kimberlites. The nephelinite does, however, have relatively high initial $^{207}\text{Pb}/^{204}\text{Pb}$, which as with the monticellite peridotite may indicate some crustal contamination. Overall, the trace element and isotope characteristics of the Schwarzeberg nephelinite provide strong evidence that the rock was produced by melting of of a source common to the Gibeon

Figure 6.11. Chondrite normalised trace element plot comparing the Schwarzeberg nephelinite (A44) with kimberlite (K35) and a primitive Bouvet basalt.



kimberlites, and similar to that of the Bouvet OIB source. This in turn is one of the clearest indications that kimberlites are linked to hotspot type magmatism.

6.4 The Grunau Province

A reconnaissance study was made on the alkaline igneous intrusions found in the Grunau area of southern Namibia (fig 2.1). The primary aim was to assess the possibility of any relationship between these rocks and the Gibeon kimberlite province. The Grunau province comprises 78 dykes and plugs, the majority of which appear to be olivine melilitites, although several (previously unrecognised) plagioclase bearing dykes of alkali basalt composition were found. All of the rocks sampled were found to have suffered moderate to severe calcite alteration, often so severe that the original mineralogy was obscured. These were unfortunately unsuitable for geochemical work, although several samples were analysed (see table 6.2).

The melilite bearing rocks consist of olivine phenocrysts, and partially resorbed clinopyroxene macrocrysts set in a groundmass of spinels, melilite, perovskite, apatite and possible monticellite. Some melilitites contained large fresh phlogopite macrocrysts (eg PK62) which could be used for radiometric dating. Typically, the groundmass minerals, and often the macrocrysts also, had been replaced by pervasive secondary calcite replacement.

Two dykes were found (PK48, PK55) of fine grained dolerite consisting of titanite and plagioclase laths with subordinate biotite, spinels and perovskite. No melilite was present in these samples. The rocks had suffered secondary calcite alteration of much of the groundmass.

Phlogopite separates from two melilitites were radiometrically dated (chapter 2) at about 520Ma using the $^{39}\text{Ar}/^{40}\text{Ar}$ technique. These rocks are therefore clearly unrelated to the Gibeon kimberlite province. At 520Ma, southern Namibia was experiencing regional metamorphism (the Pan-African event) following the closure of the 'proto-Atlantic' between South Africa and South America.

Further studies are required to assess the petrogenesis of this igneous province, though this may not be possible due to the poor preservation state of the rocks.

6.5 Conclusions

1) The Blue Hills monticellite-peridotite was produced by melting at shallower depths than the Gibeon kimberlites, in the dolomite stability field (80-110km). The degree of partial melting was higher, and occurred under higher CO_2 fugacity than melting to produce kimberlite.

2) The source region of the monticellite-peridotite is in the asthenosphere, and is geochemically and isotopically equivalent to the source of the Gibeon kimberlites, despite their age differences.

3) Monticellite peridotite is not produced by devolatilisation of a kimberlite magma.

4) Carbonatite is an independent mantle product, produced by incipient melting of a carbonated peridotite.

5) The source region of the Schwarzeberg nephelinite was produced by melting of an asthenospheric source material at depths of 50-80km, in a CO_2 rich environment. The degree of partial melting was higher than for kimberlite.

6) The source region of the nephelinite is geochemically and isotopically equivalent to the source of the Gibeon kimberlites.

7) The source of the Gibeon kimberlites and Schwarzeberg nephelinite can be temporally and spatially related to the hotspot presently related to the Vema seamount.

8) The Gibeon kimberlites and related parakimberlites all show non-Dupal type signatures.

9) The melilitites and dolerites of the Grunau province are unrelated to the Gibeon kimberlite province.

CHAPTER 7

SYNTHESIS

7.1 MANTLE SOURCE REGIONS

The isotopic and trace element composition of the Gibeon kimberlites, in common with other Group I kimberlites, is consistent with derivation from an asthenospheric source. Sr and Nd isotope ratios indicate a source which is slightly depleted relative to Bulk Earth. Pb isotope ratios indicate that the source had radiogenic Pb relative to the geochron, indicating a time integrated increase in U/Pb and Th/Pb ratios in the source, relative to an undifferentiated mantle.

Data from ocean floor and ocean island basalts reveal large variations in Nd, Sr and Pb isotopic ratios (Zindler and Hart 1986) which reflect complex evolution of mantle reservoirs. The Gibeon kimberlites show a very small range in isotopic character, suggesting derivation from a single source reservoir in the asthenosphere. This source shows great similarities to the source of the Bouvet island basalts. Group I kimberlites as a whole display a larger range in isotopic composition, though still restricted relative to the OIB range. This small compositional range evident in the literature could be due to a sampling bias towards South African kimberlites, but is likely to be real because the few North American kimberlites analysed display similar isotopic signatures.

Trace element ratio comparisons between kimberlite and OIB are difficult to assess because significant trace element fractionation occurs during the very small degree

partial melting which produces kimberlite. Trace element ratios are thus as much a function of degree of partial melting as of source characteristics. Further complications arise when certain trace elements are retained in the source by a residual phase (eg K and Rb in phlogopite). However, the La/Nb ratio appears to be relatively unaffected by these problems (see section 4.6.3) and is probably the best trace element ratio to use as a source rock indicator. The Gibeon kimberlites have the same La/Nb ratios (0.6-0.7) as Bouvet and other non-Dupal type OIB from the South Atlantic.

The Gibeon kimberlites cannot be temporally or spatially linked with the Bouvet hotspot, but do appear to coincide with the (unsampled) Vema hotspot trace. It is concluded that as the Bouvet OIB, the Gibeon kimberlites, and other southern African kimberlites (Smith 1983, Smith et al. 1985) have geochemically equivalent signatures, they must share a common widespread source. This source reservoir is isotopically distinct from the sources of MORB, Dupal-type OIB and the subcontinental lithosphere.

7.2

MELTING

The precise melting parameters for kimberlite petrogenesis are little understood. Experimental work by Brey (1978), Egglar (1978) and Wyllie (1977, 1979, 1980, 1986) has shown that kimberlites can be produced by partial melting of garnet lherzolite in the presence of CO₂, which exists in the solid state as magnesite. The presence of CO₂ at high CO₂/H₂O ratios both reduces the peridotite solidus temperature, and decreases the SiO₂ content of the melt, producing low SiO₂, high CO₂ melts (kimberlite).

The magnesite-dolomite reaction provides a minimum

depth constraint for kimberlite melting. Brey (1978) estimates that magnesite is stable on the peridotite solidus at depths in excess of 110km, which can be taken as the minimum depth for kimberlite production.

The Gibeon kimberlites, in common with other off-craton kimberlites do not carry diamonds. Boyd and Gurney (1986) ascribe the absence of diamond in off-craton kimberlites to generation at depths shallower than the diamond stability field (150km). If this is the correct explanation, the Gibeon kimberlites can be constrained to melting at depths between 110 and 150km.

Evidently, oxidised carbon in the form of carbonate is present in the asthenosphere. Elemental carbon, in the form of graphite or diamond is present in the lithosphere. A second possible explanation for the absence of diamond in the Gibeon kimberlites is that they were oxidised on ascent.

On-craton diamondiferous kimberlites however, must be derived from deeper, within the diamond stability field (>150km). Geothermobarometric studies on sheared nodules (Nixon and Boyd 1973, Nixon et al. 1981) and megacrysts (Harte and Gurney 1981) also indicate an origin from depths in excess of 150km.

The degree of partial melting cannot be constrained accurately because the relevant distribution coefficients are not available, nor is the exact composition of the source rock. Bulk distribution coefficients based on dry peridotite indicate less than 1% partial melting, but are not accurate indicators because they fail to take into account the effects of magnesite and hydrous phases such as phlogopite. If magnesite contains trace elements such as the REE, Sr and Ba, preferential melting of this phase could enhance the concentration of these elements in the melt. The presence of CO₂ also affects the stability fields of other minerals in the source (eg Eggler and

Wendlandt 1979), and thus influences the relative proportions in which they enter the melt.

Qualitative estimates of relative degree of partial melting may be obtained by comparing, for example, REE patterns of different rocks, but quantitative estimates are not yet possible. It is not considered necessary to invoke metasomatised mantle as a source rock to produce the extreme levels of REE enrichment found in kimberlites.

The REE contents of the Gibeon kimberlites show very little variation, indicating that they were all produced under very similar melting conditions. Comparison with other kimberlites (chapter 4) shows that the Gibeon kimberlites have amongst the highest LREE enrichment indicating relatively low degrees of partial melting.

7.3

ASCENT

When the kimberlite melt separates from its source rocks at the base of the lithosphere, it ascends rapidly to the surface in a matter of hours or days (McCallister et al 1979, Spera 1984). On ascending to the surface, the bulk chemical composition of the kimberlite can be modified by several processes: 1) Entrainment of mantle xenoliths and xenocrysts, 2) Fractional crystallisation, 3) Crustal contamination and 4) Assimilation of enriched subcontinental lithosphere.

Xenolith entrainment is common in kimberlites, but careful sampling can avoid xenoliths. Avoiding disaggregated xenoliths and xenocrysts is more difficult, and almost any kimberlite sample is likely to contain at least some xenocrysts. Moore (1988), however, argued that most olivine macrocrysts are phenocrysts not xenocrysts, so the effect of xenocrysts on the bulk composition is likely to be small. The effect on trace element

composition is even less.

Chapter 4 argues that fractionation is a process of minor importance during ascent, and the magma reaching the crust is very primitive. Olivine fractionation may occur, but will have little effect on the trace element composition of the magma. Crustal contamination is an ever present feature of kimberlite emplacement. Careful sampling can be concentrated on areas of minimal contamination. Because the emplacement temperatures are relatively low, crustal xenoliths tend not to be melted, so the extent of contamination can generally be judged in hand specimen. Small degrees of crustal contamination generally have little effect on the trace element composition of the kimberlite.

Assimilation of subcontinental lithosphere is a potential source of trace element enrichment. It was shown in chapter 4 that most of the Gibeon kimberlites show no evidence of lithospheric interaction, and that their isotopic and trace element signatures show little variation, and are characteristic of their asthenospheric source regions. However, kimberlite 33/K2 has assimilated time integrated trace element enriched lithosphere. Relative to the other kimberlites, K2 has increased Pb, Rb, Ba, K, Sr, P, K/Ti, Rb/Sr and Rb/Ba. This style of enrichment has been identified elsewhere (Hawkesworth et al. 1984) as a result of metasomatism by hydrous fluids. The relatively high $^{87}\text{Sr}/^{86}\text{Sr}$ ratio in 33/K2 indicates that this component is older than the kimberlite. The data are consistent with assimilation of PKP-type enriched subcontinental lithosphere.

Comparison with data from other kimberlites, using kimberlite normalised trace element plots, shows that lithospheric assimilation is not uncommon, and is one of the causes of the considerable variations in trace element compositions of kimberlite. Lithospheric assimilation can

thus mask the original asthenospheric source rock signature in kimberlites.

It is concluded that in the Gibeon kimberlites, the effects of fractionation, xenolith entrainment and crustal contamination on the whole rock composition are minimal for good samples, but lithospheric assimilation may be an important modifier.

7.4

GROUP I - GROUP II

The Gibeon kimberlites fall within the group I category of Smith (1983). Smith et al. (1985) further subdivide group I into IA (on-craton) and IB (off-craton), on chemical grounds. The Gibeon kimberlites tend to fall into group IA chemically (low Si, Pb, high Ca, Fe, Ti, K/Ti, although their REE, Ba and Sr concentrations are as high as group II kimberlites) but are located off-craton, and therefore do not support the IA/IB classification.

Kimberlite 33/K2 has trace element features which are very similar to those of group II kimberlites, especially Finsch. It appears that K2 is a mixture between an asthenospheric 'Gibeon kimberlite' component and an enriched lithospheric component. Group II kimberlites are dominated by the lithospheric component. It is not clear whether group II kimberlites are derived 1) entirely from lithospheric source rocks, or 2) from an asthenospheric melt which has interacted with metasomatised lithosphere to such an extent that its trace element and isotopic signatures are dominated by the lithospheric component.

If the latter hypothesis is correct, it would be expected that a continuous spectrum would exist from asthenospheric dominated kimberlites (eg K35) to lithospheric dominated (eg Finsch). It would appear however, that kimberlites so far examined fall into either

group I or group II, and that the two groups require separate origins. K2 is an exception as it displays features of mixing, and it is argued in chapter 4 that lithospheric assimilation can be detected in other kimberlites (eg Monastery). Accordingly, it is anticipated that future studies will discover kimberlites that are chemically and isotopically intermediate between Smith's (1983) group I and II kimberlites.

If group I and II kimberlites are derived from the asthenosphere and lithosphere respectively, as suggested by Smith (1983), separate petrogenetic origins must be invoked - group I kimberlites derived by decompression melting of a rising plume, and group II kimberlites by melting of cold, static lithosphere by an unknown heat source. Nixon (1987) proposed that this could be accommodated by the rising (group I) diapir providing heat to melt the lithosphere. However, it seems improbable that the diapir could provide enough heat to melt the colder, more refractory lithosphere, without itself melting at the same time.

The hypothesis introduced in chapter 4, suggesting that both group I and II kimberlites originated ultimately in the asthenosphere, provides a simpler more unified explanation of their origin. Also, as pointed out in chapter 4, group II kimberlites are restricted in time (114-200Ma) and space (Southern Africa) and may represent a special case, due to abnormal tectonothermal conditions in the mantle. Notably, group II kimberlites were emplaced during the period of the Karoo (120-190Ma) magmatic episode.

In conclusion, the origins of the group I - group II variations are not clear. The hypothesis preferred here is that group I kimberlites are derived directly from melting of an asthenospheric diapir, whereas group II kimberlites have assimilated significant amounts of trace element

enriched lithosphere on their ascent from their ultimately asthenospheric source. The composition of the group II kimberlite will then depend on the composition of the asthenospheric source, the nature of the enriched component, and the relative proportions of each component. In the case of K2 and Finsch, the enriched lithosphere appears to have undergone PKP type metasomatism. The scarcity of megacrysts in group II kimberlites, however, is not readily explained by this hypothesis, and remains an outstanding problem.

7.5 ASSOCIATED ROCKS

The association of kimberlites with nephelinites, melilitites and carbonatites has been explained (chapter 6) in terms of a common process (melting of a rising asthenospheric diapir) operating under different parameters (P,T, volatile composition). The relationship is not genetic (derivation by fractionation or devolatilisation).

The geochemical and isotopic similarities of the Gibeon kimberlites, the Blue Hills monticellite peridotite and the Schwarzeberg nephelinite indicate their origin in chemically equivalent source rocks. The difference in their major element composition can be explained mainly in their depth of origin. Kimberlites are produced by melting in the magnesite stability field (>110km), monticellite peridotite and melilitite in the dolomite stability field (80-110km), and nephelinite, shallower, in the CO₂ stability field (<80km). Carbonatites are produced by incipient melting at depths greater than 80km. These rock types are derivatives of asthenospheric melting. The constant cSr and cNd of the rocks investigated is not only evidence of a similar source material, but also shows that

the compositions of K35, K39 and K53 are characteristic of their source rock and have not undergone lithospheric interaction.

7.6

HOTSPOTS

The kimberlites and associated rocks studied in this work can be related in time and space to hotspots now active in the South Atlantic. It is envisaged here that two hotspot traces moved across southern Namibia. The first coincides with the Blue Hills intrusion, and the second with the Gibeon kimberlites, the Schwarzeberg nephelinite and the Vema seamount.

As the diapir rises, partial melting begins. The higher the diapir rises, the more it melts. The diapir is arrested as it reaches the base of the lithosphere, and the melt either erupts to the surface or crystallises in the mantle. The composition of the melt is therefore related to the thickness of the lithosphere. In the thick centre of the continent, kimberlites are produced, in the shallower margins, nephelinites and melilitites occur. When the hotspot moves into an oceanic environment, the diapir can rise to shallow depths, melting to form alkali basalts which form ocean islands.

In this way, kimberlites, nephelinites and OIB can share common source regions, and a common origin in terms of mantle dynamics. Their differences can then be explained in terms of different melting parameters, principally depth.

A problem arises with this hypothesis: The Blue Hills monticellite peridotite has a non-Dupal signature similar to the kimberlites, whereas the present day Discovery basalts display Dupal type enrichment. This implies either that the monticellite peridotite is unrelated to

Discovery, or else Discovery developed its Dupal signature at a later point. This observation supports the suggestion by Hawkesworth et al. (1986) that the Dupal anomaly is a shallow feature in the oceanic lithosphere. According to Hawkesworth et al. (1986), during the opening of the Atlantic, subcontinental lithosphere was delaminated from the continent and stretched out across the developing ocean basin. Ocean island basalts erupting through this enriched lithosphere could then be contaminated, to develop their enriched characteristics.

This is further supported by the fact that the Gibeon kimberlites are in the area delineated by Hart (1984) as the Dupal zone, despite the fact that they themselves are non-Dupal in character. The Gibeon kimberlites are certainly derived from depths in excess of 110km, whereas alkali basalts are produced at less than 50km.

The implications for the Dupal anomaly are either, 1) it is a shallow feature (Hawkesworth et al. 1986) which contaminates the OIB on ascent, or 2) the Dupal zone is located further north than the Gibeon kimberlites in Namibia, or 3) the Dupal zone is not continuous around the southern hemisphere.

Study of the nephelinite and monticellite peridotite has shown that they have extremely high u -values. The origin of the U/Pb fractionation is not clear, but two possibilities are 1) retention of Pb in K-richterite as a residual phase during melting, or 2) early fractionation/segregation of Pb sulphides. It is speculated that high U/Pb magmas such as the nephelinite, if arrested at some point in the lithosphere, could produce domains in the mantle with high u -values. Delamination of such high- u domains into the asthenosphere could then be a possible source of the HIMU (St Helena) end member of Zindler and Hart (1986).

It is concluded that the Gibeon kimberlites and

associated alkaline rocks can be related to present day mantle hotspots. However, there is no obvious connection between most South African kimberlites and any hotspots active today. This does not preclude their derivation from a rising mantle diapir (because a hot spot active 90ma ago need not be active today, or may not have been identified), but does present an unresolved problem.

7.7

MEGACRYSTS

The results of this study show that megacrysts are xenocrysts carried in the kimberlite host. They appear to have fractionated from an asthenospheric magma which was both crystallising the megacrysts, and assimilating lithospheric wallrock (essentially an AFC process). The parental magma was isotopically depleted relative to the kimberlites and Bulk Earth, but became more enriched as the magma evolved. The patterns of isotopic enrichment are parallel to those seen in kimberlite K2. It is not possible to clearly identify the geochemical characteristics of the source rocks, but appears to have been OIB-like isotopically, although there is evidence to suggest that the magma was broadly kimberlitic in composition. The megacrysts have apparently similar ages to the host kimberlites which may indicate that they are related to the same igneous event in a broad sense. They are not, however, directly genetically related to the kimberlite magma.

The isotopic constraints presented in chapter 5 can be accommodated by the models of Wyllie (1986), Eggler et al.(1979) and Harte and Gurney (1981). In Wyllie's model, the asthenospheric melt parental to the megacrysts is totally unrelated to the kimberlite. In this way the isotopic differences between the two magma types are

readily explained. In the models of Harte and Gurney (1981) and Eggler et al. (1979), the megacrysts are the crystallisation products of peripheral melts from the same diapir as that from which the kimberlite subsequently forms. The kimberlite, and the melt parental to the megacrysts, however, have different isotopic signatures. The megacryst melt is more depleted than the kimberlite. This implies that either (1) the plume is capable of generating two isotopically distinct melts, or (2) the peripheral parts of the diapir have interacted with depleted MORB-type mantle on ascent through the asthenosphere. Both the megacryst melt and the kimberlite may subsequently assimilate enriched subcontinental lithosphere

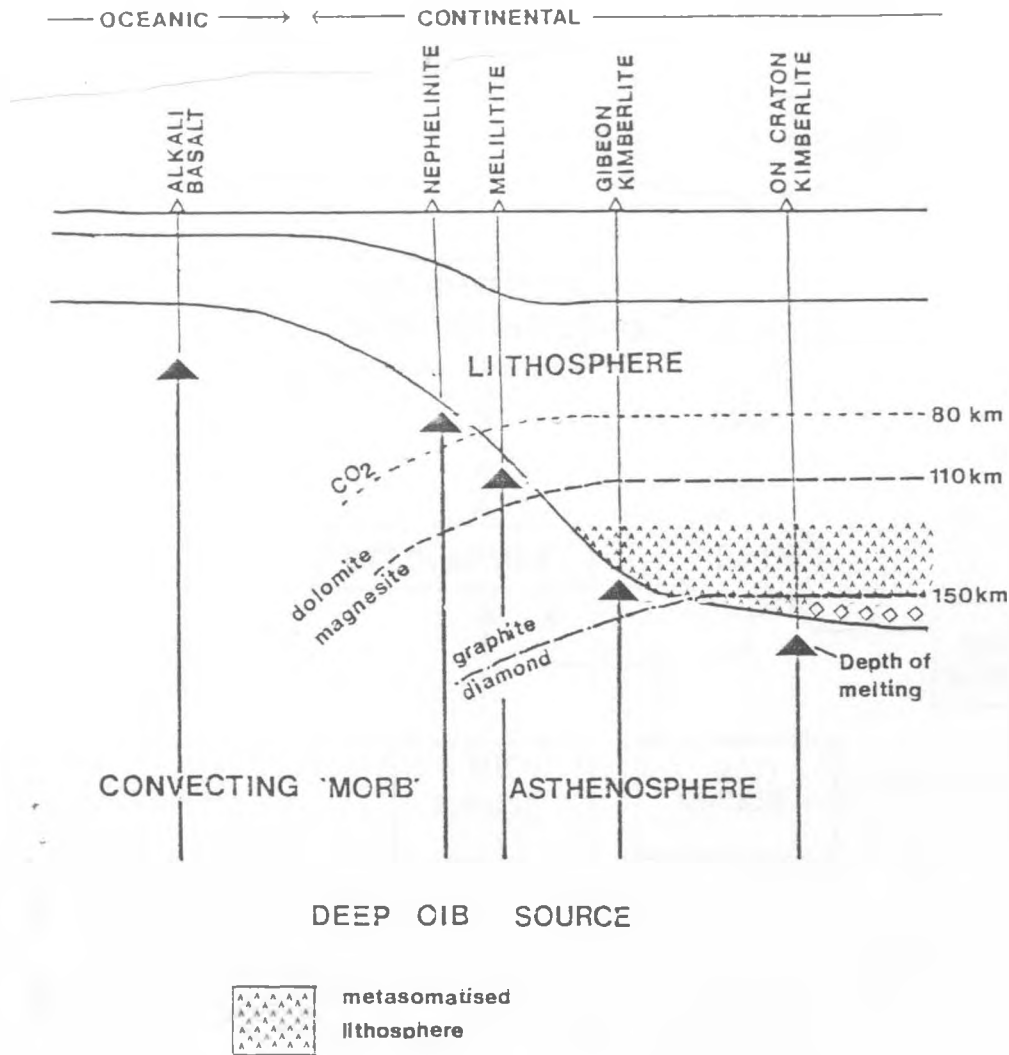


Figure 7.1. Schematic diagram showing the relationship between kimberlite and other magma types. It is envisaged that the source of the magmas is a deep OIB-type mantle plume which results in hotspot magmatism. As the source rock rises, melting begins. Melting continues until the plume/diapir reaches the base of the lithosphere, when the magma either slowly crystallises or erupts to the surface. The resultant magma type that reaches the surface depends heavily upon the depth to the base of lithosphere, as this is the point at which melting ceases and eruption begins.

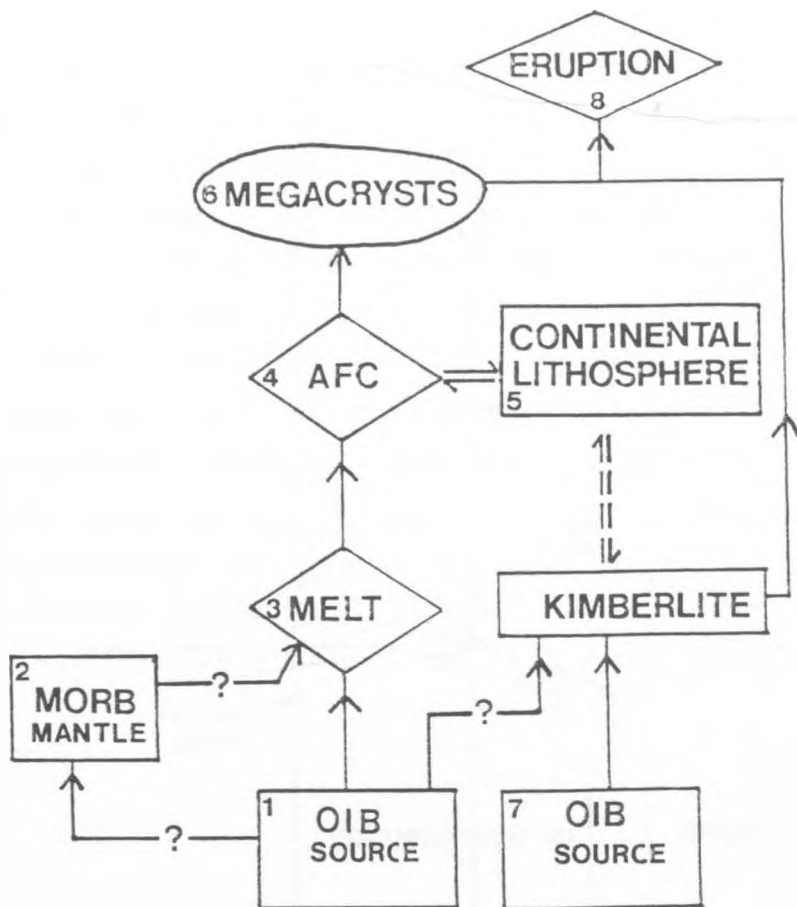


Figure 7.2. Flow diagram representing the possible sequences of events involved in megacryst formation. The megacrysts are ultimately derived from an asthenospheric source (1), which may possibly interact with the surrounding MORB-like mantle (2) during ascent and melting (3). The melt crystallises, (4) while assimilating lithospheric wallrocks (5), to produce megacrysts (6). The kimberlite, either derived from a separate mantle diapir (7) (Wyllie) or from the same diapir (1) (Harte and Gurney), erupts to the surface, entraining megacrysts en route. The kimberlite may also assimilate trace element enriched lithosphere on ascent.

REFERENCES

- Alibert C, Michard A, and Albarede F. 1983. The transition from alkali basalts to Kimberlites :isotope and trace element evidence from melilitites. Contrib min.and pet. 82 . 176-186.
- Allegre CJ, Hamelin B, Provost A, and Dupre B. 1986. Topology in isotope multispace and origin of mantle chemical heterogeneities. E.P.S.L. 81. 319-337.
- Allegre CJ, Shimizu N and Rousseau D. 1982. The History of the continental lithosphere recorded by ultramafic xenoliths. Nature.296. 732-735.
- Allegre CJ and Turcotte DL. 1985. Geodynamic mixing in the mesosphere boundary layer and the origin of oceanic islands. Geophys. Res. Lett. 12 207-210
- Allsopp HL and Barrett DR. 1975 . Rb-Sr age determinations on South African kimberlite pipes. Phys. Chem. Earth. 9. 605-617
- Allsopp HL and Kramers JD. 1977. Rb-Sr and U-Pb age determinations on South African kimberlite pipes. 2nd Int. Conf. Kimb., Santa Fe , Abstr. unpagued.
- Allsop HL, Smith CB, Bristow JW, Brown R, Kramers JD and Garvie OG. 1986. A review of radiometric dating methods applicable to kimberlites and related rocks. 4IKC Abstracts.
- Anderson DL 1984. Kimberlites and the evolution of the mantle. In:Kimberlites I. Kornprobst ed. Elsevier. 395-403.
- Aoki A. 1974. Phlogopite and potassic richterite from mica nodules in South African kimberlites. Contrib. min. and pet.48. 1-7
- Aoki A. 1975. Origin of phlogopite and potassic richterite-bearing peridotite xenoliths from South Africa. Contrib. Min. and Pet. 53 145-156.
- Apter DB, Harper FJ, Wyatt BA and Scott-Smith BH. 1984. The geology of the Mayen g kimberlite sill complex, South Africa. TIKC 1. 43-57.
- Arima M, Barnett RL and Kerrich R. 1986. Chemical and textural variations of mica in the Nickila Lake and Upper Canada Mine kimberlites, Ontario, Canada. 4IKC abstracts.

- Bailey DK. 1982. Mantle metasomatism-continuing change within the earth. *Nature*. 296. 525-530
- Ballard S, Pollack HN and Skinner NJ. 1987. Terrestrial heat flow in Botswana and Namibia. *J.G.R.* 92. 6291-6300
- Barrett DR. 1975. The genesis of kimberlite and related rocks, Sr isotope evidence. *Phys. Chem. Earth* 9. 637-653
- Barrett DR and Berg GW. 1975. Complementary petrographic and Sr isotope ratio studies of South African kimberlites. *Phys. Chem. Earth* 9. 619-636
- Basaltic Volcanism Study Project. 1981. Basaltic volcanism on the terrestrial planets. Pergamon Press. New York.
- Basu AR and Murthy VR. 1977. Kaersutites, sub-oceanic low velocity zone and the origin of mid ocean ridges. *Geology* 5. 365-368.
- Basu AR and Tatsumoto M. 1979. Samarium and Neodymium systematics in kimberlites and in the minerals of garnet lherzolite inclusions. *Science*. 205 398-401.
- Basu AR and Tatsumoto M. 1980. Nd isotopes in selected mantle derived rocks and minerals, and their implication for mantle evolution. *Contrib. Min. and Pet.* 75 43-54.
- Basu AR and Tatsumoto M. 1982. Nd isotopes in kimberlites and mantle evolution. *Contrib. Min. and Pet.*
- Boctor NZ and Boyd FR. 1980. Ilmenite nodules and associated sulphides in kimberlite from Yakutia, USSR. *Carnegie Inst. Washington Yearbook*. 79 302-304
- Boctor NZ and Meyer HOA. 1979. Oxide and sulphide minerals in kimberlite from Green Mountain, Colorado. In: Boyd and Meyer 1979, 217-228.
- Boettcher AL, O'Neil JR, Windom JE, Stewart DC and Wilshire HG. 1979. Metasomatism of the upper mantle and genesis of kimberlite and other volcanics. In: Boyd and Meyer 1979, 173-182.
- Bosch JL. 1971. The petrography of some kimberlite occurrences in the Barkly West District, Cape Province. *Trans. Geol. Soc. S. Af.* 74 75-101.
- Boyd FR. 1973. A pyroxene geotherm. *Geochim et Cosmochim. Acta.* 37-3 2533-2546.
- Boyd FR and Danchin RV. 1980. Lherzolites and kimberlites

- from some kimberlites of Angola. Am J. Sci. 280A. 528-549.
- Boyd FR and Gurney JJ. 1986. Diamonds and the African lithosphere. Science 232 472-477.
- Boyd FR, Gurney JJ, and Richardson SH. 1985. Evidence of 150 - 200 km thick lithosphere from diamond inclusion thermobarometry. Nature 315. 387
- Boyd FR and McCallister RH. 1976. Densities of fertile and sterile garnet peridotites. Geophys Res. Lett. 3 . 509-512.
- Boyd FR and Mertzman. Composition and structure of the Kaapvaal lithosphere. In: magmatic processes, Geochemical Soc. spec. publ.no.1.
- Boyd FR and Nixon PH. 1973. Structure of the upper mantle beneath Lesotho. Ann. Rep. Geophys. Lab. Washington 72 . 431-446
- Boyd FR and Nixon PH. 1975. Origins of the ultramafic nodules of some kimberlites in Northern Lesotho, and the monastery mine, S. Africa. Phys. Chem. Earth. 9 431-454
- Boyd FR and Nixon PH. 1978. Ultramafic xenoliths from the Kimberley pipes, S. Africa. Geochim. et Cosmochim. Acta. 42. 1367-1382.
- Boyd FR and Nixon PH. 1979. Discrete nodules from the kimberlites of East Griqualand, S. Africa. Ann Rep. Geophys. Lab. Washington. 79. 276-301
- Boyd FR, Jones RA, and Nixon PH. 1983. Mantle metasomatism: the kimberley dunites. Ann. Rep. Dir. Geophys. Lab. Washington. Carnegie Institution Ybk 82. 330-336
- Boyd FR, Dawson JB, and Smith JV. 1984. Granny Smith diopside megacrysts from the kimberlites of the Kimberley area and Jagersfontein, S. Africa. Geochim. et Cosmochim. Acta. 48. 381-384
- Brevart O, Dupre B and Allegre CJ. 1986. Lead-lead age of komatiite lavas and limitations on the structure and evolution of the Precambrian mantle. E.P.S.L. 77. 293-302.
- Brey G. 1978. Origin of olivine melilitites- chemical and experimental constraints. J. Volcanol. Geotherm. Res. 3 61-88.
- Brey G, Brice WR, Green DH, Harris KL and Ryabchikov ID.

1983. Pyroxenecarbonate reaction in the upper mantle. E.P.S.L. 62 63-74.
- Brey G and Green DH. 1975. The role of CO₂ in the genesis of olivine melilitite. Contrib. min. and pet. 49 93-103
- Briden JC, Rex DC, Faller AM and Tomblin JF. 1979. K-Ar geochronology and palaeomagnetism of volcanic rocks in the Lesser Antilles island arc. Phil Trans Roy Soc Lond. 291. 485-528.
- Bristow JW, Smith CB, ALLsop HL, Shee SR and Skinner EMW. 1986. Setting, geochronology and geochemical characteristics of 1600Ma kimberlites and related rocks from Kuruman Province, South Africa. 3IKC Abstracts.
- Carswell DA. 1975. Primary and secondary phlogopite and clinopyroxene in garnet lherzolite xenoliths. Phys. Chem. Earth. 9 417-430.
- Chase CG. 1981. Oceanic Island Pb: two stage histories and mantle evolution. E.P.S.L. 52 277-284.
- Clement CR. 1975. The emplacement of some diatreme facies kimberlites. Phys. Chem. Earth 9 51-59.
- Clement CR. 1979. The origin and infilling of kimberlite pipes. In kimberlite Symposium II, Cambridge (extended abstracts) pp 71-73.
- Clement CR. 1982. A comparative geological study of some major kimberlite pipes in the Northern Cape and Orange Free State. Ph.D. Thesis, Univ Cape Town.
- Clement CR and Skinner EMW. A textural-genetic classification of kimberlites. 1985. Trans. Geol. Soc. S. Africa. 88 403-409 Clement CR, Skinner EMW and Scott Smith BH 1984. Kimberlite redefined. J.Geol. 32 223-228.
- Clifford TN 1970. The structural framework of Africa. in: African magmatism and tectonics. Clifford and Gass, Eds. Oliver and Boyd. London.
- Cohen RS and O'Nions RK. 1982b. Identification of recycled continental material in the mantle from Sr, Nd and Pb isotope investigations. E.P.S.L. 61 73.
- Cohen RS, O'Nions RK, and Dawson JB. 1984. Isotope geochemistry of xenoliths from East Africa: Implications for development of mantle reservoirs and their interaction. E.P.S.L. 68. 209
- Cox KG. 1978. Flood basalts, subduction and the break-up of

- Gondwanaland. Nature. 274 47-49
- Cox KG. 1983. The Karoo province of Southern Africa: origin of trace element enrichment patterns. 139-157. In: Continental volcanics and mantle xenoliths. Eds.: Hawkesworth CJ and Norry MJ. Shiva Press.
- Cox KG and Hawkesworth CJ. 1984. Relative contribution of crust and mantle to flood basalt magmatism in the Deccan Traps. Phil. Trans Roy. Soc. A310 627-641
- Crough ST, Morgan WJ and Hargraves RB. 1980. Kimberlites: their relationship to mantle hotspots. E.P.S.L. 50 260-274
- Davis GL. 1976. The ages of zircons from kimberlites from South Africa. Carnegie institute of Washington yearbook 75. 821
- Davis GL. 1977. The ages and Uranium content of zircons from kimberlites and associated. Ext. Abs. 2nd Kim. Conf. Arizona.
- Davis GL. 1978. Zircons from the mantle. Carnegie Institute of Washington yearbook 77. 895
- Dawson JB. 1980. Kimberlites and their xenoliths. Springer Verlag, New York.
- Dawson JB and Hawthorne JB. 1973. Magmatic sedimentation and carbonatitic differentiation in kimberlite sills at Benfontein, South Africa. J. Geol. Soc. London 129 61-85
- Dawson B. 1987. The MARID suite of xenoliths in kimberlite: relationship to veined and metasomatised peridotite xenoliths. in Mantle Xenoliths, PH Nixon Ed.
- Dawson JB and Smith JV. 1975. Chemistry and origin of phlogopite megacrysts in kimberlite. Nature 253 336-338
- Dawson JB, Smith JV and Hervig RL. 1977. Late stage diopside in kimberlite groundmass. N. Jahrbuch Min. Monatshefte 1977. 529
- Dawson JB, Smith JV and Hervig RL. 1980. Heterogeneity in upper mantle lherzolites and harzburgites. Phil. Trans. Roy. Soc. Lond. A297, 323-331.
- Delaney JS, Smith JV, Carswell DA and Dawson JB. 1980. Chemistry of micas from kimberlites and xenoliths - I: micaceous kimberlites. Geochem. et Cosmochim. Acta 44 857-872.

- DePaulo DJ and Wasserburg GJ. 1976. Nd isotopic variations and petrogenetic models. *Geophys. Res. Lett.* 3 249-252.
- Dickin AP. 1987. Cerium isotope geochemistry of OIBs. *Nature* 326 283.
- Edgar AD, Arima M, Baldwin DK, Bell DR, Shee SR, Skinner EMW and Walker EC. 1986 High pressure melting experiments on an aphanitic kimberlite from the Wesselton mine, Kimberley, South Africa. *4IKC*. 170-172.
- Eggler DH. 1978. The effect of CO₂ upon partial melting of peridotite. *American Journal of Science*. 278 305-343
- Eggler DH, McCullum ME and Smith CB. 1979. Megacryst assemblages in kimberlite from Northern Colorado and Southern Wyoming: Petrology, Geothermometrybarometry and areal distribution. *2IKC* 213-226
- Eggler DH and Wendlandt RF. 1979. Experimental studies on the relationship between kimberlite magmas and partial melting of peridotite. *2 IKC* 2, 313-226.
- Erlank AJ, Marsh JS, Miller RA, Hawkesworth CJ, Betton PJ and Rex DC. 1984. Geochemistry and petrogenesis of Etendeka volcanic rocks from S.W.A. *Spec. Pub. Geol. Soc. S. Afr.* 13. 195.
- Erlank AJ, Waters FG, Haggerty SE and Hawkesworth CJ. 1986. Characterisation of metasomatic processes in peridotite nodules contained in kimberlite. *4IKC*. 232-235.
- Erlank AJ, Waters FG, Hawkesworth CJ, Haggerty SE, Allsop HL, Rickard RS and Menzies M. 1987. Evidence for mantle metasomatism in peridotite nodules from the Kimberley pipes, South Africa. In *Mantle Metasomatism*. Eds Menzies and Hawkesworth, Academic Press . p221-311.
- Fairhead JD and Henderson NB. 1977. The seismicity of Southern Africa. *Tectonophysics* 41. T19-26.
- Fairhead JD and Reeves CV. 1976. Teleseismic delay times, Bouguer anomalies and inferred thickness of the African lithosphere. *E.P.S.L.* 36. 63-76.
- Faure G. 1977. Principles of isotope geology. Wiley, New York. 464pp.
- Ferguson J, Martin H, Nicolaysen LO and Danchin RV. 1975. Gross Brukkaros: A kimberlite-carbonatite volcano. *Phys. Chem. Earth.* 9 219
- Fesq HW, Kable EJD, Gurney JJ. 1975. Aspects of the

- geochemistry of kimberlite from Premier mine and other South African occurrences with particular reference to the Rare Earth elements. *Phys. Chem. Earth.* 9 686-707
- Fischer DE, Joensuu O and Bostrom K. 1969. Elemental abundances in ultramafic rock and their relation to the upper mantle. *J.G.R.* 74 3865-3873
- Foley SF, Venturelli G, Green DH, and Toscani L. 1987. The Ultrapotassic rocks: characteristics, classification and constraints for petrogenetic models. *Earth Sci. Rev.* 24. 81
- Frankel JJ. 1956. An inclusion bearing olivine melilitite from Mukorob, South West Africa. *Trans. Roy. Soc. S. Afr.* 35(2) 115-123.
- Fraser KJ. 1987. Petrogenesis of kimberlites from South Africa and Lamproites from Western Australia and North America. PhD. Thesis. Open University.
- Fraser KJ, Hawkesworth CJ, Erlank AJ, Mitchell RH, and Scott-Smith BH. 1985. Sr, Nd and Pb isotopes and trace elements of lamproites and kimberlites. *E.P.S.L.* 76. 57
- Frey FA, Roden MF, and Zindler A. 1980. Constraints on mantle source composition imposed by Phosphorus and the Rare Earth Elements. *Contrib. Min. & Pet.* 75 165-173.
- Galer S and O'Nions RK. 1985. Residue time of Th, U and Pb in the mantle with implications for mantle convection. *Nature* 316. 778
- Gaspar JC and Wyllie PJ. 1982. Barium phlogopite from the Jacupiranga carbonatite, Brazil. *Amm. Mineral.* 67. 997-1000
- Gromet LP, Dymek RF, Haskin LA and Korotev RL. 1984. The north American shale composite: its compilation major and trace element characteristics. *Geochim. and Cosmochim. Acta.* 48. 2469
- Haggerty SE. 1983. The mineral chemistry of new titanates from the Jagersfontein kimberlite, S. Africa: implications for metasomatism in the upper mantle. *Geochim. et Cosmochim. Acta.* 47. 1833-1854.
- Haggerty SE, Hardie RB and McMahon RM. 1979. The mineral chemistry of ilmenite nodule associations from the monastery diatrema. *2nd Int. Kim. Conf.* 2. 249-256.
- Hariya Y and Terada S. 1972. Stability of richterite tremolite solid solution at high pressures and possible

presence of sodium calcic amphibole under upper mantle conditions. E.P.S.L. 18 72-75.

Hart SR. 1984. A large scale isotopic anomaly in the Southern hemisphere mantle. Nature 309. 753

Hart SR and Brooks C. 1980. Sources of terrestrial basalts: an isotopic view point. In: Basaltic volcanism of the terrestrial planets. ch7

Harte B. 1983. Mantle peridotites and processes - the kimberlite sample. in continental basalts and mantle xenoliths. In Hawkesworth and Norry Eds p46-91 Shiva publishing, Cheshire.

Harte B and Gurney JJ. 1981. The mode of formation of Cr poor megacryst suites from kimberlites. Journal of Geology 89 749-753.

Harte B, Jackson, and MacIntyre. 1981. Age of mineral equilibria in granulite facies nodules from kimberlites. Nature. 291. 147.

Hartnady CJM and LeRoex AP. 1985. Southern Ocean hotspot tracks and the Cenozoic absolute motion of the African, Antarctic and South American plates. E.P.S.L. 75 245-257.

Hawkesworth CJ, Fraser KJ and Rogers NW. 1986. Kimberlites and lamproites: extreme products of mantle enrichment processes. Trans. Geol. Soc. S. Afr. Karoo Vol

Hawkesworth CJ, Mantovani MSM, Taylor PN and Palacz Z. 1986. Evidence from the Parana of S. Brazil for a continental contribution to Dupal basalts. Nature 322. 256

Hawkesworth CJ and Menzies MA. 1983. Kimberlites revisited. Nature 302.

Hawkesworth CJ, Norry MJ, Roddick JC and Vollmer R. 1979. Nd and Sr ratios from the Azores and their significance in LIL element enriched mantle. Nature 280. 28-31

Hawkesworth CJ, Rogers NW, Van Calsteren PWC, and Menzies MA. 1984 Mantle enrichment processes. Nature 311 331

Hawkesworth CJ, VanCalsteren P, Rogers NW and Menzies MA. 1987. Isotope variations in recent volcanics: A trace element perspective. In: Mantle metasomatism. Eds Menzies and Hawkesworth, Academic Press. 365-388.

Hawthorne JB. 1975. Model of a kimberlite pipe. Phys. Chem. Earth. 9 1-15

- Henderson P. 1982. Inorganic Geochemistry. Pergammon Press.
- Higuchi H and Nagasawa H. 1969. E.P.S.L. 7 281-287.
- Hoffman AW, Jochum KP, Seufert M and White WM. 1986. Nd and Pb in oceanic basalts- new constraints in mantle evolution. E.P.S.L. 79. 33
- Hops JJ, Gurney JJ and Harte B. 1986. Megacrysts and deformed nodules from the Jagersfontein kimberlite pipe. 4IKC. abstracts. 256-258.
- Huppert HE, Sparks RSJ, Turner JS and Arndt NT. 1984. Emplacement and cooling of komatiite lavas. Nature 309. 19-22
- Ilupin IP and Lutz BG. 1971. The chemical composition of kimberlite and questions on the origin of kimberlite magmas. Sovietskaya Geol 6, 61-73
- Irifune T, Sekine T, Ringwood AE and Hibberson WO. 1986. The eclogitegarnetite transformation at high pressure and some geophysical implications. E.P.S.L. 77. 245-256.
- Irving . 1986. Polybaric magma mixing in alkalic basalts and kimberlites: evidence from corundum, zircon and ilmenite megacrysts. 4IKC abstracts 262-264
- Irving AJ and Frey FA. 1984. Trace element abundances in megacrysts and their host basalts: constraints on partition coefficients and megacryst genesis. Geochim. Cosmochim Acta. 48. 1201-1221.
- Jacobson SB and Wasserburg GJ. 1980. Sm-Nd isotopic evolution of chondrites. E.P.S.L. 50. 139
- Janse AJA. 1964. Kimberlites and related rocks of the Nama plateau SWA. PhD. thesis. Univ. Leeds.
- Janse AJA. 1969. Gross Brukkaros, a probable carbonatite volcano in the Nama plateau of SWA. Geol. Soc. Am. Bull. 83. 573-586.
- Janse AJA. 1971. Monticellite bearing porphyritic peridotite from Gross Brukkaros SWA. Trans. Geol. Soc. S. Afr. 74. 45-55.
- Janse AJA. 1975. Kimberlites and related rocks from the Nama plateau of SWA. Phys. Chem. Earth 9. 81-94.
- Jensen B. 1973. Patterns of trace element partitioning. Geochim. et Cosmochim Acta. 37. 2227-2242.
- Jones MQW. 1981. Heatflow and heat production studies in the

Namaqua mobile belt and Kaapvall Craton. Ph.D. thesis, University of the Witwatersrand, Johannesburg, South Africa.

- Jones MQW. 1987. Heat flow and heat production in the Namaqua mobile belt, South Africa. J.G.R. 92 B7 6273-6289.
- Jones RA. 1984. Geochemical and isotopic studies of some kimberlites and included ultrabasic xenoliths from South Africa. PhD thesis, Univ Leeds.
- Jones RA. 1987. Sr and Nd isotopic and rare earth element evidence for the genesis of megacrysts in kimberlites of southern Africa. In Nixon 87.
- Kramers JD. 1977. Pb and Sr isotopes in Cretaceous kimberlites and mantle derived xenoliths from Southern Africa. E.P.S.L. 34.
- Kramers JD. 1979. Pb,U,Sr,K,Rb in inclusion bearing diamonds and mantle derived xenoliths from R.S.A. E.P.S.L. 42. 58
- Kramers JD, Roddick JCM, and Dawson JB. 1983. Trace element and isotopic studies on veined, metasomatic and MARID suite xenoliths from Bultfontein S. Africa. E.P.S.L. 65. 90
Kramers JD, Smith JV, Lock N, Harmons R and Boyd FR. 1981. Can kimberlites be generated from an ordinary mantle? Nature 291. 53
- Kroner A. 1973. Comments on "Is the African Plate stationary?" Nature 243 29-30
- Langmuir CH, Bender JF, Bence AE, Hanson GN and Taylor SR. 1977. Petrogenesis of basalts from the FAMOUS area: mid Atlantic ridge. E.P.S.L. 36 133-156
- Langmuir CH, Vocke RD, Hanson GN and Hart SR. 1978. A general mixing equation with applications to Icelandic basalts. E.P.S.L. 37. 380.
- Lasaga AC. Multicomponent exchange and diffusion in silicates. G.C.A. 43. 455.
- LeMaitre RW. 1982. Numerical petrology. Developments in Petrology. vol 8
- LeRoux AP. 1987. Geochemical correlation between S. African ~~basalts and S. Atlantic hotspots.~~ Nature 324. 243.
- Lloyd FE and Bailey DK. 1975. Light Element metasomatism of the continental mantle: the evidences and the consequences. Phys. Chem. Earth. 9 389-416.

- Lock BE and Marsh JS. 1981. Tertiary phonolite volcanism in the Klinghardt mountains of South-West Africa. *Trans. Geol. soc. S. Afr.* 84. 1-6.
- Marsh JS. 1973. Relationships between transform directions and alkaline rock lineaments in Africa and S. America. *E.P.S.L.* 18. 317.
- Marsh JS. 1987. Evolution of a strongly differentiated suite of phonolites from the Klinghardt Mountains, Namibia. *Lithos* 20 41-58
- McCulloch MT, Jaques AL, Nelson DR and Lewis JD. 1983. Nd and Sr isotopes in kimberlites and lamproites from western Australia: an enriched mantle origin. *Nature* 302. 400
- McFaddon PL. 1977. A palaeomagnetic determination of the emplacement temperature of some South African kimberlites. *J.G.R.* 50 587-604
- McKenzie D. 1986. Magma extraction. *E.P.S.L.* 74. 81.
- McKenzie D and O'nions RK. 1983. Mantle reservoirs and ocean island basalts. *Nature* 301. 229.
- Newsom HE, White WM, Jochum KP and Hoffman AW. 1986. Siderophile and chalcophile element abundances in oceanic basalts. Pb isotope evolution and growth of the earths core. *E.P.S.L.* 80. 299.
- McLennan S and Taylor SR. 1979. Rare earth element mobility associated with U mineralisation. *Nature* 282. 247.
- Menzies MA and Hawkesworth CJ (Eds) 1987. *Mantle Metasomatism*. Academic Press London.
- Menzies MA and Wass SY. 1983. CO₂ and LREE rich mantle below E. Australia: a REE and Isotopic study of alkaline magmas and apatite rich mantle xenoliths from Australia. *E.P.S.L.* 65. 287.
- Menzies M, Rogers N, Tindle A and Hawkesworth CJ. 1987. Metasomatic and enrichment processes in lithospheric peridotites, and the effect of asthenosphere - lithosphere interaction. In *mantle metasomatism*. Menzies and Hawkesworth Eds. Academic Press. p312
- Mikhayenko VI and Nenashev VI. 1962. Absolute age of kimberlites of Yakutia. *Int. Geol. Rev.* 4 914-924
- Mitchell RH. 1984. Garnet lherzolites from the Hanaus I and Louwrensia kimberlites of Namibia. *Contrib. Min and*

Pet. 86. 178.

Mitchell RH. 1986. Kimberlites ; mineralogy, geochemistry and petrology. Plenum press, New York.

Mitchell RH. 1987. Megacrysts in kimberlites from the Gibeon field, Namibia. Neues Jahrbuch Miner. Abh. 157. 267-283.

Moore AE. 1976. Controls of post-Gondwanaland alkaline volcanism in southern Africa. E.P.S.L. 31. 291.

Morgan WJ. 1971. Convection plumes in the lower mantle. Nature 230 42-43.

Morgan WJ. 1983. Hotspot tracks and the early rifting of the Atlantic. tectonophysics 94 123-39.

Mysen BO and Boettcher AL. 1975. Melting of a hydrous mantle II: Geochemistry of crystals and liquid formed by anatexis of mantle peridotite at high pressure and temperature as a function of controlled activities of H₂O and CO₂. J. Pet. 16

Nelson DR, Chivas AR, Chappell BW and McCulloch MT. 1987. Geochemical and isotope systematics in carbonatites and implications for the evolution of ocean island sources. Geochim. et Cosmochim. Acta. 52 1-17

Nixon PH. 1973. Lesotho Kimberlites. Lesotho National Development Corporation Maseru.

Nixon PH. 1987. Mantle Xenoliths. PH Nixon Ed, John Wiley and Sons, New York.

Nixon PH and Boyd FR. 1973a. Petrogenesis of the granular and sheared ultrabasic nodule suite in kimberlites. In Nixon 1973, 48-56.

Nixon PH and Boyd FR. 1973b. The discrete nodule association in kimberlites in northern Lesotho. In Nixon 1973, 67-75.

Nixon PH and Boyd FR. 1979a. The SE Lesotho-E Griqualand kimberlite field and the nature of the edge cratonic lithosphere. Kimberlite Symposium II, Cambridge.

Nixon PH and Boyd FR. 1979b. Garnet bearing lherzolites and discrete nodule suites from the Malaita alnoite, Solomon Is. SW Pacific, and their bearing on oceanic mantle composition and geotherm. 2nd Int. Kim. Conf. 2 400-423.

Nixon PH, Rogers NW, Gibson, Grey. 1981. Depleted and fertile

mantle xenoliths from southern African kimberlites.
Ann. Rev. Earth Planet Sci 1981. 285

- Olafsson M and Eggler DH. 1983. Phase relations of amphibole-carbonate and phlogopite-carbonate peridotite: Petrologic constraints on the asthenosphere. E.P.S.L. 64 305-315.
- O'Nions RK. 1984. Isotopic abundances relevant to the identification of magma sources. Phil. Trans. Roy. Soc. Lond. A310 591
- O'Nions RK, Hamilton PJ and Evensen NM. 1977. Variations in Nd/Nd and Sr/Sr ratios in oceanic basalts. E.P.S.L. 34 13-22.
- Parsons I, Rex DC, Guise P and Halliday AN. 1988. Argon loss by Alkali Feldspars
Geochim et Cosmochim Acta. 52 1097-1112
- Pearce JA and Norry MJ 1979. Petrogenetic implications of Ti, Zr, Y and Nb variations in volcanic rocks. Contrib. Min. and Pet. 69. 33.
- Peterman ZE, Hedge CE and Tourtelot HA. 1970. Isotopic composition of Sr in sea water throughout phanerozoic time. Geochim. et cosmochim. Acta. 34 105-120
- Provost A and Allegre CJ. 1979. Process identification and search for optimal differentiation parameters from major element data. General presentation with emphasis on the fractional crystallization process. G.C.A. 43. 487.
- Rawlingson PJ and Dawson JB. 1979. A quench pyroxene-ilmenite xenolith from Kimberley: implications for pyroxene-ilmenite intergrowths. 2nd int. kim. conf. vol. 2
- Reeves CV. 1976. Gravity studies in Botswana and their contribution to regional geophysics in Southern Africa. PhD Thesis. Leeds Univ.
- Richardson SH, Erlank AJ and Hart SR. 1985. Kimberlite borne garnet peridotite xenoliths from old enriched subcontinental lithosphere. E.P.S.L. 75. 116.
- Richardson SH, Gurney JJ, Erlank AJ and Harris JW. 1984. Origins of diamonds in old enriched mantle. Nature 310. 198-202.
- Richter FM 1986. Simple models for trace element fractionation during melt segregation. E.P.S.L. 77. 333-344.

- Rogers NW, Hawkesworth CJ, Parker RJ and Marsh JS. 1985. The geochemistry of potassic lavas from Vulcini, central Italy, and implications for mantle enrichment processes beneath the Roman region. *Contrib. Min. and Pet.* 90. 244.
- Rolfe DG. 1973. The geology of the Kao kimberlite pipes. In Nixon 1973.
- Schilling JG, Thompson RN, Kingsly and Humphris. 1985. Hotspot-migrating ridge interaction in the S. Atlantic. *Nature* 313.
- Schreyer W, Massonne HJ and Chopin C. 1987. Continental crust subducted to depths near 100km: implications for magma and fluid genesis in collision zones. The Geological Society Spec. pub. no 1. Ed B.O. Mysen.
- Schulze DJ. 1985. Evidence for primary kimberlitic liquids in megacrysts from kimberlites in Kentucky, USA. *J. Geol* 93 75-79
- Schulze DJ. 1987. Megacrysts from alkalic volcanic rocks. In Nixon 1987.
- Scott BH. 1979. Petrogenesis of kimberlites and associated lamprophyres from central west Greenland. In Boyd and Meyer (1979a) 190-205.
- Scott BH. 1981. Kimberlite and lamproite dykes from Holsteinborg, west Greenland Meddr. Groenland Geosci. 4 22
- Skinner EMW. 1986. Contrasting group I and group II kimberlite petrology: towards a genetic model for kimberlites. 4IKC. 202-204.
- Skinner EMW and Clement CR. 1979. Mineralogical classification of Southern African kimberlites. 2IKC. 129-139.
- Shee SR. 1984. The oxide minerals of the Wesselton Mine kimberlite, Kimberley. 3IKC 59-75.
- Smith CB. 1983. Pb, Sr, and Nd isotopic evidence for sources of southern African Cretaceous kimberlites. *Nature* 304. 51.
- Smith CB, Gurney JJ, Skinner EMW, Clement CR and Ebrahim. 1985. Geochemical character of S. African kimberlites: a new approach based on isotopic constraints. *Trans. Geol. Soc. S. Afr.* 88. 267.

- Smith CB, Allsop HL, Kramers JD Gurney JJ and Jagoutz E. 1986. Isotopic and geochemical studies of kimberlite and included xenoliths. 4IKC 329-331.
- Smith JV, Brennesholtz R and Dawson JB. 1978. Chemistry of micas from kimberlites and xenoliths. I: Micaceous kimberlites. Geochim. et cosmochim. Acta 42 959-971.
- Smith JV and Hervig 1979. K,Rb,Ba in micas from kimberlite and peridotitic xenoliths- implications for origin of basaltic rocks. Proc 2nd Int. Kim. Conf.
- Sun SS. 1980. Lead isotopic study of young volcanic rocks from mid ocean ridges, ocean islands and island arcs. Phil. Trans. Roy. Soc. Lond. A297. 409-445.
- Sun SS and McDonough WF. 1988. Chemical and isotopic systematics of oceanic basalts: Implications for mantle composition and processes. In: Magmatism in ocean basins. (Eds Saunders and Norry).
- Takahashi E, and Scarfe CM. 1985. Melting of peridotite to 14 GPa and the genesis of komatiite. Nature 315. 566.
- Takahashi E, Ito E and Scarfe CM. 1986. Melting and subsolidus phase relation of mantle peridotite up to 25GPa. 4IKC.208-210.
- Tankard AJ, Jackson MPA, Eriksson KA, Hobday DK, Hunter DR and Minter WEL. 1982. Crustal evolution of Southern Africa. Springer Verlag, New York.
- Taylor HP. 1980. Affects of AFC on $180/160$ and $87\text{Sr}/86\text{Sr}$. E.P.S.L. 47. 243.
- Taylor SR and McLennan S. 1981. The composition and evolution of the continental crust. Phil. Trans. Roy. Soc. A301. 381.
- Taylor SR and McLennan S. 1985. The continental crust: it's composition and evolution. Blackwell Scientific Publications.
- Taylor WR and Green DH. 1988. Measurement of reduced peridotite COH solidus and implications for redox melting of the mantle. Nature 332 349-52
- Thompson RN. 1984. Dispatches from the basalt front. Proc. Geol. Ass. 95. 249.
- Thompson RN, Morrison A, Matthey D, Dickin PA and Moorbath S. 1980. An assessment of the Th-Hf-Ta diagram as a discriminant for tectonomagmatic classifications and the detection of crustal contamination of magmas.

Verwoerd WJ. 1967. The carbonatites of South Africa and South West Africa. S. Af. Geol. Surv. Handbook no.6.

Wagner PA. 1914. The diamond fields of Southern Africa. Transvaal Leader, Johannesburg.

Weaver BL and Tarney J. 1981. Lewisian gneiss geochemistry and Archaean crustal development models. E.P.S.L. 1981. 171.

Weaver BL, Wood, Tarney J and Joron. 1986. Role of subducted sediment in the genesis of OIBs in the S. Atlantic. Geology 14. 275.

Wedepohl KH and Muramatsu Y. 1979. The chemical composition of kimberlites compared with the average composition of three basaltic magma types. 2IKC 300-312.

Weis D and Demaiffe D. 1975. A depleted mantle source for kimberlites from Zaire: Nd, Sr and Pb isotopic evidence. E.P.S.L. 73. 268

Wendlandt RF. 1976. Barium Phlogopite from Haystack Butte, Highland Mountains, Montana. Carnegie Institute of Washington yearbook 76 534-539

White AW. 1985. Sources of oceanic basalts: radiogenic isotope evidence. Geology 13 115-118

White AW and Hoffman WM. 1982. Sr and Nd isotope geochemistry of oceanic basalts and mantle evolution. Nature 296. 821.

White and McKenzie 1988. In Press.

Williams AF. 1932. The Genesis of Diamond. Ernest Benn Ltd, London.

Wyllie PJ. 1977. Mantle fluid compositions buffered by carbonates in peridotite-CO₂-H₂O. J. Geol. 85 187-208.

Wyllie PJ. 1978. Mantle fluid compositions buffered in peridotite-CO₂-H₂O by carbonates, amphiboles and phlogopite. J. Geol. 86. 687-713.

Wyllie PJ. 1980. The origin of kimberlite. J.G.R. 85 6902-6910

Wyllie PJ. 1986. Genesis and migration of kimberlites and other low-SiO₂, high-alkali magmas. 4IKC. 214-216.

Wyllie PJ. 1987. Metasomatism and fluid generation in mantle

xenoliths. In Nixon 1987.

Wyllie PJ and Huang WL. 1975. Peridotite, kimberlite and carbonatite explained in the system CaO-MgO-SiO₂-CO₂. *Geology* 3 621-624.

Zindler A and Hart SR. Chemical geodynamics. *Ann. Revs. E.P.S.L.* 1986. 493-571.

APPENDIX 1

A1.1 PREPARATION AND XRF ANALYSIS OF WHOLE-ROCK SAMPLE

1.1.1 Crushing

Whole rock samples were either taken from drill cores (kimberlites) or from the field (parakimberlites etc). Samples were as large as possible, typically weighing about 2kg. Weathered surfaces of field samples were cut off with a diamond saw. Kimberlite samples with visible crustal xenoliths were avoided as much as possible. Samples were reduced with a hydraulic splitter, then crushed in a hardened steel mortar to chips less than 2mm. A steel jaw crusher was not used as a precaution against trace metal contamination. An 80g portion was removed for powdering in an agate tema mill, and the remainder was used for mineral separation (see section A1.7.1). The whole rock sample was ground in the tema for 8-12 minutes until all the sample passed through a 100 mesh seive. Powders were stored in cleaned glass bottles.

A1.1.2 Preparation of discs for XRF major element analysis

Fused discs were prepared for XRF analysis of major elements. 0.400g of rock powder plus 4.000g of lithium borate spectroflux (Johnson and Matthey Spectroflux 110) was weighed accurately into a platinum crucible. These were well mixed with a teflon stirring rod, then heated in a furnace for 30 minutes at 1000°C. After cooling, the sample was made up to 4.400g with more flux. The weight loss was due partially to water loss from the flux, and partially from volatile loss from the rock. The sample was reheated and melted over bunsen burners, then cast into

copper discs on a hotplate, using an aluminium plunger to flatten the disc. The discs were then cooled, labelled and stored in plastic bags.

A1.1.3 Preparation of discs for XRF minor element analysis

Pressed powder discs were prepared for XRF analysis of minor elements. 15.0g of rock powder was mixed with 2ml of Moviol agglutinate in a plastic beaker. The mixture was pressed to a disc in a toughened steel jacket in a hydraulic press, to a pressure of 10 tons per square inch. the pellet was then dried in an oven at over 100°C for 1 hour. The pellet was stored in a plastic bag. The pellet was placed in a vacuum desiccators shortly before use.

A1.1.4 Measurement of Loss on Ignition

Loss on ignition was measured by placing 1 gram of rock powder in a ceramic dish, and heating in a furnace at 1000°C for 30 minutes. the sample was then reweighed and the loss calculated as a percentage.

A1.1.5 XRF Machine conditions and analytical errors

Samples were analysed using a Phillips PW1400 X-ray fluorescence spectrometer. Running parameters for major elements were 40kV, 60mA. minor elements were analysed at 50kV, 50mA. Two cycles of measurements were routinely run to correct for machine drift. All data is corrected for mass absorption and matrix affects by computer program. The standard major element analytical program and an assesment of the errors in analysis is given by Downes (1983). The effects of machine drift are corrected for by reference to an internal standard which always occupies one of the sample chamber positions. Errors are thought to

be +/- 5-20% for minor elements and +/- 1% for major elements (A Gray pers comm.).

A1.2 ANALYSIS OF REE BY ICP SPECTROSCOPY

REE were analysed using a Phillips PV8210 1.5m inductively coupled plasma (ICP) spectrometer. ICP spectrometry is a multi-element technique which relies on atoms being excited, and on falling back to their groundstate, releasing energy in the form of light. A high temperature plasma is formed by means of a radio frequency generator. The sample, in solution, is injected into the flame which reaches very high temperatures (6000-10000K), resulting in many spectral lines being emitted from both ionic and atomic species. This is important for REE since many have complex ionic spectra, thus giving a wide choice of sensitive spectral lines, but also considerable problems of spectral overlap.

Spectral lines used for REE analysis (Walsh et al. 1986)

		interfering element
La	398.85nm	Ca
Ce	418.66nm	Sr
Pr	422.20nm	Ce, Sr, Ca
Nd	403.36nm	Ba
Sm	359.26nm	Nd, Gd
Eu	381.97nm	Nd
Gd	335.05nm	Ca
Dy	353.17nm	
Ho	345.60nm	
Er	390.63nm	
Yb	328.94nm	
Lu	261.50nm	

A1.2.1 Sample separation

The technique of Crock et al. (1986) was used to prepare samples, by separation of REE in solution.

1.000g of powdered rock sample was weighed into a platinum crucible and dissolved in a mixture of HCl, HF and HOCl. The sample was then evaporated to dryness and redissolved in 50ml of 1M HCl. The sample was then loaded onto preconditioned cation exchange columns and eluted in 50ml 2.0M HCl then 50ml 2.0M HNO₃. The REE were then collected in 50ml 6M HCl followed by 50ml 8M HNO₃. The sample was evaporated to dryness, then made up to a 10.0ml solution in water. Two blanks were run using the same procedure as the samples.

A1.2.2 Standards

Standards were analysed between every 3 samples to correct for machine drift, and to correct for interference. Several standards were analysed. One standard contained all the REE, one only Nd and Ce, one Ba, one Sr and another, Ca.

Raw data was corrected using a computer programme which corrected each measurement for drift, then (if necessary) for interfering elements, and finally subtracted the analytical blank. Because of the high interference on Pr from Ce, Sr and Ca the corrected data was of rather poor quality, and was discarded.

A1.3 ANALYSIS OF REE AND Th, U, Ta AND Hf by INAA

REE and several trace elements were determined by Instrumental Neutron Activation Analysis (INAA) following the techniques reported in Potts et al. (1981, 1985). Rock powders were dried in an oven at 105°C overnight, and 0.3g of each powder were then weighed into polythene capsules.

The capsules were sealed by soldering. Ten capsules were placed in a polythene irradiation tube, together with an international (Whin Sill) and internal (Ailsa Craig) standard in a predesignated order. Capsules were separated by laquered iron foils.

Samples were irradiated within a core tube at the University of London Reactor Centre, Ascot in a thermal flux of $5 \times 10^{12} \text{ n cm}^{-2} \text{ s}^{-1}$ for 24-30 hrs of reactor time. After 'cooling' for 5 days they were counted at the Open University by N Rogers, using two detectors; a planar low energy photon spectrometer (LEPS) and a coaxial Ge(Li) detector. Data were processed using spectroscopy amplifiers and a multichannel analyser. Full details of counting conditions for the foils and samples, peak fitting, corrections for overlaps and neutron flux discrepancies and calibration are given in Potts et al (1981,1985).

A1.4 MINERAL ANALYSIS BY ELECTRON MICROPROBE

Major element mineral analyses presented in this work were measured on the Joel JXA-50A electron microprobe which is fitted with an energy dispersive system (link 860 series 2). All ZAF corrections were made on-line. The elements analysed were calibrated with the following standards:

Si	Wollastonite	Mg	Periclase
Ti	Rutile	Ca	Wollastonite
Al	Corundum	Ni	Ni metal
Cr	Cr metal	Na	Jadeite
Fe	Fe metal	K	Orthoclase
Ni	Ni metal		

The beam current used was approximately 1 nanoamp, the accelerating voltage was 20kV and the count time was 100 sec. Errors for major elements are generally +/-2%, but are larger for trace elements in low concentrations. Elements present at less than 1 wt per cent have errors of +/-5%. Analyses of elements less than 0.1% were discarded as these were below the detection limit (Condliffe pers comm).

A1.5 Sr, Nd and Pb ISOTOPE ANALYSIS

Chemistry for Sr and Nd isotope analysis was performed at the Leeds University laboratory which has a positive pressure (relative to atmospheric) produced by filtered air. Samples were dissolved in teflon beakers (or bombs). All teflon beakers were cleaned by rinsing, followed by soaking in dilute HNO₃, then in hot (80°C) conc. HNO₃ for 24hrs. The beakers were then soaked in distilled-deionised (d-d)water. Prior to use the beakers were boiled twice in d-d water. All reagents used for chemistry were of Analar grade, and were further purified by sub-boiling twice in a quartz distill (SBQD).

A1.5.1 whole rock Sr and Nd chemistry

15-150 mg of ground whole-rock powder was weighed into a teflon beaker. Spike (if used) was then added to, and weighed with, the sample. Dissolution was accomplished by adding 2ml conc HF and 8ml conc HNO₃ and leaving overnight. the sample was then dried under an evaporation hood. The sample was then dissolved in 6M HCl and dried again, followed by further dissolution in 1ml of 2.5M HCl. The sample was placed in an ultrasonic bath to aid dissolution, then centrifuged to remove any insoluble residue.

The dissolved sample was loaded onto preconditioned cation exchange columns, and washed on with 2 x 1ml 2.5M HCl. The sample was eluted with 2.5 M HCl and Rb, and Sr collected at calibrated intervals, and evaporated to dryness. REEs and Ba were collected in 2M HNO₃. The columns were then cleaned with 6M HCl and water and reconditioned with 2.5MHCl. The Sr separate was then dissolved again in 2.5M HCl and passed through the cation exchange columns again to purify it. The Sr separate was then dried and stored in a sealed teflon microbeaker.

The REE fraction was dried under an evaporation hood, then dissolved in concentrated HNO₃ and dried again. The dried precipitate was then dissolved in 1ml of a mixture of 75% acetic acid/25% nitric acid and loaded onto a second set of cation exchange columns. The sample was washed onto the column with 2 x 1ml of a mixture of 90% acetic acid/10% nitric acid. The sample was eluted with a calibrated amount of 90/10 acetic/nitric acid, then the REE fraction was collected in 5ml 0.05M HNO₃ and evaporated to dryness.

The REE fraction was dissolved in 0.5ml 0.125M HCl and loaded onto a third set of (PTFE) cation exchange columns to separate Nd. The sample was eluted with 0.125M HCl for 150 minutes at a fixed (calibrated) head of pressure, then collected in 0.25M HCl over a timed interval. The calibration of the PTFE columns was sensitive to temperature and disturbance of the resin bed, hence frequent recalibrations were necessary. The Nd collected was evaporated to dryness and stored in a sealed microbeaker until loaded onto a bead for analysis.

A1.5.2 Whole rock Pb chemistry

All Pb chemistry was performed in a laminar flow fume cupboard in an ultraclean laboratory, which was under a

positive pressure generated by filtered air, and specially reserved for Pb chemistry. All Pb chemistry was done in ultraclean teflon beakers. These were cleaned by several rinsings in 6M HCl and H₂O, followed by soakings in 6M HCl, 8M HNO₃, and finally H₂O. Before use, the beakers were rinsed again in H₂O. All reagents used were purified twice by sub-boiling distillation (SBQD).

Samples were weighed into the teflon beakers, and if used, ²⁰⁸Pb spike was added and weighed as well. The sample was then dissolved in a mixture of 8ml conc. HF/1ml 1M HBr and left overnight. The sample was then dried and dissolved again in 5ml 1M HBr. An ultrasonic bath was used to aid dissolution if the sample was found not to be in complete solution. The dried sample was dissolved in 1ml 1M HBr and loaded onto preconditioned anion exchange columns using pre-cleaned disposable PVP pipette tips. The Pb sample was eluted with HBr and collected in 6M HCl. The Pb fraction was then dried, redissolved in HBr, and passed through the columns a second time. A drop of perchloric acid was added to collectant, and the Pb fraction was then evaporated to a small droplet which was then loaded onto a bead for analysis in the mass spectrometer.

A1.5.3 Mass Spectrometry

Samples were loaded onto outgassed filaments of Re or Ta ribbon welded onto pins mounted in glass beads.

Sr. A drop of phosphoric acid was placed on a single Ta bead and evaporated to incipient dryness by passing a small current through the filament. The Sr sample was dissolved in a small drop of SBQD H₂O and loaded onto the filament with a micro-pipette and dried. The filament was heated until phosphoric acid fumes were produced, then cooled.

Ba. Ba was loaded using the same procedure as Sr.

Rb. The sample was dissolved in SBQD H₂O and loaded onto the two side filaments of a triple Ta bead. The filament was then heated until it glowed red, and was then cooled.

Nd & REE. The sample was dissolved in a small drop of SBQD H₂O and loaded onto the two Ta side filaments of a triple filament bead (the centre filament being Re), and dried to a salt.

Pb. Pb samples were dissolved in a small drop of 1M HPO₃ and loaded onto a single Re filament, onto which a large drop of silica gel had been dried to incipient dryness.

Sr and REE samples were run automatically on a VG 54E thermal ionisation mass spectrometer. Nd, Pb, Rb and Ba samples were run manually on a Micromass MM30 thermal ionisation mass spectrometer. All elements were analysed at $<10^{-7}$ atmospheres and with an accelerating potential of 8.0 kV. 100 ratios were routinely measured for Sr, about 700 for Nd, and 600 for Pb. The number of scans across the mass spectrum was less for more stable beams.

A1.5.4 Standards

During the course of this work, international standards were routinely run.

The Sr standard NBS 987 was run twice in each turret of 16 samples, in the VG 54E. The measured values of this standard varied after two periods of machine maintenance:

Before 1-5-87: average NBS987 $^{87}\text{Sr}/^{86}\text{Sr}=0.710278$ (n>300)
After 1-5-87: average NBS987 $^{87}\text{Sr}/^{86}\text{Sr}=0.710265$ (n>140)
After 7-88: average NBS987 $^{87}\text{Sr}/^{86}\text{Sr}=0.710250$ (n 25)

The measurements were corrected to the internationally agreed value of NBS 987 $^{87}\text{Sr}/^{86}\text{Sr}=0.71022$. Mass fractionation was corrected internally by the operating

programme assuming $^{88}\text{Sr}/^{86}\text{Sr} = 0.1194$, and that mass fractionation is linearly dependent upon mass difference.

The Nd standard 'La Jolla' was routinely run on the MM30 giving an average $^{143}\text{Nd}/^{144}\text{Nd}=0.511905$ on 20 samples during the period of study. The measurements were corrected to BCR-1, $^{143}\text{Nd}/^{144}\text{Nd}=0.512665$. Mass fractionation was corrected internally by the operating programme assuming $^{148}\text{Nd}/^{144}\text{Nd}= 0.7219$.

The Pb standard SRM981 was run with every turret of 6 samples on the MM30. Fractionation was monitored and corrected for by the repeated analysis of this standard. The average of 19 analyses of precision $\pm 0.015\%$ (2 σ) was:

$$\begin{aligned}^{207}\text{Pb}/^{206}\text{Pb} &= 0.91462 \\ ^{208}\text{Pb}/^{206}\text{Pb} &= 2.16165 \\ ^{206}\text{Pb}/^{204}\text{Pb} &= 16.895\end{aligned}$$

which was corrected to the agreed value of:

$$\begin{aligned}^{207}\text{Pb}/^{206}\text{Pb} &= 0.91464 \\ ^{208}\text{Pb}/^{206}\text{Pb} &= 2.1681 \\ ^{206}\text{Pb}/^{204}\text{Pb} &= 16.937\end{aligned}$$

giving an average mass fractionation of -1.27% per mass unit. The samples then had their measured values corrected by this factor.

A1.5.5 Analytical blanks

Analytical blanks for Sr and Nd were each less than 2ng which was insignificant in all cases. Pb blanks, which were analysed with each batch of 6 samples, were 0.4 to 1ng

A1.5.6 Data presentation

For principles of isotope systematics, the reader is referred to Faure and Powell (1972), Faure (1977) and Hawkesworth and Van Calsteren (1984). Measured isotope data are recalculated to initial ratios at time (t), the age of emplacement using the following isochron equations:

$$\left(\frac{^{143}\text{Nd}}{^{144}\text{Nd}}\right)_m = \frac{^{147}\text{Sm}}{^{144}\text{Nd}}(e^{\lambda t} - 1) + \left(\frac{^{143}\text{Nd}}{^{144}\text{Nd}}\right)_i$$

$$\left(\frac{^{87}\text{Sr}}{^{86}\text{Sr}}\right)_m = \frac{^{87}\text{Rb}}{^{86}\text{Sr}}(e^{\lambda t} - 1) + \left(\frac{^{87}\text{Sr}}{^{86}\text{Sr}}\right)_i$$

$$\left(\frac{^{206}\text{Pb}}{^{204}\text{Pb}}\right)_m = \mu(e^{\lambda t} - 1) + \left(\frac{^{206}\text{Pb}}{^{204}\text{Pb}}\right)_i$$

$$\mu = \frac{^{238}\text{U}}{^{204}\text{Pb}}$$

$$\left(\frac{^{207}\text{Pb}}{^{204}\text{Pb}}\right)_m = \kappa(e^{\lambda t} - 1) + \left(\frac{^{207}\text{Pb}}{^{204}\text{Pb}}\right)_i$$

$$\kappa = \frac{^{235}\text{U}}{^{204}\text{Pb}}$$

$$\left(\frac{^{208}\text{Pb}}{^{204}\text{Pb}}\right)_m = \frac{^{232}\text{Th}}{^{204}\text{Pb}}(e^{\lambda t} - 1) + \left(\frac{^{208}\text{Pb}}{^{204}\text{Pb}}\right)_i$$

For Sr and Nd isotopes, the ϵ notation of DePaulo and Wasserberg (1976) is generally employed for representation of isotopic data formed at time (t) relative to a uniform reservoir (UR) at that same time. For Nd analyses the UR is assumed to be chondritic (CHUR). Thus:

$$\epsilon_{Nd} = \left[\frac{(^{143}\text{Nd}/^{144}\text{Nd})_{\text{sample}(t)}}{(^{143}\text{Nd}/^{144}\text{Nd})_{\text{CHUR}(t)}} - 1 \right] \times 10^4$$

$$\epsilon_{Sr} = \left[\frac{(^{87}\text{Sr}/^{86}\text{Sr})_{\text{sample}(t)}}{(^{87}\text{Sr}/^{86}\text{Sr})_{\text{CHUR}(t)}} - 1 \right] \times 10^4$$

The T^{Nd} age is the time at which a sample of particular present day Sm/Nd and $^{143}\text{Nd}/^{144}\text{Nd}$ ratios has the same $^{143}\text{Nd}/^{144}\text{Nd}$ ratio as CHUR (Hawkesworth and Van Calsteren 1984). Thus:

$$T_{\text{CHUR}}^{\text{Nd}} = 1/\lambda \ln \left[\frac{(^{143}\text{Nd}/^{144}\text{Nd})_{\text{m}} - (^{143}\text{Nd}/^{144}\text{Nd})_{\text{CHUR}}}{(^{147}\text{Sm}/^{144}\text{Nd})_{\text{m}} - (^{147}\text{Sm}/^{144}\text{Nd})_{\text{CHUR}}} + 1 \right]$$

where:

- $\lambda ^{147}\text{Sm} = 6.54 \times 10^{-12} \text{ y}^{-1}$
- $(^{143}\text{Nd}/^{144}\text{Nd})_{\text{CHUR}} = 0.51264$
- $(^{147}\text{Sm}/^{144}\text{Nd})_{\text{CHUR}} = 0.1967$
- $\lambda ^{87}\text{Sr} = 1.42 \times 10^{-11}$
- $(^{87}\text{Sr}/^{86}\text{Sr})_{\text{UR}} = 0.7047$
- $(^{87}\text{Rb}/^{86}\text{Sr})_{\text{UR}} = 0.0847$
- $\lambda ^{238}\text{U} = 1.55125 \times 10^{-10} \text{ y}^{-1}$
- $\lambda ^{235}\text{U} = 9.8485 \times 10^{-10} \text{ y}^{-1}$
- $\lambda ^{232}\text{Th} = 4.948 \times 10^{-11} \text{ y}^{-1}$

Spike correction calculations.

During the Nd analysis of the CPX megacrysts, it became apparent that the samples had been contaminated by trace amounts of a REE spike which was currently in use in the lab. The point at which the contamination was picked up was never defined, but it is thought that it may have occurred when the sample was passed through a set of REE separation columns. As the samples were irreplaceable within the time constraints of this work, it was necessary to calculate their composition. As the composition of the spike is known precisely, it is possible to use the double-spike calculations of Dodson (1970) to calculate the correct composition of the sample, and the amount of spike present (Dodson pers comm.). The samples ran extremely well and all natural Nd isotope ratios were measured.

The measured ratios were corrected for fractionation using the equation:

$$f = \frac{1}{1+P_k} \left[\frac{N_5}{M_5} - 1 + P_k \left(\frac{S_5}{M_5} - 1 \right) \right]$$

or

$$f = \frac{1}{2(1+P_k)} \left[\frac{N_6}{M_6} - 1 + P_k \left(\frac{S_6}{M_6} - 1 \right) \right]$$

where: N_5 = $^{145}\text{Nd}/^{144}\text{Nd}$ of the sample (0.348417)
 N_6 = $^{146}\text{Nd}/^{144}\text{Nd}$ of the sample (0.7219)
 S_5 = $^{145}\text{Nd}/^{144}\text{Nd}$ of the spike (26.9469)
 S_6 = $^{146}\text{Nd}/^{144}\text{Nd}$ of the spike (3.61088)
 M_5 = $^{145}\text{Nd}/^{144}\text{Nd}$ of the mixture (measured)
 M_6 = $^{146}\text{Nd}/^{144}\text{Nd}$ of the mixture (measured)

and
$$P_k = \frac{\frac{N_6}{M_6} - 2 \frac{N_5}{M_5} + 1}{\frac{S_6}{M_6} - 2 \frac{S_5}{M_5} + 1}$$

The corrected sample ratios are given by :

$$N_i = M_i + P_k(M_i - S_i) \equiv M_i(1 + P_k) - P_k S_i$$

where

$$i = 143/144, 145/144, 146/144$$

It is quite possible that the spike contaminant was accompanied by a small amount of sample from a previous user. A worst case calculation was performed to assess the effects of the possibilities of sample contamination. The worst case would involve the smallest megacryst sample mixing with an old crustal sample. Old crustal samples, and recent mantle samples had been run in the lab previous to this incident. The measured composition and spike and sample weights of the potential contaminants was known, and a calculation was made using the least radiogenic crustal sample together with the highest sample/spike ratio. The highest amount of spike present in the megacryst represented 0.03% of the worst case crustal sample/spike mix. The mixture of this worst case contaminant with the smallest megacryst produced a reduction in the megacryst $^{143}\text{Nd}/^{144}\text{Nd}$ ratio of 0.000008, which is within analytical error. All of the megacrysts were analysed to a precision of better than +/- 0.000020.

It is therefore concluded that the contamination by another sample is negligible, and that the spike contamination is adequately dealt with. The calculation was repeated for non-radiogenic ratios which confirmed the validity of Dodson's calculation method. Also, when age corrected, many of the samples were found to have the same initial ratios, lending support to the conclusion.

A1.6 COMPARISON OF ANALYTICAL TECHNIQUES

In the course of this work, several elements were analysed by more than one analytical technique. Comparison of data produced from the same samples by different techniques was used to gauge the precision and accuracy of those techniques. The results highlight the problems of comparing data produced by different laboratories or by using different techniques.

Rb	XRF	ID	INAA	
Sr	XRF	ID		ICP
REE	XRF		INAA	ICP

Rb. Rb was analysed by XRF, ID and INAA. Figure A1a (Rb by XRF v Rb by ID) shows that XRF and ID determinations agreed to a high level of precision, with data points scattering about the XRF:ID = 1:1 line with an average discrepancy of +/-3%.

There was a much higher level of discrepancy between INAA and ID than with XRF and ID. The INAA determinations were always higher than ID determinations, by up to 50% at low concentrations (<20ppm) and up to 20% at high concentrations (>100ppm).

The ID Rb data was used in this work

Sr. Sr was analysed by isotope dilution (ID), XRF and ICP. Figure A1b (Sr by XRF v Sr by ID) shows that Sr determinations by ID are consistently higher than XRF determinations, and plot on a best fit line of gradient 0.92 ID determinations are on average 8% higher than XRF. XRF determinations plot close to the best fit line at all concentrations from <100ppm to >1500ppm. ID is usually considered to be a very precise and accurate analytical technique with errors <<1% (Cliff pers comm). Thus it is

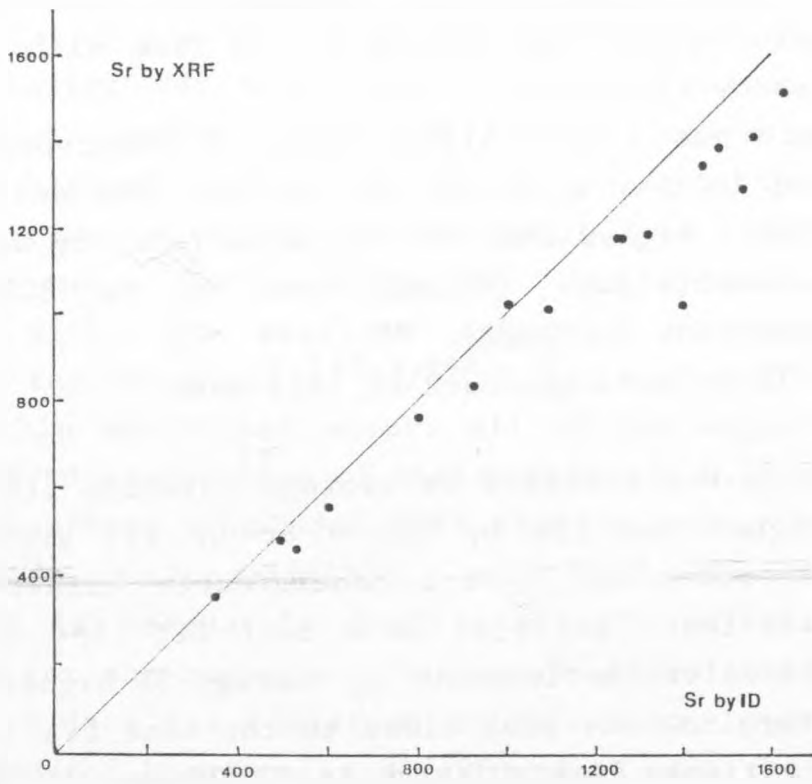
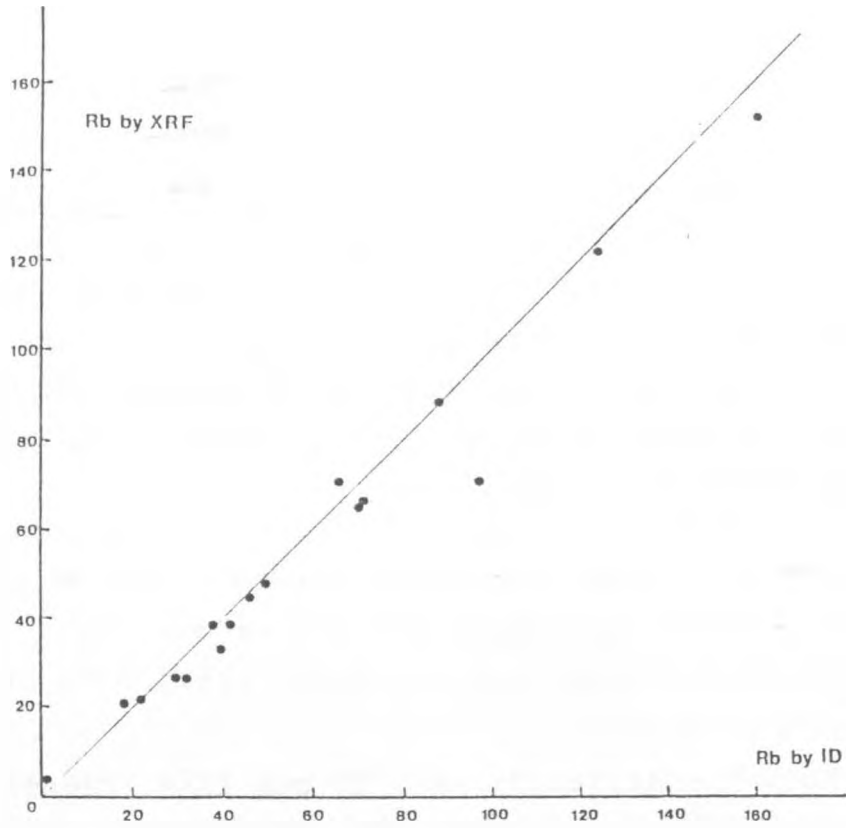
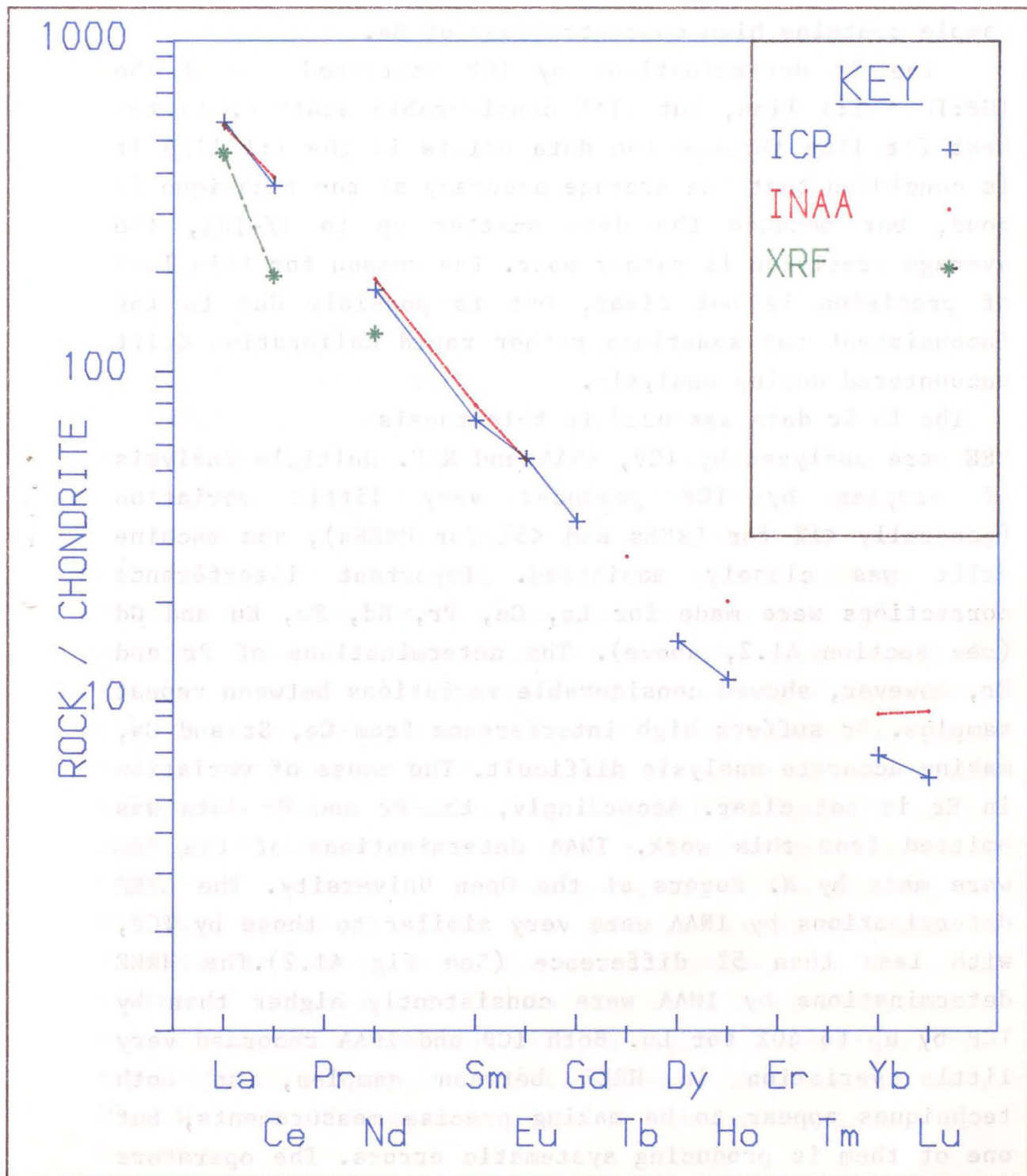


Figure A1.1.a Comparison of analytical techniques: (a) Rb analysed by XRF v Rb by ID, (b) Sr by XRF v Sr by ID.

Figure A1.2. Comparison of analytical techniques for REE analysis: analyses of K35 by ICP, INAA and XRF. The discrepancies between techniques was consistent between different samples.



concluded that the XRF technique used on the Leeds machine gave reasonable precision (about 2% average deviation from the best fit line, but poor accuracy, consistently measuring about 8% low. C.B. Smith (pers comm) suggested that the XRF technique is not accurate for Sr when the sample contains high concentrations of Ba.

The Sr determinations by ICP scattered around the ICP:ID = 1:1 line, but with considerable scatter. As the best fit line through the data points is the 1:1 line it is concluded that the average accuracy of the technique is good, but because the data scatter up to +/-10%, the average precision is rather poor. The reason for this lack of precision is not clear, but is possibly due to the inconsistent and sometimes rather rapid calibration drift encountered during analysis.

The ID Sr data was used in this thesis REE were analysed by ICP, INAA and XRF. Multiple analysis of samples by ICP produced very little variation (generally <1% for LREEs and <5% for HREEs), and machine drift was closely monitored. Important interference corrections were made for La, Ce, Pr, Nd, Sm, Eu and Gd (see section A1.2, above). The determinations of Pr and Er, however, showed considerable variations between repeat samples. Pr suffers high interference from Ce, Sr and Ca, making accurate analysis difficult. The cause of variation in Er is not clear. Accordingly, the Pr and Er data was omitted from this work. INAA determinations of the REE were made by N. Rogers at the Open University. The LREE determinations by INAA were very similar to those by ICP, with less than 5% difference (See fig A1.2). The HREE determinations by INAA were consistently higher than by ICP by up to 40% for Lu. Both ICP and INAA recorded very little variation in HREE between samples, so both techniques appear to be making precise measurements, but one of them is producing systematic errors. The operators

of each facility claimed the best precision. The ICP data is used in this work because all of the samples were analysed by ICP, whereas only half could be analysed by INAA.

La, Ce and Nd were also analysed by XRF. XRF determinations were consistently low compared to ICP and INAA, and showed considerable scatter between samples. XRF data was discarded. It is recommended that XRF determinations of REE be treated with considerable caution.

A1.7 ANALYSIS OF MINERAL SEPARATES

A1.7.1 Phlogopite separation

Phlogopite was separated from whole rock kimberlite samples during rock crushing (see section A1.1.1). The crushed whole rock sample was split into two portions, the first being used for a whole rock analysis, the remainder for phlogopite separation. The latter portion was crushed further by steel mortar or jaw crusher to about 1mm grains. Phlogopite was separated from the rock by use of the 'paper shaking' technique. The crushed rock was spread onto a sheet of paper, which was then shaken so that rounded grains could be shaken off, whilst the flat phlogopite grains remained on the paper. Repeated paper shaking and the use of a magnetic separator recovered mica separates consisting of >95% phlogopite. The phlogopite was then washed in dilute detergent and repeatedly rinsed in water to remove dust. The cleaned phlogopite was then separated into magnetic (containing ulvospinel inclusions) and non-magnetic fractions using a magnetic separator. The non-magnetic phlogopite fractions were then sieved with 30, 60 and 100 mesh sieves to obtain various size fractions.

The cleaned phlogopite separates were hand-picked under a binocular microscope to select fresh grains. Grains with alteration or inclusions were rejected. The fresh separates were leached in 2M HCl for 5-10 minutes. Leaching removed any calcite from cracks along cleavage planes. The phlogopite was then washed several times in SBQD water and dried. The dried grains were weighed into teflon beakers and spiked using the Leeds University 'Green' mixed Rb/Sr spike. The sample was then dissolved in a mixture of HF and conc. HNO_3 , for Rb and Sr separation as with wholerock samples (above).

A1.7.2. Megacryst Preparation

Individual megacrysts were crushed in a hardened steel mortar and examined under a binocular microscope. The megacrysts which produced the most fresh material were then crushed further to -30 mesh grain size and sieved with 60 and 90 mesh nylon sieves to give three size fractions, -90, -60 and +60. The crushed grains were then washed in distilled water to remove dust. The grains were then individually hand-picked so that only fresh grains were selected, and any grains with the slightest alteration, or cracks or inclusions were rejected. The selected grains were then placed in a petri dish filled with analytical grade pure ethanol and exhaustively hand-picked again with bright illumination under a powerful binocular microscope. The use of ethanol eliminates surface reflections from the grains producing a very clear image, so that tiny cracks and inclusions can be seen much better. Only the totally pure fresh grains were selected. The majority of megacrysts failed to provide enough pristine material to analyse.

The selected megacryst samples were then washed in SBQD water and then leached. Pyroxene (Diopside and

orthopyroxene) samples were mildly leached in 2.5 M HCl for 10 minutes in an ultrasonic bath. Garnet megacrysts were leached for 10 minutes in 6M HCl for 10 minutes, also in an ultrasonic bath. The megacrysts were then immediately washed in QDSB water and dried. The dried samples were crushed in an agate ball mill designed for small samples.

The pyroxene samples were weighed into teflon beakers and spiked for Ba, Rb, Sr, U, and Pb, then dissolved in an HF/HNO₃ mixture. When fully dissolved the samples were loaded onto Pb columns and Pb chemistry was performed as described above. The elutant, containing Rb, Sr and REE was collected and dried, then redissolved in HNO₃. This sample was then aliquoted into two portions, the larger (85%) to be analysed for Ba, Rb, Sr and Nd, the smaller (15%) was spiked for REE analysis with the Leeds mixed REE spike.

The element separation chemistry used was as for major elements (above). REE were separated using calibrated REE columns. The REE sample was dried, then dissolved in a 1ml mixture of 75% HNO₃/25% CH₃COOH and loaded onto the REE columns. The sample was eluted in a calibrated volume of 90/10 HNO₃/CH₃COOH, and collected in 10ml 0.05M HNO₃. The sample was dried and redissolved in 0.5ml of 75/25 HNO₃/CH₃COOH and passed through a second (smaller) set of REE clean-up columns. The sample was again collected in 0.05M HNO₃, then dried in a microbeaker ready for loading onto a filament for analysis.

Garnet megacrysts were dissolved in bombs as they are much less soluble than diopside. The bombs used were cleaned meticulously to reduce analytical blanks as garnet has very low concentrations of REE, Rb and Sr. The powdered garnet samples were weighed into the bombs and spiked for Rb and Sr. 2ml conc HF and 8ml conc HNO₃ were added and the bombs were closed, sealed and placed in an oven at 120°C. The bombs were removed after one week and

cooled. The bombs were opened and inspected. A fluoride precipitate had formed in the liquid. The samples were then subjected to several cycles of drying, dissolution in conc. then dilute HNO_3 and heating in the oven. When the garnet had finally gone completely into solution the sample was aliquoted into two portions for REE analysis and Rb, Sr and Nd analysis as with the pyroxene samples. The REE portion was then spiked with the Leeds mixed REE spike. The element separation chemistry was performed as described above.

APPENDIX 2

MICROPROBE DATA

ULVOSPINEL

K2

ELEMENT	%OXIDE 1	2	3	4	5	6	7	8	9
SiO ₂	.15	.34	.31	.46	.28	.35	.46	.32	.16
TiO ₂	30.78	18.54	13.18	12.34	10.81	14.07	13.02	13.56	13.75
Al ₂ O ₃	-	.54	2.61	4.31	3.92	3.10	3.55	3.01	3.13
V	.46	.34	-	.10	-	-	-	.11	-
Cr ₂ O ₃	.84	.75	-	-	-	-	-	-	.13
Fe ₃ ⁺	42.50	34.15	44.85	43.80	47.02	42.21	43.56	43.21	42.96
Fe ₂ ⁺	21.45	37.09	23.02	26.11	22.94	27.17	26.28	23.62	23.98
MnO	.13	.56	1.00	.95	.91	1.15	1.01	1.13	.84
MgO	3.32	6.25	12.13	10.27	10.96	10.28	10.39	11.86	12.12
CaO	.31	1.24	.58	.36	.34	.42	.58	.57	.51
NiO	-	-	-	-	.13	.19	-	-	-
Zn	-	-	-	.23	.16	-	.12	.19	.16
TOTAL	100.0	99.8	97.9	99.0	97.6	99.0	99.0	97.6	97.9

K2

ULVOSPINEL

ELEMENT	%OXIDE AS15	AS17	AS18	AS19	AS21	AS22	AS23
SiO ₂	.30	1.06	.37	.24	.49	.28	.30
TiO ₂	14.57	15.28	14.32	13.05	10.91	10.76	14.70
Al ₂ O ₃	2.97	3.16	2.68	3.79	3.41	4.65	3.16
V	-	.12	-	-	-	-	-
Cr ₂ O ₃	.37	-	-	.10	-	.28	-
Fe ₃ ⁺	41.39	37.48	42.50	44.25	47.97	47.43	42.37
Fe ₂ ⁺	29.78	31.19	25.54	27.58	24.84	23.84	26.73
MnO	.60	.75	.93	.72	.88	.80	.81
MgO	9.59	8.75	11.34	9.95	10.08	10.01	11.29
CaO	.18	1.17	.47	.51	.63	.31	.62
NiO	.12	.20	.18	-	.20	.21	-
Zn	-	-	.21	-	-	.14	-
TOTAL	99.9	99.3	98.6	100.3	99.5	99.7	100.2

K2

K2

OLIVINE

XENOCRYST

ELEMENT	%OXIDE					
	AS6	AS7	AS8	AS10	AS11	AS12
SiO ₂	41.19	40.76	40.60	40.76	39.94	40.47
TiO ₂	-	-	-	-	-	-
Al ₂ O ₃	.10	-	-	.33	-	-
Cr ₂ O ₃	-	-	-	-	-	-
FeO	8.10	8.56	10.12	10.30	9.93	8.27
MnO	.10	-	-	-	.10	-
MgO	50.37	49.68	48.18	48.57	48.35	49.20
CaO	-	.11	.11	.11	.26	-
NiO	.44	.39	.50	.30	.39	.40
TOTAL	100.6	99.7	99.7	100.5	99.0	98.6
mq Number =	91.5	91.1	89.4	89.3	89.6	91.3

APATITE

ELEMENT	%OXIDE	
	AS24	AS26
SiO ₂	.52	
FeO	.20	.18
MnO	-	-
MgO	.12	.11
CaO	54.53	54.14
SrO	1.62	1.92
P ₂ O ₅	42.39	40.86
ClO ₀	-	-
TOTAL	99.4	97.2

K2

OLIVINE

PHENOCRYST

ELEMENT	%OXIDE							
	AS1	AS2	AS3	AS4	AS5	3	4	7
SiO ₂	40.73	40.56	41.11	40.70	41.04	40.36	40.71	41.17
TiO ₂	-	-	-	-	-	-	-	-
Al ₂ O ₃	-	-	-	-	.14	-	-	-
Cr ₂ O ₃	-	-	-	-	-	-	-	-
FeO	8.84	8.10	8.70	8.45	8.64	11.06	9.06	5.30
MnO	-	.16	-	.18	-	.17	.11	.37
MgO	49.52	49.79	49.75	49.56	49.76	48.73	50.49	53.17
CaO	-	-	-	.10	-	.22	.07	.76
NiO	.26	.44	.35	.40	.40	.30	.51	-
TOTAL	99.4	99.1	100.1	99.4	100.1	100.9	101.1	100.9
mq Number =	90.8	91.5	91.0	91.1	91.1			

K2

PHLOGOPITE

ELEMENT	%OXIDE AS28	AS10	AS11	AS12	AS13	Q22	Q23	Q24
SiO ₂	36.77	34.72	33.87	35.19	34.03	35.16	34.54	36.76
TiO ₂	4.33	1.28	1.41	.62	1.51	.99	1.62	.89
Al ₂ O ₃	15.82	16.29	17.46	8.21	16.73	16.20	15.49	16.17
Cr ₂ O ₃	.74	-	-	-	-	-	-	-
FeO	4.76	2.95	4.16	2.99	3.16	2.93	2.65	2.24
MnO	-	-	-	-	-	-	-	-
MgO	20.27	23.76	23.88	23.28	23.77	25.25	23.84	26.52
CaO	-	-	.21	14.62	.53	-	.58	-
Na ₂ O	-	-	-	-	-	.28	.63	-
K ₂ O	10.47	8.15	7.67	4.19	8.37	8.11	8.23	8.49
NiO	-	-	-	-	-	-	-	-
BaO	1.00	8.30	9.68	6.24	8.13	7.21	7.50	6.92
TOTAL	94.6	95.7	98.8	95.6	96.7	96.2	95.2	98.2

K2

CHROMESPINEL

ELEMENT	%OXIDE AS13	AS14	AS16	AS20
SiO ₂	.61	.35	.52	.48
TiO ₂	1.66	1.88	3.08	3.04
Al ₂ O ₃	15.53	15.02	22.29	20.78
V	-	-	.15	.18
Cr ₂ O ₃	49.18	49.18	39.01	39.29
Fe ₃ ⁺	3.93	4.80	4.66	4.95
Fe ₂ ⁺	14.56	14.41	14.33	15.20
MnO	.14	.43	.13	.20
MgO	14.27	14.00	15.90	14.78
CaO	.11	.16	-	.14
NiO	.24	-	.33	.17
Zn	-	.19	-	.02
TOTAL	100.34	100.5	100.4	99.2

MONTICELLITE

ELEMENT	%OXIDE AS14	AS16	AS17	AS20
SiO ₂	36.66	36.49	37.00	36.78
TiO ₂	-	-	-	.22
Al ₂ O ₃	-	.51	.17	-
Cr ₂ O ₃	-	-	-	-
FeO	11.27	11.41	11.05	4.43
MnO	.29	.38	.20	.16
MgO	18.40	18.86	19.07	22.92
CaO	32.98	32.31	32.47	34.68
TOTAL	99.7	100.0	100.1	99.2

K35

K35

<u>OLIVINE</u>	<u>PHENOCRYST</u>									
ELEMENT	%OXIDE AS21	AS22	AS23	AS24	AS26	AS27	B41	B42	B43	B54
SiO ₂	39.23	40.91	40.23	40.66	41.08	37.61	39.98	39.96	40.32	40.17
TiO ₂	-	-	-	-	-	-	-	-	-	-
Al ₂ O ₃	.37	.26	-	.29	.23	.32	-	-	-	-
Cr ₂ O ₃	-	.13	-	-	-	-	-	-	-	-
FeO	13.54	10.20	11.58	11.74	8.52	11.83	10.45	9.85	11.21	8.22
MnO	-	-	.22	.16	-	-	.10	.12	.14	.12
MgO	46.14	48.93	47.75	48.25	50.27	45.84	49.12	48.88	49.24	49.67
CaO	.52	-	-	-	-	2.25	-	.10	-	-
NiO	-	.37	.24	.39	.41	-	.30	.23	.31	.31
TOTAL	99.9	100.8	100.0	101.5	100.5	98.1	100.0	99.3	101.2	98.6
mg Number =	85.8	89.5	87.8	87.8	91.3	87.3	89.2	89.7	88.6	91.4

K35

<u>OLIVINE</u>	<u>MACROCRYST</u>					
ELEMENT	%OXIDE B44	B45	B46	B47	B51	B52
SiO ₂	40.36	40.29	40.74	39.49	40.52	39.84
TiO ₂	-	.11	-	-	-	-
Al ₂ O ₃	.26	-	-	-	-	-
Cr ₂ O ₃	-	-	-	-	-	-
FeO	11.25	9.72	8.75	14.40	8.72	8.58
MnO	.18	-	.11	.17	-	-
MgO	48.52	49.43	50.07	46.25	49.88	49.94
CaO	.15	-	-	-	-	-
NiO	-	.32	.27	-	.39	.41
TOTAL	100.9	100.0	100.1	100.3	99.7	98.9
mg Number =	88.3	90.0	91.0	85.0	91.0	91.1

K35

ULVOSPINEL

ELEMENT	%OXIDE AS68	AS75	AS77	AS62	AS64	B1	B2	B4	B6	B8
SiO ₂	.37	.35	.25	.23	2.04	.54	.31	.39	.32	.29
TiO ₂	16.38	19.13	15.25	15.72	14.29	15.24	17.87	17.08	16.35	18.92
Al ₂ O ₃	1.72	1.48	1.60	1.74	1.66	1.64	1.40	2.53	2.05	1.17
V	-	-	-	.13	-	-	-	-	-	-
Cr ₂ O ₃	2.96	.69	1.07	1.62	1.21	.75	.69	1.19	6.04	2.29
Fe ₃ ⁺	61.95	62.25	70.21	19.95	63.66	42.82	38.70	38.42	35.93	35.50
Fe ₂ ⁺	-	-	-	22.57	-	21.52	23.06	22.34	20.64	24.85
MnO	1.43	1.63	.86	1.26	1.22	1.68	1.62	1.56	1.58	1.47
MgO	13.70	14.11	10.91	13.60	12.04	14.31	14.73	14.90	15.62	14.29
CaO	.49	1.25	.14	.40	2.43	.43	.35	.31	.31	.44
NiO	-	.24	-	.22	-	.14	-	.25	.17	.11
Zn	.17	-	-	-	.17	-	.17	.11	-	.17
TOTAL	99.4	101.1	100.3	97.5	98.9	99.2	99.0	99.1	99.0	99.5

K35

ULVOSPINEL

ELEMENT	%OXIDE B9	B11	B12	B15	B18
SiO ₂	.23	.36	.40	.33	.35
TiO ₂	17.33	15.62	16.80	17.44	18.63
Al ₂ O ₃	1.75	2.30	1.56	1.28	1.52
V	-	-	-	-	-
Cr ₂ O ₃	1.01	1.58	1.55	2.62	.72
Fe ₃ ⁺	38.70	41.62	38.89	37.95	38.02
Fe ₂ ⁺	23.06	21.91	22.62	22.43	25.98
MnO	1.46	1.47	1.60	1.41	1.43
MgO	14.40	13.79	13.82	14.78	13.84
CnO	.34	1.45	.97	.64	.37
NiO	.16	.15	.25	.17	.26
Zn	-	-	.22	.23	-
TOTAL	98.5	100.3	98.7	99.3	101.1

ULVOSPINEL

ELEMENT	%OXIDE AS41	AS42	AS43
MgO	13.66	14.63	15.19
Al ₂ O ₃	-	.26	.10
SiO ₂	.18	.23	.24
CaO	-	.17	.59
TiO ₂	54.70	55.52	54.12
V ₂ O ₃	.16	-	-
Cr ₂ O ₃	2.63	.43	4.01
MnO	.57	.55	.58
FeO	28.06	28.44	25.05
NiO	.11	.13	.21
ZnO	.17	-	-
TOTAL	100.3	100.4	100.1

K35

PHLOGOPITE GROUND MASS

ELEMENT	%OXIDE AS39	AS72	B19	B20	B21	B22	B23	B25	B26	B27
SiO ₂	34.19	37.21	37.72	39.13	36.06	32.04	34.78	36.91	36.09	36.05
TiO ₂	2.00	.79	1.07	.79	1.04	1.99	1.22	1.08	1.22	1.32
Al ₂ O ₃	17.17	15.45	15.85	15.02	15.04	15.04	14.71	15.53	15.83	16.94
Cr ₂ O ₃	-	.15	.20	.15	.50	-	-	.12	.13	-
FeO	6.33	4.21	3.92	2.42	9.82	4.56	2.71	4.71	5.35	2.58
MnO	.17	-	-	-	.11	.20	-	-	-	-
MgO	24.65	24.43	25.15	26.58	26.53	23.63	24.00	26.12	26.52	25.30
CaO	1.06	.25	.17	-	.37	3.17	3.59	.12	.32	.15
Na ₂ O	.25	.28	.13	.75	.22	.61	.45	.33	-	.66
K ₂ O	8.04	10.15	10.25	10.68	9.43	6.82	7.46	8.51	8.16	8.36
NiO	-	-	-	-	-	-	-	-	-	-
BaO	6.61	1.50	1.70	1.72	1.27	8.41	6.77	4.86	5.06	7.07
TOTAL	100.5	94.5	96.2	97.3	100.3	96.6	95.2	98.4	98.8	98.5

K35

PHLOGOPITE GROUND MASS

PEROVSKITE

ELEMENT	%OXIDE B29	B30	B31	AS31	AS34	AS36	AS73	ELEMENT	%OXIDE AS65
SiO ₂	34.52	31.42	36.81	34.41	34.27	34.64	37.93	MgO	-
TiO ₂	1.50	1.69	1.31	1.28	1.32	1.06	.78	Al ₂ O ₃	-
Al ₂ O ₃	16.87	15.92	16.45	18.35	18.33	17.54	15.74	SiO ₂	.57
Cr ₂ O ₃	-	.38	.11	-	-	-	-	CaO	31.94
FeO	4.29	7.61	2.25	2.21	2.16	2.22	2.90	TiO ₂	50.38
MnO	-	.23	.14	-	-	-	-	V ₂ O ₃	-
MgO	25.34	24.46	24.85	25.19	25.09	24.36	24.49	Cr ₂ O ₃	-
CaO	.26	.55	2.63	-	-	-	.27	MnO	-
Na ₂ O	.63	.11	.13	.29	-	-	.25	FeO	1.74
K ₂ O	7.80	6.85	7.98	7.62	7.12	7.50	10.20	NiO	-
NiO	-	-	-	-	-	.13	-	ZnO	-
BaO	8.51	7.34	7.00	10.46	11.50	10.32	1.44	ZrO ₂	-
TOTAL	96.6	96.6	99.7	100.0	100.0	97.8	94.1		

K35

<u>PHILOGOPITE PHENO</u>			<u>ILMENITE</u>			<u>CHROMESPINEL</u>	
ELEMENT	%OXIDE AS30	AS73	ELEMENT	%OXIDE B13	B16	ELEMENT	%OXIDE B17
SiO ₂	40.30	40.03	SiO ₂	.29	.36	SiO ₂	.20
TiO ₂	5.59	4.83	TiO ₂	54.65	55.20	TiO ₂	.14
Al ₂ O ₃	12.48	13.79	Al ₂ O ₃	-	.56	Al ₂ O ₃	27.60
Cr ₂ O ₃	.24	.46	V	-	-	V	-
FeO	6.42	5.18	Cr ₂ O ₃	4.00	.12	Cr ₂ O ₃	41.25
MnO	-	-	Fe ₃ ⁺	6.87	6.26	Fe ₃ ⁺	2.00
MgO	20.18	20.84	Fe ₂ ⁺	18.56	24.43	Fe ₂ ⁺	13.58
CaO	-	-	MnO	.76	.35	MnO	.38
Na ₂ O	-	-	MgO	16.51	14.16	MgO	14.56
K ₂ O	10.76	10.79	CaO	.56	-	CaO	.13
NiO	-	-	NiO	-	-	NiO	.22
BaO	-	-	Zn	-	-	Zn	.31
TOTAL	96.2	96.0	TOTAL	102.3	101.5	TOTAL	100.4

K35

PHILOGOPITE MACROCRYST

ELEMENT	%OXIDE AS15	AS17	AS19	AS20	B94	B95	B96	B97	B98	B100
SiO ₂	38.68	40.98	38.90	42.27	39.07	39.20	36.57	39.24	41.97	37.98
TiO ₂	4.95	4.55	5.46	.40	4.72	4.49	1.16	5.93	.76	4.71
Al ₂ O ₃	13.38	11.74	13.22	11.65	13.38	13.22	15.58	13.36	10.65	13.08
Cr ₂ O ₃	.97	-	.75	.57	1.27	1.44	.26	.29	.37	1.07
FeO	4.93	6.02	5.39	3.75	4.67	4.58	2.15	5.13	4.54	4.46
MnO	-	-	-	-	-	-	-	-	-	.11
MgO	20.39	21.52	19.44	25.30	20.74	21.42	24.99	21.36	24.92	20.71
CaO	-	.13	-	-	-	-	-	.10	-	-
Na ₂ O	.43	.41	-	.64	.50	.67	-	.40	.47	-
K ₂ O	10.66	10.83	10.65	10.86	10.28	10.41	9.11	10.45	10.78	10.27
NiO	-	-	.17	.21	.13	.22	-	.20	-	.26
BaO	-	-	-	.24	.18	.12	5.05	.14	-	.57
TOTAL	94.5	96.3	94.0	95.8	94.9	95.9	94.9	96.5	94.6	93.3

K39

K39

<u>OLIVINE</u>		<u>PHENOCRYST</u>								
ELEMENT	%OXIDE AS1	AS2	AS3	AS4	AS5	AS6	B56	B64	B65	B66
SiO ₂	40.74	40.99	40.81	40.44	40.43	39.30	40.13	40.52	40.52	39.23
TiO ₂	-	-	-	-	-	.17	-	-	-	-
Al ₂ O ₃	.17	.51	.22	.33	.24	-	-	-	-	-
Cr ₂ O ₃	-	-	-	-	-	-	-	-	.20	-
FeO	7.91	8.71	7.84	7.77	9.19	10.58	10.05	8.40	8.72	13.70
MnO	.10	-	.21	-	-	.16	.11	-	.14	.17
MgO	49.06	49.82	50.53	50.35	49.03	47.14	48.49	50.44	50.00	45.28
CaO	-	-	-	-	-	.10	-	-	-	-
NiO	.47	.51	.35	.41	.48	.27	.47	.34	.44	.11
TOTAL	99.4	100.7	100.0	99.4	99.5	97.7	99.3	99.7	100.1	98.7
mg Number =	91.7	91.0	91.8	91.9	90.4	-	89.5	-	91.0	85.3

K39

<u>OLIVINE</u>		<u>MACROCRYST</u>						
ELEMENT	%OXIDE B57	B58	B59	B69	B70	B71	B75	B76
SiO ₂	40.38	40.03	40.30	40.40	40.00	39.79	40.17	40.73
TiO ₂	-	-	-	-	-	-	-	-
Al ₂ O ₃	-	-	-	-	-	-	-	.30
Cr ₂ O ₃	.13	-	-	-	-	-	.13	-
FeO	8.38	11.85	9.67	7.85	11.84	9.87	9.56	8.09
MnO	-	.17	-	-	.20	-	.14	.13
MgO	49.82	47.55	48.90	50.48	47.07	48.49	49.17	50.61
CaO	-	-	-	-	-	.12	-	-
NiO	.25	.40	.32	.40	.37	.33	.39	.39
TOTAL	99.0	100.0	99.3	99.2	99.5	97.7	99.6	100.3
mg Number =	91.3	87.6	90.0	91.9	87.4	89.7	90.0	91.7

K39

(1)

ULVOSPINEL

ELEMENT	%OXIDE AS1	AS2	AS52	AS54	AS55	AS59	AS60	B79	B80	B83
SiO ₂	.29	.30	.41	.44	.32	.27	.39	.48	.35	.33
TiO ₂	18.32	18.84	17.94	19.10	19.22	18.03	18.13	14.86	19.15	19.11
Al ₂ O ₃	1.40	1.50	1.41	1.80	1.20	1.24	1.17	2.42	1.58	1.60
V	.27	.14	.14	.11	-	-	.16	-	-	-
Cr ₂ O ₃	.73	.48	.87	.69	.55	3.30	.59	.62	.49	.61
Fe ₃₊	61.68	62.52	59.96	61.13	61.00	61.74	61.73	42.13	34.36	35.42
Fe ₂₊	-	-	-	-	-	-	-	20.38	25.22	28.13
MnO	1.30	1.18	1.82	1.39	1.61	1.42	1.73	1.66	1.07	1.02
MgO	15.61	14.91	16.69	16.25	16.20	14.64	16.01	14.31	14.27	12.77
CaO	.55	.63	.38	.24	.41	.14	.32	.94	.22	.33
NiO	-	-	.28	-	-	.11	.14	-	-	-
Zn	.26	-	.15	-	.23	.11	-	-	-	.23
TOTAL	100.4	100.59	100.3	101.3	100.9	101.0	100.4	97.8	96.7	99.5

K39

ULVOSPINEL

ELEMENT	%OXIDE B85	B86	B87	B88
SiO ₂	.22	.44	.49	.35
TiO ₂	18.04	19.21	18.08	17.61
Al ₂ O ₃	1.39	1.68	.84	1.58
V	-	-	-	-
Cr ₂ O ₃	3.20	.81	1.62	.81
Fe ₃₊	35.74	34.04	37.08	34.96
Fe ₂₊	24.03	25.88	24.61	22.78
MnO	1.15	1.27	1.70	1.22
MgO	14.34	13.35	14.04	13.21
CaO	.18	1.13	.19	1.47
NiO	.13	-	-	.22
Zn	.15	.12	-	.12
TOTAL	98.8	97.9	98.76	94.3

CHROMESPINEL

ELEMENT	%OXIDE B82	B84
SiO ₂	.36	.29
TiO ₂	10.58	.59
Al ₂ O ₃	.96	15.64
V	-	-
Cr ₂ O ₃	28.34	49.24
Fe ₃₊	22.07	5.65
Fe ₂₊	22.51	15.26
MnO	1.16	.27
MgO	11.51	12.70
CaO	.15	-
NiO	-	.24
Zn	.15	.30
TOTAL	97.45	100.1

K39

K39

<u>OLIVINE</u>				<u>PHENOCRYST</u>			<u>PHLOGOPITE</u>			<u>GROUND MASS</u>			<u>PEROVSKITE</u>	
ELEMENT	%OXIDE B67	B68	B72	ELEMENT	%OXIDE AS18	B99	B101	ELEMENT	%OXIDE B92			ELEMENT	%OXIDE B92	
SiO ₂	40.38	39.98	40.82	SiO ₂	34.07	37.03	34.49	SiO ₂	.37			TiO ₂	50.54	
TiO ₂	-	-	-	TiO ₂	1.12	1.27	1.43	TiO ₂				Al ₂ O ₃	.20	
Al ₂ O ₃	.20	-	-	Al ₂ O ₃	17.33	13.77	15.41	Al ₂ O ₃				V	-	
Cr ₂ O ₃	-	-	-	Cr ₂ O ₃	-	.22	-	V	-			Cr ₂ O ₃	.74	
FeO	7.86	8.72	8.19	FeO	2.26	3.10	2.46	Fe ₃₊	2.40			Fe ₂₊	1.48	
MnO	.12	-	-	MnO	-	-	-	Fe ₂₊				MnO	-	
MgO	50.92	50.43	50.55	MgO	24.58	26.03	24.73	MnO	-			MgO	1.09	
CaO	-	-	-	CaO	.10	.41	.25	MgO				CaO	32.94	
NiO	.38	.41	.34	CaO	-	-	-	NiO	.20			NiO		
TOTAL	99.8	99.6	100.1	NiO	-	-	-	TOTAL	90.0			TOTAL		
mq Number =	91.9	91.1	91.6	BaO	8.39	3.96	8.09	Zn	-			TOTAL	90.0	
				TOTAL	96.3	94.9	94.8							

K39

<u>ILMENITE</u>				<u>CALCITE</u>			<u>ZrO₂</u>	
ELEMENT	%OXIDE B90	B91	B93	ELEMENT	%OXIDE C1	C2	ELEMENT	%OXIDE AS58
SiO ₂	.30	.40	.24	SiO ₂	.44	1.16	MgO	.41
TiO ₂	52.30	54.40	52.17	TiO ₂	-	-	Al ₂ O ₃	-
Al ₂ O ₃	.12	-	-	Al ₂ O ₃	.12	.23	SiO ₂	.43
V	-	-	-	Cr ₂ O ₃	-	-	CaO	.79
Cr ₂ O ₃	4.55	2.76	3.79	FeO	.27	.34	TiO ₂	.40
Fe ₃₊	6.88	3.75	9.87	MnO	-	-	V ₂ O ₃	-
Fe ₂₊	17.83	22.01	12.17	MgO	.39	.85	Cr ₂ O ₃	-
MnO	.72	.58	.95	CaO	54.00	51.90	MnO	-
MgO	15.41	14.85	16.63	NiO	-	-	FeO	.59
CaO	.93	.14	3.39	TOTAL	55.3	54.6	NiO	-
NiO	-	.18	-				ZnO	-
Zn	-	-	-				ZrO ₂	101.27
TOTAL	99.1	99.1	99.2				TOTAL	103.9

K53

K53

<u>OLIVINE</u>	<u>PHENOCRYST</u>									
ELEMENT	%OXIDE A510	A511	A512	A19	A21	A22	A23	A24	A30	A31
SiO ₂	40.90	40.04	40.63	39.85	40.26	40.36	40.16	39.69	39.88	39.87
TiO ₂	-	-	-	-	-	-	-	-	-	-
Al ₂ O ₃	.65	.31	.23	-	.35	.17	-	-	-	-
Cr ₂ O ₃	-	.15	.11	-	-	-	-	-	.10	-
FeO	8.03	8.82	9.24	9.93	10.72	10.92	12.07	11.89	10.89	11.65
MnO	.22	.17	.16	.14	.13	.14	.21	.12	.14	.28
MgO	50.16	49.50	49.18	49.27	49.46	48.60	48.10	47.65	48.48	48.05
CaO	-	.18	.16	.11	.11	.12	.13	.12	-	.30
NiO	.35	.38	.43	.27	.26	.40	.24	-	.16	.16
TOTAL	100.4	99.5	100.1	99.6	101.3	100.8	101.0	99.7	99.8	100.4
mg Number =	91.6	90.8	90.3	89.7	89.0	88.7	87.5	87.6	88.7	87.8

K53

<u>OLIVINE</u>	<u>PHENOCRYST</u>					<u>OLIVINE</u>	<u>MACROCRYST</u>	
ELEMENT	%OXIDE A16	A50	A52	A57	A58	ELEMENT	%OXIDE A24	A25
SiO ₂	40.96	40.44	40.83	40.49	40.09	SiO ₂	39.87	40.03
TiO ₂	-	-	-	-	-	TiO ₂	.10	-
Al ₂ O ₃	.22	.14	.35	.39	-	Al ₂ O ₃	-	.16
Cr ₂ O ₃	-	-	.13	.21	-	Cr ₂ O ₃	-	-
FeO	9.91	9.25	9.21	9.01	9.70	FeO	11.43	12.18
MnO	.13	-	-	-	-	MnO	.15	.24
MgO	49.29	49.65	49.01	49.75	48.55	MgO	47.60	46.55
CaO	.13	-	-	-	.19	CaO	.12	.33
NiO	.35	.36	.38	.28	.44	NiO	.11	.35
TOTAL	101.0	100.1	100.0	100.4	99.2	TOTAL	99.4	99.9
mg Number =	89.7	90.5	90.4	90.7	89.8	mg Number =	88.0	87.0

K53



<u>OLIVINE</u>		<u>MACROCRYST</u>							
ELEMENT	%OXIDE A9	AS10	A20	A25	A26	A29	A15	A17	A23
SiO ₂	40.49	41.13	39.77	39.87	40.04	39.78	40.42	40.19	39.63
TiO ₂	-	-	.16	-	-	-	-	-	-
Al ₂ O ₃	.43	.65	-	.30	-	-	-	-	-
Cr ₂ O ₃	-	-	.10	-	.12	.13	-	-	.16
FeO	11.15	8.07	11.60	16.36	8.32	12.81	11.07	11.23	11.50
MnO	.25	.22	-	.21	-	.16	.25	-	.13
MgO	48.38	50.43	48.01	44.70	49.93	48.19	46.99	48.21	46.93
CaO	-	.11	.14	-	.17	.31	.75	.11	.12
NiO	-	.36	.10	-	.45	.38	.40	.50	.25
TOTAL	100.8	100.9	100.0	101.6	99.1	101.8	100.0	100.5	98.7
mg Number = 88.3	-	-	88.0	82.8	91.4	86.9	88.1	88.4	87.8

K53

<u>CHROMESPINEL</u>					
ELEMENT	%OXIDE AS79	AS1	AS8	AS11	AS13
SiO ₂	.68	.32	.37	.23	1.10
TiO ₂	5.64	3.33	4.16	4.97	4.84
Al ₂ O ₃	8.91	5.54	1.56	.80	1.96
V	-	.35	.37	.29	.17
Cr ₂ O ₃	33.86	37.29	34.27	28.69	28.79
Fe ₃ ⁺	15.68	19.57	25.99	30.08	29.05
Fe ₂ ⁺	25.36	23.93	25.48	25.33	25.74
MnO	.63	.69	.91	1.10	.94
MgO	8.17	6.93	6.14	5.83	7.07
CaO	.23	.18	.10	.27	-
NiO	.15	-	-	.10	.10
Zn	.15	-	-	-	-
TOTAL	99.5	98.2	99.6	97.7	99.8

K53

ULVOSPINEL

ELEMENT	OXIDE AS2	AS3	AS4	AS5	AS7	AS9	AS10	AS12
SiO ₂	.54	.22	.28	.26	.48	2.69	.37	.33
TiO ₂	9.33	8.14	7.89	7.19	8.32	7.82	7.66	7.99
Al ₂ O ₃	.54	.30	.40	.39	.65	.30	-	.30
V	.39	.37	.46	.25	.38	.31	.33	.34
Cr ₂ O ₃	4.91	4.83	11.01	5.27	9.00	4.20	3.20	4.01
Fe ₃ ⁺	46.54	81.06	43.01	49.79	43.90	49.34	50.66	49.67
Fe ₂ ⁺	30.44	-	28.93	29.43	30.48	27.77	31.31	30.09
MnO	.74	.64	.73	.78	1.01	1.00	.83	.74
MgO	5.01	4.70	5.33	4.69	4.84	8.04	3.59	4.77
CaO	1.31	.39	.22	.15	.31	1.25	.22	.17
NiO	.10	.26	.33	.11	.20	.24	.21	.16
Zn	-	.13	.12	-	-	.16	.10	.10
TOTAL	99.9	101.04	98.7	98.3	99.6	103.1	98.5	99.7

K53

ULVOSPINEL

ELEMENT	OXIDE AS80	AS81	AS83	AS85	AS86
SiO ₂	.15	.46	.39	.33	.85
TiO ₂	8.22	8.14	7.71	8.26	11.26
Al ₂ O ₃	.39	.32	.68	.41	-
V	-	-	-	-	-
Cr ₂ O ₃	6.90	3.58	14.79	4.77	-
Fe ₃ ⁺	46.78	49.22	40.19	48.70	44.54
Fe ₂ ⁺	29.99	31.30	29.73	30.47	32.18
MnO	.82	.84	.66	.70	1.37
MgO	4.79	4.10	5.34	4.67	3.98
CaO	-	.16	-	.23	1.15
NiO	.23	.19	.19	.26	-
Zn	.11	-	.11	-	.14
TOTAL	98.5	98.3	99.9	98.8	95.6

K53

PHLOGOPITE MACROCRYST

ELEMENT	%OXIDE AS1	AS2	AS3	AS4	AS5	AS6
SiO ₂	38.39	37.59	37.58	35.45	38.01	37.71
TiO ₂	4.82	4.55	4.39	1.86	4.77	4.58
Al ₂ O ₃	15.01	16.11	15.88	17.51	16.26	16.00
Cr ₂ O ₃	1.15	.92	.95	-	-	-
FeO	5.25	4.93	5.34	3.41	5.34	5.26
MnO	-	-	-	-	-	-
MgO	21.12	20.62	21.23	24.30	21.17	20.90
CaO	-	-	-	.13	-	-
Na ₂ O	.28	-	.74	.53	.66	.49
K ₂ O	10.73	10.40	10.71	8.36	10.54	10.43
H ₂ O	-	-	-	-	-	-
BaO	.18	.61	.59	7.97	.28	.54
TOTAL	97.1	95.9	97.5	99.7	97.2	96.1

K51

PEROVSKITE

ELEMENT	%OXIDE AS6	AS79	AS82	AS51
SiO ₂	.29	.28	1.11	.24
TiO ₂	56.90	56.51	55.42	57.18
Al ₂ O ₃	.17	.22	.35	.25
V	.17	-	-	.21
Cr ₂ O ₃	.25	.20	-	.86
Fe ₃₊	.86	-	-	-
Fe ₂₊	-	.89	1.71	.24
MnO	-	-	-	40.58
MgO	-	.19	.28	.14
CaO	40.21	40.07	39.02	-
H ₂ O	-	-	-	-
Zn	.16	.23	-	-
BaO	-	-	-	-
TOTAL	99.0	98.6	98.2	99.7

PHLOGOPITE GROUND MASS

ELEMENT	%OXIDE AS6	AS7	AS9
SiO ₂	34.51	35.17	35.06
TiO ₂	1.72	.97	.84
Al ₂ O ₃	16.98	17.17	17.44
Cr ₂ O ₃	-	.15	.13
FeO	2.63	3.10	2.64
MnO	-	-	-
MgO	24.19	24.94	24.32
CaO	.86	.25	-
Na ₂ O	.21	.33	-
K ₂ O	8.62	8.16	8.09
H ₂ O	-	-	-
BaO	6.95	8.44	8.67
TOTAL	96.8	98.7	97.3

SCIMARZEBERG

TITANOMAGNETITE

ELEMENT	%OXIDE AS11	AS12	AS13	AS14	AS15	AS16	AS17	AS18	AS19	AS20
SiO ₂	.62	.24	.61	.44	.45	.41	.39	.37	.73	.42
TiO ₂	17.32	16.67	18.30	19.36	18.84	18.81	17.76	17.70	18.34	17.90
Al ₂ O ₃	2.88	2.71	2.33	2.35	2.67	2.25	2.43	2.35	2.47	2.60
V	-	-	-	-	-	-	-	-	-	-
Cr ₂ O ₃	.15	.18	.11	-	.12	-	.17	.28	.14	.10
Fe ₃ ⁺	30.78	33.13	27.90	27.27	28.62	26.97	30.61	30.58	26.47	30.41
Fe ₂ ⁺	40.97	41.34	42.54	44.31	42.22	42.17	41.59	42.93	42.28	41.90
MnO	1.12	1.22	1.22	1.20	1.18	1.21	1.21	1.04	1.24	1.00
HgO	3.37	2.58	2.40	2.20	3.10	2.51	2.90	2.26	2.60	2.90
CaO	.18	.18	.28	.21	.30	.41	.15	.13	.20	.20
NiO	-	-	.14	-	.19	-	.12	.12	-	-
Zn	.26	-	-	.11	.25	.17	.19	-	-	-
TOTAL	97.6	98.1	95.9	97.5	97.9	94.9	97.5	97.8	94.5	98.0

SCHWARZBERG

PYROXENE

ELEMENT	%OXIDE AS61	AS62	AS63	AS65	AS67
SiO ₂	47.27	45.40	44.68	49.63	42.85
TiO ₂	2.40	3.00	2.92	1.58	4.09
Al ₂ O ₃	5.45	9.05	8.23	5.53	11.16
Cr ₂ O ₃	-	-	-	.33	.12
FeO	6.74	7.07	6.86	4.83	7.09
MnO	.23	-	.11	-	-
HgO	12.29	11.93	11.50	14.45	11.01
CaO	24.11	24.54	23.87	23.99	23.85
Na ₂ O	-	-	.31	.39	-
K ₂ O	-	-	-	-	-
NiO	-	-	-	-	-
BaO	-	-	-	-	-
TOTAL	98.5	101.0	98.6	100.9	100.3

NEPHELINE

ELEMENT	%OXIDE AS64	AS68
SiO ₂	41.13	42.08
TiO ₂	.12	-
Al ₂ O ₃	32.58	33.02
Cr ₂ O ₃	-	-
FeO	1.05	1.00
MnO	-	-
HgO	-	-
CaO	.72	.84
Na ₂ O	13.12	13.10
K ₂ O	9.23	8.93
NiO	-	-
BaO	-	.26
TOTAL	97.9	99.3

<u>ULVOSPINEL</u>		<u>PK2</u>					
ELEMENT	%OXIDE AS2	AS3	AS4	AS7	AS8	AS9	AS10
SiO ₂	.27	.26	.38	.34	.37	1.05	.28
TiO ₂	.68	7.59	2.38	4.56	5.30	6.37	1.30
Al ₂ O ₃	.30	3.84	.58	.10	.71	2.85	.51
V	-	-	-	-	-	-	-
Cr ₂ O ₃	.17	-	-	-	-	.14	.15
Fe ₃ ⁺	65.65	51.94	63.26	58.75	57.07	52.44	66.86
Fe ₂ ⁺	27.34	25.56	25.40	30.42	30.18	24.40	24.58
MnO	.66	.87	.67	.47	.31	.91	.35
HgO	1.69	7.62	4.28	2.52	3.28	7.34	4.58
CaO	.31	.13	.22	-	-	.74	.28
NiO	.18	-	-	-	-	.17	-
Zn	.12	.14	-	.15	.18	-	-
TOTAL	97.4	98.0	97.3	97.4	97.6	96.5	98.9

APPENDIX 3 - ORDER OF CRYSTALLISATION

The order of crystallisation described on page 74 was determined by petrographic examination. The mineralogy can be divided into early (phenocryst) phases and late (groundmass) phases.

The first phase to crystallise was chromite, which forms small equant grains. Chromite was sometimes found as inclusions within olivine macrocrysts, indicating their early precipitation. Olivine was the second phase to crystallise, and appears to have formed over a large temperature range, because of their size and compositional variations. The olivines are usually well formed phenocrysts with few inclusions. Occasionally, however, some olivine phenocrysts were found to contain small ilmenite inclusions indicating that ilmenite fractionation began before olivine fractionation ceased. The apparent Mg enrichment trend (p66) observed (by microprobe) in the ilmenites was due to the rising Mg content of the melt after cessation of olivine fractionation. Ilmenite is therefore considered to have continued fractionating after olivine had ceased. Macrocryst phlogopite laths clearly were formed before groundmass crystallisation, but their origin as phenocrysts or xenocrysts is not clear (p69).

Ulvospinel and perovskite are microphenocryst phases in the groundmass which were precipitated after the above phenocryst phases. Ulvospinel forms either equant cubic grains or overgrowths over ilmenite or chromite, indicating it's later crystallisation. Perovskite forms as equant-subequant grains or as overgrowth rims over ulvospinels (p68). Groundmass phlogopite, monticellite and calcite were the last three phases to form. Phlogopite forms micro-laths in the groundmass with abundant inclusions of ulvospinel. the onset of groundmass phlogopite precipitation was late, but zonation trends (p70-76) and poikilitic texture indicate relatively rapid crystal growth once crystallisation began. Monticellite forms interstitially between the phlogopites and spinels and crystallised after them. Primary calcite was probably the last phase to crystallise. It forms in small interstitial patches which were perhaps tiny volatile rich segregations.